

AD-A149 037

A COMPREHENSIVE STUDY ON SUBLAMINATE CRACK GROWTH
STABILITY AND ITS EFFEC. (U) DREXEL UNIV PHILADELPHIA
PA DEPT OF MECHANICAL ENGINEERING AN. A S WANG ET AL.

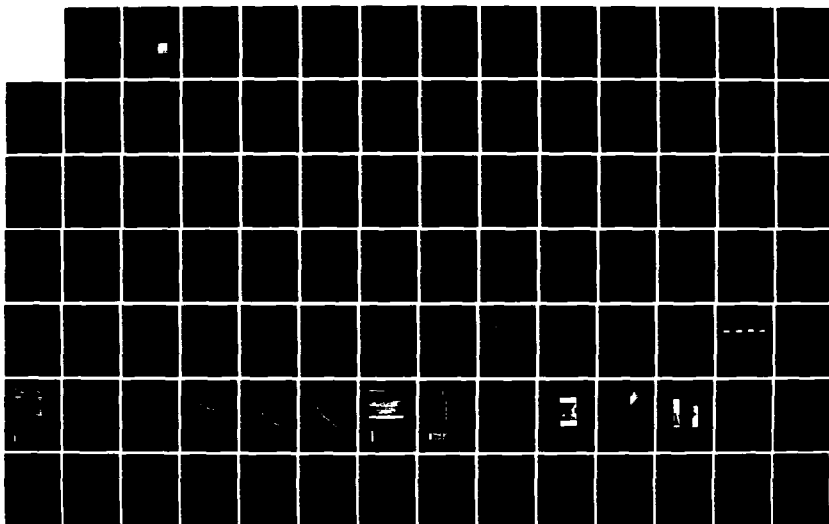
172

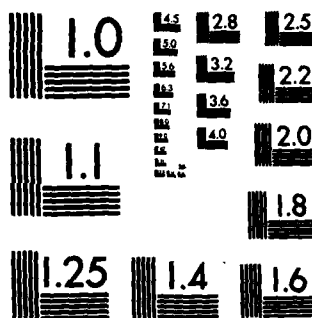
UNCLASSIFIED

MAR 84 AFOSR-TR-84-1127 F49620-79-C-0206

F/G 11/4

NL





MICROCOPY RESOLUTION TEST CHART
NATIONAL BUREAU OF STANDARDS-1963-A

AFOSR-TR- 84-1127

9

AD-A149 037

A COMPREHENSIVE STUDY ON SUBLAMINATE
CRACK GROWTH STABILITY AND ITS EFFECTS
ON THE LOAD-CARRYING CAPACITY

A. S. D. Wang
Drexel University

and

F. W. Crossman
Lockheed Palo Alto Research Laboratory

Drexel
University



College of Engineering
Department of
Mechanical Engineering
and Mechanics
Philadelphia, PA 19104

(215) 895-2352-53

DTIC FILE COPY

Approved for public release;
distribution unlimited.

DTIC
S
DEC 27 1984
E

84 12 14 015

9

A COMPREHENSIVE STUDY ON SUBLAMINATE
CRACK GROWTH STABILITY AND ITS EFFECTS
ON THE LOAD-CARRYING CAPACITY

A. S. D. Wang
Drexel University

and

F. W. Crossman
Lockheed Palo Alto Research Laboratory

March, 1984

Final Contract Report

October 1, 1981 to September 30, 1983

Contract No. F 49620-79-C-0206

Approved for Public Release: Distribution Unlimited
for

Director of Aerospace Sciences
Air Force Office of Scientific Research
Bolling AFB, Washington, DC 20332

STG
DEC 1984
E

AIR FORCE OFFICE OF SCIENTIFIC RESEARCH (AFOSR)
NOTICE OF TRANSMISSION
This technical report is approved for public release and distribution.
MATTHEW J. KERNAN
Chief, Technical Information Division

UNCLASSIFIED

DECLASSIFICATION OF THIS PAGE (When Data Entered)

REPORT DOCUMENTATION PAGE		READ INSTRUCTIONS BEFORE COMPLETING FORM	
1. REPORT NUMBER AFOSR-TR-84-1127		12. GOVT ACCESSION NO. AD-A149037	
4. TITLE (and Subtitle) A COMPREHENSIVE STUDY ON SUBLAMINATE CRACK GROWTH STABILITY AND ITS EFFECTS ON THE LOAD-CARRYING CAPACITY		5. TYPE OF REPORT & PERIOD COVERED FINAL: 01 OCT 81-30 SEP 83	
7. AUTHOR(s) A. S. D. Wang and F. W. Crossman		6. PERFORMING ORG. REPORT NUMBER	
9. PERFORMING ORGANIZATION NAME AND ADDRESS DREXEL UNIVERSITY DEPARTMENT OF MECHANICAL ENGINEERING PHILADELPHIA, PA 19104		8. CONTRACT OR GRANT NUMBER(s) F49620-79-C-0206	
11. CONTROLLING OFFICE NAME AND ADDRESS AFOSR/NA Bolling AFB DC 20332-6448		10. PROGRAM ELEMENT, PROJECT, TASK AREA & WORK UNIT NUMBERS 61102F 2307/B2	
14. MONITORING AGENCY NAME & ADDRESS (if different from Controlling Office)		12. REPORT DATE March, 1984	
		13. NUMBER OF PAGES 180	
		15. SECURITY CLASS. (of this report) UNCLASSIFIED	
		15a. DECLASSIFICATION/DOWNGRADING SCHEDULE	
16. DISTRIBUTION STATEMENT (of this Report) Approved for public release; Distribution unlimited			
17. DISTRIBUTION STATEMENT (of the abstract entered in Block 20, if different from Report)			
18. SUPPLEMENTARY NOTES			
19. KEY WORDS (Continue on reverse side if necessary and identify by block number) Composite laminates; graphite-epoxy; sublaminates cracks; transverse cracks; delaminates; fracture mechanics; random flaw distribution; crack growth processes; crack interactions; three-dimensional stress analysis; contour delamination simulation; failure of load-carrying plies.			
20. ABSTRACT (Continue on reverse side if necessary and identify by block number) This report highlights the development of a unified method for the formation mechanisms of matrix-dominated cracks in a class of structural laminates that are made using unidirectionally fiber reinforced composite plies. Because of the collimated reinforcement structure exhibited in this class of laminates, the growth of an individual matrix crack is confined either in the fiber-matrix interface or in the ply-to-ply interface. The former occurs as intraply crack caused primarily by in-ply stresses, while the latter occurs as			

DD FORM 1 JAN 73 1473

EDITION OF 1 NOV 65 IS OBSOLETE

UNCLASSIFIED
SECURITY CLASSIFICATION OF THIS PAGE (When Data Entered)84 12 14 015
REPRODUCED AT GOVERNMENT EXPENSE

UNCLASSIFIED

SECURITY CLASSIFICATION OF THIS PAGE (When Data Entered)

TK-84-1127

interply crack caused by interlaminar stresses. These are the two fundamental modes exhibited in matrix cracking.

Experiments using graphite-epoxy composite systems have established that matrix cracking is actually a process in which a great number of similar cracks occur during the course of loading. The multiplicity in the crack formation process stems from the existence of material flaws which distribute randomly throughout the laminate, and from the internal reinforcement structure which inhibits individual crack from growing into large proportions.

When viewed at the ply level, growth of a matrix crack is essentially brittle in nature; its growth path initially follows one of the two fundamental modes. When blunted, the initial mode may turn to the other mode. Thus, the individual growth path may be considered as piece-wise self-similar.

The general methodology developed in this study invokes the fundamental concepts of ply elasticity which assumes that the material ply in the laminate is individually elastic, homogeneous and anisotropic. The constitutive properties can be represented by a set of effective constants and the failure properties are governed by randomly distributed material flaws. The latter is characterized by an effective flaw distribution which is considered a basic ply property. Thus, for each individual flaw, its propagation behavior is governed by criteria derived from the classical fracture mechanics, while the flaw distribution enables the description of the multiplicity and the stochastic nature of the matrix cracking process.

This report highlights these methodical developments, along with illustrative experimental and analytical results.

Three technical papers are appended to this report. These papers contain the details of the development and much more results. Although each paper was written in self-contained format, they collectively represent the bulk of the technical development accomplished in this research program.

UNCLASSIFIED

SECURITY CLASSIFICATION OF THIS PAGE (When Data Entered)

REPRODUCED AT GOVERNMENT EXPENSE

A COMPREHENSIVE STUDY ON SUBLAMINATE CRACK GROWTH
STABILITY AND ITS EFFECTS ON THE LOAD-CARRYING CAPACITY

A. S. D. Wang
Drexel University
Philadelphia, PA 19104

and

F. W. Crossman
Lockheed Palo Alto Research Laboratory
Palo Alto, CA 94304

ABSTRACT

Accession For	
NTIS GRA&I	<input checked="" type="checkbox"/>
DTIC TAB	<input type="checkbox"/>
Unannounced	<input type="checkbox"/>
Justification	
By	
Distribution /	
Availability Codes	
Dist	Special
A-1	

This report highlights the development of a unified method for the formation mechanisms of matrix-dominated cracks in a class of structural laminates that are made using unidirectionally fiber reinforced composite plies.

Because of the collimated reinforcement structure exhibited in this class of laminates, the growth of an individual matrix crack is confined either in the fiber-matrix interface or in the ply-to-ply interface. The former occurs as intraply crack caused primarily by in-ply stresses, while the latter occurs as interply crack caused by interlaminar stresses. These are the two fundamental modes exhibited in matrix cracking.

Experiments using graphite-epoxy composite systems have established that matrix cracking is actually a process in which a great number of similar cracks occur during the course of loading. The multiplicity in the crack formation process stems from the existence of material flaws which distribute randomly throughout the laminate, and from the internal reinforcement structure which inhibits individual crack from growing into large proportions.

↓
When viewed at the ply level, growth of a matrix crack is essentially brittle in nature; its growth path initially follows one of the two fundamental modes. When blunted, the initial mode may turn to the other mode. Thus, the individual growth path may be considered as piece-wise self-similar. ↗

The general methodology developed in this study invokes the fundamental concepts of ply elasticity which assumes that the material ply in the laminate is individually elastic, homogeneous and anisotropic. The constitutive properties can be represented by a set of effective constants and the failure properties are governed by randomly distributed material flaws. The latter is characterized by an effective flaw distribution which is considered a basic ply property. Thus, for each individual flaw, its propagation behavior is governed by criteria derived from the classical fracture mechanics, while the flaw distribution enables the description of the multiplicity and the stochastic nature of the matrix cracking process.

This report highlights these methodical developments, along with illustrative experimental and analytical results.

Three technical papers are appended to this report. These papers contain the details of the development and much more results. Although each paper was written in self-contained format, they collectively represent the bulk of the technical development accomplished in this research program.

Foreword

This is the final technical report for Phase-II Study under the Contract No. F49620-79-C-0206 from the Air Force Office of Scientific Research. The contract was led to Drexel University with a sub-contract to Lockheed Palo Alto Research Laboratory, covering the period from September 1, 1979 to September 30, 1983.

The contracted research program consisted two phases. The Phase-I Study spanned the period from September 1, 1979 to September 30, 1981; and the Phase-II Study spanned the period from October 1, 1981 to September 30, 1983.

Dr. A. S. D. Wang of Drexel University was the principal investigator, and Dr. F. W. Crossman of Lockheed was the co-principal investigator. Dr. Wang was assisted by his former and present students, principally Dr. G. E. Law, Jr., Dr. N. N. Kishore and Mr. C. A. Li. Dr. Crossman was assisted by Mr. W. J. Warren.

The authors would like to thank Dr. Anthony K. Amos and Major David A. Glasgow, both of AFOSR. Dr. Amos was the contract monitor for Phase-I Study and Major Glasgow was the contract monitor for Phase-II Study.

I. INTRODUCTION

This report contains the results of a research program conducted under the auspices of the Air Force Office of Scientific Research. The stated objectives of the research are (1) to investigate the basic mechanisms of sub-laminate cracks in a class of aerospace structural laminates; and (2) to develop a rational modelling procedure by which the formation and growth processes of the observed sublaminar cracks can be described in terms of engineering quantities.

The particular class of laminates considered in this study included those fabricated using continuous fiber reinforced resin systems, e.g. the unidirectional graphite-epoxy prepreg tape. Sublaminar failure in this class of laminates begins generally with local matrix cracks at low stress levels. The individual growth paths of these cracks almost always follow either the fiber/matrix interface or the ply-to-ply interface. Hence, there are only two fundamental modes for matrix crack growth, the intraply cracking mode and the interply cracking mode. The present research is concerned with the physical mechanisms of the two fundamental cracking modes as well as their mutual interactions.

Consequently, a comprehensive effort was made during the research period which embodied both an experimental and an analytical investigation.

The first phase of the research was directed to the basic mechanics of intraply and interply crackings individually, whereby a unified energy method was developed for their formation mechanisms. Several technical papers were published on one or more aspects related to the development of the analytical model (see Refs. [1] to [8], Appendix A). An overall exposition of the first phase study results was contained in Ref. [9], Appendix A.

The second phase of the research was directed to the understanding of multiple cracks and cracking modes interaction. These sublaminate failures occur following the onset of one of the fundamental modes of matrix cracking.

Multiple cracks and their mutual interactions presented both conceptual and physical difficulties. The former is related to the rational derivation of the desired analytical model, while the latter is related to the mathematical and/or numerical techniques necessary to execute the model for real problems. In this regard, several major developments are noted. First, the concept of "effective flaw distribution" was introduced which replaces the conventional strength concept for the basic ply material. It is assumed that these flaws cause multiple sublaminate cracks. Rational arguments based on experimental observations and simple testing techniques are devised in order to characterize these flaws as a ply material property.

Secondly, computer simulation procedures based on 3-D finite element method and incorporating fracture mechanics criteria were developed in order to describe the interacting and stochastic nature of multiple cracks.

Finally, extensive experiments were conducted in concert with each of the analytical development phases. These experiments involve the most up-to-date destructive and non-destructive damage inspection techniques, which provide not only a visual description of the various matrix cracks in the laminates but also a chronological documentation of the crack formation processes during the course of loading. Both are essential to the initial formulation and the final correlation of the analytical model.

This report contains the results of the second phase of research.

II. RESULTS

Major results obtained in the second phase study have been presented in a series of three technical papers. These papers are listed in Appendix A as Ref. [10], [11] and [12], and are appended to this report as Appendix B, C and D.

The first paper (in Appendix B) is entitled "Fracture Mechanics of Sub-Laminate Cracks in Composite Laminates." In this paper, a detailed account is given for the mechanics of transverse cracking and for the mechanics of free edge delamination; the concept of effective flaws is augmented to simulate multiple cracks and their mutual interactions. Results from two case studies are included to provide a comparison between the analysis and the experiment. In the first case study, 90° -ply transverse cracks in the family of $[0_2/90_n]_s$, $n = 1, 2, 3$, laminates are tested and simulated. In the second case study, the family of $[\pm 25/90_n]_s$, $n = 1/2, 1, 2, 3, 4, 6, 8$, laminates are tested and simulated. It is noted that delamination mode is not involved in the first case study, while both transverse cracking and delamination are involved in the second case study. Depending on the value of n of the latter case, one cracking mode can be induced before the other. Generally, the analytical model can reliably predict the various cracking events.

The second paper (in Appendix C) is entitled "Influence of Ply Thickness on Damage Accumulation and Final Fracture." The paper documents the experimental finding for a series of graphite-epoxy laminate families in the form $[\pm \theta/90_n]_s$, where the thickness of the 90° -ply varies from 2 to 16 plies ($n = 1$ to 8) and the angle " θ " takes on values of 0° , 25° , 30° and 60° . Incremental tensile loading followed by x-radiographic damage inspection were conducted to document chronologically damage accumulation in the laminates; depleting experiments and real-time x-ray during tensile loading were also used

to monitor the details nearing imminent laminate failure. It is shown in this experimental study that matrix cracking modes and their propagative behavior change with laminate stacking sequence and ply thickness in a manner that supports the analytical model based on the criteria of fracture mechanics. Furthermore, the effects of sub-laminate cracks on the primary load-carrying plies were also evaluated experimentally.

The final paper (in Appendix D) is entitled "On Crack Development in Graphite Epoxy $[0_2/90_n]_s$ Laminates Under Uniaxial Tension." This paper makes use of the experimental data reported in the previous paper. The particular laminates chosen belong to the family of $[0_2/90_n]_s$, $n = 1, 2$, and 4 . When these laminates are subjected to uniaxial tension, transverse cracks in the 90° -ply develop at tensile strain as low as 0.3% . As the applied tension increases, the cracks continue to form in increasing numbers. At some critical late stage of loading, however, several other modes of matrix cracking emerge, all stemming from the sites of the transverse cracks. Among them are (1) splitting cracks in the 0° -ply that span across one or more 90° -ply transverse cracks, (2) localized delamination in the $0^\circ/90^\circ$ interface, emanating from the point where a 0° -ply split intersects a 90° -ply transverse crack; and (3) localized edge delamination in the $0^\circ/90^\circ$ interface emanating from the corner point where a 90° -ply transverse crack meets the free edge of the laminate coupon. These late stage matrix crackings seem to precipitate weakening of the load-carrying ply of the laminate, resulting in lowered apparent strength. This paper attempts to analytically describe all these important cracking events by means of the previously developed fracture mechanics/effective flaw method. Emphasis is placed on explaining qualitatively and quantitatively why a certain mode of cracking occurs while other modes do not; especially for the cracking state which exists during late

stage loading, an analysis is made to explain why that state is critical to the apparent laminate strength reduction. As stated, all predictions are compared to the experimentally obtained data.

Although each of the three separate papers is written in self-contained format, they do maintain the essential continuity in contents and consistency in presentation. Collectively, these three papers represent the bulk of the second phase study results.

A list of technical presentations made during both the first phase and the second phase studies is included in Appendix A.

APPENDIX A

(1) Papers and Reports Published:

- [1] A. S. D. Wang, F. W. Crossman and G. Law, "Interlaminar Failure in Epoxy Based Composite Laminates," Proceedings, 29th Symp. Advanced Composites-Design and Applications, National Bureau of Standards, 1979, p. 255.
- [2] A. S. D. Wang and G. E. Law, "An Energy Method for Multiple Transverse Cracks in Graphite-Epoxy Laminates," Modern Developments in Composite Materials and Structures, ASME, 1979, p. 17.
- [3] A. S. D. Wang and Frank W. Crossman, "Initiation and Growth of Transverse Cracks and Edge Delamination in Composite Laminates, Part I. An Energy Method," Jour. Comp. Mat'ls., Suppl. Vol. 1980, p. 71.
- [4] F. W. Crossman, W. T. Warren, A. S. D. Wang and G. E. Law, "Initiation and Growth of Transverse Cracks and Edge Delamination in Composite Laminates, Part II. Experimental Correlation," Jour. Comp. Mat'ls., Suppl. Vol. 1980, p. 88.
- [5] A. S. D. Wang, "Growth Mechanisms of Transverse Cracks and Ply Delamination in Composite Laminates," Proc. ICCM-III, Paris, Vol. 1, 1980, p. 170.
- [6] G. E. Law, Jr., "Fracture Analysis of [+25/90]_ns Graphite-Epoxy Composite Laminates," Ph.D. Thesis, Drexel University, 1981.
- [7] F. W. Crossman and A. S. D. Wang, "The Dependence of Transverse Cracking and Delamination on Ply Thickness in Graphite-Epoxy Laminates," ASTM-STP 775, 1982, p. 118.
- [8] A. S. D. Wang, N. N. Kishore and W. W. Feng, "On Mixed-Mode Fracture in Off-Axis Unidirectional Graphite Epoxy Composites," Proc. ICCM-4, Tokyo, Japan, Vol. 1, 1982, p. 599.
- [9] A. S. D. Wang and F. W. Crossman, "Fracture Mechanics of Sublaminar Cracks," Technical Report prepared under Contract F49620-79-C-0206, October, 1982. Also as AFOSR-TR-83-0594, 1983.
- [10] A. S. D. Wang, "Fracture Mechanics of Sub-Laminar Cracks in Composite Laminates," Proc. 1983 AGARD Specialist Meeting on Defects in Composite Materials, London (1983). Also in Composite Technology Review, Vol. 6, (1984), pp. 45-62.
- [11] F. W. Crossman, W. J. Warren and A. S. D. Wang, "Influence of Ply Thickness on Damage Accumulation and Final Failure," in Advances in Aerospace Structures, Materials and Dynamics, ASME AD-06, 1983, p. 215.
- [12] A. S. D. Wang, N. N. Kishore and C. A. Li, "On Crack Development in Graphite-Epoxy [0/90]_ns Laminates Under Uniaxial Tension," Paper to be presented at International Symposium on Composites: Materials and Engineering, University of Delaware, September 1984.

(2) Papers Presented in National and International Conferences:

- [1] "An Energy Method for Multiple Transverse Cracks in Graphite Epoxy Laminates," presented at ASME Winter Annual Meeting, New York, December 1979.
- [2] "Growth Mechanisms of Transverse Cracks and Ply Delamination in Composite Materials," presented at International Conference on Composite Materials-III, Paris, August 1980.
- [3] "The Dependence of Transverse Cracking and Delamination on Ply Thickness in Graphite Epoxy Laminates," presented at ASTM Symposium on Damages in Composite Materials, Bal Harbon, December 1980.
- [4] "The Fracture Mechanics of Transverse Cracking and Delamination in Composites," presented at 2nd USA-USSR Symposium on Fracture of Composite Materials, Lehigh University, August 1981.
- [5] "On Mixed-Mode Fracture in Off-Axis Unidirectional Graphite Epoxy Composites," presented at International Conference on Composite Materials-IV, Tokyo, October 1982.
- [6] "Fracture Mechanics of Sublaminar Cracks in Composite Laminates," presented at AGARD Specialists Meeting on Defects in Composite Materials, London, May 1983.
- [7] "Interlaminar Stress Fields as Influenced by Interacting Flaws," presented at Symposium on NDE and Criticality of Defects in Composite Laminates, Philadelphia, May 1983.
- [8] "Effects of Curing Stresses on Intralaminar Cracking in Graphite Epoxy Laminates," presented at 20th Society of Engineering Science Annual Meeting, University of Delaware, August 1983.
- [9] "A Stochastic Model for the Growth of Matrix Cracks in Composite Laminates," presented at ASME Winter Annual Meeting, Boston, November 1983.
- [10] "Influence of Ply Thickness on Damage Accumulation and Final Failure," presented at ASME Winter Annual Meeting, Boston, November 1983.
- [11] "On Crack Development in Graphite Epoxy [0₂/90₈] Laminates Under Uniaxial Tension," to be presented at International Symposium on Composites: Materials and Engineering, University of Delaware, September 1984.
- [12] "3-D Stress Fields Near Several Interacting Matrix Cracks in Composite Laminates," to be presented at 21st Society of Engineering Science Annual Meeting, VPI & SU, October 1984.
- [13] "On Mathematical Modelling of Multiple Cracks in Composite Materials," to be presented at International Symposium on Fundamental Questions and Critical Experiments on Fatigue, Dallas-Fort Worth, October 1984.

APPENDIX - B

FRACTURE MECHANICS OF SUBLAMINATE CRACKS
IN COMPOSITE LAMINATES*

A. S. D. Wang

Drexel University

Philadelphia, PA 19104

*Paper presented to 1983 NATO, AGARD Specialist Meeting
on Defects in Composite Materials, London, April, 1983.

Proceeding No. 355, pp. 15-1 to 15-19. (Also to appear
in Composite Technology Review, Vol. 6, 1984.

FRACTURE MECHANICS OF SUBLAMINATE CRACKS IN COMPOSITE LAMINATES

A. S. D. Wang

Drexel University

Philadelphia, PA. 19104

ABSTRACT

This paper presents an overview of a fracture mechanics approach to some of the most frequently encountered matrix-dominated, sub-laminate cracks in epoxy-based composite laminates. By "sub-laminate", it is meant that the cracks are internal to the laminate, generally invisible macroscopically; but are much larger in size than those microcracks considered in the realm of micromechanics. The origin of sub-laminate cracks is assumed to stem from the coalescence of natural material flaws (also microcracks) which occur under a certain favorable laminate stress condition. Thus, the modeling of the mechanisms of sub-laminate crack initiation and propagation is essentially mechanistic and probabilistic in nature. Some specific results from several analytical/experimental investigations using graphite-epoxy laminates are presented and discussed in this paper.

KEY WORDS. macroscopic analysis; fracture mechanics; transverse cracks; delamination; mechanistic modeling; stochastic simulations; sub-laminate cracks interaction; final failure mechanisms; failure modes sequence.

INTRODUCTION

Failure mechanisms in structural composite laminates have been viewed at several dimensional levels. Consider, for instance, the curved laminated panel shown in Figure 1(a). Failure of this structural component may be caused by a loss of the global stiffness when the applied load reaches a certain critical value. To describe analytically the associated failure mechanisms and hence to determine the critical load, structural mechanics methods such as buckling and post-buckling theories are employed, which relate the change of the structural geometry to the applied load. In this type of analysis, the stiffness of the laminated panel and the kinematics of its displacements are among the most predominant factors.

On the other hand, the same panel may fail due to a loss of strength at a local defect; for example, at a bolt-hole, Figure 1(b). In this case, rupture of material will begin at the hole and may propagate into a large crack whenever a certain load condition is reached. But in order to define the conditions for rupture initiation and propagation, a knowledge of the actual stress field around the hole, and the physical mechanisms of the material rupture process is essential. To this end, it will be necessary to focus further on the local defect area at a much smaller dimensional level. As illustrated in Figure 1(c), for instance, the lamination details of the panel, such as layer interfaces and the stacking sequence are now identifiable. Consequently, quantities of size comparable to the layer thickness become important; the influence of a local interface defect, a transverse crack, a fiber split in the 0-layer, etc. are new factors to be considered. For it is believed that the development of rupture around the hole is precipitated by these sub-laminate cracking activities.

Any failure analysis performed at this dimensional level must address the individual mechanisms of the various sub-laminate cracks as well as their interaction and coalescence mechanisms as they occur simultaneously and/or sequentially.

It is well known that the formation and propagation mechanisms of a crack are governed by the conditions that exist in the close vicinity of the crack front. In the case of the sub-laminate cracks mentioned above, further focusing of the crack front region will reveal the microstructure of the composite system, Figure 1(d). Here, a clear distinction can be made between the fiber and the matrix phases of the material. At this dimensional scale, one also finds a random distribution of material microflaws, be it voids, broken fibers, matrix crack, debonded fiber-matrix interfaces, just to mention a few, see Figure 1(e).

Although the inherent microflaws are small in size, usually on the order of the fiber diameter, they may behave as local stress risers under the applied load. When a certain local condition is reached, the microflaws interact and coalesce to form an actual crack, much larger in size and identifiable at the sub-laminate level. Hence, a proper analysis of the mechanisms must be capable of delineating the individual behavior of the various types of stress risers, and their interactions when one is located near another. All these will depend profoundly on the probabilistic nature of the microflaws in terms of their size, location and density distributions.

The physical process of material failure as portrayed in the preceding discussions is seen to span a wide range of dimensions. Though the entire process is essentially one continuous event, failure analysis could

be conducted only within isolated dimensional regimes. As illustrated in Figure 1, the entire dimensional spectrum is separated roughly into three analysis regimes; namely the structural mechanics, the macromechanics and the micromechanics regimes. Within each analysis regime, the material failure process involves a distinct set of material and geometrical parameters.

Analytical and experimental treatments on laminate failure at the structural mechanics level have generally been approached by using the classical lamination theory (see [1]). Stiffness-predominant structural responses such as panel buckling and post-buckling have been successfully analyzed [2]. The effect of local material damage (e.g. from a bolt-hole, a delamination caused by impact, etc.) upon the global response can also be evaluated [3]. But, a more detailed description about the damage formation and propagation mechanisms always required separate treatment.

For a class of epoxy-based composite laminates, e.g. graphite-epoxy systems, material damage mechanisms around a bolt-hole or near the tip of a line-notch have been modeled by an empirical formulae which is derived from the classical fracture mechanics for structural metals [4-6]. Essentially, the notched laminate is regarded as a 2-dimensional body, and failure from the notch is assumed in the form of a line crack propagation. In order for the fracture formula to correlate with a body of experimental data, the notch size parameter must be adjusted to include an empirically defined "intense energy region" at the crack tip. Thus, together with the laminate's fracture toughness (K_c or G_c), yet to be fitted experimentally, the model consists of two disposable parameters which can be adjusted only when a suitable set of test data is given.

Clearly, the approach is totally empirical in nature. The term "intense energy region" is in fact a gross representation of local sub-laminate cracking activities at the ply level. Consequently, both the "intense energy region" and the "fracture toughness" parameters may differ from one lamination to another lamination. It would be ideal, therefore, to be able to perform failure analysis at the ply level so as to understand how sub-laminate cracks occur, and how they lead to damage development near the bolt-hole or the line-notch in the laminate.

Early studies on failure in fiber composite systems have dealt mainly mechanisms in the micromechanics regime. For instance, a considerable amount of theoretical and experimental treatments was given to the subject of fiber-matrix interface mechanics [7 -10]. Fracture models for such microflaws as those depicted in Figure 1(e) have been characterized in terms of energy absorption processes [11]. Although modeling the various types of microflaws is essential for an understanding of the strengthening mechanics of the composite system, these "micro" models have not yet provided a further analysis on the mutual interaction and the coalescence mechanisms amongst the microflaws. Indeed, it would be ideal again to have a unified model which not only accounts for the mechanistic failure behavior but also the statistic nature of the microflaws. Such an analysis can then bring the knowledge about microcrack mechanisms to the regime of macromechanics.

Several mechanistic/probabilistic failure models have been developed in the past. Zweben and Rosen [12] studied, for example, the tensile strength properties of unidirectional composites by assuming the microflaws in the form of local broken fibers. Though the basic concept of material flaw distribution can theoretically be extended to multi-

directional laminated systems, the complexity in geometry as well as the multiplicity in the sub-laminate cracking modes make this type of approach so far unproductive.

In recent years, increased attention has been given to fracture modeling within the frame work of ply-elasticity and the theory of the classical fracture mechanics. At this level of analysis, the individual material plies in the laminate are replaced by homogeneous and anisotropic bodies, where no distinction of the fiber and the matrix phases need be made. Specifically, the stiffness property of the material ply is represented by a set of "effective" constants to be determined experimentally; while the strength property is governed by a distribution of material flaws whose fracture events lead to multiple failures at the sub-laminate level. Since by a "homogeneous" approximation the true identities of the inherent material flaws are lost, their effects on the formation and propagation of multiple cracks are retained through an introduction of a new concept; namely, the concept of "effective" material flaw distribution, as a basic ply property.

As it will be discussed in more detail later in this paper, the macroscopic view point incorporating the effective flaw concept enables a rational formulation of a unified fracture model which is applicable to a class of sub-laminate cracking phenomena observed in brittle matrix systems, such as graphite-epoxy composites.

Early investigations on composite failure, notably by Corten [13], Wu [14], Kanninen, et. al. [15], have already articulated the viability of such an approach. Advances have since been made, due largely to the ever-expanding computational capabilities and the ever-revealing damage inspection techniques. These modern facilities have provided a means for more rational correlations between experiments and analyses.

In a series of papers [16 - 22], Wang, Crossman, et. al. developed a unified energy model within the context of macromechanics. It describes the growth mechanisms in a class of matrix-predominant sub-laminate cracks. The specific cracks considered included interlaminar (delamination) and intralaminar(transverse) crackings. These sub-laminate failure modes have been found most prevalent in graphite-epoxy laminates.

The main objective of this paper is to give an overview on the theoretical development, and to present some of their major results.

FRACTURE CONSIDERATIONS IN MACROMECHANICS

The energy model developed by Wang and Crossman is formulated on the energy release rate concept of the linear elastic fracture mechanics (LEFM). All variables in the model are defined within the context of the macromechanics. Since fibrous composites possess some unique characteristics, special considerations had to be given to defining some of the variables.

Application of the Griffith Criterion

The essence of the LEFM is that material failure is not defined from the stand-point of strength as a constant material property. Rather, it is determined by an analysis of the kinetics of the actual process of fracture propagation. The classical result of Griffith [23] pertained to an elastic plate which is uniformly stretched in one direction by σ . The plate has a through crack of size $2a$, orientated normal to the direction of σ . The length of the crack is assumed small but finite; and, the material is homogeneous and isotropic. Griffith postulated that at the instance of crack extension, a loss of the stored elastic strain energy U results; and this energy is assumed to be converted entirely into the

surface energy of the crack. A balance of energy during a stable crack extension leads to the criterion

$$\frac{\partial U}{\partial a} = \frac{\partial S}{\partial a} \quad (1)$$

Equation (1) defines the general condition under which the existing crack begins self-similar propagation in the direction of the crack.

For the plate problem, the critical stress at the instance of crack extension can be derived from (1), giving

$$\sigma_c = \left(\frac{2E\gamma}{\pi a} \right)^{1/2} \quad (2)$$

where γ is the free surface energy density of the material.

When applied to engineering problems, the Griffith theory is often modified for practical considerations. For instance, Equation (2) becomes unbounded as $a \rightarrow 0$. Certainly, no real material can sustain an infinite stress. This limitation, however, can be circumvented by invoking the existence of material flaws. That is to assume for the material some characteristic distribution of flaws; the worst of which, having a size of $2a_0$, acts like a real crack. It then determines a finite critical stress according to Equation (2).

Of course, flaws do exist in real materials, especially in fibrous composite systems. But the physical identity is lost at the dimensional level where the analysis is performed. The quantity a_0 can be defined only empirically as an effective material property. As it will be discussed later, the quantity a_0 is in fact a random variable, representing the size distribution of the material flaws.

Another practical consideration is related to the definition of γ , the free surface energy density of the material. For crack in brittle material such as glass, then γ is as defined. For most other engineering materials, crack extension is found to associate a certain degree of inelastic deformation near the crack-tip region. Furthermore, the crack extension path, or the crack surface, shows a certain degree of ruggedness, depending on the heterogeneity of the material viewed at a micro-scale. Early studies by Irwin [24], Orowan [25] and others on structural metals considered the right-hand side of Equation (1) the irreversible work required to create a unit crack surface area. Hence, the quantity γ can be interpreted as the energy dissipated in the crack-tip region during crack extension. Clearly, γ will then depend on the inelasticity as well as the microscopic heterogeneity of the material locally (near the crack-tip). It, therefore, must also be regarded as an intrinsic property of the material to be defined at the macromechanics level. Conceivably, γ has to be an averaged value over a relatively large crack surface area for fibrous composites in order for it to be a macroscopic property.

These considerations are of fundamental importance when a crack-like failure is modeled at the macroscopic dimensional level. For only in this context can a macroscopic fracture model be developed along the rational arguments of the classical fracture mechanics.

In common practice, the right-hand side of Equation (1) is replaced by G_c ($= 2\gamma$), known as the critical energy release rate of the material. The left-hand side is a function of the applied load, the geometry of the body and the size of the crack. Thus, for a crack propagating in its own direction, the Griffith criterion is expressed commonly as,

$$G(\sigma, a) = G_c \quad (3)$$

In view of the foregoing discussions, a successful model for some of the sub-laminate cracks may be formulated if a judicious use of Equation (3) is made. But, unlike in the classical fracture problems where the crack length a and the fracture toughness G_c are usually well defined, these two quantities are generally difficult to determine for fibrous composites. In addition, calculation of the function $G(\sigma, a)$ for a crack propagating in layered media can also be mathematically complicated; invariably, some numerical procedure is required. All these aspects will be further elaborated in the following.

The Concept of Effective Flaw Distribution.

In laminate stress analysis, the fundamental approach has been the so-called ply-elasticity theory [1]. The theory pertains primarily to laminates that are composed of unidirectional plies pressed together with each ply orientated in some designed direction. The individual plies, though consisting fiber and matrix phases, are assumed macroscopically homogeneous having uniform properties. This assumption enables characterization of the unidirectional ply by two sets of material constants. The first set consists of the ply deformation property; and the second set is associated with the ply strength property. The stiffness matrix C_{ij} in the generalized Hooke's law, and the strength constants in the quadratic failure criterion are practical examples:

$$\sigma_i = C_{ij} \epsilon_j \quad i, j = 1, 6 \quad (4)$$

$$F_{ij} \sigma_i \sigma_j + F_j \sigma_j = 1 \quad i, j = 1, 6$$

It is noted that the constants C_{1j} , F_{1j} , etc. are "uniform" properties of the ply material. And, in particular, the quadratic failure criterion governs only the first failure of the ply. But, in a laminate, multiple failures in a single ply can occur at a range of ply stress magnitudes. Thus, the ply failure property cannot be assumed uniform.

The conceptual argument for sub-laminate cracks is that randomly distributed material flaws exist in the microstructures of the unidirectional ply; the flaw distributional characteristics are inherent to the basic material system used and, perhaps also to the laminate's fabrication processes. But, within the frame work of ply-elasticity, the true identity of the inherent material flaws cannot be practically determined. The alternative is, therefore, the concept of "effective" flaws.

This concept assumes that a characteristic distribution of "effective" flaws can be determined for a given representative volume of the unidirectional ply; each of the flaws can act like a small crack in the same sense as the Griffith crack. So, individually, the behavior of the flaw can be described by the criterion (3). Collectively, they form the source of the observed sub-laminate cracks.

To define the effective flaw distribution, let a be the size of the flaw, and S be the relative position between two neighboring flaws. Both a and S are generally random variables. The probability density functions $f(a)$ and $f(S)$ then define completely the effective flaw distribution.

For each effective flaw, the size a , the geometry and location relative to the layering structure of the laminate are defined. It remains then to suitably calculate the available energy release rate function $G(\sigma, a)$ under the given laminate load σ . For this, one uses the theory of ply-elasticity and the methods available in fracture mechanics.

Accordingly, the development of the fracture model for sub-laminate cracks rests upon the calculation of $G(\sigma, a)$ and the physical measurement of G_c .

The Calculation of $G(\sigma, a)$

In the theory of the LEFM, the singular stress field near a crack tip in a homogeneous, isotropic elastic body is represented by analytical functions in the theory of complex variables [26]. The near-field stresses are obtained for three particular modes of crack extension. These are known as the opening mode (I), the sliding mode (II) and the anti-plane shearing mode (III). For each mode, the stresses are expressed in terms of the associated stress intensity factor K [27]; and consequently, the associated $G(\sigma, a)$ is computed in terms of K . Since the relation between K and G is one-to-one, Equation (3) reduces to the form

$$K(\sigma, a) = K_c$$

Similar relations between K and G for orthotropic media having a crack orientated along one of the major axes can also be obtained [28]. But the analytical solutions for the singular stress field often require tedious mathematical derivations.

Direct solution methods for $G(\sigma, a)$ have been available; among them are the well-known J-integral method [29, 30] and the method of virtual crack closure technique by Irwin [31].

Irwin [31] observed that the elastic strain energy released during a virtual crack extension Δa is equal to the work done in closing it again. The closing of Δa provides the solution for the surface tractions $\bar{\sigma}$

over Δa . The crack-tip energy release rate is then represented by

$$G = \lim_{\Delta a \rightarrow 0} \frac{1}{2\Delta a} \int_0^{\Delta a} (\bar{\sigma} \cdot \Delta \bar{u}) da \quad (5)$$

where $\Delta \bar{u}$ is the crack opening displacement vector over Δa .

If the crack extension involves all three modes (I, II, III), the vector product in Equation (5) will give a sum of three scalars, associated respectively with G_I , G_{II} , and G_{III} .

The virtual crack-closure representation is particularly adaptive to machine computations. Rybicki and Kanninen [32] suggested a 2-dimensional finite element technique to evaluate G for a line crack in a plane. The crack-tip stress vector $\bar{\sigma}$ and the displacement vector $\Delta \bar{u}$ in Equation (5) are approximated by the nodal forces and displacements respectively, in a finite element representation (for detail, see [18]).

Wang and Crossman applied this technique in a generalized plane strain finite element routine [33], which can simulate a line crack propagation in the 2-dimensional cross-section of a laminate. Since a general laminate under load may suffer cross-sectional warping, the routine actually computes 3-dimensional stresses and displacements [33].

If a laminate is subjected to the far-field stress σ_0 and a sub-laminate crack is to be simulated, the crack-tip energy release rate can be expressed in the general form

$$G_e = C_e (a/t) \cdot t \cdot (\sigma_0 / E_0)^2 \quad (6)$$

where E_0 is laminate stiffness in σ_0 direction, and t is a characteristic length, taken usually as the thickness of the ply. C_e is a function dependent only on the crack size a , which is routinely generated for a

given type of crack in a given laminate.

Similarly, if the laminate is subjected to a uniform temperature load ΔT , and if a thermally induced crack opening results; then the associated energy release rate at the crack tip can be expressed by,

$$G_T = C_T(a/t) \cdot t \cdot (\Delta T)^2 \quad (7)$$

Generally, ΔT is characterized to represent the temperature load due to laminate curing; but it can include subsequent environmental (e.g. humidity) relaxation effects before mechanical load is applied [22]. The combined temperature and mechanical load effects on the stress field are linearly additive; and the total available energy release rate is expressed as,

$$G = [(C_e)^{1/2} \cdot e_o + (C_T)^{1/2} \cdot \Delta T]^2 \cdot t \quad (8)$$

where e_o is the far-field strain ($= \sigma_o/E_o$).

It is seen that the finite element technique is extremely versatile, and can be efficiently executed for simulating complicated sub-laminate cracking such as delamination.

Nonetheless, the accuracy of the technique has been a subject of concern of many analysts, because of its approximate nature in representing a mathematically singular stress field. As has been demonstrated by Raju and Crews [34], Spilker and Chou [35], and Wang and Choi [36], the finite element stress solutions could lose significant accuracy in the small vicinity of the singular point; the region in which the stress becomes inaccurate is generally much smaller than, say, a fiber diameter, due to the very nature of the singularity [36]. However, it can also be demonstrated that the stresses in that small region do not contribute significantly to the crack opening energy release rate, especially for a crack size much larger in proportion.

Figure 2 shows a close comparison between the finite element computed G and the elasticity solution counter-part, for a transverse crack located in the mid-layer of a 3-layer laminate (see inset of Figure 2). The extreme layers are designated as material 1 and the mid-layer as material 2. Both were assumed homogeneous and isotropic materials. The exact solution for G as a function of the crack size a is given by Isida [37], using complex stress potentials; while the finite element solution is computed using a rather coarse constant-strain, triangular element mesh. It is seen that the finite element solution for $G(a)$ compares well with the exact solution. To obtain more accurate stresses near the crack tip, however, one may need to deploy a finer element mesh, a singular element or a higher-order element formulation [38]. But, such extreme measures are often unnecessary for the computation of G .

The Evaluation of G_c

When fracture occurs in the material, the energy required in the process is expected to depend on the morphology of the fracture surface, which must be examined at the microscale. Fibrous composites are known to possess complex fracture surface details, even in matrix-predominant cracks. The observed delamination surfaces in graphite-epoxy composites show, for instance, a considerable raggedness because the crack must pass around the reinforcing fibers. But, at the macroscopic level, the crack surface details are "smoothed out"; and their effects are reflected in the measured quantity of the fracture resistance G_c .

For this reason, G_c measured for some matrix-predominant fractures in epoxy-based composites has been found to depend on the direction of fracture propagation. Cullen [39] and Williams [40] considered two different

cases of delamination as illustrated in Figure 3. The first case is $0^\circ/0^\circ$ delamination in which the crack path is in the fiber direction, while the second is $90^\circ/90^\circ$ delamination where the crack path is transverse to the fiber direction. The experiments were performed using a graphite-epoxy unidirectional laminate, subjected to mode-I cracking condition. They found that the microscopic morphology of the $90^\circ/90^\circ$ delamination surface exhibited considerably more raggedness than the $0^\circ/0^\circ$ delamination surface. This resulted in marked differences for the measured G_c . Note that these two fracture events occur essentially in the same interface when viewed macroscopically. Yet, the respective G_c values can differ greatly depending on the direction of the crack propagation.

Hence, when the Griffith formula (3) is applied for cracks in composites, the term G_c requires a precise qualification. Similarly, when a test method is devised to measure G_c , it is also necessary to consider the dimensional and directional characteristics of the measured data.

Mode-I interlaminar G_{Ic} . A commonly used test method to determine interlaminar G_{Ic} is the splitting cantilever beam. Cullen [39] and Wilkins [41] have used this method to determine the interlaminar G_{Ic} when the crack is propagating in the direction of the fibers ($0^\circ/0^\circ$ delamination). For some graphite-epoxy systems, they found that G_{Ic} at room temperature is about 0.85 lb/in, or 130 J/m^2 . This value is about twice the G_{Ic} measured for pure epoxy resin. Williams [40] used a compact specimen which simulates roughly a $90^\circ/90^\circ$ delamination. He found, for the same material system, a G_{Ic} value of 1.3 lb/in, about three times that of the pure resin. Williams explained that the fracture surface in his specimens showed fiber breakage as well as fractured epoxy debris; this had resulted in a higher value for G_{Ic} than that found for $0^\circ/0^\circ$ delamination by Cullen [39].

In another paper by Wilkins, et. al. [42], it is reported that G_{Ic} in delamination of $0^\circ/90^\circ$ interface is also higher than that of $0^\circ/0^\circ$ delamination. All these findings indicate the directional dependent nature of G_{Ic} .

Mixed-mode interlaminar $G_{(I, II)c}$. The splitting cantilever beam method has also been used in mixed-mode cracking experiment. In this case, it is necessary to apply different loads at the top and the bottom parts of the split so as to create both an opening (I) and a sliding (II) action. Vanderkley [43] and Wilkins [41] conducted tests on the same graphite-epoxy system (used for their mode-I tests), and found the total energy release rate $G_{(I, II)c} = G_{Ic} + G_{IIc}$ which exhibited a strong dependence on the G_{II}/G_I ratio.

This phenomenon is not uncommon in mixed-mode fracture. Similar observations were reported for brittle metals as well as pure epoxy resins [44]. It is, perhaps, more pronounced in fibrous composites. Generally, it is thought that the increased fracture resistance is the result of excessive matrix yielding under shear, as well as crack-closure friction due to the sliding action.

In an experiment on double-notched off-axis unidirectional graphite-epoxy laminates, Wang, et. al. [45] measured the mixed-mode $G_{(I, II)c}$ as a continuous function of G_{II}/G_I , see Figure 4. It is seen that $G_{(I, II)c}$ is monotonically increasing with G_{II}/G_I .

But in the same experiment, it shows also that the opening part G_{Ic} remains roughly independent of G_{II}/G_I . This suggests that mixed-mode crack is essentially controlled by mode-I. Of course, such a suggestion is only temporary; more study is needed to fully understand the true nature of the mixed-mode crack mechanisms.

MECHANICS OF TRANSVERSE CRACKS

Physical Mechanisms at the Macroscale

Transverse cracks are found in epoxy-based laminates, even at a low loading level. When viewed at the macroscopic scale, the cracking action is simply a sudden separation of fibers by breaking the epoxy bond. To illustrate, consider as an example a $[0/90]_s$ type laminate such as shown by the inset in Figure 2. There, material 1 is the 0° -layer and material 2 is the 90° -layer. Under the far-field tensile load, material 2 could suffer multiple transverse cracks. Generally, the sequence of events is as follows: A single crack forms first when the applied load reaches a certain critical value, which defines the "onset" of the events; as the applied load increases, more similar cracks are formed. If there is no other failure mode setting in at high load (e.g. 0° -rupture, delamination, etc.), the number of transverse cracks will continue increasing, until it reaches a saturation density.

Figure 5 shows a load-sequence x-radiographs taken for a $[0/90]_s$ graphite-epoxy laminate under ascending tensile load. Transverse cracks in the 90° -layer are seen to form in increasing numbers. From these photographs, a plot of crack density (e.g. cracks per inch of specimen length) versus the applied load can be obtained. Figure 6 shows a family of such experimental plots for a series of $[0/90_n/0]$ laminates, $n = 1, 2, 3, 4$.

Examination of the plots in Figure 6 reveals several interesting features. First, the onset load for the first transverse crack seems to be influenced profoundly by the 90° -layer thickness, especially when it is very thin. Take, for example, the case of $n = 1$ in Figure 6, the onset load is almost twice that of $n = 2$.

Secondly, the crack density also shows dependence on the same thickness factor. Generally, the laminate with thinner 90°-layer is capable of yielding a higher crack density. (But, for the case of $n = 1$, failure of 0°-layer at high load interrupted the development of more transverse cracks).

The 90°-layer thickness effect on transverse cracking was first documented experimentally by Bader, et. al. [46]. They attributed the effect to the constraining actions of the adjacent 0°-layers. Observing that a transverse crack can be no larger than the 90°-layer thickness, the energy release rate which drives the crack is thus limited by the same factor. It is the total strain energy trapped in the 90°-layer which determines the onset of the cracking, not the in-situ tensile stress.

As for the effect on crack density, it has been explained by the existence of a "shear-lag" zone at the transverse crack root [46 - 48]. That is an interlaminar shear stress is developed on the 0/90 interface where a transverse crack terminates. This shear stress is singular at the crack root, but decays exponentially a distance away [20]. Similarly, the in-situ tensile stress in the 90°-layer is nil at the transverse crack, but it regains its far-field value outside the shear-lag zone. Thus, ideally, any two adjacent cracks should be spaced by the shear-lag distance. Since this distance is proportional to the 90°-layer thickness [20], hence the observed thickness effect on crack density [46].

Although the shear-lag concept is ideally correct, the so-called "characteristic" spacing of transverse cracks does not occur exactly in practice, due to the random nature of material flaws. However, transverse cracks may cause other failure modes, such as delamination [21]. Failure modes interactions will be discussed later in this paper.

At the microscopic level, the mechanisms of a transverse crack are much more perplexing. For example, the exact kinematics of crack formation is not fully known. Post-test SEM examination of the crack surfaces generally gives a very ragged appearance; tiny epoxy debris and sometimes broken fibers are also seen [40]. Figure 7 shows an x-ray plane view of a $[+25/90_2]_s$ laminate after transverse cracking, left, and an edge-view micrograph on the right. It is seen that the transverse crack is practically a plane crack of a rectangular dimension, which is bounded by the width of the specimen and the 90° -layer thickness. There is no evidence to indicate that the crack formation is progressive in nature. In fact, all experiments tend to suggest a sudden dynamical formation.

This dynamical nature, though still conjectured, has been qualified by many who monitored the acoustics emitted during the crack formation (see, e.g. [49]).

While it is difficult to reduce these physically observed facts into a general law, they nevertheless provide the necessary rationale for the formation of an analytical model. In what follows, an energy formulation is presented, which describes the most essential observed characteristics of the transverse cracking phenomenon.

The Energy Formulation

For purpose of clarity, consider a $[0/90]_s$ type laminate, as shown in Figure 8. It will be assumed that, in the 90° -layer, the material has a random distribution of microflaws. The gross effects of the microflaws at the macroscopic scale are represented by a characteristic distribution of "effective" flaws which cannot be physically seen. But, under stress, these effective flaws are capable of propagating suddenly into transverse

cracks, which are physically real. The individual size of the effective flaws is denoted by $2a$; and any two adjacent flaws are spaced by a distance S , see Figure 8.

Given a unit length of the specimen, there is a probability density function $f(a)$, and a probability density function $f(S)$. For sake of no evidence to suggest otherwise, the two functions are assumed to take a form for normal distributions [50];

$$f(a) = \frac{1}{a\sqrt{2\pi}} \exp [-(a - \mu_a)^2/2\sigma_a^2] \quad (9)$$

$$f(S) = \frac{1}{S\sqrt{2\pi}} \exp [-(S - \mu_s)^2/2\sigma_s^2] \quad (10)$$

where μ and σ are the mean and the standard deviation of the respective distribution functions.

Among the effective flaws, the size of the "worst" one is denoted by $2a_o$. For definiteness, assume a_o the 99 percentile of $f(a)$. That is 99% of the flaws are smaller than $2a_o$.

Then, under the far-field load, say e_o , the "worst" flaw $2a_o$ will become the first transverse crack. The critical value for e_o at the onset is calculated by substituting Equation (8) into the Griffith criterion (3):

$$[(C_e)^{1/2} \cdot e_o + (C_T)^{1/2} \cdot \Delta T]^2 \cdot t = G_c \quad (11)$$

where C_e and C_T are evaluated at $a = a_o$.

As has been detailed earlier, the energy release rate coefficients C_e and C_T are generated numerically by the finite element crack-closure routine, given the geometry and material moduli of the laminas. Thus, in Equation (11), all quantities except e_o will be given: ΔT is the tem-

perature load due to cooling and possibly also environmental relaxation; t is a characteristic length (thickness of one ply) and G_c is measured experimentally simulating mode-I $90^\circ/90^\circ$ delamination (see Figure 3-b).

Now, the difficulty rests upon the choice of a_0 , or for the same matter, the choice of μ_a and σ_a in the distribution functions in (9).

Clearly, $2a_0$ must be smaller than the 90° -layer thickness. But the latter can be made arbitrarily large. Hence, a finite bound on a_0 exists even if the 90° -layer thickness is unbounded.

As an example, consider the experimental results reported in [21]. The tensile strength of T300/934 $[90_8]$ laminates averaged $\sigma_u \sim 7000$ psi. Assume that the "largest" effective flaw in the $[90_8]$ laminate has a size $2a_0$ (parallel to the fiber); this flaw will determine the laminate's tensile strength given by the Griffith formula (2). From which one obtains

$$a_0 = G_c E / \pi \sigma_u^2 \quad (12)$$

With $E = 1.7 \times 10^6$ psi and $G_c = 0.9$ lb/in for $0^\circ/0^\circ$ mode-I delamination, Equation (12) determines $a_0 \sim 0.01$ ", or about 2 times the ply thickness of the T300/934 systems.

It may thus be inferred that the largest flaw in an unbounded 90° laminate (or in a $[0/90_n]_s$ type laminate with $n \gg 2$) should be no greater than $a_0 \sim 0.01$ ". Indeed, in several experimental correlations conducted by Wang and Crossman [19, 20, 21], using the same material system, a_0 is found in the order of 0.0075 ", or 1.5 times the ply thickness.

Numerical Examples by Monte-Carlo Simulation

In what follows, the transverse cracking phenomenon will be simulated numerically by the so-called Monte-Carlo random search technique. The

considered laminates are in the form $[0_2/90_n]_s$, $n = 1, 2$ and 3 . The material system is the AS-3501-06 graphite-epoxy system (for the material moduli, see [51]). The nominal ply thickness of this system is $0.0052''$.

In order to define the parameters μ and σ in the $f(a)$ and $f(S)$ distribution functions, the following values are chosen for the laminates $n = 2$ and 3 :

$$\mu_a = 0.0036'', \sigma_a = 0.0013'' \quad (13)$$

$$\mu_s = 0.0125'', \sigma_s = 0.0046'' \quad (14)$$

These are chosen to reflect the fact that a_o , being over 99% of $f(a)$, may take a value (see [50]),

$$a_o = \mu_a + 3\sigma_a \sim 0.0075'' \quad (15)$$

and that for $\mu_s = 0.0125''$ it implies 80 effective flaws to the inch. The choice of the standard deviations is a matter of adjusting to the actual data scatter [51].

As for the laminates of $n = 1$, the thickness of the 90° -layer is only $0.0104''$, or $a_o < 0.0052''$. For this case, the choice of μ_a and σ_a are as follows:

$$\mu_a = 0.0021'', \sigma_a = 0.00075'' \quad (16)$$

so that

$$a_o = \mu_a + 3\sigma_a \sim 0.0044'' \quad (17)$$

The choice of the spacing parameters remains the same for $n = 1$.

The Monte-Carlo simulation procedures start with the generation of a set of N ($= 80$) flaws whose random sizes and spacings are represented by the respective density functions (9) and (10). This is done by generating first a set of N random values in the interval $(0,1)$. Then, by equating the cumulative function of $f(a)$ to each of the random values, a random set $\{a_i\}$, $i = 1, N$ is computed. Among the values in $\{a_i\}$, the probability of the largest to be equal or greater than a_0 as defined in (15) or (17) is about 99%.

Similarly, a random set $\{S_i\}$, $i = 1, (N - 1)$, is also generated by the random number scheme. S_i is then assigned to be the spacing between the i th and the $(i + 1)$ th flaws.

Thus, a computer research follows, which determines the flaw most likely to become a transverse crack. The first to occur, clearly, is the worst flaw in the $\{a_i\}$ set, and the corresponding applied load for the onset of the first crack is then determined using Equation (11).

After the first crack is formed, another flaw in the $\{a_i\}$ set will become a crack at a slightly higher load. But this flaw is located at a random distance from the first crack. And the presence of the physical (real) crack has a stress reducing effect on the rest of the flaws. Thus, if the second flaw to become a crack is located outside the shear-lag zone, it will not feel the presence of the first crack; and hence, its available energy release rate at the instant of cracking is given by $G_0(\sigma, a)$, the same as in Equation (8).

On the other hand, if the second flaw is located inside the shear-lag zone, then the available energy release rate is reduced by a factor de-

pending on its distance from the first crack.

Generally, for the flaw to become the k th crack, one must search to the left and to the right for the nearest cracks. If so, the energy release rate at the instance of the k th crack is given by

$$G_k(\sigma, a) = R(S_l) G_o(\sigma, a) R(S_r) \quad (18)$$

where S_l is the distance to the left crack, S_r the distance to the right crack.

In Equation (18), $R(S)$ is the energy rate retention factor which is generated by the finite element routine for a flaw of $2a$ ($< 2a_o$) and is placed at varying distance S from a transverse crack, see Figure 9.

For the laminate family $[0_2/90_n]_s$, a single $R(S)$ curve can be generated if expressed in terms of S/nt , t being the thickness of one 90° -ply, see Figure 9. Note that 100% energy rate retention is expected beyond $S = 9nt$; the latter is actually the size of the shear-lag zone [19].

The applied load, corresponding to the k th crack is determined from

$$G_k(\sigma, a) = G_c \quad (19)$$

The search essentially simulates the cracking process as it would occur naturally. Each random simulation represents an actual test case; and repeated simulations represent actual tests on replicas. Table A illustrates the flow-chart for the Monte-Carlo simulation.

Figures 10, 11, and 12 show the simulated crack-density versus load plots for respectively, $[0_2/90]_s$, $[0_2/90_2]$ and $[0_2/90_3]$ laminates. In the simulations, the quantities appearing in Equation (11) are assigned as follows:

$$\Delta T = 225^{\circ}\text{F}, t = 0.0052", G_c = 1.3 \text{ lb/in} \quad (20)$$

The shaded band in each of these plots is the corresponding experimental data band from 4 test specimens. These test data were reported earlier in Reference [52]; and the details for the simulation computer routine are reported in Reference [51].

MECHANICS OF FREE EDGE DELAMINATION

The Classical Free-Edge Problem

The free edge delamination problem has attracted increased research interest ever since the advent of composite laminates. The reason is that delamination is one of the most damaging sub-laminate failure modes. Generally, it is a plane crack which forms along the laminate free edge and propagates inward along an interface of two adjacent layers.

Figure 13 shows an x-ray plane view of a $[\pm 45/0/90]_s$ graphite-epoxy laminate under uniaxial tension (left). Delamination is seen to occur along both edges of the laminate, with essentially uniform growth toward the center. An edge view of this crack is shown on the right, which indicated that the crack is basically contained inside the 90° -layer, not necessarily in any one given layer interface. Moreover, the cracked plane is quite zig-zagged along the length of the free edge.

Similar photographs, taken for a $[\pm 25/90_{1/2}]_s$ laminate after failure, are shown in Figure 14. Here, the edge crack is seen to have formed inside the 90° -layer, but branched to the $25/90$ interface as it propagated. The branch-out is due to the skewed cracks which occur in the 90° -layer ahead of the edge delamination front.

Note that both laminates have a 90° -layer; and they could suffer transverse cracking under the tensile load. But, because the thickness of the 90° -layer is thin, a high load is required for transverse cracking according to the energy theory presented earlier. Instead, in this case, edge delamination is induced as the first event of sub-laminate failure.

Analytical studies of the free edge delamination problem have originated from the much celebrated work of Pipes and Pagano [53], who formulated and computed the boundary-layer interlaminar stress solutions for a long symmetric laminate under tension. The formulation is based on the macroscopic ply-elasticity theory, which regards the material layers as individually homogeneous media; material and geometrical discontinuities exist only across the layer interfaces.

Generally, the free edge stress field is three-dimensional, and is singular at the intersection of the free edge with a layer interface [36]. Hence, interface delamination is caused by the highly concentrated edge stresses, especially the interlaminar normal stress σ_z .

In a series of tensile strength tests, Bjeletich, et. al. [54] examined the failure modes of six families of quasi-isotropic laminates by alternating the stacking sequence of the 0° , 90° and $\pm 45^\circ$ layers. Edge stress analysis indicated a compressive σ_z along the free edge of the $[0/90/\pm 45]_s$ laminate, while a tensile σ_z for the $[\pm 45/0/90]_s$ laminate. The latter developed extensive delamination; and the growth of it had led to a much lowered tensile strength. Clearly, knowledge of the free-edge stresses can provide an explanation why delamination occur; but a quantitative prediction for its occurrence requires a more precisely defined criterion.

In a study on delamination for similar graphite-epoxy laminates, Rodini, et. al. [55] determined experimentally the critical tensile loads at the onset of free edge delamination in a $[\pm 45_n / 0_n / 90_n]_s$, $n = 1, 2, 3$ family. They found that the critical laminate tensile stress $\bar{\sigma}_x$ varied greatly with the value of n . Specifically, the critical $\bar{\sigma}_x$ decreases at the rate of about \sqrt{n} , even though an edge stress analysis yields identical $\bar{\sigma}_z$ for the same $\bar{\sigma}_x$ for all values of n .

Such a 90° -layer thickness dependent behavior is related to that found in the transverse cracking problems, suggesting the observed phenomenon is again fracture in nature.

The Energy Criterion

In the work of Wang and Crossman [18], it is assumed that material flaws exist randomly on any one of the interfaces between the material layers. Those flaws which are located within the free-edge stress zone form an "effective" flaw having a size a_0 at the instance of onset of delamination, see inset in Figure 15. Following the finite element crack-closure procedure by allowing virtual extension of a_0 along the layer interface, an energy release rate curve is generated, such as shown in Figure 15.

It is seen that the energy release rate G increases sharply with a , but reaches an asymptote at $a \sim a_m$. Generally, the value of a_m is about one-half the layer-thickness which contains the delamination [18]. Thus, the layer thickness affect the value of a_m , and also the value of G .

Expressing the computed energy release rate, Equation (6),

$$G(e_0, a) = [\sqrt{C_e(a)} e_0 + \sqrt{C_T(a)} \Delta T]^2 t \quad (21)$$

and applying the Griffith criterion (3) for the onset of delamination, one obtains the critical far-field strain,

$$(e_o)_{cr} = [\sqrt{G_c/t} + \sqrt{G_T(a)} \Delta T] / \sqrt{G_e(a)}, \quad a = a_o \quad (22)$$

Note that in (22), the thermal residual effect is also included. But such thermal effect on free edge delamination is generally minimal [56].

The problem comes down to two important questions; namely, what value is a_o , and which interface is likely to delaminate?

To answer the first question, recall the earlier discussions about a_o in unbounded 90° laminates. As inferred from the Griffith's criterion, a_o is in the order of 0.01", or 2 times the ply thickness for commercial graphite-epoxy systems. It is believed that a_o for delamination is at least of this magnitude if not larger, because of possible additional cutting flaws along the free edge. In any event, if a_m in Figure 15 is less than 2 times of the ply thickness, one simply uses $a = a_m$ and predicts from Equation (22) the minimum possible load for the onset of delamination. Thus

$$(e_o)_{cr} = [\sqrt{G_c/t} - \sqrt{G_T(a)} \Delta T] / \sqrt{G_e(a)}, \quad a = a_m \quad (23)$$

The answer to the second question, however, is complicated, if not inconcise. Consider as an example a $[90_2/0_2/\pm 45_2]_s$ under uniform compression. Interlaminar tensile σ_z is developed in this laminate and edge delamination is induced before global buckling, see Figure 16. A 3-dimensional through-thickness display of σ_z is shown in Figure 17(a). It is seen that the largest σ_z is located on the 45/-45 interface (in fact, this σ_z

is singular at the free edge). On the other hand, σ_z along the mid-plane ($z = 0$) is finite at the free edge. In addition, there is also a singular interlaminar shear stress τ_{xz} along the 45/-45 interface. Thus, the stress analysis suggests the 45/-45 interface as the most probable delamination site.

However, according to the energy release rate argument as well as the "effective" flaw hypothesis, one must calculate the energy release rate curves along all possible interfaces in order to determine the interface most energetically favorable for delamination.

The finite element crack-closure results of the $G(a)$ curves for this example problem is shown in Figure 17(b). Actually, for $a > t$, the mid-plane interface yields a much larger energy release rate than the 45/-45 interface. For $a < t$ however, the energy release rate on 45/-45 interface is slightly larger than that on the mid-plane. For all likelihood, the worst interface flaw size a_0 is larger than t ; and the most energetically favorable delamination site should be the mid-plane.

This conclusion is confirmed by experiments conducted by Wang and Slomiana [57], who also investigated compression-induced delamination in $[0_2/90_2/\pm 45_2]_s$ and $[0/90/0/90/\pm 45/\pm 45]_s$ laminates. In all cases, mid-plane and mode-I delamination was predicted and observed. Using the energy criterion of Equation (23), and setting $G_c = 1.0$ lb/in, the predicted minimum onset loads ($\bar{\sigma}_x$) for these laminates are tabulated below, along with the corresponding test data (average of 3 specimens each):

<u>Laminates</u>	<u>Predicted onset of $\bar{\sigma}_x$</u>	<u>Experimental Finding</u>
$[90_2/0_2/\pm 45_2]_s$	43.9 ksi	45.7 ksi
$[0_2/90_2/\pm 45_2]_s$	50.9	52.0
$[0/90/0/90/\pm 45/\pm 45]_s$	59.1	62.0

Edge Delamination and Transverse Cracking: Their Interactions

In the previous examples, edge delamination is the first and only sub-laminate failure mode before laminate buckling. The onset load for delamination is synonymous to the final laminate failure load. In most other cases, edge delamination and transverse cracking are often two competing failure modes, which interact each other through a complicated mechanisms.

Examine again the photomicrographs shown in Figures 13 and 14, where a $[\pm 45/0/90]_8$ and a $[\pm 25/90_{1/2}]_8$ laminates were loaded by axial tension. The thickness of the 90° -layer in both laminates is so small that transverse cracking is possible only at a high load. Instead, an edge delamination is induced as the first sub-laminate failure mode. Nonetheless, the stress field in the 90° -layer, which contains the delamination, appears to be extremely complex. The skewed cracks shown in Figure 14 are indicative of the complex stress field ahead of the delamination front. But, just how profoundly these secondary cracking events influence the delamination growth is far from known.

On the other hand, Figure 18(a) shows an x-ray plane view of a $[\pm 25/90_2]_8$ laminate after delamination. Actually, this laminate suffered first transverse cracks in the 90° -layer; subsequent edge delamination in the $25/90$ interface developed at a higher load. It is seen from the picture that delamination actually caused many more transverse cracks because of stress concentration along the curved delamination front. On the other hand, in the undelaminated portion only a few transverse cracks are in fact present. This phenomenon has repeatedly been observed in experiments [21]; but no serious account has been attempted to analytically model the mechanisms.

Law [56] assumed that when transverse cracks occur in the 90° -layer, the tensile modulus E_T and the Poisson ratio ν_{TL} of the 90° -layer both reduce to nearly zero. With reduced moduli in the 90° -layer, the overall laminate becomes energetically delamination prone in the 25/90 interface, resulting in a mixed-mode cracking (I, II). Some details of Law's analysis will be discussed later in a case study.

Figure 18(b) shown an x-ray plane view for a $[\pm 25/90_4]_s$ laminate soon after transverse cracking took place. In this case, scattered transverse cracks appeared first, which immediately caused delamination on both 25/90 interfaces in the area where they occurred. The delamination is, in fact, a combined effect stemming from the transverse crack-tip and free edge stress concentrations. Figure 19 illustrates this combined effect in an isometric view. The interface shear stress τ_{xz} , which is developed at the transverse crack root, tends to delaminate the 25/90 interface in the x-direction; and the interlaminar normal stress, σ_z , which is a free edge effect, tends to open up the same interface in the y-direction. The combined action gives rise to a mixed-mode, delta-shaped delamination. Evidence of this type of delamination can be found by examining Figure 18b.

Law [56] approximated the combined effect by first computing G_x for the x-direction delamination by a 2-dimensional analysis, and then by computing G_y for the y-direction as in the case of free edge delamination. Since both G_x and G_y are considered crack-driving forces, their vector sum is used to predict the onset of the delta-shaped delamination. Obviously, such an approximate approach is only tentative; the problem remains to be treated more rigorously by a truly 3-dimensional analysis simulating a "contoured" plane delamination. But, as it will be shown in the next section, Law's approach was at least qualitatively correct.

It is now apparent that sub-laminate cracking , especially delamination, are physically complicated even under simple tension. The energy method just presented should be applicable if the interaction mechanisms amongst different sub-laminate crack modes could be more accurately simulated. this topic, however, remains to be further developed.

An Experimental Case Study

An experimental case study on transverse cracking, free edge delamination and their mutual interaction was conducted by Crossman and Wang [21]. They chose a family of graphite-epoxy laminates (T300/934) in the form of $[+25/90_n]_s$. By varying the single parameter $n = 1/2, 1, 2, 3, 4, 6$ and 8 , they were able to control the occurrence of the various competing failure modes in the laminates when loaded in tension. Both x-radiography and microphotography were used to monitor the sub-laminate cracking development as a function of the applied load. For clarity, a graphical summary of their experimental findings is shown in Figure 20. For $n = 1/2$ and 1 , the laminates are classified as having a "thin" 90° -layer. Transverse cracking is suppressed due to the lack of sufficient strain energy stored in the 90° -layer. Hence, free edge delamination occurs as the first sub-laminate failure mode. For $n = 1/2$, a stable mode-I delamination is produced during the loading until final failure. For $n = 1$, however, transverse cracks are induced in the area of delamination. Because of these cracks, the delamination plane is often branched to the $25/90$ interface. This latter appearance is indicative of an interaction taking place between the two failure modes.

When $n = 2$ and 3 , the laminates are denoted as having "thick" 90° -layer. In both, transverse cracks occur first long before delamination. It may be thought that the onset of transverse cracking is an independent

event, while delamination is caused, at least partially, by the presence of the multiple transverse cracks. Indeed, the delamination plane in the case of $n = 2$ resembles that for $n = 1$; and the delamination plane in the $n = 3$ laminate is entirely in the 25/90 interface. Also, for $n = 3$, the growth of delamination becomes more rapid.

The laminates with "very thick" 90°-layer are those for $n = 4, 6$, and 8. In all cases transverse cracks occur first followed immediately by delta-shaped delaminations emanating from the transverse crack roots. These soon coalesce to form large scale 25/90 delamination, resulting in premature laminate failure.

Figure 21(a) summarizes the various onset loads $\bar{\epsilon}_x$ for each of the laminates (signified by the value of n). Since the laminates' longitudinal Young modulus \bar{E}_x varies with the value of n , it is sometimes more convenient to use the laminate tensile strain, $\bar{\epsilon}_x$, as a measure of the applied load. Note that except for $n = 1/2$ and 1, transverse cracking is the first sub-laminate failure event. Generally, growth of multiple cracks is fully developed, followed by interlayer delamination. However, as $n > 3$, the load-gap between the transverse cracking and delamination events grows closer. In fact for $n = 8$, these two events are closely linked to the final laminate failure.

Note also that except for $n = 1/2, 1$ and 2, onset of delamination and final failure are separated only by less than 5% of loading.

By means of the energy model presented earlier, Law [56] conducted a computer simulation of the transverse cracking and delamination processes in the $[+25/90_n]_s$ family. The numerical results are shown in Figure 21(b), which is superscribed on the experimental results shown in Figure 21(a).

Law has actually conducted four types of crack simulations: (a) onset of transverse cracking in the 90° -layers for all values of n ; (b) mid-plane ($z = 0$), mode-I delamination for $n = 1/2, 1, 2$, and 3 ; (c) $25/90$ interface delamination for $n = 2, 3$, and 4 (the 90° -layer is saturated with transverse cracks; and is represented by reduced moduli); and (d) transverse crack root/free edge combined delamination of the $25/90$ interface for $n = 3, 4, 6$ and 8 (as illustrated in Figure 19).

It is seen from Figure 21b that the predicted onset loads for transverse cracking agree well with the experiment, while the predicted delamination loads (represented by 3 curves) form an envelope to which the experimental points fall below. Although the predicted delamination loads for $n = 6$ and 8 are off considerably from the experimental points, the energy analysis seems to capture the physical mechanisms of these various failure modes; the analysis gives correctly the trend of the failure loads.

Final Failure Mechanisms

In the case study discussed above, the sub-laminate failure sequence is seen to lead to the final rupture of the laminate. It is generally thought that final failure is determined essentially by the strength of the load-carrying plies; i.e. in the case of the $[\pm 25/90_n]_s$ family, the ± 25 -plies should carry practically all the load. But, what determines the strength of the ± 25 -plies? And, is it adversely influenced by the sub-laminate cracking events that preceded the final laminate rupture? These questions relate to the final failure modes and their associated fracture mechanisms.

Crossman and Wang [58] conducted an extensive experimental investigation into the failure sequence of several families of laminates under uni-

axial tension. Some of his results may help to answer the above questions.

Consider first the effect of thickness of the load-carrying plies by examining the results in Table B.

It is noted that the final failure mode of $[\underline{+25}/\underline{+25}]_s$ is due simply to fiber breaking across the laminate, while the final failure mode of $[25_2/\underline{-25}_2]_s$ involves a major transverse crack in the center core (-25_4° -layer) followed by multiple fiber-splitting in the 25_2 -layer. In particular, there is no fiber breakage involved in the latter case, see Figure 22.

An energy analysis of the respective failure modes indicated that the transverse cracking mode in the $[\underline{+25}/\underline{+25}]_s$ is suppressed by the actual thickness of the 25° -layer; there is not enough strain energy to cause this failure mode at a lower load level. Hence, it forces a fiber breakage instead. However, by doubling the layer thickness, in the case of $[25_2/\underline{-25}_2]_s$, the transverse cracking mode emerges at a much lower load. The difference in the failure modes results in the difference in the applied ultimate loads.

Clearly, the strength of the so-called "load-carrying" plies in a laminate depends also on the particular fracture modes that cause failure. In the examples above, the ply-thickness factor is seen again to play a profound role in the final failure mechanisms.

When the respective load-carrying plies are laminated with a 90° -layer, such as in $[\underline{+25}/\underline{+25}/90_2]_s$ and $[25_2/\underline{-25}_2/90_2]_s$, transverse cracks in the 90° -layer and edge delamination are found to proceed any failure in the 25° -plies. From the results displayed in Table B, it is seen that the sub-laminate cracking events neither changed the failure mode of the $\underline{+25^\circ}$ -plies, nor decreased the final ultimate loading, although the presence of the 90° -layer in $[25_2/\underline{-25}_2/90_2]_s$ slightly increased the lami-

nate load-carrying capacity. The reason is that $[25_2/-25_2]_s$ has four (4) 25°-plies in the core, while $[25_2/-25_2/90_2]_s$ has only two (2) 25°-plies scattered by the presence of the 90°-layer in the core.

However, adverse effects of sub-laminate cracking on laminate final failure modes are seen from the test results displayed in Table C. Here, the failure modes in $[+0/90_2]_s$ and $[+0/90_8]_s$ are compared. Note that the 90°-layer thickness in the latter is exaggerated in order to separate widely the respective sub-laminate crack modes.

In the cases of $[0_2/90_8]_s$ and $[+25/90_8]_s$, the final failure mode in the load-carrying plies involves multiple fiber-splitting in 0° or 25° layers over the root of a 90°-layer transverse crack; see Figure 22. On the other hand, there is no fiber-splitting in the $[0_2/90_2]_s$ or the $[+25/90_2]_s$ laminates.

A three dimensional stress analysis by Wang, et.al.[59] has shown that over the 90°-layer transverse crack root, stress concentration can be amplified several times by the presence of the laminate free edge. In particular, the size of the stress concentration zone is proportional to the 90°-layer thickness; which explains why the considerable difference in the final loads between $[0_2/90_2]_s$ and $[0_2/90_8]_s$; and between $[+25/90_2]_s$ and $[+25/90_8]_s$, see Table C.

Fiber-splitting of the outer ply seems to trigger the final rupture of the $[0_2/90_8]_s$ and $[+25/90_8]_s$ laminates. The splitting mechanisms is due to the existence of the tensile stress normal to the fibers, which is magnified in amplitude by the 90°-layer transverse crack root.

Similar stress condition also exists in the $[+30/90_8]_s$ laminates. But in this case, the tensile stress (normal to +30°-fibers) is not large enough

to cause fiber splitting; see also Table C. As a result, the final failure modes for $[+30/90_2]_s$ and $[+30/90_8]_s$ all involve fiber breaking; and their final failure load are essentially the same. Thus, a mere increase in the angle from 25° to 30° changes the failure modes in $[+25/90_8]_s$ and $[+30/90_8]_s$.

Clearly, the final failure modes in the "load-carrying" plies can be influenced by nature from the sub-laminate cracking. Moreover, there are probably a host of other possible modes that are competing for dominance. The specific failure occurrence in a given laminate is generally determined by the lamination geometry as well as the intrinsic material properties. And, of course, there are always the statistical uncertainties in the "intrinsic" material properties.

CONCLUSIONS

This paper has attempted to give an overview of a fracture mechanics approach to some of the frequently observed sub-laminate cracks in epoxy-based composite laminates. The laminates discussed in the paper served mainly to illustrate how a certain failure sequence is developed and how the predictive model is constructed. They are certainly not the ones which may be used in practical design applications. The major objective here is to enable to see through the various fracture mechanisms and try to understand them; to this end, one often had to exaggerate the geometric parameters (e.g. the thickness of 90° -layer) in order to ascertain their full range of influence.

Indeed, the field of fracture in composites seems infinitely complex. Yet, numerous past and present investigators have toiled the field with many successes. And, new discoveries are being continuously made to further its advancement. The results reported in this paper represent but one effort to fill the dimensional span from micromechanics to structural mechanics in composite failure analysis.

Acknowledgments. Many results reported in this paper were obtained in collaboration with Drs. F. W. Crossman, G. E. Law, H. Miller and N. N. Kishore; and with Mr. C. Lei and Ms. M. Slomiana, graduate students at Drexel University. Financial supports have been provided by the U. S. Air Force Office of Scientific Research, Wright Aeronautical Laboratory and the Naval Air Development Center. The contents in this paper was presented at the AGARD Structural and Material Specialists Meetings; April, 1983; London.

REFERENCES

- [1] Tsai, S. W. and Hahn, H. T., "Introduction to Composite Materials," Technomics, 1980.
- [2] Starnes, J. H. and Rouse, M., "Post-Buckling and Failure Characteristics of Selected Flat Rectangular Graphite-Epoxy Plates Loaded in Compression," Proc. AIAA/ASME/ASCE/AHS, 22nd Structures, Structural Dynamics and Materials Conference, 1981.
- [3] Starnes, J. H. and Williams, J. G., "Failure Characteristics of Graphite-Epoxy Structural Components Loaded in Compression," NASA-TR-84552, 1982.
- [4] Waddoups, M. E., Eisenmann, J. R. and Kaminski, B. E., "Macroscopic Fracture Mechanics of Advanced Composite Materials," Journal of Composite Materials, Vol. 5, 1971, p.466.
- [5] Cruse, T. A., "Tensile Strength of Notched Composites," Journal of Composite Materials, Vol. 7, 1973, p.218.
- [6] Whitney, J. M. and Nuismer, R. J., "Stress Fracture Criteria for Laminated Composites Containing Stress Concentrations," Journal of Composite Materials, Vol. 8, 1974, p.253.
- [7] Cooper, G. A. and Kelly, A., "Role of the Interface in the Fracture of Fiber-Composite Materials," ASTM STP 452, 1969, p. 90.
- [8] Greszczuk, L. B., "Theoretical Studies of the Mechanisms of the Fiber-Matrix Interface in Composites," ASTM STP 452, 1969, p. 42.
- [9] Kelly, A., "Interface Effects and the Work of Fracture of a Fibrous Composites," Proc. Royal Society, Vol. A-319, 1970, p.95.
- [10] Phillips, D. C. and Tetelman, A. S., "The Fracture Toughness of Fiber Composites," Composites, Vol. 3, 1972, p. 216.
- [11] Piggott, M. R., "Theoretical Estimation of Fracture Toughness of Fibrous Composites," Journal of Material Science, Vol. 5, 1970, p.669.
- [12] Zweben, C. and Rosen, B. W., "A Statistical Theory of Material Strength with Application to Composite Materials," Journal of Mechanics and Physics of Solids, Vol. 18, 1970, p.189.
- [13] Corten, H. T., "Fracture Mechanics of Composites," Fracture, Vol. 7, Ed. H. Liebowitz, Academic Press, N.Y., 1972, p. 676.
- [14] Wu, E. M., "Application of Fracture Mechanics to Anisotropic Plates," Journal of Applied Mechanics, Vol. 34, 1967, p.967.

- [15] Kanninen, M. F., Rybicki, E. F. and Brinson, H. F., "A Critical Look at Current Applications of Fracture Mechanics to the Failure of Fiber-Reinforced Composites," Composites, Vol. 8, 1977, p. 17.
- [16] Wang, A. S. D., Crossman, F. W. and Law, G. E., "Interlaminar Failure in Epoxy-Based Composite Laminates," Proc. 29th MFPG Symp. Advance Composites-Design and Applications, NBS, 1979, p. 255.
- [17] Wang, A. S. D. and Law, G. E., "An Energy Method for Multiple Transverse Cracks in Graphite-Epoxy Laminates," in Modern Dev. in Composite Materials and Structures, Ed. J. Vinson, ASME, 1979, p. 17.
- [18] Wang, A. S. D. and Crossman, F. W., "Initiation and Growth of Transverse Cracks and Edge Delamination in Composite Laminates: Part 1. An Energy Method," Journal of Composite Materials, Suppl. Vol., 1980, p. 71.
- [19] Crossman, F. W., Warren, W. T., Wang, A. S. D. and Law, G. E., "Initiation and Growth of Transverse Cracks and edge delamination in Composite Laminates: Part 2. Experimental Correlation," Journal of Composite Materials, Suppl. Vol., 1980, p. 88.
- [20] Wang, A. S. D., "Growth Mechanisms of Transverse Cracks and Ply-Delamination in Composite Laminates," Proc. ICCM-III, Vol. 1, Paris, 1980, p. 170.
- [21] Crossman, F. W. and Wang, A. S. D., "The Dependence of Transverse Cracks and Delamination on Ply Thickness in Graphite-Epoxy Laminates," ASTM STP 725, 1982, p. 170.
- [22] Wang, A. S. D. and Crossman, F. W., "Fracture Mechanics of Sub-laminate Cracks", Technical Report, prepared under Contract No. F49620-79-C-0206, Air Force Office of Scientific Research, Aug., 1982.
- [23] Griffith, A. A., "The Phenomena of Rupture and Flow in Solids," Phil. Trans. Royal Society, Vol. A-221, 1920, p. 163.
- [24] Irwin, G. R., "Fracture Dynamics," in Fracture of Metals, ASM, Cleveland, 1948, p. 147.
- [25] Orowan, E. O., "Fundamentals of Brittle Behavior of Metals," in Fatigue and Fracture of Metals, W. M. Murray, Ed. Wiley & Sons, N.Y., 1950, p. 139.
- [26] Muskhelishvili, N. I., "Some Basic Problems From the Mathematical Theory of Elasticity," Noordhoff, Holland, 1953.
- [27] Sneddon, I. N., "Integral Transform Methods," in Methods of Analysis and Solutions of Crack Problems, Noordhoff, Holland, 1973, p. 315.
- [28] Lekhnitsky, S. G., "Theory of Elasticity of an Anisotropic Elastic Body," Holden-Day, San Francisco, 1963.

- [29] Rice, J. R., "A Path Independent Integral and Approximate Analysis of Strain Concentration by Notches and Cracks," Journal of Applied Mechanics, Trans. ASME, 1968, p.379.
- [30] Bucci, R. J., Paris, P. C., Landis, J. D. and Rice, J. R., "J-Integral Estimation Procedures," in Fracture Toughness, ASTM STP 514, 1972, p.40.
- [31] Irwin, G. R., "Fracture," Handbuch der Physik, Vol. 5, Springer-Verlag, 1958, p. 551.
- [32] Rybicki, E. F. and Kanninen, M. F., "A Finite Element Calculation of Stress Intensity Factors by a Modified Crack-Closure Integral," Engineering Fracture Mechanics, Vol. 9, 1977, p.931.
- [33] Wang, A. S. D. and Crossman, F. W., "Some New Results on Edge Effects in Symmetric Composite Laminates," Journal of Composite Materials, Vol. 11, 1977, p.92.
- [34] Raju, I. S. and Crews, J. H., "Three Dimensional Analysis of [0/90] and [90/0] Laminates With a Central Circular Hole," Composites Technology Review, Vol. 4, 1982, p.116.
- [35] Spilker, R. L., and Chou, S. C., "Edge Effects in Symmetric Composite Laminates: Importance of Satisfying the Traction Free Edge Condition," Journal of Composite Materials, Vol. 14, 1980, p.2.
- [36] Wang, S. S. and Choi, I., "Boundary Layer Effects in Composite Laminates," Part 1 and Part 2, Journal of Applied Mechanics, Vol. 49, 1982, p.541.
- [37] Isida, M., "Method of Laurant Series Expansion for Internal Crack Problems," in Methods of Analysis and Solutions of Crack Problems, Ed. G. C. Sih, Noordhoff, 1973, p. 56.
- [38] Whitcomb, J. D., Raju, I. S. and Goree, J. G., "Reliability of the Finite Element Method for Calculating Free Edge Stresses in Composite Laminates," Computers & Structures, Vol. 15, 1982, p. 23.
- [39] Cullen, J. S., "Mode-I Delamination of Unidirectional Graphite Epoxy Composite Under Complex Load Histories," M. S. Theses, Texas A & M Univeristy, 1981.
- [40] Williams, D., "Mode-I Transverse Cracking in an Epoxy and a Graphite Fiber Reinforced Epoxy," M. S. Thesis, Texas A & M University, 1981.
- [41] Wilkins, D. J., "A Comparison of the Delamination and Environmental Resistance of a Graphite-Epoxy and a Graphite-Bismaleimide," NAV-GD-0037, Naval Air System Comm., 1981.
- [42] Wilkins, D. J., Eisenmann, J. R., Camin, R. A., Margolis, W. S. and Benson, R. A., "Characterizing Delamination Growth in Graphite-Epoxy," ASTM STP 775, 1982, p. 168.

- [43] Vanderkley, P. S., "Mode-I and Mode-II Delamination Fracture Toughness of an Unidirectional Graphite-Epoxy Composite," M. S. Thesis, Texas A & M University, 1981.
- [44] Bascom, W. D., Cottoington, R. L. and Timmons, C. O., "Fracture Design Criteria for Structural Adhesive Bonding - Promise and Problems," Naval Engineering Journal, Aug., 1976, p.73.
- [45] Wang, A. S. D., Kishore, N. N. and Feng, W. W., "On Mixed-Mode Fracture in Off-Axis Unidirectional Graphite-Epoxy Composites," Proc. ICCM-IV, Vol. 1, Tokyo, 1982, p. 599.
- [46] Bader, M. G., Bailey, J. E., Curtis, P. T. and Parvizi, A., "The Mechanisms of Initiation of Development of Damage in Multi-Axial Fiber-Reinforced Plastics Laminates," in Mechanical Behavior of Materials, ICM-3, Vol. 3, 1979, p. 227.
- [47] Aveston, J. and Kelly, A., "Theory of Multiple Fracture of Fibrous Composites," Journal of Material Science, Vol. 8, 1973, p.352.
- [48] Reifsnider, K. L. and Masters, J. L., "Investigation of Characteristic Damage States in Composites Laminates," ASME Paper No. 78-WA-AERO-4, 1978.
- [49] Chou, S. C., Brockelman, R., Broz, A., Hinton, Y. and Shuford, R., "Analytical and NDE Techniques for Determining Crack Initiation in Graphite-Epoxy Laminates," ASTM Symp. Effects of Defects in Composite Materials, San Francisco, 1982.
- [50] Juvinall, R. C., "Stress, Strain and Strength," McGraw Hill, N.Y., 1967, p. 346.
- [51] Wang, A. S. D., Chou, P. C., Lei, C. S. and Bucinell, "Cumulative Damage Model for Advanced Composite Materials", Final Report, prepared under Contract No. F33615-80-C-5039, AFWAL, Aug. 1983.
- [52] Chou, P. C., Wang, A. S. D. and Miller, H. R., "Cumulative Damage Model for Advanced Composite Materials," AFWAL-TR-82-4083, U. S. Air Force Wright Aeronautical Lab., 1982.
- [53] Pipes, R. B. and Pagano, N. J., "Interlaminar Stresses in Composite Laminates Under Uniform Axial Tension," Journal Composite Materials, Vol. 4, 1970, p.538.
- [54] Bjeletich, J. G., Crossman, F. W. and Warren, W. J., "The Influence of Stacking Sequence on Failure Modes in Quasi-Isotropic Graphite-Epoxy Laminates," Failure Modes in Composites - IV, AIME, 1979.
- [55] Rodini, B. T. and Eisenmann, J. R., "An Analytical and Experimental Investigation of Edge Delamination in Composite Laminates," in Fibrous Composites in Structural Design, Ed. E. M. Lenoe, et. al., Plenum Press, N.Y., 1978, p. 441.

- [56] Law, G. E., "Fracture Analysis of [+25/90] Graphite-Epoxy Composite Laminates," Ph.D. Thesis, Drexel University, 1981.
- [57] Wang, A. S. D. and Slomiana, M., "Fracture Mechanics of Delamination - Initiation and Growth," NADC-TR-79056-60, Jan., 1982.
- [58] Crossman, F. W., Warren, W. J. and Wang, A. S. D., "Influence of Ply Thickness on Damage Accumulation and Final Fracture," Proc. Symposium on Mechanics of Composite Materials and Structures, ASME, WAM. Boston, Nov. 1983.
- [59] Wang, A. S. D., Kishore, N.N. and Li, C. A., "A Three Dimensional Finite Element Analysis of Contoured Interlaminar Cracks", Final Report, prepared under Contract No. F62269-82-C-0250, NADC, Oct., 1983.

TABLE A FLOW-CHART FOR MONTE-CARLO SIMULATION

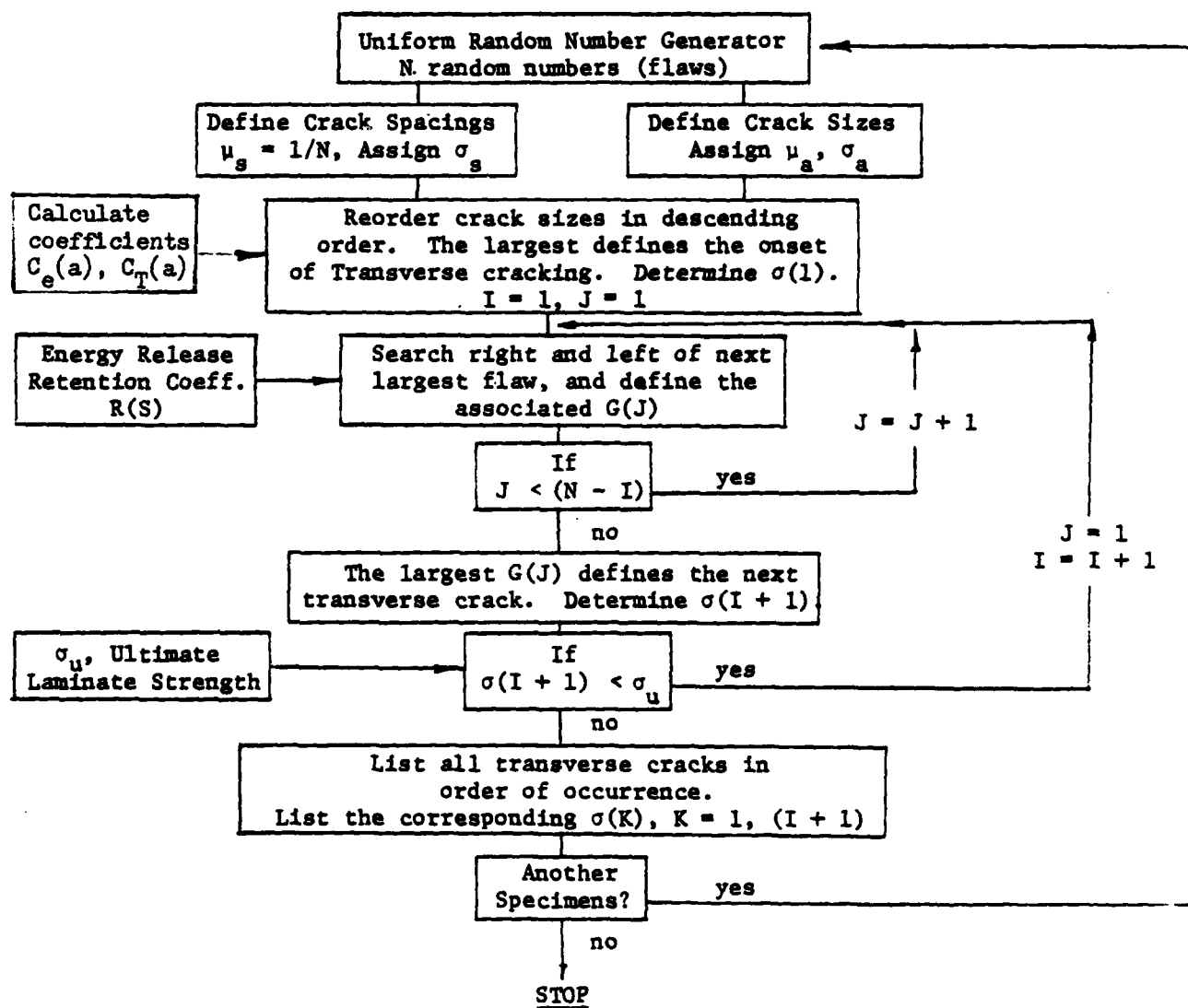


TABLE B EXPERIMENTAL DAMAGE SEQUENCE AND FINAL FAILURE LOAD P_u

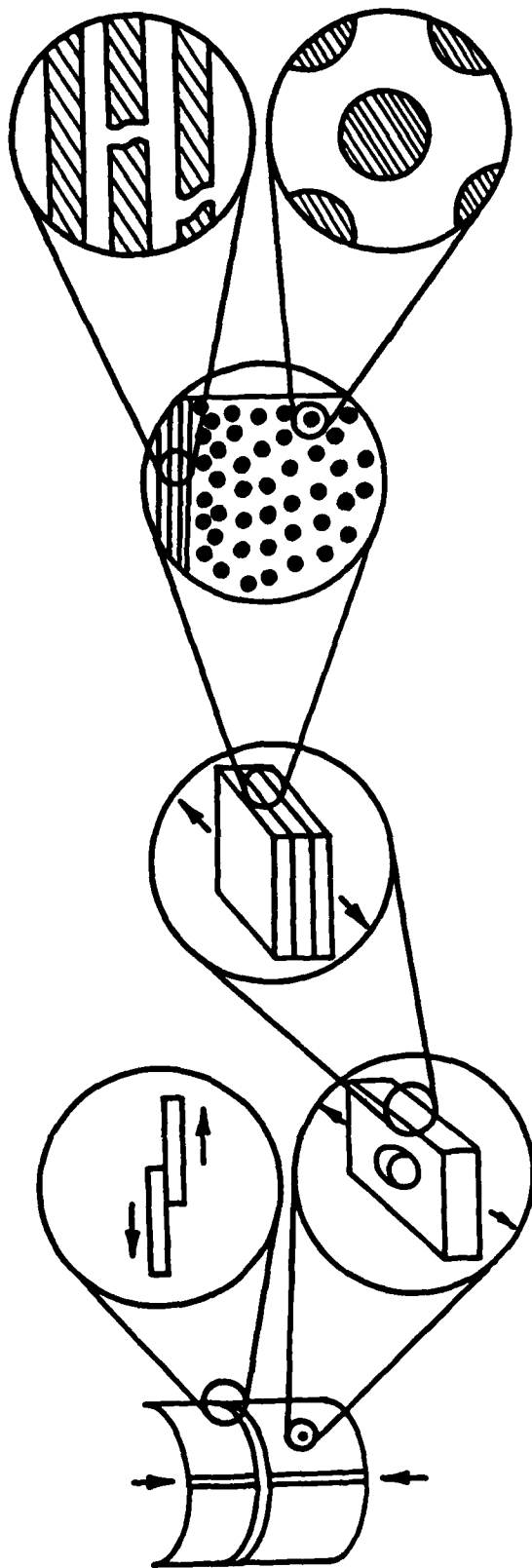
<u>Laminate</u>	<u>Sequence of Failure Modes</u>	<u>Total load in lbs.*</u>
$[\underline{+25}/\underline{+25}]_s$	no transverse cracking no edge delamination cross-section fiber break	<u>3103(2895-3245)</u>
$[25_2/\underline{-25}_2]_s$	single transverse crack in -25-layer, followed by multiple transverse cracks in the +25-layer	occur at 98% P_u
	final failure involved no fiber break	<u>2272(2001-2480)</u>
$[\underline{+25}/\underline{+25}/90_2]_s$	transverse cracks in 90-layer stable edge delamination	occur at 80% P_u occur at 90% P_u
	cross-section fiber break in the 25-layers	<u>3040(3001-3250)</u>
$[25_2/\underline{-25}_2/90_2]_s$	transverse cracks in 90-layer rapid edge delamination	occur at 90% P_u occur at 98% P_u
	fiber-split in 25-layer	<u>2648(2500-2830)</u>

* Number is for average of 4 specimens; (range of test data at failure).

TABLE C EXPERIMENTAL DAMAGE SEQUENCE AND FINAL FAILURE LOAD P_u

<u>Laminate</u>	<u>Sequence of failure modes</u>	<u>Total load in lbs.*</u>
$[\underline{+25}/90_2]_s$	transverse cracks in 90-layer stable edge delamination cross-section fiber break in 25-layers	occur at 85% P_u occur at 95% P_u <u>1802(1747-1893)</u>
$[\underline{+25}/90_8]_s$	scattered transverse cracks local delamination from T.C. tip; combined with edge delam. fiber split in 25-layer few fiber break in 25-layer	occur at 95% P_u <u>1606(1500-1660)</u>
$[0_2/90_2]_s$	transverse cracks in 90-layer no edge delamination cross-section fiber break of 0-layer	occur at 80% P_u <u>5163(4600-5730)</u>
$[0_2/90_8]_s$	scattered transverse cracks local delamination from T.C. tip; local fiber-split in 0-layer above transverse crack coalescence of fiber-splits in 0-layer final 0-layer failure	occur at 75% P_u occur at 85% P_u <u>4220(4120-4320)</u>
$[\underline{+30}/90_2]_s$	transverse crack in 90°-layer stable edge delamination cross-section fiber break in 30-layer	occur at 80% P_u occur at 95% P_u <u>1650(1625-1670)</u>
$[\underline{+30}/90_8]_s$	transverse crack in 90°-layer local edge delamination from T.C. tip; fiber break in 30-layer	occur at 80% P_u occur at 85% P_u <u>1622(1620-1625)</u>

* Number is for average of 4 specimens; (range of test data at failure).



STRUCTURAL MECHANICS

GEOMETRIC-
IMPERFECTION

LOCALIZED-
DAMAGE ZONE

BUCKLING

(a)

MACROMECHANICS

SUBLAMINATE-
CRACKING

DELAMINATION,
ETC.

(c)

MICROMECHANICS

MICROFLAW-
DISTRIBUTION

CRACK-
COALESCENCE

(d)

INTERFACE-
MECHANISMS

DEBONDING,
ETC.

(e)

Fig. 1 Dimensional Regimes of Failure Analysis in Composite Materials

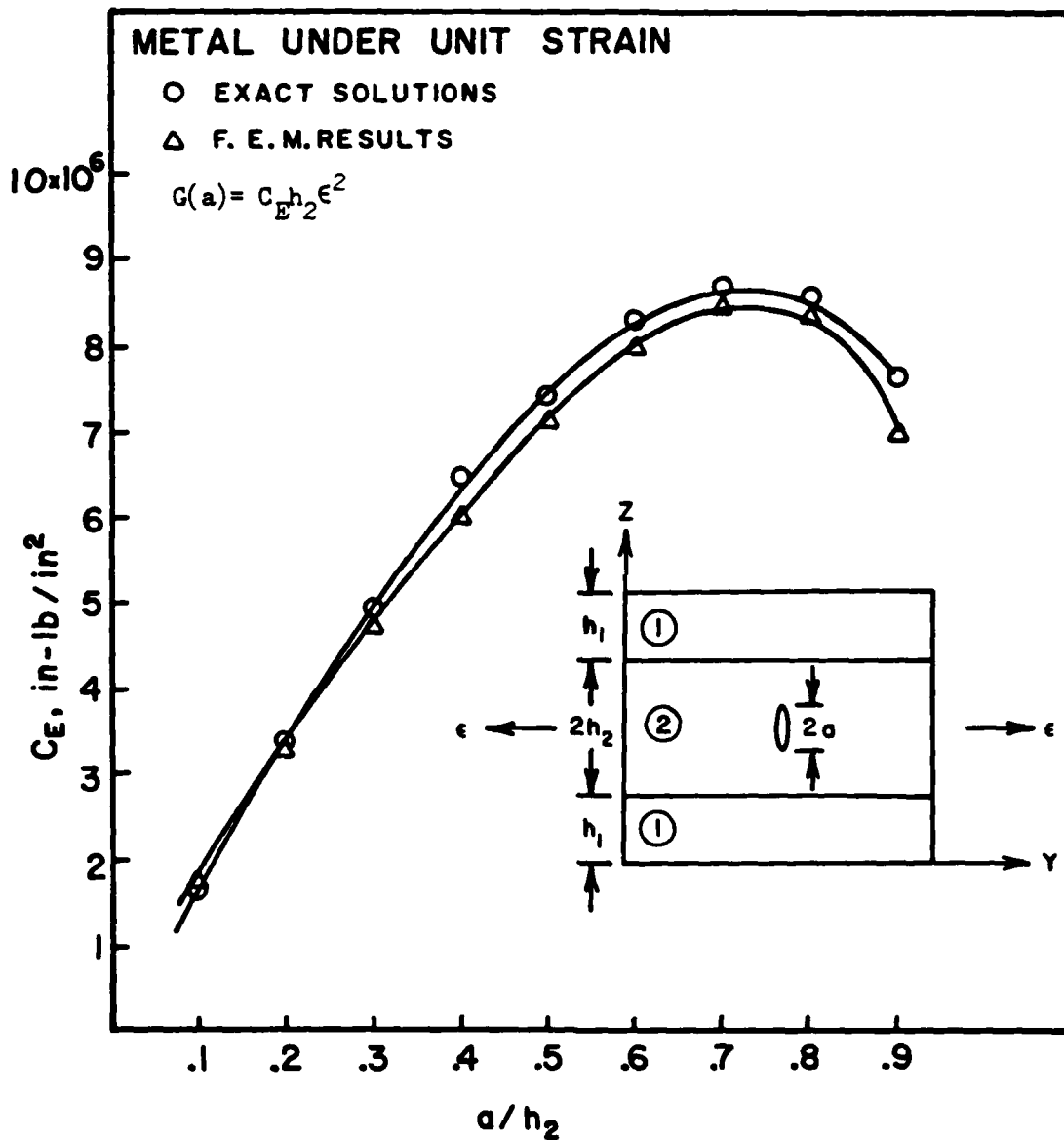


Fig. 2 Comparison of the Exact and the Finite Element Solutions for $G(a)$; $E_1/E_2 = 5$; $h_1 = h_2$; $\nu_1 = \nu_2 = 1/3$.

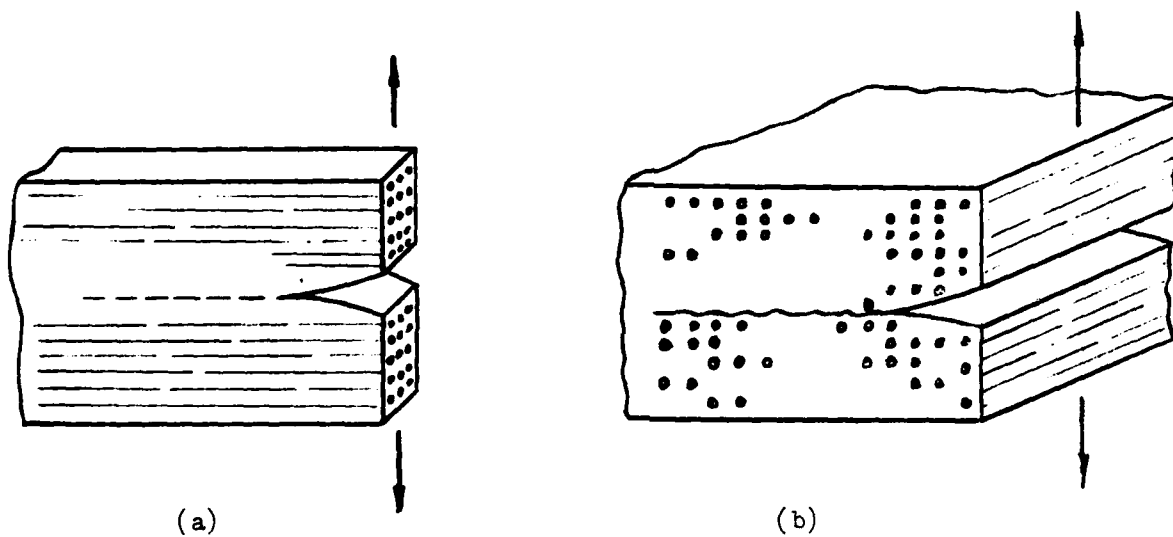


Fig. 3(a) $0^\circ/0^\circ$ Mode-I Delamination; (b) $90^\circ/90^\circ$ Delamination.

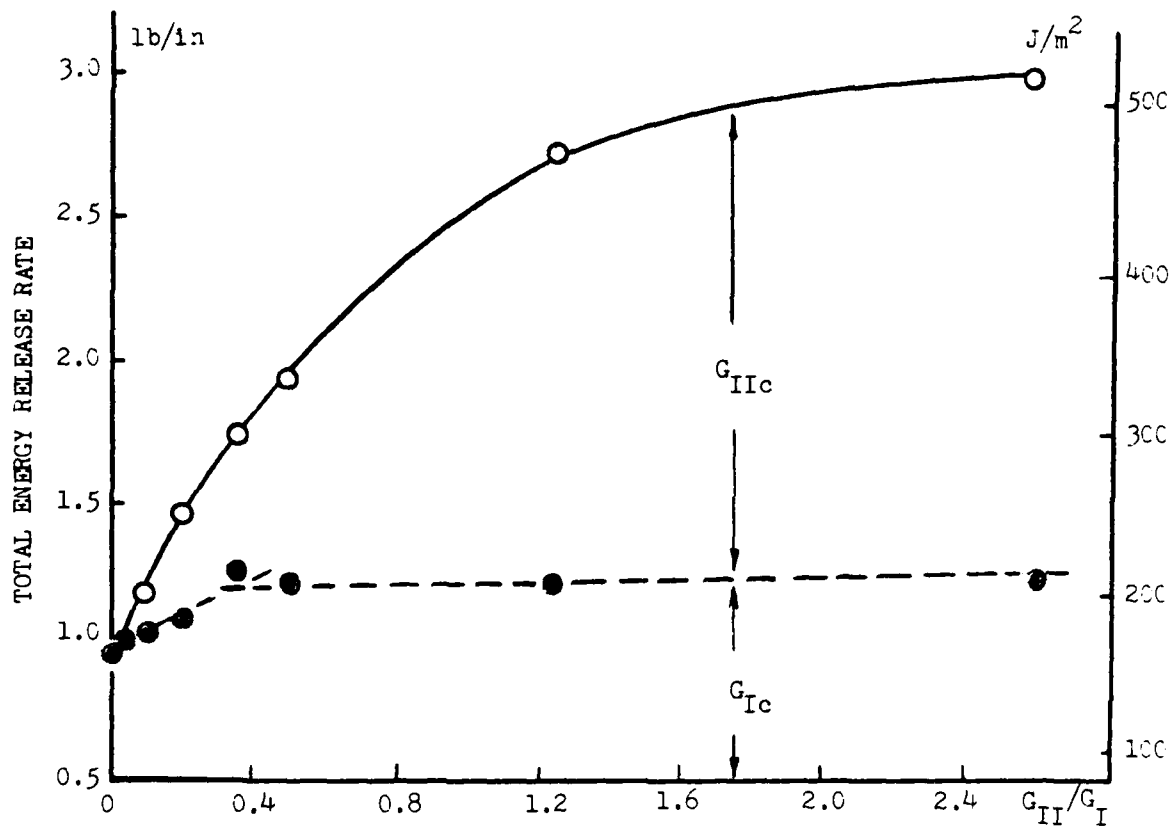


Fig. 4 Mixed-Mode $G_c (= G_{Ic} + G_{IIc})$ vs. G_{II}/G_I Ratio. Ref.[45].

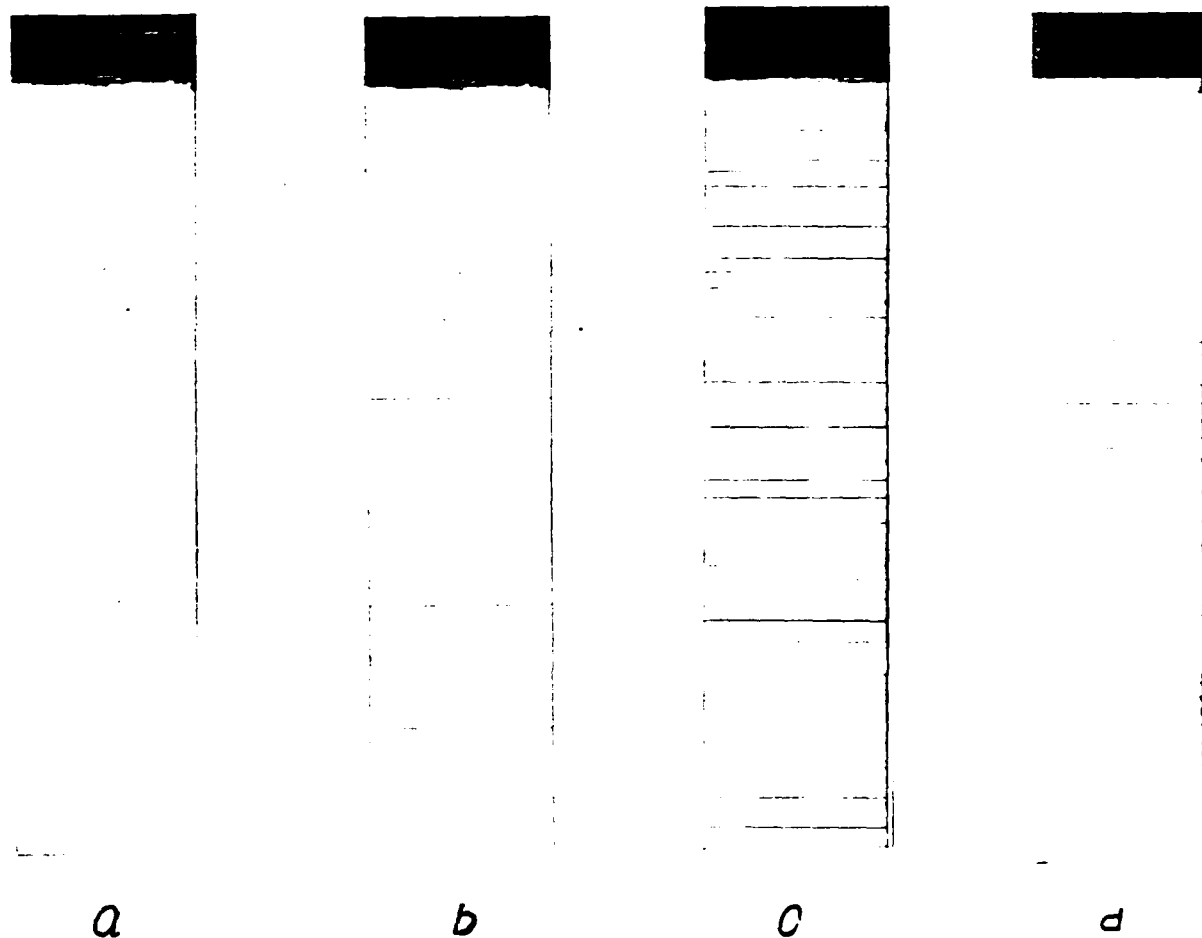


Fig. 5 X-Radiographs of Transverse Cracks Formation Under Increasing Loading. T300/934 $[0/90]_s$ Laminate.

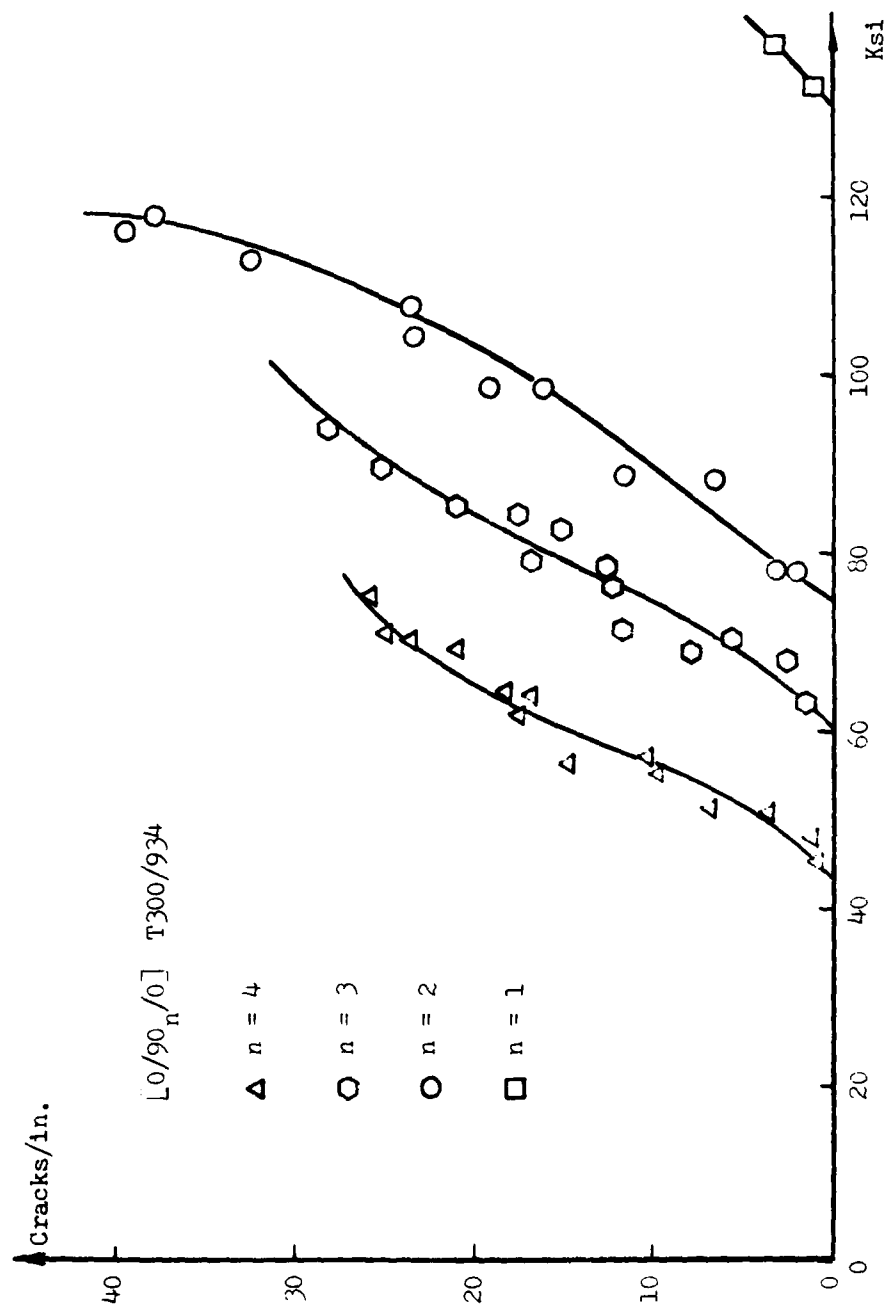


Fig. 6 Transverse Crack Density vs. Applied Tensile Stress. Ref.[21].

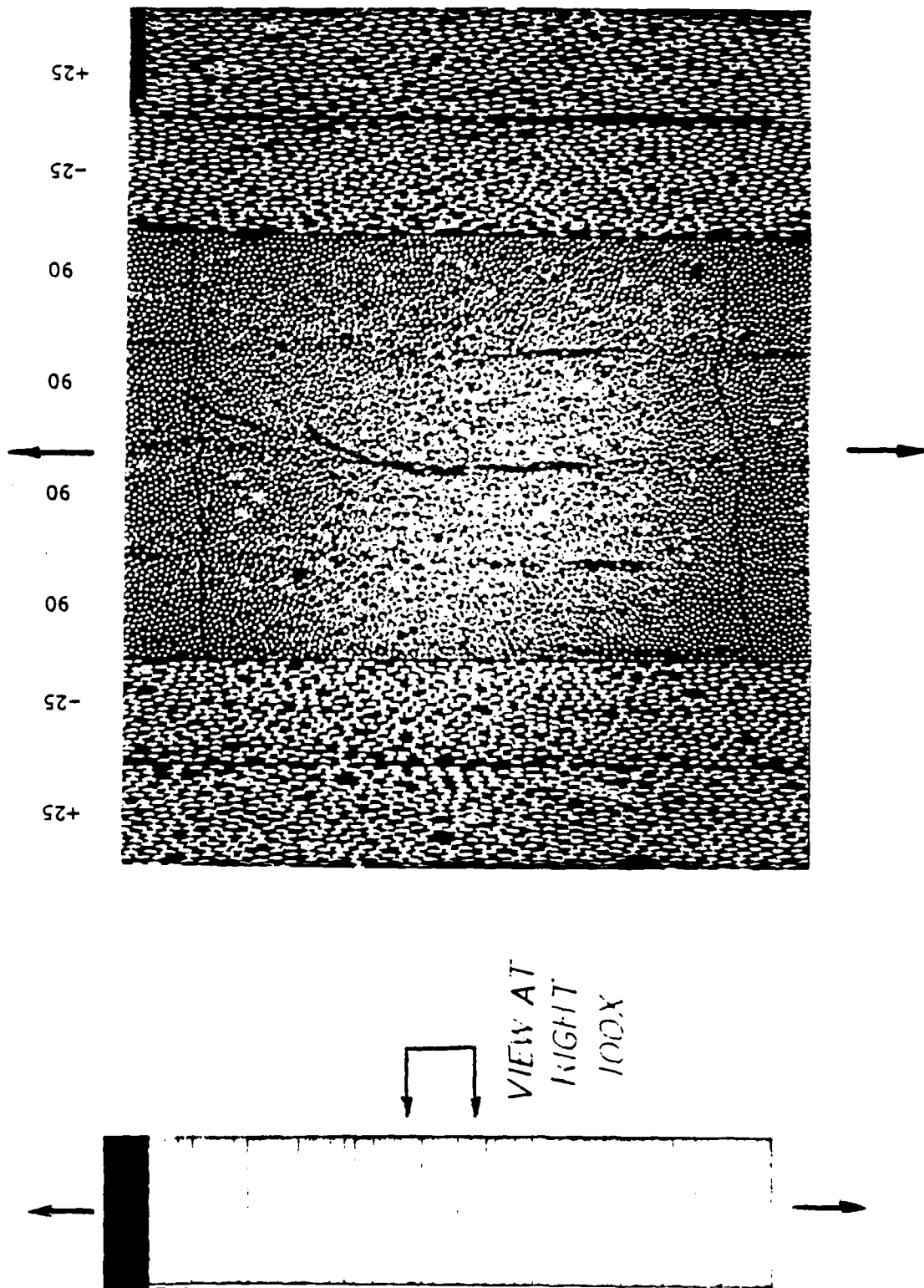


Fig. 7 Micrograph(right) Showing Two Transverse Cracks In A [+25/90₂]_s Laminate.

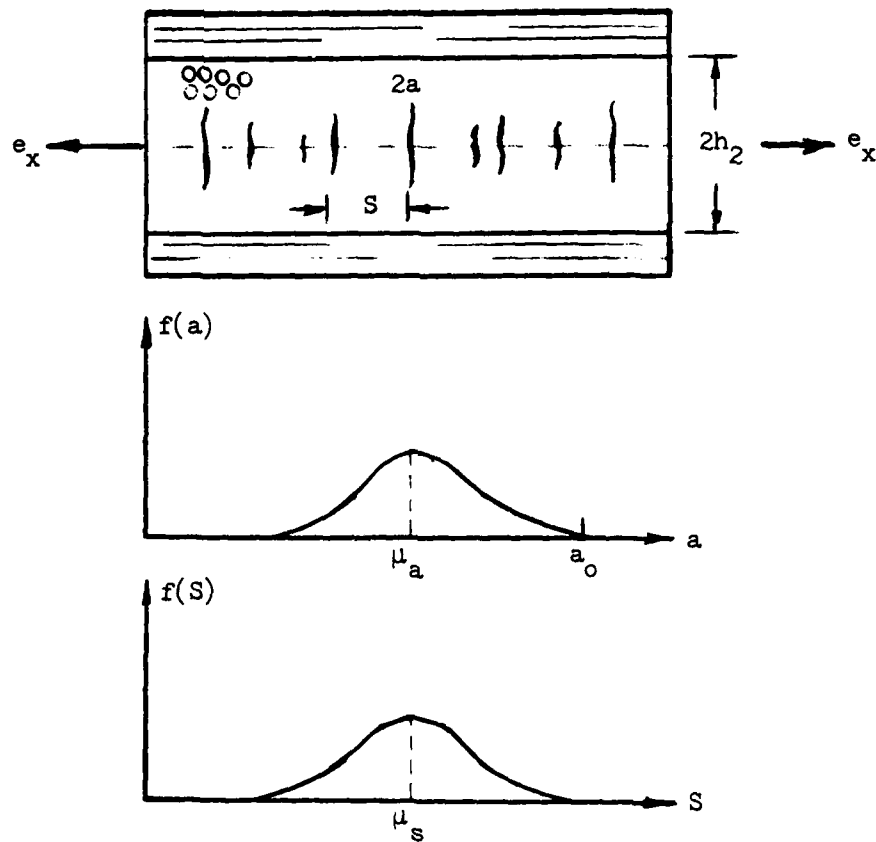


Fig. 8 Effective Flaws in 90° Layer(top); Size a and Spacing S Distributions(below).

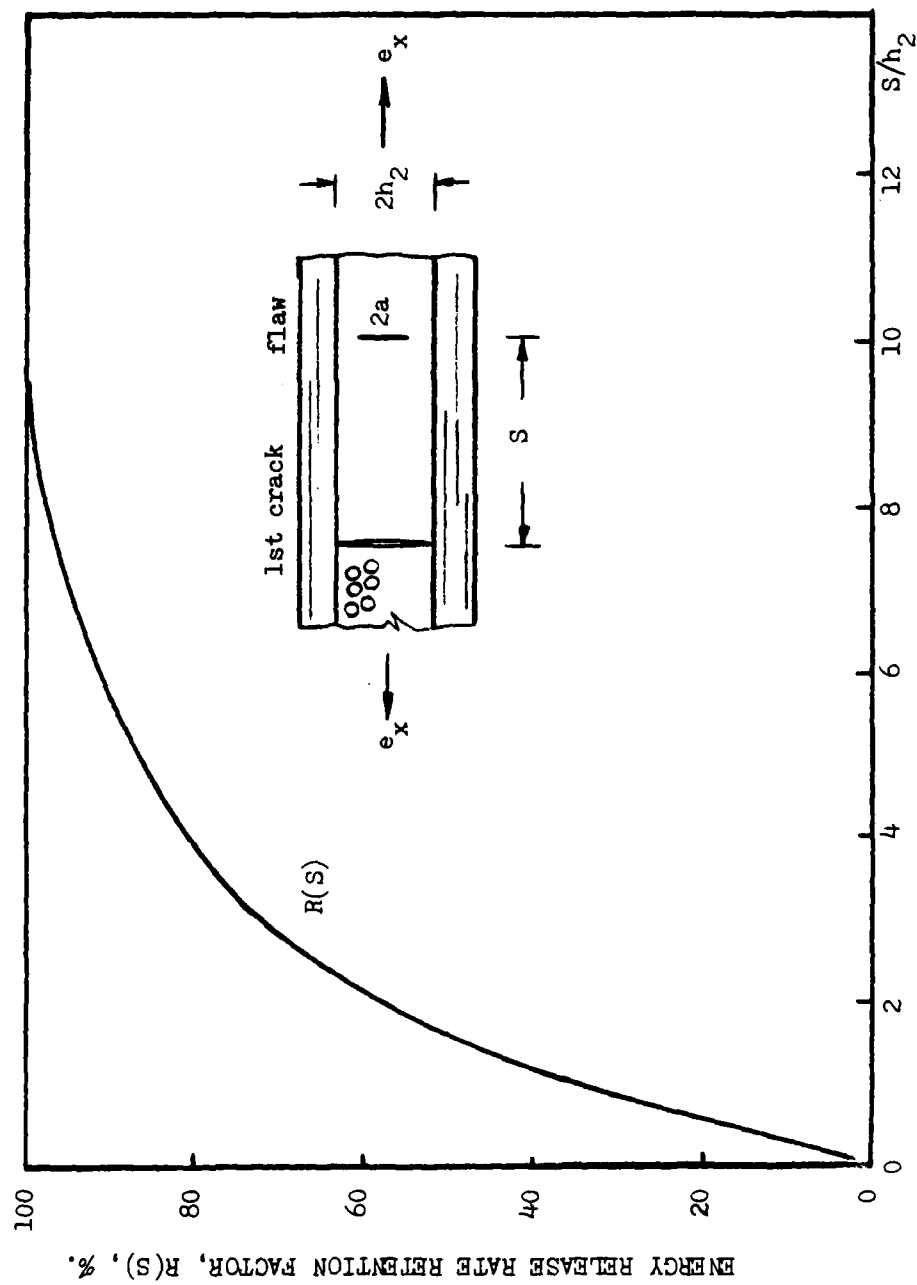


Fig. 9 Energy Release Rate Retention Factor $R(S)$ for a Flaw Located at a Distance S from a Transverse Crack.

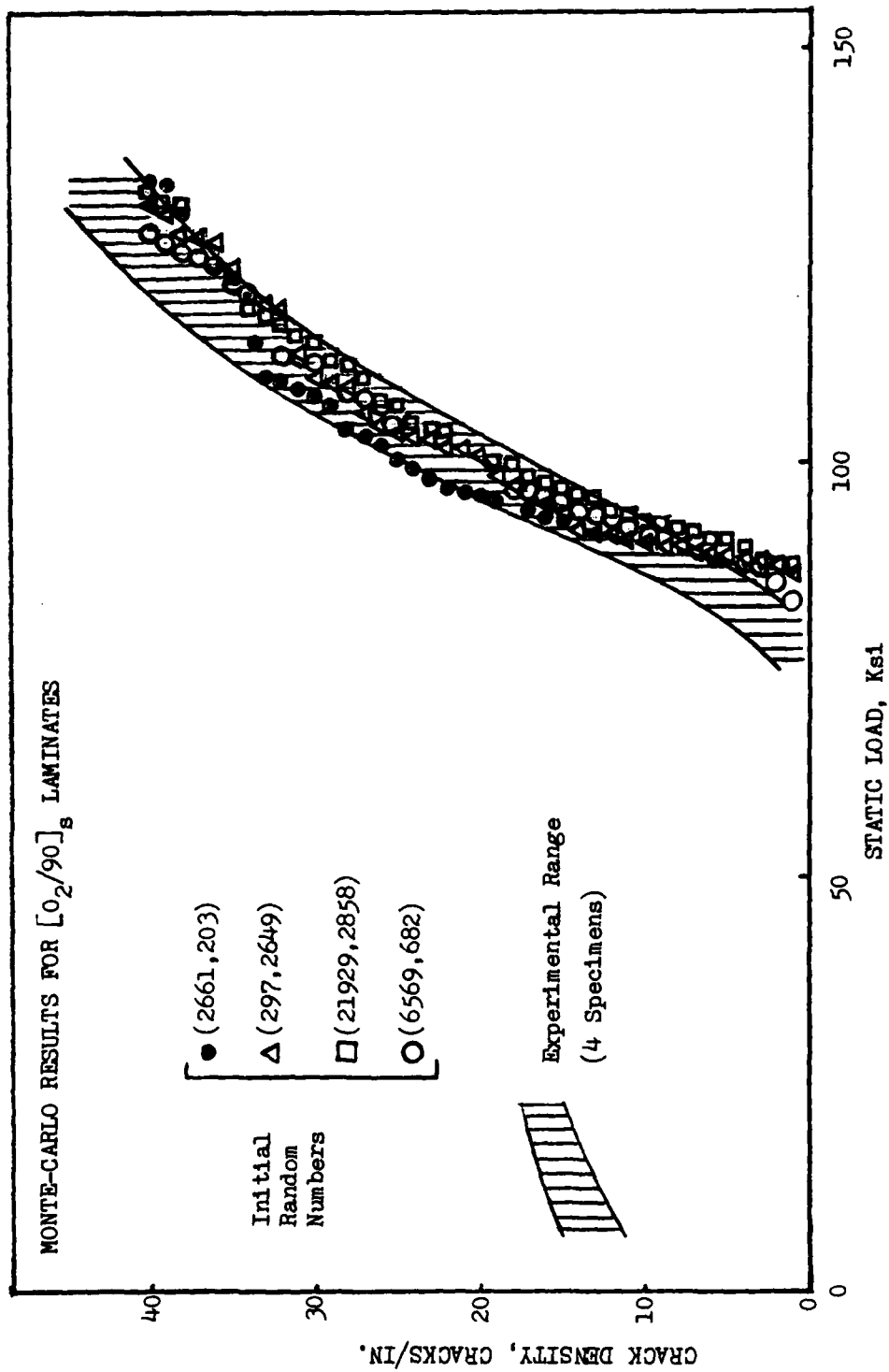


Fig. 10 Comparison of Experiment and the Monte-Carlo simulations of Transverse Cracks.

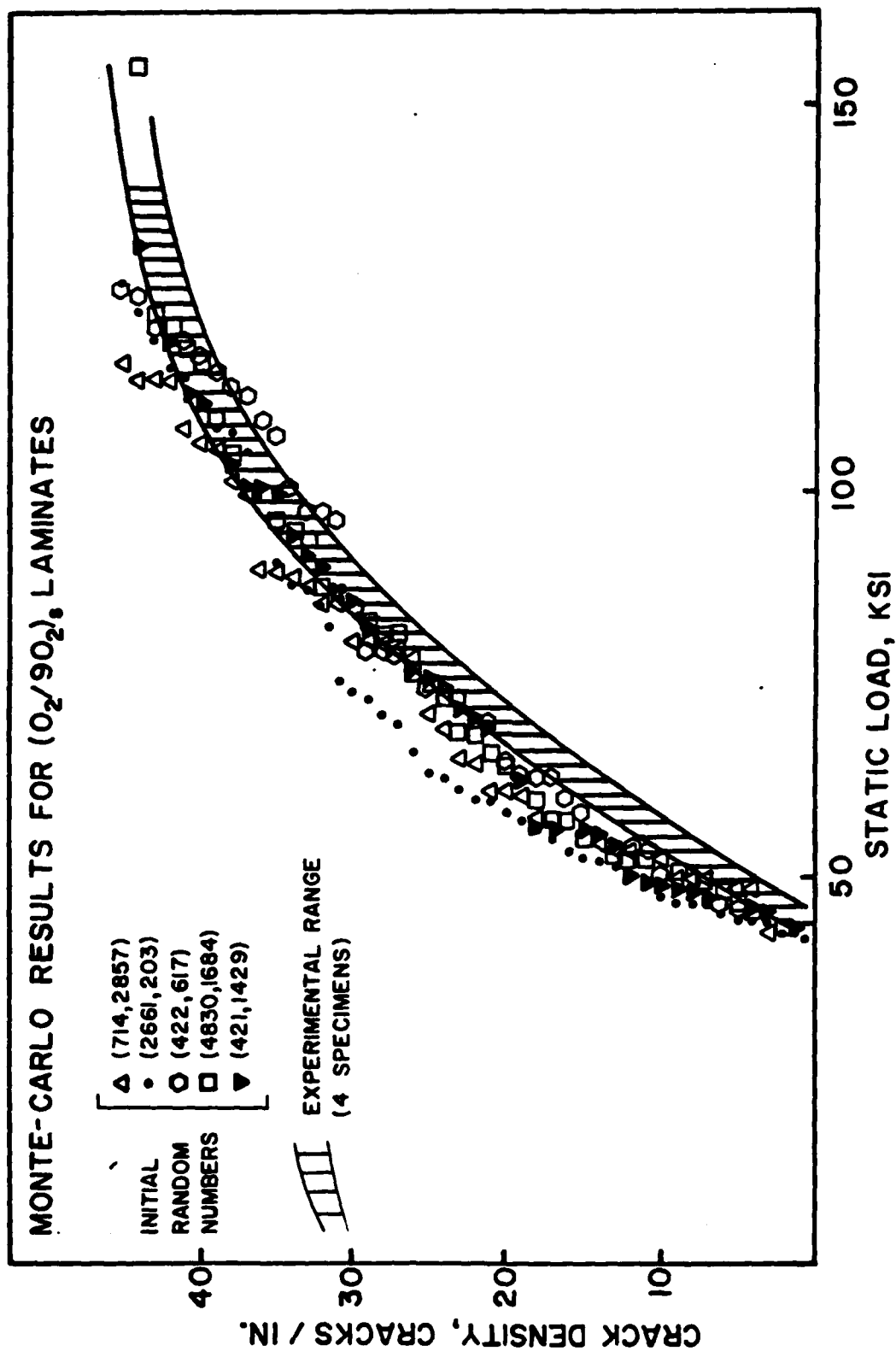


Fig. 11 Comparison of Experiment and the Monte-Carlo Simulations of Transverse Cracks.

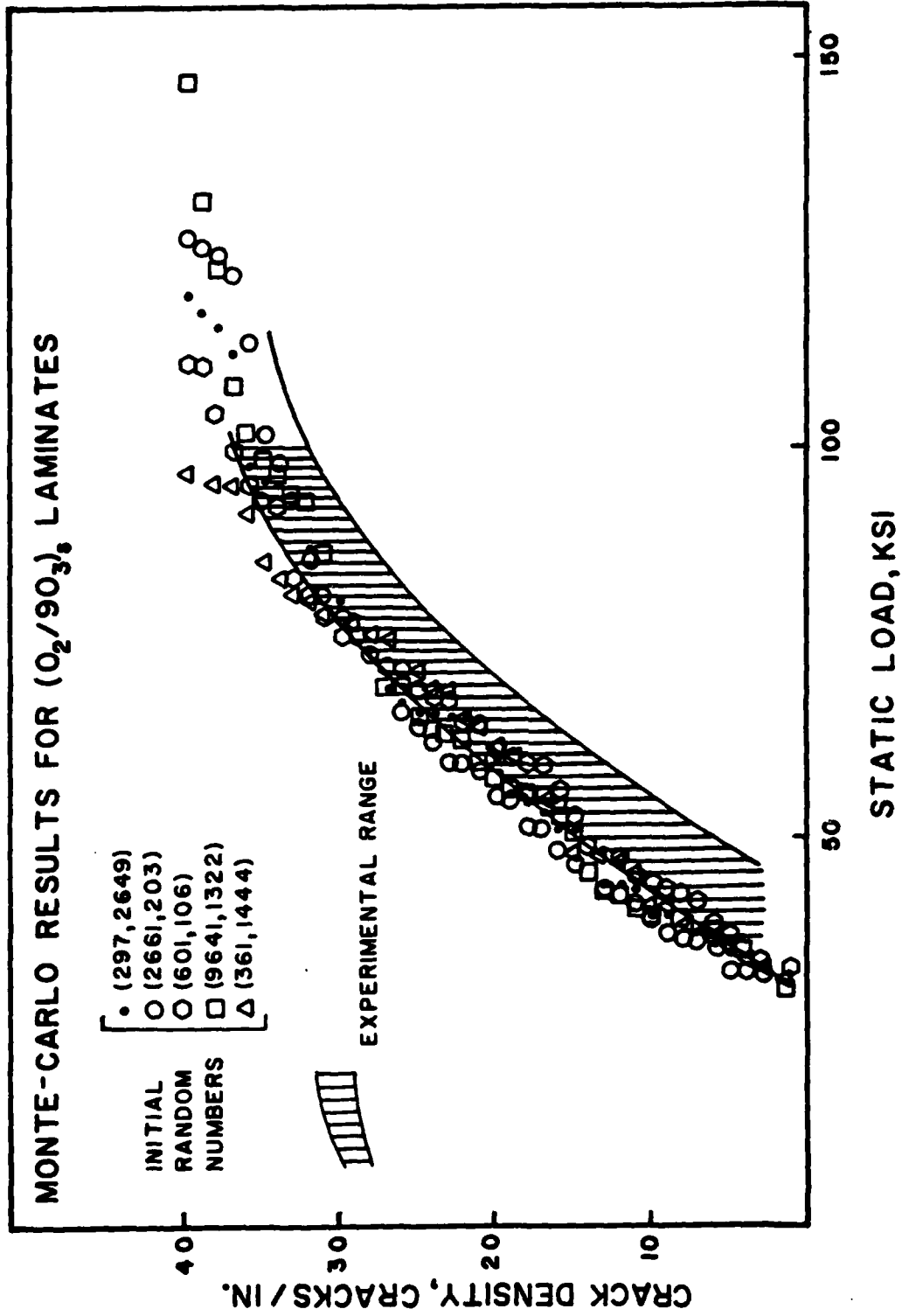
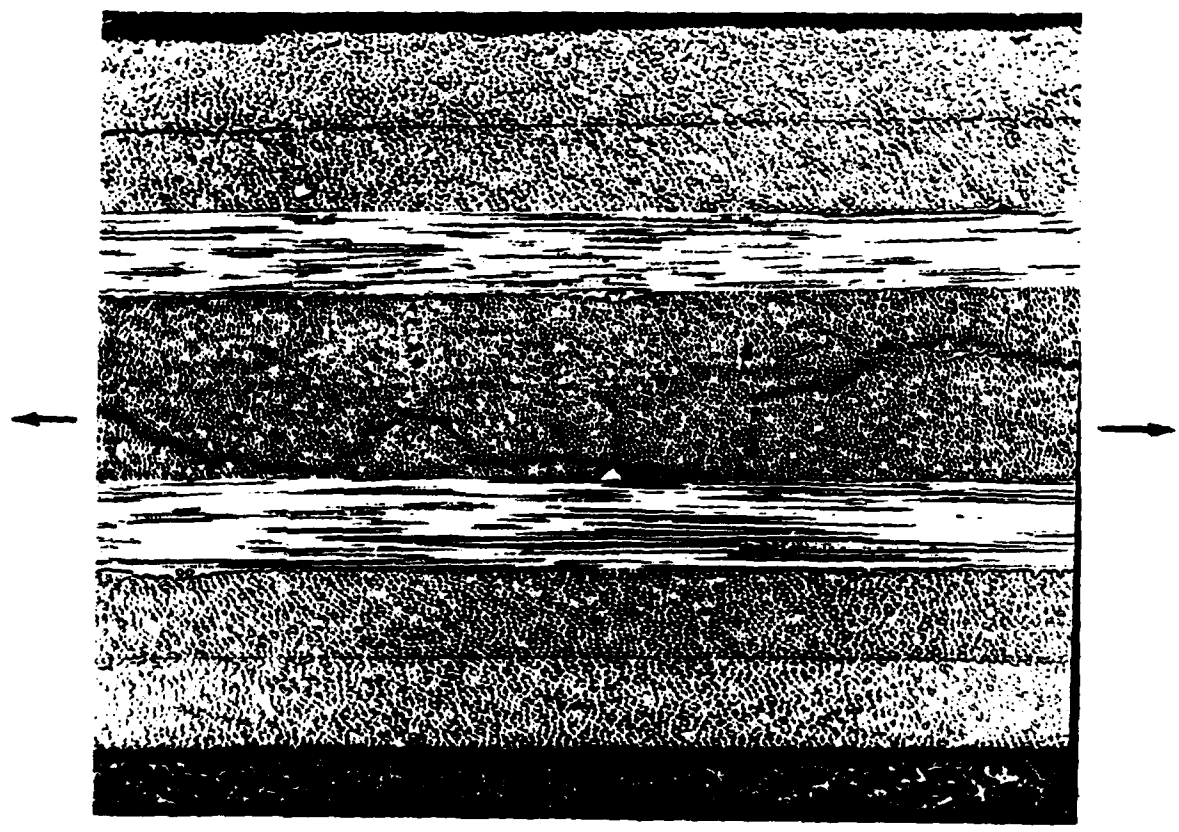
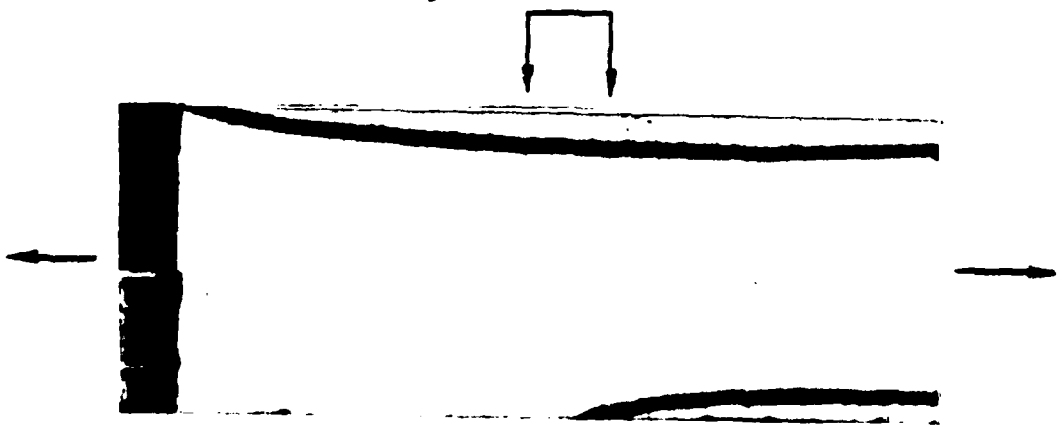


Fig. 12 Comparison of Experiment and the Monte-Carlo Simulations of Transverse Cracks.



VIEW AT
RIGHT
80X



Micrograph(right) Showing the effect of illumination in A $[+45/45]$ laminate.

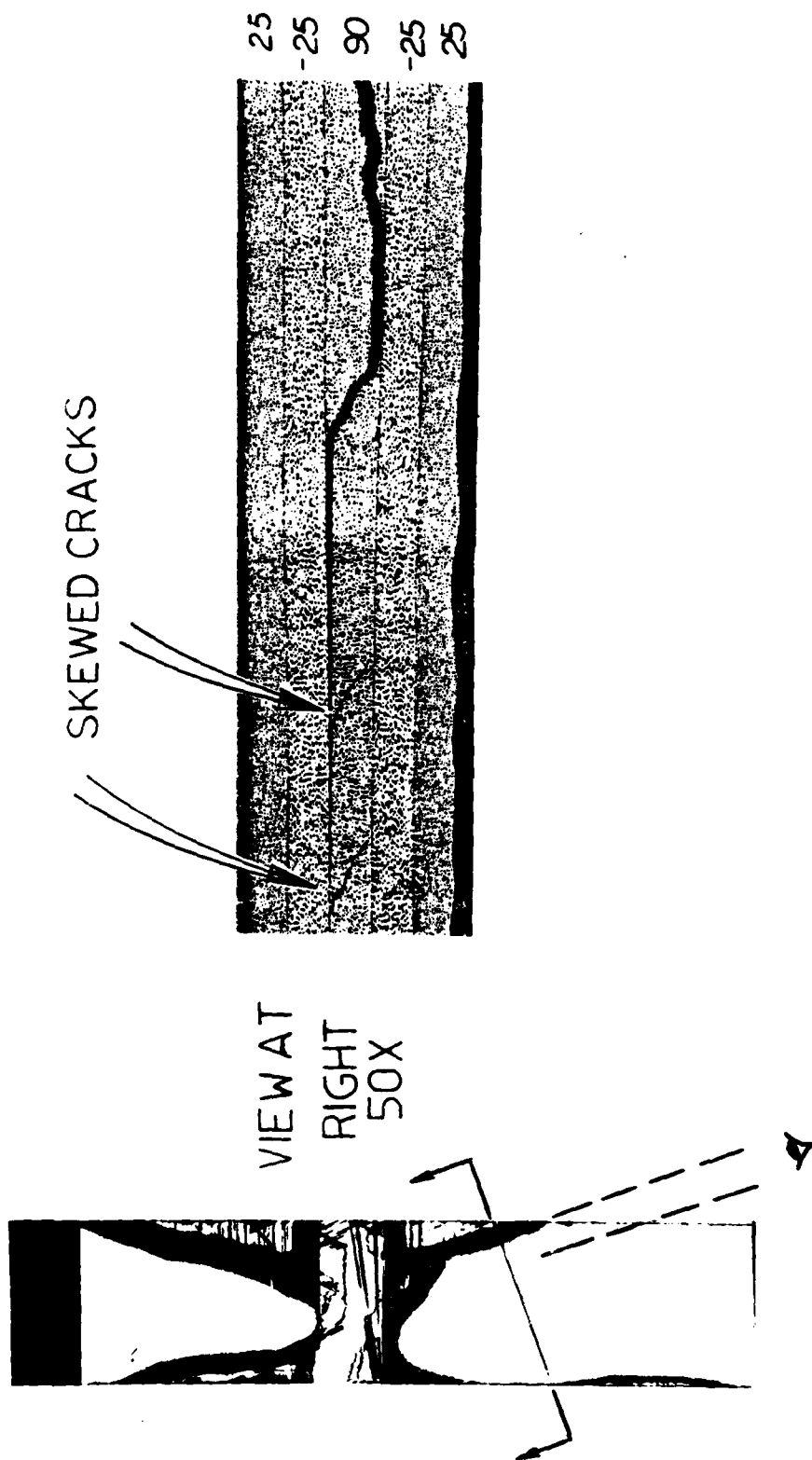


Fig. 14 Microphotograph(right) Showing Free Edge Delamination of a $[\pm 25/90]_2$ Laminate After Final Failure. Note Skewed Cracks Ahead of Delamination.

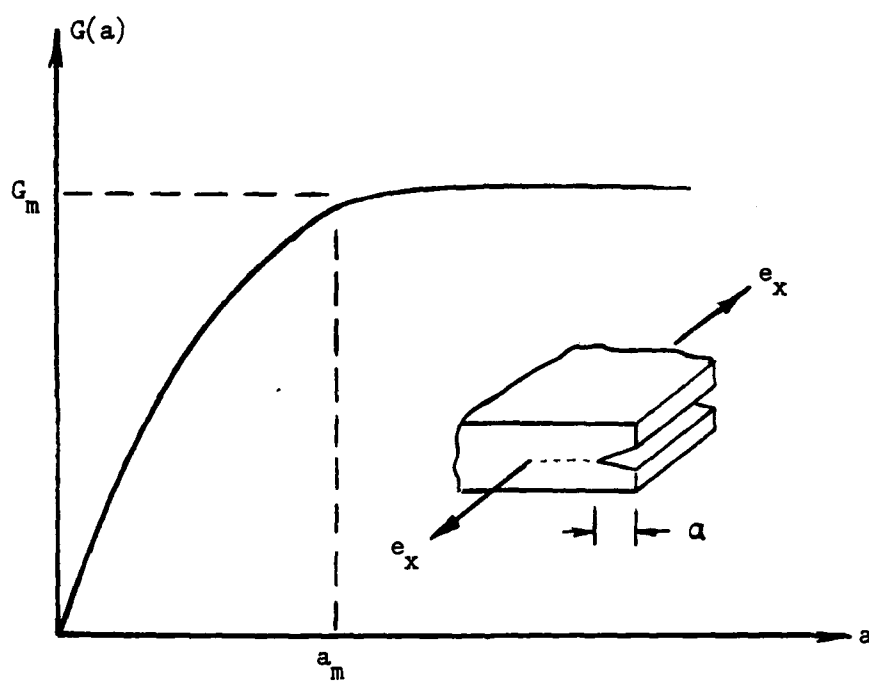
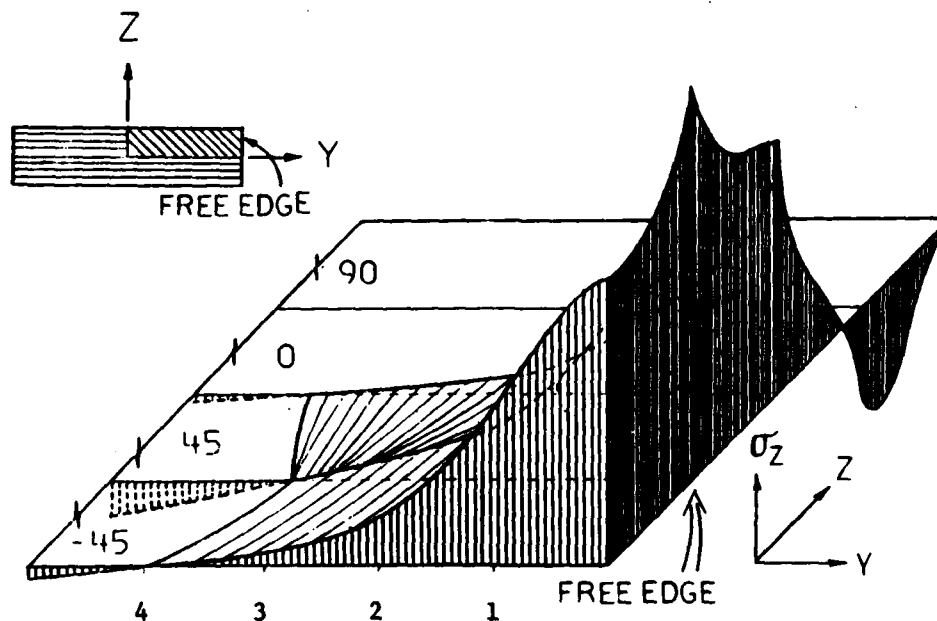


Fig. 15 Typical Shape of Energy Release Rate $G(a)$ for Delamination.



Fig. 16 Free Edge Delamination Induced by Compression.
AS-3501-06 $[90_2/0_2/\pm 45_2]_s$.



Interlaminar Normal Stress Distribution

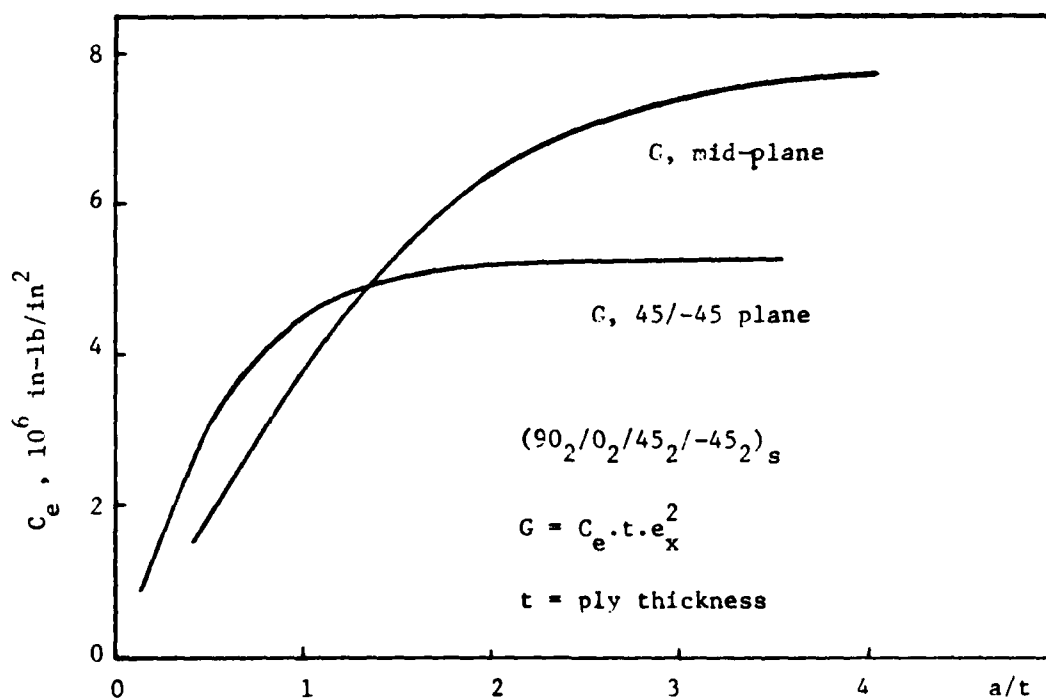
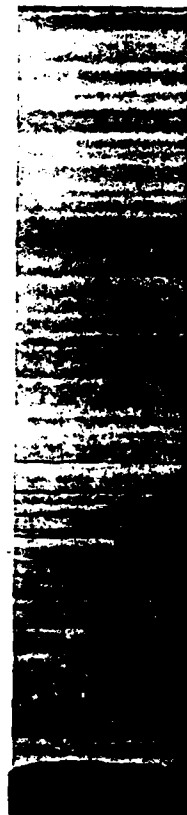


Figure 17 Interlaminar Normal Stress Distribution and Energy Release Rate Coefficients for $(90_2/0_2/\pm 45_2)_s$ Under Compression. Ref.[57].



a



b

Fig. 18 (a) Delamination Induces Transverse Cracks, $[\pm 25/90_2]_s$;
 (b) Transverse Cracks induce Delaminations, $[\pm 25/90_4]_s$.

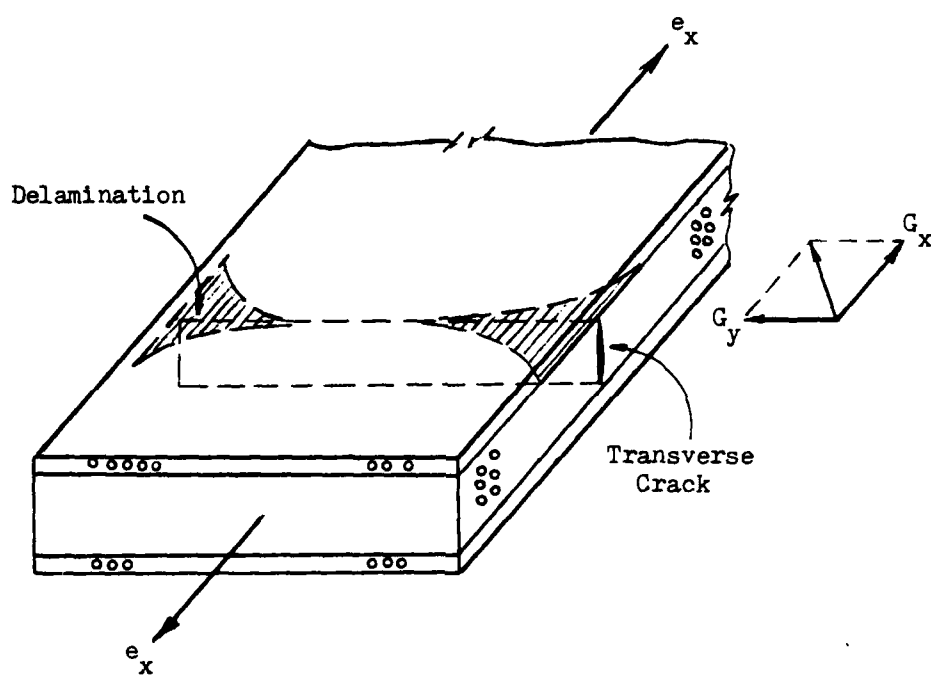


Fig. 19 Transverse Crack/Delamination Interaction.

T300/934 $(\pm 25/90)_n_s$, $n=1/2, 1, 2, 3, 4, 6, 8$.

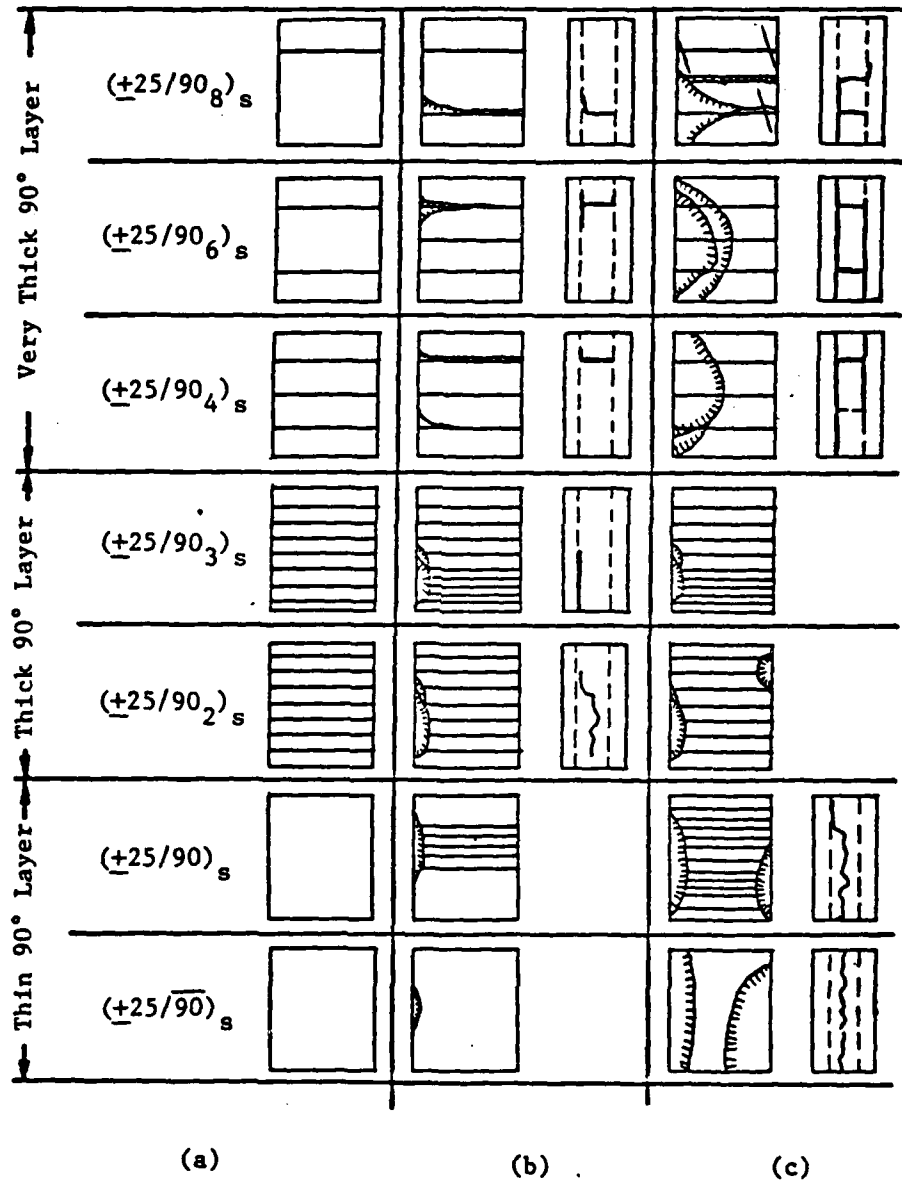
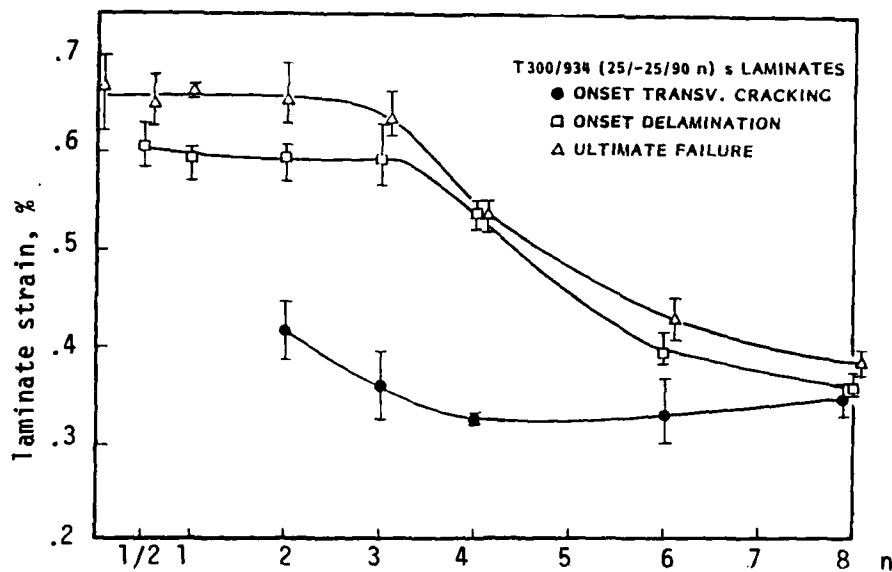
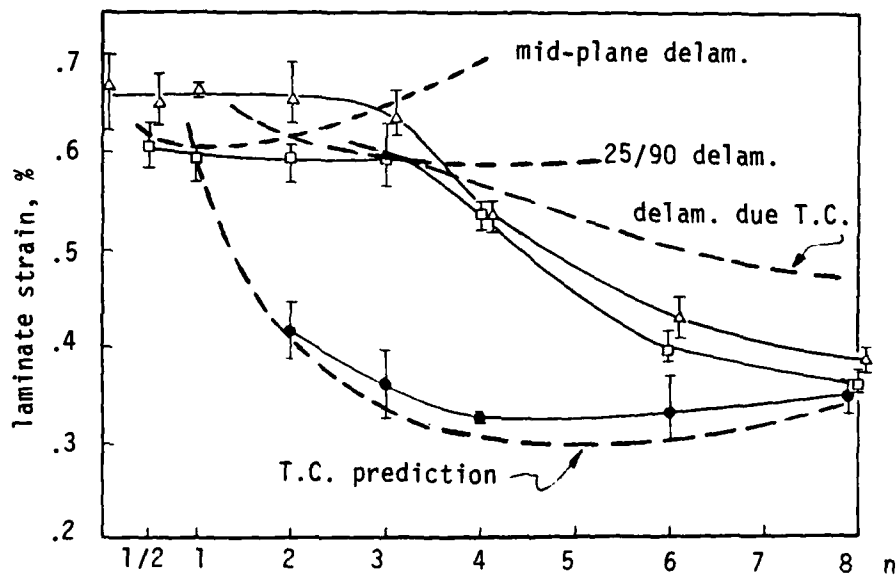


Fig. 20 SCHEMATIC OF THE FRACTURE SEQUENCE IN THE $(\pm 25/90)_n_s$ LAMINATES
 (a) JUST PRIOR TO EDGE DELAMINATION, (b) SUBSEQUENT TO EDGE
 DELAMINATION, (c) JUST PRIOR TO FINAL FAILURE. Ref.[21].



(a) Experimental Results



(b) Comparison with Predicted Results

Fig. 21 Onset Loads at Transverse Crack, Edge Delamination and Final Failure for the $[\pm 25/90]_n$ s Laminate Series, Ref.[22].

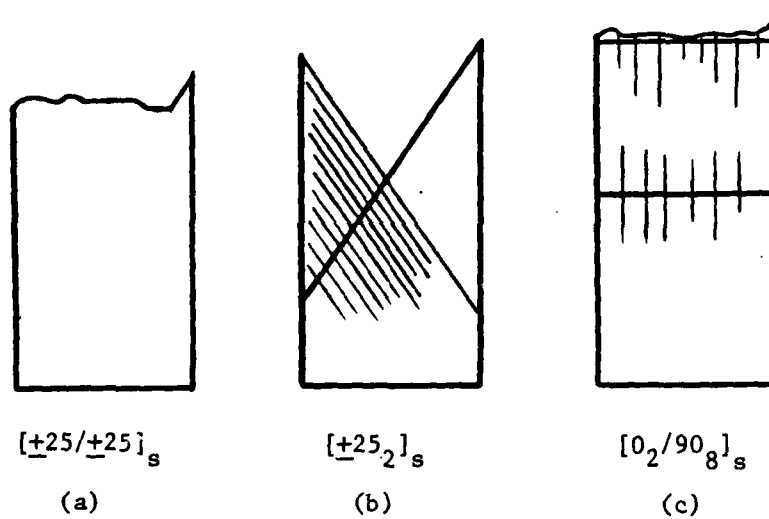


Figure 22 Final Failure Modes: (a) Cross-sectional Fiber Break; (b) 25-layer Transverse Cracks; (c) 0-layer Fiber Splits over 90-layer Transverse Cracks.

APPENDIX - C

INFLUENCE OF PLY THICKNESS ON DAMAGE ACCUMULATION
AND FINAL FAILURE*

F. W. Crossman and W. J. Warren
Lockheed Palo Alto Research Laboratory
Palo Alto, CA 94304

and

A. S. D. Wang
Drexel University
Philadelphia, PA 19104

*Paper presented to ASME Winter Annual Meeting, Boston,
November, 1983.

Advances in Aerospace Structures, Materials and
Dynamics, ASME AD-06, 1983, pp. 215 - 226.

INFLUENCE OF PLY THICKNESS ON DAMAGE ACCUMULATION AND FINAL FRACTURE

F. W. Crossman and W. J. Warren
Applied Mechanics Laboratory
Lockheed Palo Alto Research Laboratories
Palo Alto, CA 94304

and

A. S. D. Wang
Department of Mechanical Engineering and Mechanics
Drexel University
Philadelphia, PA 19104

ABSTRACT

This paper examines the sequence of sub laminate fracture and the damage state which exists just prior to laminate failure under tensile loading. Tests were conducted on T300/934 symmetric laminates of $[\theta, -\theta, 90]_s$ type, in which the thickness of the 90 degree ply varies from 2 to 16 plies and the angle "theta" takes on values of 0, 25, 30, and 60 degrees. Incremental tensile loading followed by DIB enhanced x-radiography is the primary means of documentation. Deploying experiments and real-time x-ray radiography during tensile loading are also described. Failure sequence and mode are shown to change with stacking sequence and ply thickness in a manner which supports a model of fracture based on a through-the-thickness local redistribution of stress to the primary load carrying ply.

INTRODUCTION

This paper presents a detailed investigation of the sub-laminate fracture modes which exist just prior to laminate fracture in a series of laminates of the $[\theta/\theta/90]_s$ family where the angle "theta" takes on values of 0, 25, 30, 60 degrees. This paper has been preceded by a series of experimental and analytical studies which have addressed the fracture of unnotched tensile coupons of the T300/934 graphite-epoxy material. Previous experimental investigations have included the documentation of fracture mode and sequence of fracture in quasi-isotropic $[0/90/45/-45]_s$ laminates by metallographic means [1] and the description of fracture sequence in $[25/-25/90]_s$ laminates by radio opaque dye penetration of edge cracks and x-radiography [2].

Transverse cracking of the 90 deg and off axis plies and delamination at the free edges of the coupon were observed to occur at tensile loads sufficiently lower than the ultimate strength that these fracture modes could be viewed as important precursors to laminate fracture. Analytical methods based on strain energy release rate [3] and stochastic processes [5] have been successful in predicting the onset and accumulation of transverse cracks under both static and cyclic loading. The utility of strain energy release rate analysis to predict the onset of free-edge delamination and local delamination induced by transverse cracking has also been established under tensile loading conditions [4]. However, more recent analyses of delamination under fatigue cycling [6,7] have demonstrated that delamination growth under mixed mode crack opening is not simply related to knowledge of delamination initiation and growth under Mode I crack opening and static loading conditions.

The detailed analysis of transverse cracking and isolated delaminations provide examples of what Reifsnider and colleagues have termed the "inductive" approach to composite failure analysis [8]. This approach requires that the analytical models account for the detailed experimentally observed micro-structural fracture processes for their interaction. A detailed review and historical perspective of the experimental observations and analytical modeling of laminate fracture under static and cyclic loads is provided in [8].

An important corollary to the inductive approach is that SOME of the observed sub-laminate fracture modes may not have to be modeled and analyzed in detail if the prediction of final laminate fracture is of primary concern [12]. What is needed is a fracture model which accounts for the development of the sub-laminate fracture condition ("damage state") which exists just prior to fracture and an understanding of why that condition is critical.

The purpose of this paper is to document the sequence of sub-laminate fracture processes and to describe the final damage state of a series of simple laminate constructions. The results of this study indicate a strong dependence of that final state on fiber angle, ply thickness, and stacking sequence. With few exceptions, the final fracture event is triggered not by a sharp stress concentration but by a stress redistribution between plies in a region that is small compared to the size of the coupon.

EXPERIMENTAL PROCEDURE

Laminates were fabricated from Fiberite T300/934 prepreg tape and autoclave cured at 450 K according to the manufacturer's recommended cure procedure. Nominal fiber volume ranged from 64 to 68 percent, and ply thickness ranged from .0119 to .0127 cm. The 30 cm by 30 cm panels were cut by diamond saw to a coupon length of 22.5 cm and a width of 2.5 cm. Fiber-glass tabs of length 3.75 cm were bonded to each end of the coupon. Coupons

were stored at ambient laboratory conditions (20-23 deg. C and 55-65 percent humidity) and tested 6-12 months after fabrication. All tests were conducted on an Instron Test Machine at a controlled displacement rate of 25mm/mm. An average ultimate tensile strength for each type of laminate was determined by ramp tension testing of two replicas. Stress strain curves were based on the measured output of 1/4 in. EA-13-125TM-120 type strain gages.

Three to five replicas of each laminate type were step loaded to approximately 50, 70, 80, and 90 percent of the average UTS, and then, based on the audible cracking which the experienced operator observed, the coupon was step loaded in progressively smaller increments to failure. The first load step was chosen to coincide with the onset of transverse cracking as determined in previous studies [2, 11]. At least two coupons of each series were step loaded to between 97-99 percent of UTS and examined prior to final failure. The total number of step loadings varied between 5 and 10 for a given coupon.

The examination after each step loading and unloading consisted of (1) removing the coupon from the tensile tester, (2) swabbing the edges of the coupon with di-iodobutane (DIB) solution to penetrate the cracks, (3) wiping off the excess DIB after 30 s, and (4) placing the coupon atop a Polaroid film (Type 55 Positive/Negative ASA 50) in a Faxatron 804 point source x-ray chamber for a 1.25 min. exposure at 30 KV. Following the x-ray exposure the specimen was optically examined on edge at 30X to document the through-the-thickness location of ply cracks and delamination.

Several coupons of $[0/0/90_n]_s$ ($n=1, 2, 4, 8$) and $[25/-25/90_n]_s$ ($n=8$) were depled following tensile loading to 70 percent of UTS. The depleting procedure developed by Freeman [9] was used and consisted of heating to 700 K for 1.25 hrs to facilitate the separation of the plies. Depled 0 and 25 deg. layers were then examined under scanning electron microscopy (SEM) for damage to the

fibers in the load carrying plies.

Several coupons of $[25/-25/90_n]_s$ ($n=8$) type were examined under real-time x-ray exposure during tensile loading. The Lockheed HERTIS (High Energy Real Time Inspection System) facility was used for this purpose. The system consisted of a 45KV/10mA soft x-ray source with a 4mm focal point on one side of the coupon being loaded in a portable 5000 lb (22. 2kN) hydraulic test frame and fluorescent screen and vidicon tube to pick up the x-ray image on the other side of the coupon. At increments of 20 percent of the specimen UTS, the specimen was unloaded and the coupon edges were coated with DIB X-ray enhancing penetrant. Two vidicon tubes capable of imaging a 1 by 1 cm and 12 by 12 cm area respectively were used in the experiments. The vidicon signal was then digitally processed and signal enhanced for viewing in real time and on a video tape system.

EXPERIMENTAL RESULTS

Method of Presentation

The cataloging of x-ray and optical observations of sub-laminate fracture of the laminate series tested in this program resulted in hundreds of individual photographs which provide a snapshot of damage accumulation and which, taken as a whole, provide some measure of failure mode and sequence variability within a given laminate construction.

In the presentation of these results we have chosen to represent the damage state obtained just prior to laminate failure by a set of schematic drawings and graphs which succinctly compare the accumulation of damage within a given series of similar laminates.

Fig. 1 presents a summary of fracture sequence in $[0/0/90_n]_s$ ($n=1, 2, 4, 8$) laminates. The diagram labeled (A) in Fig. 1(a) represents the center portion of the gage length of the $n=1$ type tensile coupon as recorded on the DIB enhanced

x-radiograph. The tensile axis is vertical and the width direction is horizontal in this view.

The diagram labeled (B) in Fig. 1(a) depicts a view of the specimen edge. The tensile axis is vertical and the through-the-thickness direction is horizontal in this view. The dotted lines indicate ply boundaries at the (0/0) and (0/90) ply interfaces. In subsequent schematics the (θ/θ) and ($-\theta/90$) boundaries are dotted.

The third diagram labeled (C) in Fig. 1(a) presents an optical view of the gage length of the specimen after laminate fracture. The tensile axis is vertical and the width direction is horizontal in this view.

To the right of these three diagrams is a graph in histogram form containing the range of onset stresses for each of several individual sub-laminate fracture modes. All four graphs in Fig. 1 have the same horizontal stress scale to facilitate a comparison of fracture sequence and to provide the developer of fracture process models with some sense of the interaction between fracture modes within a given family of laminates. The onset data for a given fracture mode is displayed at progressively higher vertical positions on each graph according to the order in which each occurs during tensile loading.

$[0_n/90_m]_s$ Laminates.

Fig. 1 summarizes the sub-laminate fracture sequence in a series of $[0_n/90_m]_s$ laminates where $n=1,2,4,8$. The damage noted by (1) in Fig. 1(a) denotes transverse cracking which occurs early during tensile loading of all four laminates. The damage mode noted by (2) in Fig. 1(b) indicates the presence of local delamination at the $[0/90]$ interface which accompanies the initiation of 90 deg transverse cracks. These local delaminations are observed to initiate more frequently at stresses approaching the UTS of the laminate. The first transverse cracks which initiate do not exhibit this characteristic delamination.

The damage near note (3) in Fig. 1(d) denotes the presence of transverse cracks in the 0 deg. ply. Under tensile loading only the $n=8$ laminates were found to exhibit this ply splitting mode. Reifsnider et al. [8] have found splitting to be much more common in $[0/90]_s$ type laminates during fatigue cycling.

Examination of the final fracture diagrams in Fig. 1 indicates that the amount of 0 deg. layer splintering increases as n increases. This observation is consistent with the increased delamination between the 0 and 90 deg. plies for increasing n . The $n=8$ shattering of the 0 deg. plies closely resembles the fracture mode of unidirectional 0 deg. tensile specimens. With the exception of the 0 deg. splitting in the $n=8$ laminate, there is no obvious precursor to failure of the load carrying ply. The initiation and accumulation of transverse cracks in the 90 deg. ply appears to have little influence on the failure of the 0 deg layer in all of the other laminates.

Fig. 2 presents a summary of incremental tensile tests conducted on a general series of $[0_n/90_m]_s$ laminates in which the 0 deg. layer was located at either the surface (a,c,d) or midplane (b). While the onset for transverse cracking is clearly influenced by temperature (due to altered thermal residual stresses [11]), the results in Fig. 2(c) show no similar temperature dependence of UTS. Indeed, the only case where a lower than expected UTS occurs is in the testing of the $[0/90/0]$ laminate. As shown in Fig. 2(d) it is the only laminate in which transverse cracking is not observed prior to failure.

Fiber damage has been observed in deplie 0 deg. layers at the tip of transverse 90 deg. cracks in fatigue loaded specimens [8]. In this study $[0/0/90_n]_s$ $n=8$ laminates were deplie after tensile loading to 70 percent of UTS and examined for fiber damage. The results shown in the Fig. 3 SEM photographs indicate that far less than one percent of 0 deg. fibers are broken in the vicinity

of transverse cracks under static loading. The possibility exists, however, that the initiation of a new 90 deg. crack at higher stresses could trigger the sufficient fiber damage that the 0 deg. layer fails prematurely, since the energy release rate from transverse cracking increases with the square of the stress [3].

$[25/-25/90]_n$, n=2,8 Laminates

Fig. 4 summarizes the sub-laminate fracture of $[25/-25/90]_n$ laminates tested in this program. A more extensive summary including n=1/2,1,3,4,6 laminate types is found [2]. The region marked by (1) in Fig. 4(a) denotes the prevalent free-edge delamination which is at the -25/90 interface. Delamination initiates at load very close to UTS but incremental loading of these laminates shows that it is the initiation of 25 deg. transverse cracking denoted by (2) in Fig. 4(b) that triggers the final failure.

In Fig. 5(a) one can observe dark horizontal bands on the 25 deg. fiber layer in locations where x-rays taken prior to failure indicated the presence of transverse cracks and local -25/90 interface delamination. These regions are marked by (1) in Fig. 5(a). Examination of the 25 deg. ply surface in these regions by SEM shows that the bands are caused by the pattern of resin adherence and do not show any damage to the fibers. This observation was verified by examination of depled n=8 laminates as well.

HERTIS real time x-ray experiments were conducted on $[25/-25/90]_n$ n=8 laminates loaded in tension. In Fig. 5(d) a video image of one specimen at 99 percent of ultimate load indicates the presence of a 90 deg. transverse crack and an associated [-25/90] local delamination at location (2) in the figure.

Stop action playback of the video taped failure of this specimen showed that the final fracture occurred at this location by the propagation of a crack transverse to the tensile axis from the edge toward the center of the specimen. After propagating by fiber breakage to about half way across the specimen the

remaining 25 deg. layers failed by shearing parallel to the 25 deg. fiber axis. Thus the critical event appears to involve sufficient load redistribution into the uncracked 25 deg. ply that fiber failure can be triggered and propagate transverse to the tensile axis.

$[30/-30/90_n]_s$ and $[60/-60/90_n]_s$ Laminates

Figs. 6 and 7 summarize the results of incremental tensile testing of $\theta = 30$ deg. and $\theta = 60$ deg. laminates. Transverse cracking in these laminates occurs irregularly and most often in association with the initiation of another fracture mode as at location (1) in Figs. 6 and 7. The transverse cracking of the 30 degree plies near the free edge of the laminate is found to accompany the initiation of free-edge delamination at the $-30/90$ interface as at locations (2) in Fig. 6. In many cases the transverse 30 degree crack causes a local delamination at the $30/-30$ interface and then transverse cracking of the -30 deg. ply. With the exception of 90 deg. transverse cracking, all of these events occur very near the UTS of this laminate. The highest density of 90 degree transverse cracks are located under the delaminated edges.

In $n=1$ laminates transverse cracking is virtually absent prior to failure. Furthermore, the delamination plane runs randomly through the 90 deg. layer, while for $n=2,4,8$ the $-30/90$ interface is the preferred plane.

In the $\theta=30$ deg. laminates, the final fracture is by propagation of a fiber breaking crack transverse to the tensile axis accompanied by a small percentage of shear out of 30 deg. layers near the edge of the coupon.

In $\theta=60$ deg. laminates, the critical fracture event changes from the initiation of a 60 deg. transverse crack for $n=1,2$ to the initiation of a 90 deg. transverse crack in $n=4,8$ laminates. In either case the presence of the first transverse crack in one ply triggers the initiation of several transverse cracks in the other type of ply.

In the $n=4$ laminate the 90 deg. crack triggers only internal splitting

of the -60 and 60 layers which are observed after the DIB penetrates to these cracks along the 90 transverse crack which is open to the coupon edge. This is noted at location (2) in Fig. 7.

For $n=1, 2$ the final failure occurs by propagation of the transverse crack in the outer 60 deg. ply and a fiber breaking crack transverse to the tensile load in the -60 deg. ply. In $n=4, 8$ the failure is almost entirely due to shear of the 60 deg. layers with very little fiber breakage,

Closer examination of the fracture patterns in Figs. 4, 6, and 7 shows that the distribution of transverse cracking and delamination along the gage length of the specimen is very irregular. It is unlikely that strain measurement via a single small strain gage or global strain measurement via extensometers spanning the gage length can provide sufficient information regarding the local redistribution of stresses due to the interaction of these fracture modes. The "stiffness" changes associated with the $[\theta/-\theta/90]_s$ family of laminates are clearly highly dependent on the location and size of the zone over which strain is measured.

Effect of 90 deg. Ply Thickness

If stiffness measurements provide little of value in assessing the fracture criterion for these $[\theta, -\theta, 90]_s$ laminates, we are left with a need to detail the degree of local damage and determine whether the undamaged plies at a given cross-section of the laminate can carry the entire tensile load. It is important to understand that cracked plies can still carry some load even in a direction normal to the crack plane. The density of transverse cracks in the region of greatest damage in the $[\theta, -\theta, 90]_s$ laminates is high just prior to laminate fracture. Fig. 8 plots the inverse of crack density normalized to the thickness of the 90 deg. ply. Most of the laminates tested have S/T values between 1-2.

Finite element analyses [10, 12] of cracked 90 deg. layers in a $[0/90]_s$ laminate have shown that the effective transverse modulus of the 90 deg. layer is reduced to 0.65 of its initial value at $S/T = 2.0$ and to 0.40 at $S/T = 1.0$. Furthermore, if the transverse cracks cause a local delamination at the theta/90 interface the 90 deg. ply is more fully isolated from the theta load carrying plies.

On the basis of these results and the observed high density of transverse 90 cracks, it is realistic to consider that the tensile load carried by the 90 deg. plies is very small compared to that carried by the theta plies. This assumption is borne out when the ultimate tensile load is plotted for each of the laminate sequences in this study, as shown in Fig. 9. For $n=1, 2, 4$ there is very little dependence of ultimate load on the thickness of the 90 deg. ply. For $\theta = 0, 25$ deg. and $n=8$ there is a drop in load carrying ability, while for $\theta = 30, 60$ and $n=8$, the load carrying ability is slightly enhanced. The existence of large regions of locally delaminated theta/90 interface in the $\theta = 0, 25$ deg. and $n=8$ laminates is a possible cause of the observed degradation.

Stacking Sequence Studies in $[25/-25/90]_s$

To further investigate the concept of local stress redistribution as a model for predicting final failure, a series of laminates were prepared from the $[25/-25/90]_s$ family and incrementally tensile tested by the procedures already described. The laminate sequences tested are shown in Fig. 10(a-d). Because of differences in stacking sequence, the edge view diagrams for cases (a, c, d) must be explained. In Fig. 1(a) the layup has no 90 deg. ply and the transverse cracks drawn across the center layer in the diagram are simply to connect the transverse cracks which are continuous across the inner -25 layers. In Fig. 10(c, d) the outer layer is taken to be only the outer 25 deg.

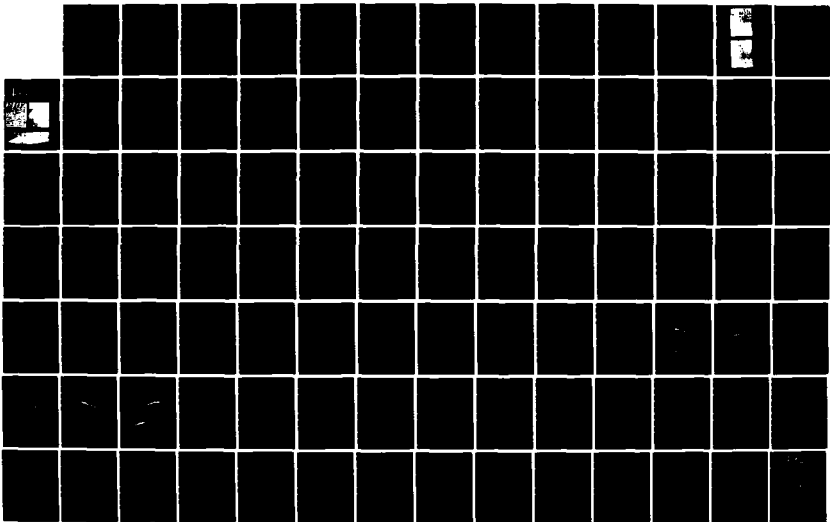
AD-A149 037

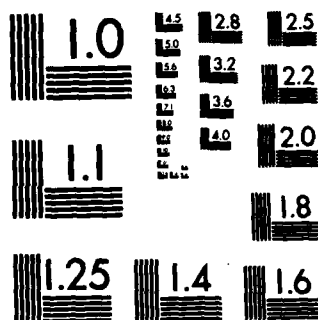
A COMPREHENSIVE STUDY ON SUBLAMINATE CRACK GROWTH
STABILITY AND ITS EFFEC. (U) DREXEL UNIV PHILADELPHIA
PA DEPT OF MECHANICAL ENGINEERING AN. A S WANG ET AL.
MAR 84 AFOSR-TR-84-1127 F49620-79-C-0206 F/G 11/4

2/2

UNCLASSIFIED

NL





ply, the next dotted layer actually contains the next three 25 type plies, and the center layer is the 90 ply.

The layups in Fig. 10(a) and 10(b) contain double layers of 25 deg. plies adjacent to each other. In an earlier study [2] the doubling up of 25 deg. plies resulted in altering the failure mode from one of fiber breakage to one of transverse cracking and shear out parallel to the 25 deg. fiber axis. These results were duplicated here for cases (a) and (b).

In the $[25/25/-25/-25]_g$ laminate, the critical fracture event was the initiation of a single transverse crack in the outer 25 deg. ply. This was followed immediately by a fine transverse splitting of the inner two plies of -25 deg. and subsequent shear out of the remaining 25 deg. ply.

The $[25/25/-25/-25/90/90]_g$ laminate developed a high density of transverse 90 deg. ply cracks early in the tensile loading, followed by the initiation of -25/90 delamination at the free edge and a rapid unstable propagation of delamination toward the specimen centerline from both edges. The speed with which the delamination growth takes place is evident in the waviness of the final delamination front near the centerline of the specimen. Earlier studies [3, 4] have shown that the driving force (strain energy release rate) drops off rapidly as the delamination approaches the center line thus allowing this region to remain undelaminated until final laminate fracture.

The stacking sequences in (c) and (d) show the same early failure modes of transverse cracking of the 90 deg. ply and 25/90 interface delamination. As in laminate (b) the outer 25 degree ply tends to transverse crack near the coupon free edges. However, in the case of (c) and (d) a local delamination is formed between the outer 25 deg. ply and the inner 25 deg. plies and transverse crack do not form in the adjacent -25 deg. ply. Because the cracks in the outer 25 deg. ply are isolated from the adjacent 25 deg. plies by local

delamination, further ply degradation is inhibited until another 5-10 KSI is carried by the laminate. As a result, laminates (c) and (d) have a higher UTS than laminate (b) and exhibit a mode of failure dominated by fiber breakage rather than shear out.

Fig. 11 provides a summary of the range of ultimate loads carried by the four laminates described in Fig. 10. If one compares the $[25/25/-25/-25]_s$ results for $[25/25/-25/-25/90/90]_s$, the addition of the 90 layer contributes little to the tensile load carrying ability of the laminate, as observed in the $[\theta, -\theta, 90]_s$ series. However, when the 25/-25 plies are alternated as in the second two layups, one finds that the load carrying ability of the laminate is significantly improved. The onset stresses for each of the three fracture modes in the latter two layups (c) and (d) in Fig. 10 show no significant differences, yet the sequence (d) which provides a symmetric $[25/-25/-25/25]$ layer on each side of the 90 layer show significantly higher load carrying capacity. It is postulated that some loss of strength is associated with the twisting of the non-symmetric layup $[25/-25/25/-25]$ in a region where it is effectively debonded from the 90 degree ply because of the extensive edge delamination.

CONCLUSIONS

It is not the purpose of this paper to provide a detailed comparison between the experimental observations of fracture sequence and analytical models for prediction of the initiation and growth of specific fracture modes. The references cited in this paper provide information on the more successful approaches to modeling individual fracture modes. Rather we have concentrated on the documentation of the interaction of fracture modes immediately prior to failure and the differences in the modes and their interaction within a given series of laminates.

From the observed diversity of fracture mode type and interaction found in this series of laminates, it is difficult to conclude that any analytical model which accounts for fracture mode initiation and growth and the interactions of modes in a given laminate can be applied "a priori" to predict the tensile strength of a different layup sequence. The detailed modeling of failure mode interactions provides primarily a quantitative understanding of the mechanics of that interaction and a confidence that a particular mode interaction resulting in lower strength or stiffness will not occur.

With the exception of the $[25/-25/25/-25/90/90]_s$ and $[25/-25/-25/25/90/90]_s$ laminates and laminates containing very thick 90 deg. plies, the strength of these $[\theta, -\theta, 90]_s$ laminates is found to be very simply estimated by ignoring stress concentrations associated with transverse cracking and delamination and assuming that, near the UTS, the load will be carried entirely by the primary load carrying ply. The plots of ultimate load in Figs. 9 and 11 bear this out.

If one assumes that eventually all of the tensile load is redistributed onto the primary load carrying plies, a lower bound on strength can be established. For more complex laminates like the $[0/45/-45/90]_s$ family this assumption will be very conservative for certain stacking sequences in which delamination is not observed under static tension [1]. On the other hand, this lower bound estimate of strength was successfully utilized by Ryder [12] to predict the tension-tension fatigue life and strength of quasi-isotropic laminates.

The results described in this paper reinforce the argument that some detailed experimental observations of the particular fracture sequence in a given laminate are clearly necessary for accurate strength prediction, although the trends observed in a similar laminate construction may be sufficient to place some useful bounds on the predicted strength.

ACKNOWLEDGEMENTS

This work was performed at the Lockheed Palo Alto Research Laboratories through a sub-contract from Drexel University under Air Force Office of Scientific Research, Contract F49620-79-C-0206.

REFERENCES

- [1] Bjeletich, J. G., Crossman, F. W., Warren, W. J., "The Influence of Stacking Sequence on Failure Modes in Quasi-Isotropic Graphite-Epoxy Laminates", Failure Modes in Composite IV, AIME, 1979, p. 118
- [2] Crossman, F. W. and Wang, A. S. D., "The Dependence of Transverse Cracking and Delamination on Ply Thickness in Graphite-Epoxy Laminates", ASTM STP 775, 1982, p. 118
- [3] Wang, A. S. D. and Crossman, F. W., "Initiation and Growth of Transverse Cracks and Edge Delamination in Composite Laminates", J. Comp. Mat., Suppl Vol. 14, 1980, p. 72
- [4] Law, G. E., "The Fracture Behavior of $[25/-25/90_n]_s$ Graphite-Epoxy Composite Laminates", ASTM Symposium on the Effects of Defects in Composite Materials, San Francisco, Dec. 1982, To be published as ASTM STP in 1983
- [5] Wang, A. S. D., Chou, P. C., Lei, S. C., "A Stochastic Model for the Growth of Matrix Cracks in Composite Materials" Proc. Symposium on Mechanics of Composite Materials and Structures, ASME WAM, Boston, Nov. 1983
- [6] O'Brien, T. K., "Mixed Mode Strain-Energy Release Rate Effects on Edge Delamination of Composites", ASTM Symp. on Effects of Defects in Composite Materials, San Francisco, Dec. 1982, To be pub. as ASTM STP in 1983
- [7] Ramkumar, R. L., "Performance of a Quantitative Study of Instability-Related Delamination Growth", NASA Contractor Report 166046, March 1983
- [8] Reifsnider, K. L. and Jamison, R. D., "Advanced Fatigue Damage

Development in Graphite Epoxy Laminates", AFWAL. TR-82-3103 December 1982

[9] Freeman, S. M., Damage Progression in Graphite-Epoxy by a De-plying Technique", AFWAL-TR-81-3157, Dec. 1981

[10] O'Brien, T. K., Ryder, J. T., and Crossman, F. W., "Stiffness, Strength, and Fatigue Life Relationships for Composite Laminates", Proc. Seventh Annual Mechanics of Composites Review, Oct. 1981

[11] Flaggs, D. L. and Kural, M. H., "Experimental Determination of the In-Situ Transverse Lamina Strength in Graphite-Epoxy", J. Comp. Mat., Vol 16, 1982, p. 103

[12] Ryder, J. T. and Crossman, F. W., "A Study of Stiffness, Residual Strength, and Fatigue Relationships For Composite Laminates", NASA CR 172211, Oct. 1983

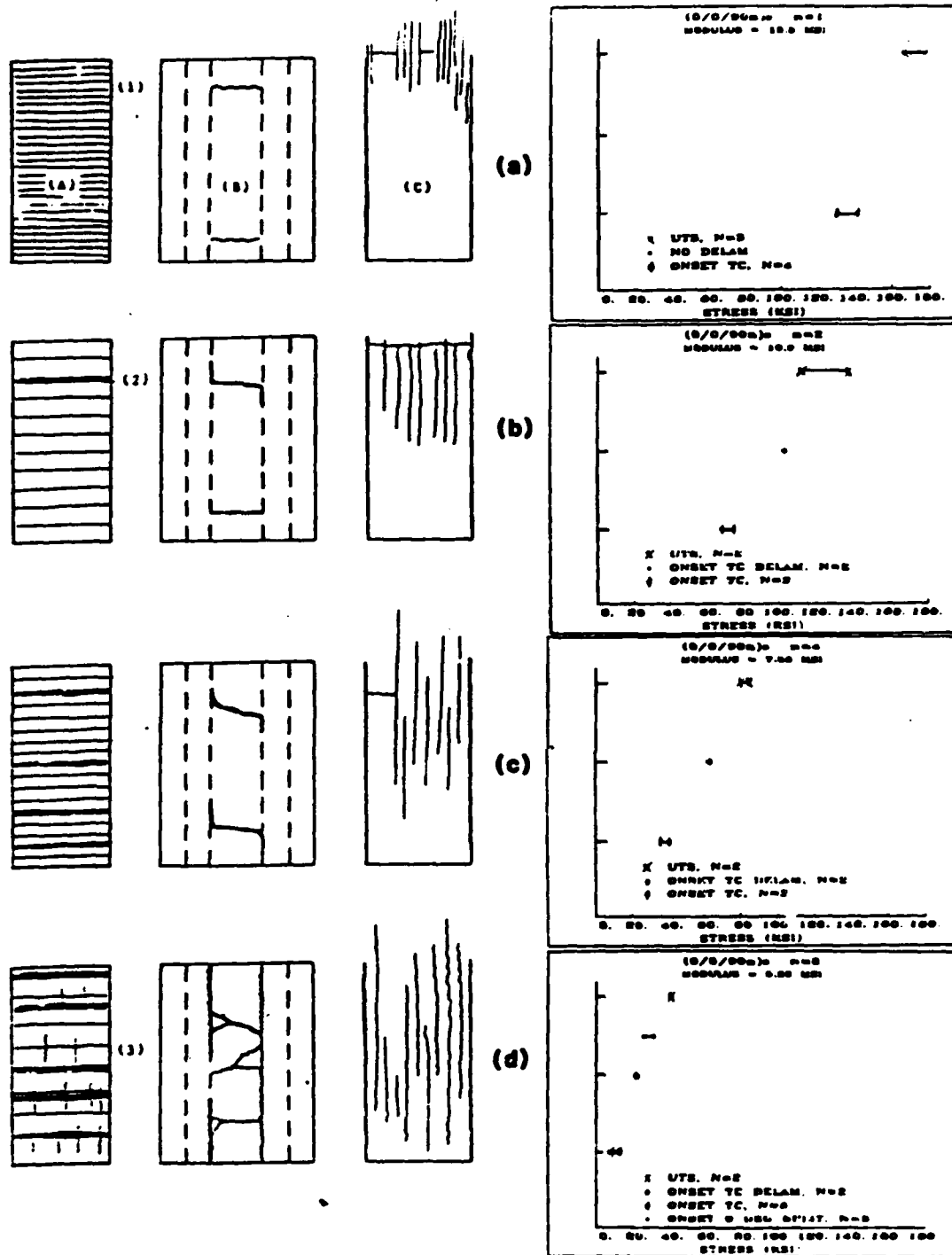


Figure 1. Sequence of Fracture in $(0_2/90_n)_s$ Laminates. (a) $n = 1$; (b) $n = 2$; (c) $n = 4$; (d) $n = 8$.

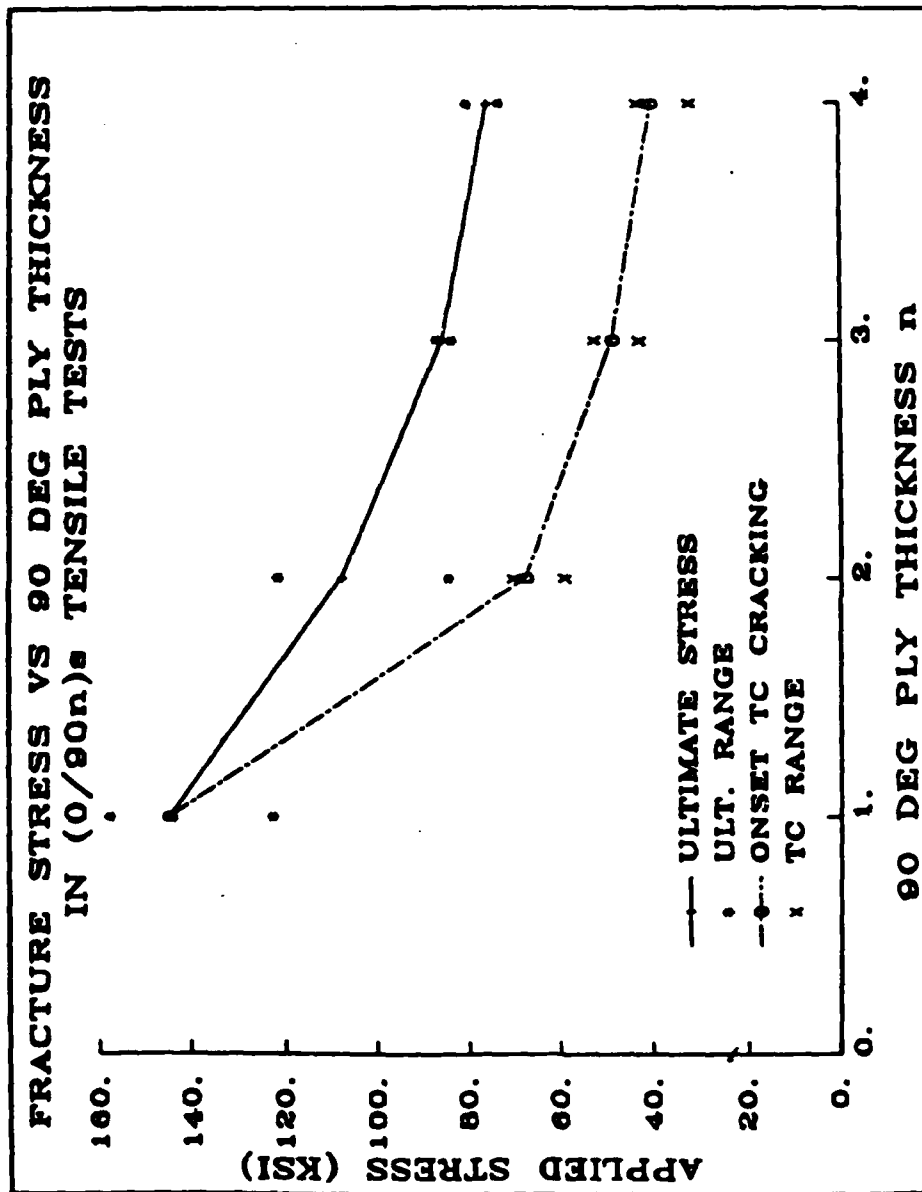


Figure 2(a) 90-Degree Ply Cracking(TC) Onset Stress and Ultimate Tensile Strength As Influenced by the Thickness of the 90-Degree Layer.

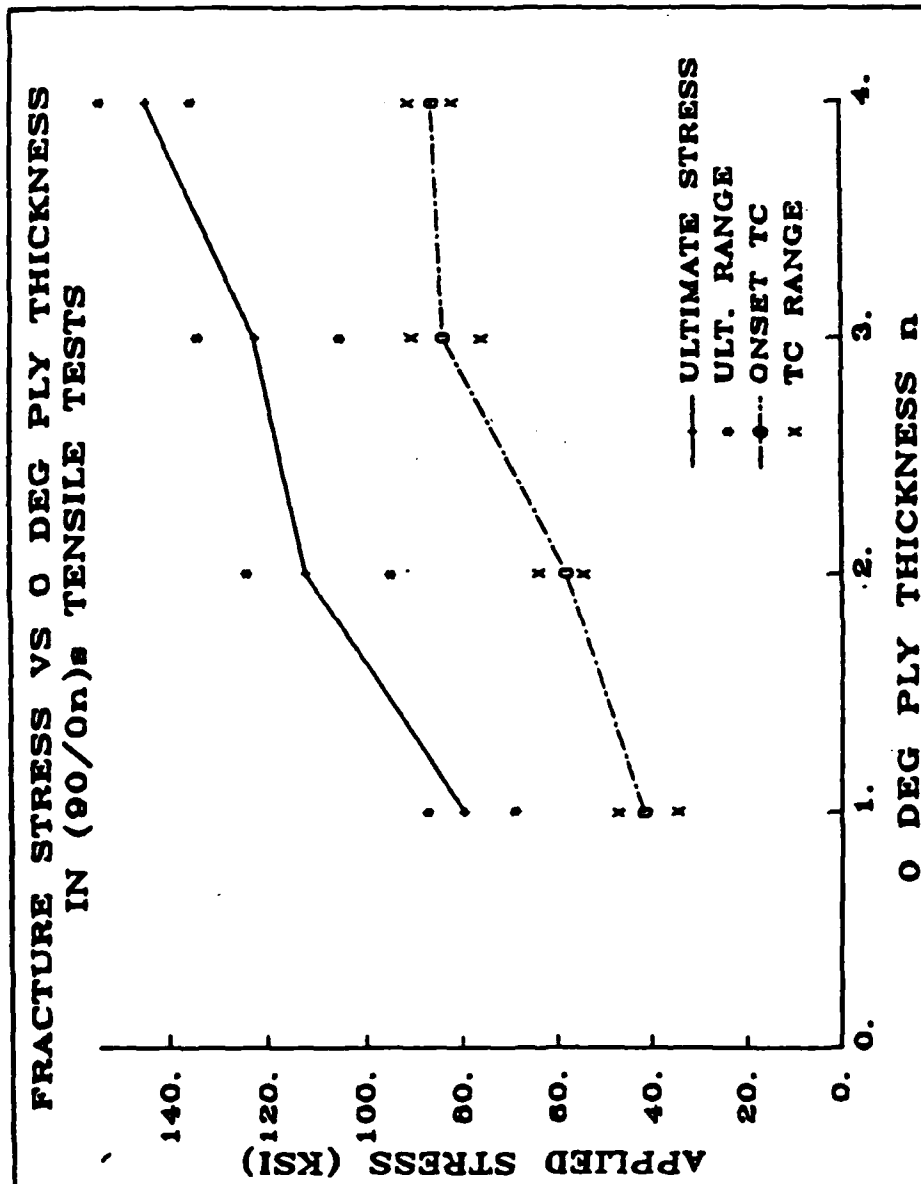


Figure 2(b) 90-Degree Ply Cracking(TC) Onset Stress and Ultimate Tensile Strength As Influenced by the Thickness of the 0-Degree Layer.

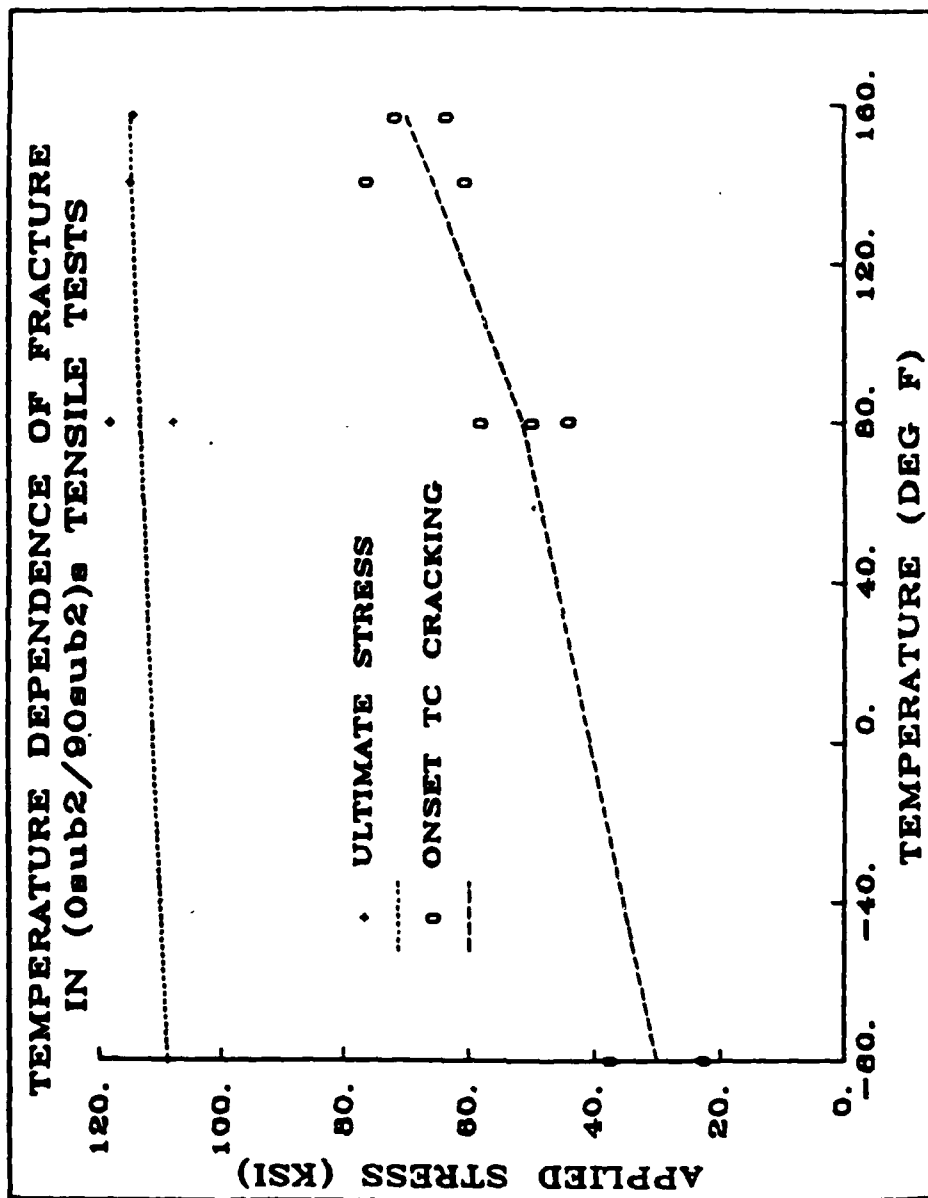


Figure 2(c) 90-Degree Ply Cracking(TC) Onset Stress and Ultimate Tensile Strength As Influenced by Temperature.

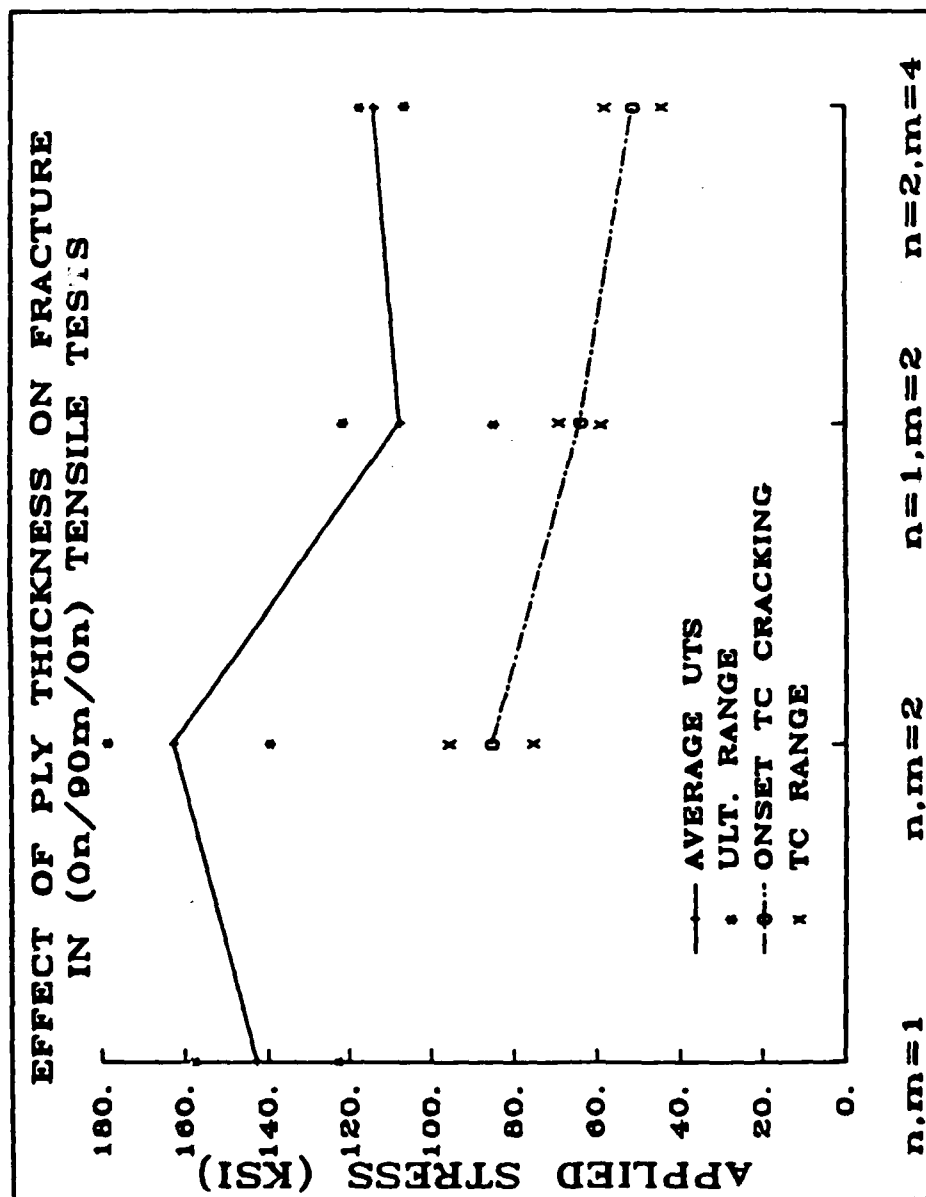
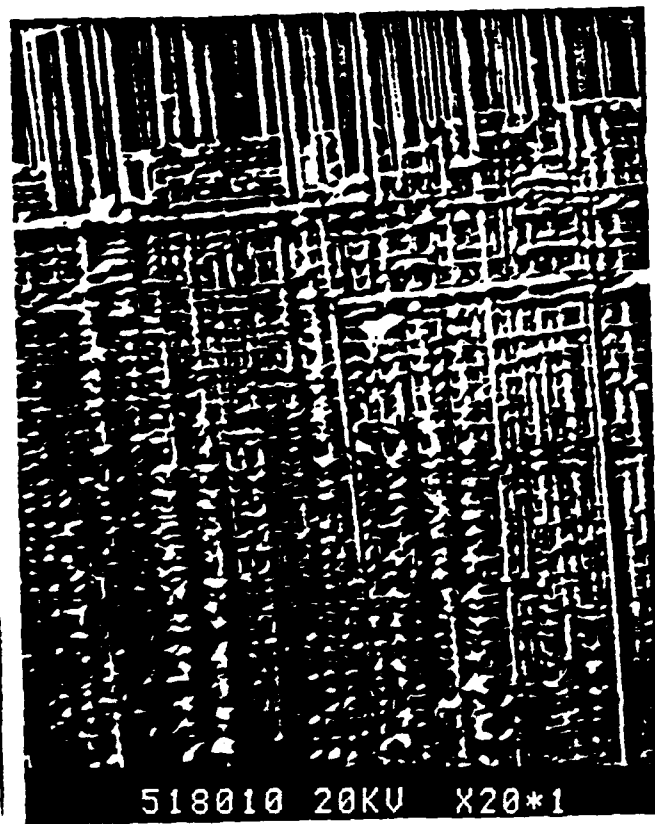


Figure 2(d) 90-Degree Ply cracking(TC) Onset Stress and Ultimate Tensile Strength; Summary.



(a)



(b)

FIG. 3 SEM Microscopy at (a) 20X and (b) 200X of a 0 deg layer of a (0sub2/90sub8)s T300/934 Laminate Loaded to 70 Percent of UTS Prior to Deploying

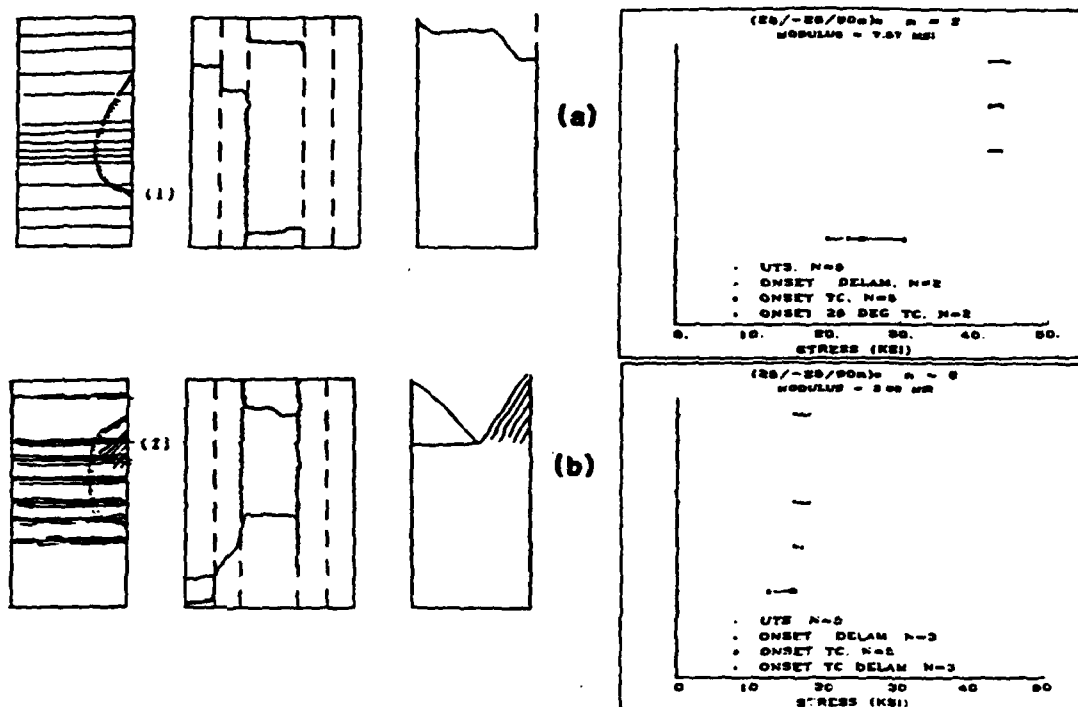
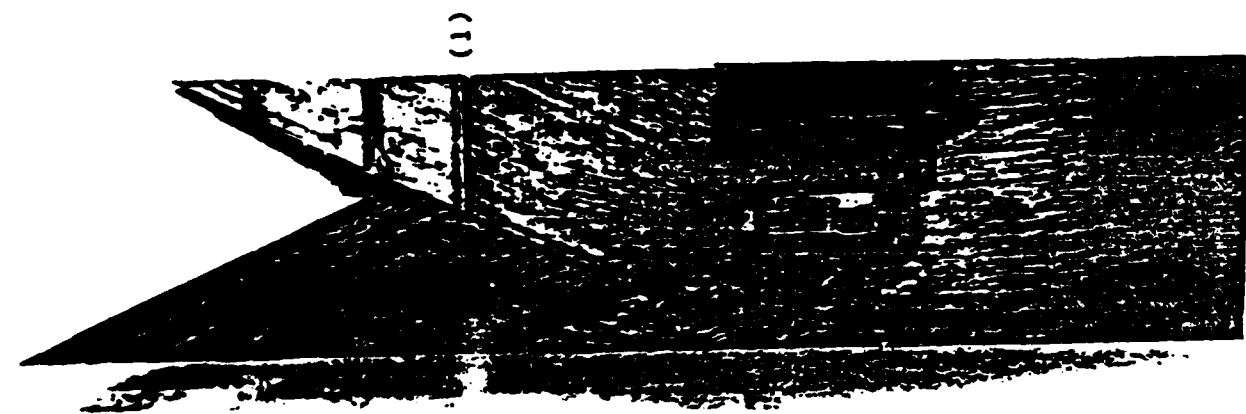
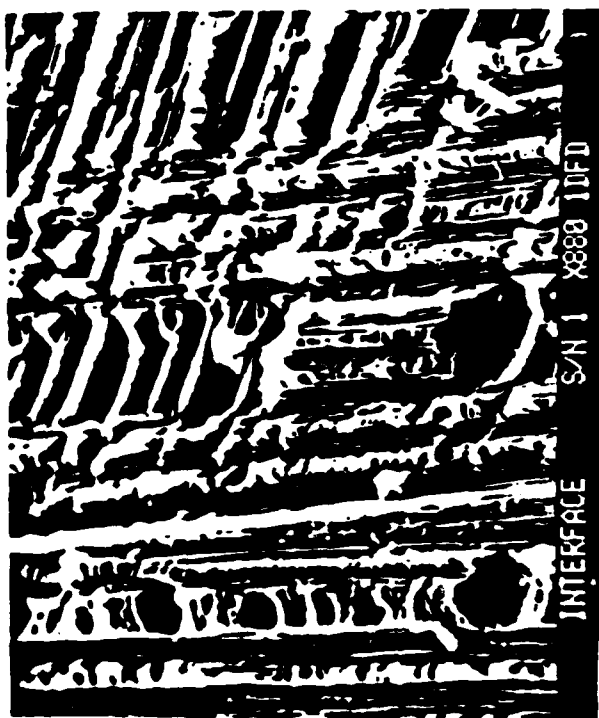


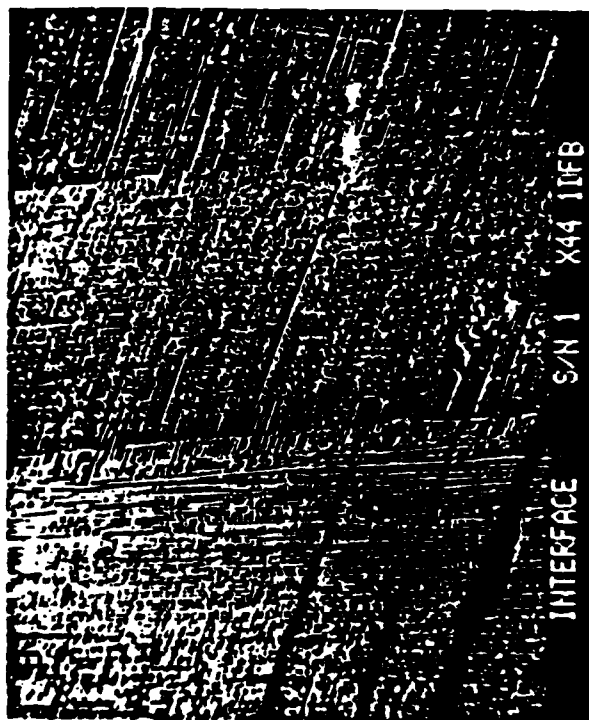
Figure 4. Sequence of Fracture in $(25/-25/90)_n$ Laminates. (a) $n = 2$;
(b) $n = 8$.



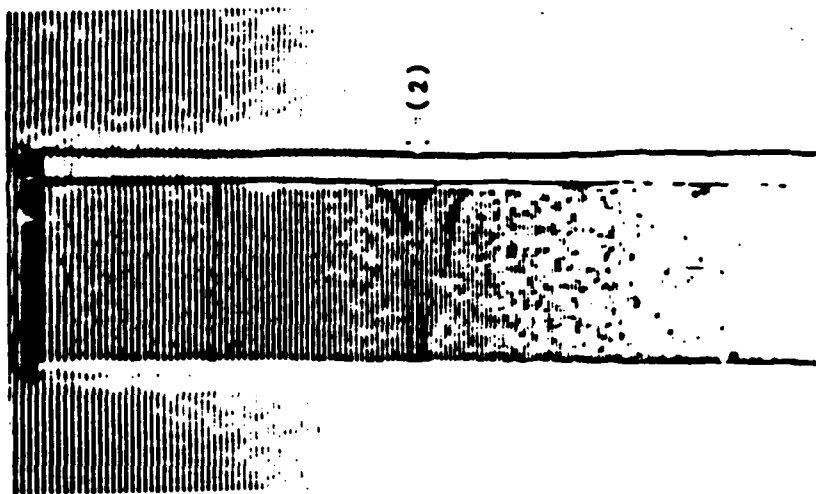
(a)



(c)



(b)



(d)

FIG. 5 Macroscopic View (a), SEM Photographs at (b) 44X and (c) 880X, and HERTIS Scan (d) of the (25/90) Delamination at the tip of 90 deg. TC's in a (25/-25/90sub8) T300/934 Laminate Loaded to Failure

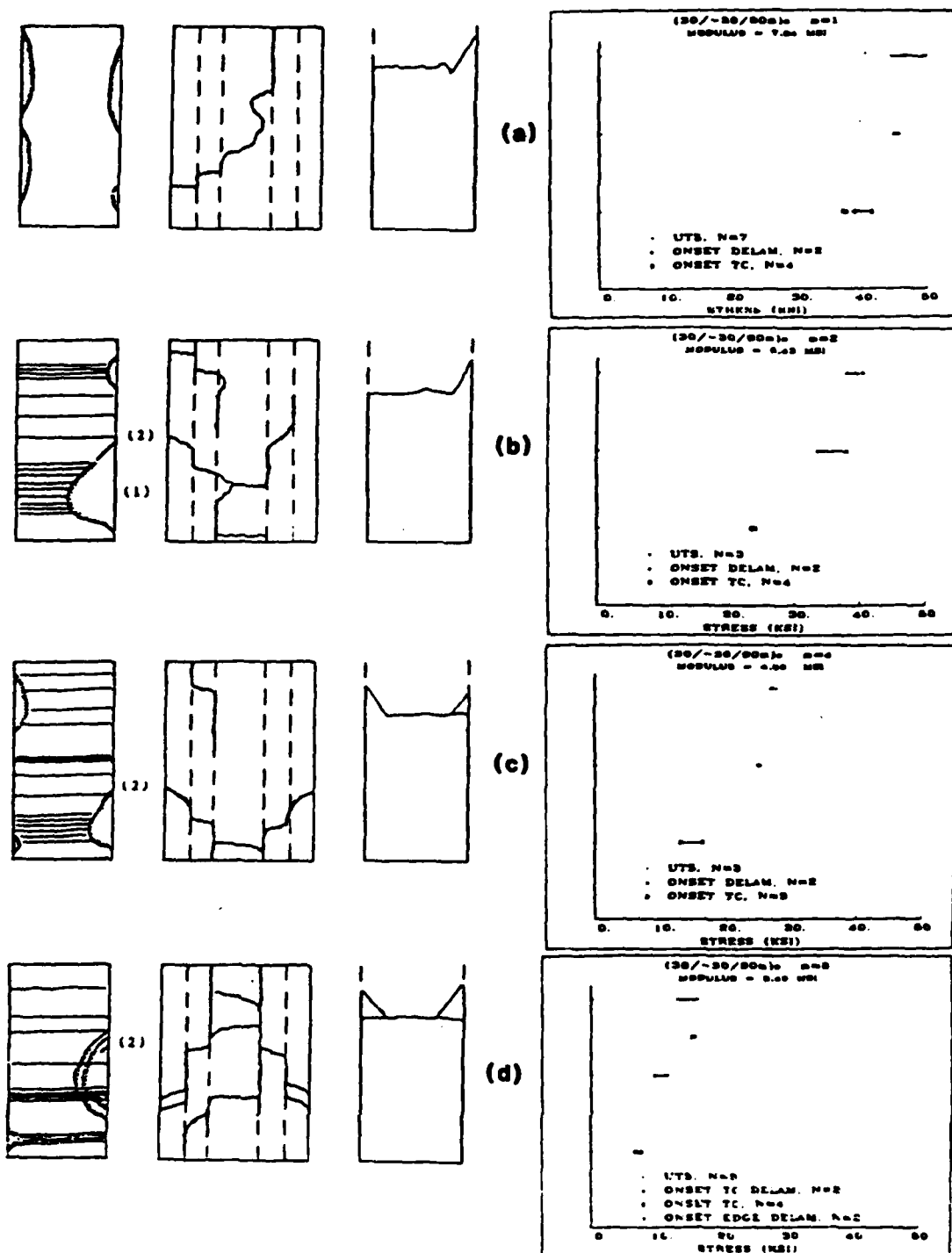


Figure 6. Sequence of Fracture in $(30/-30/90)_n$ Laminates. (a) $n = 1$; (b) $n = 2$; (c) $n = 4$; (d) $n = 8$.

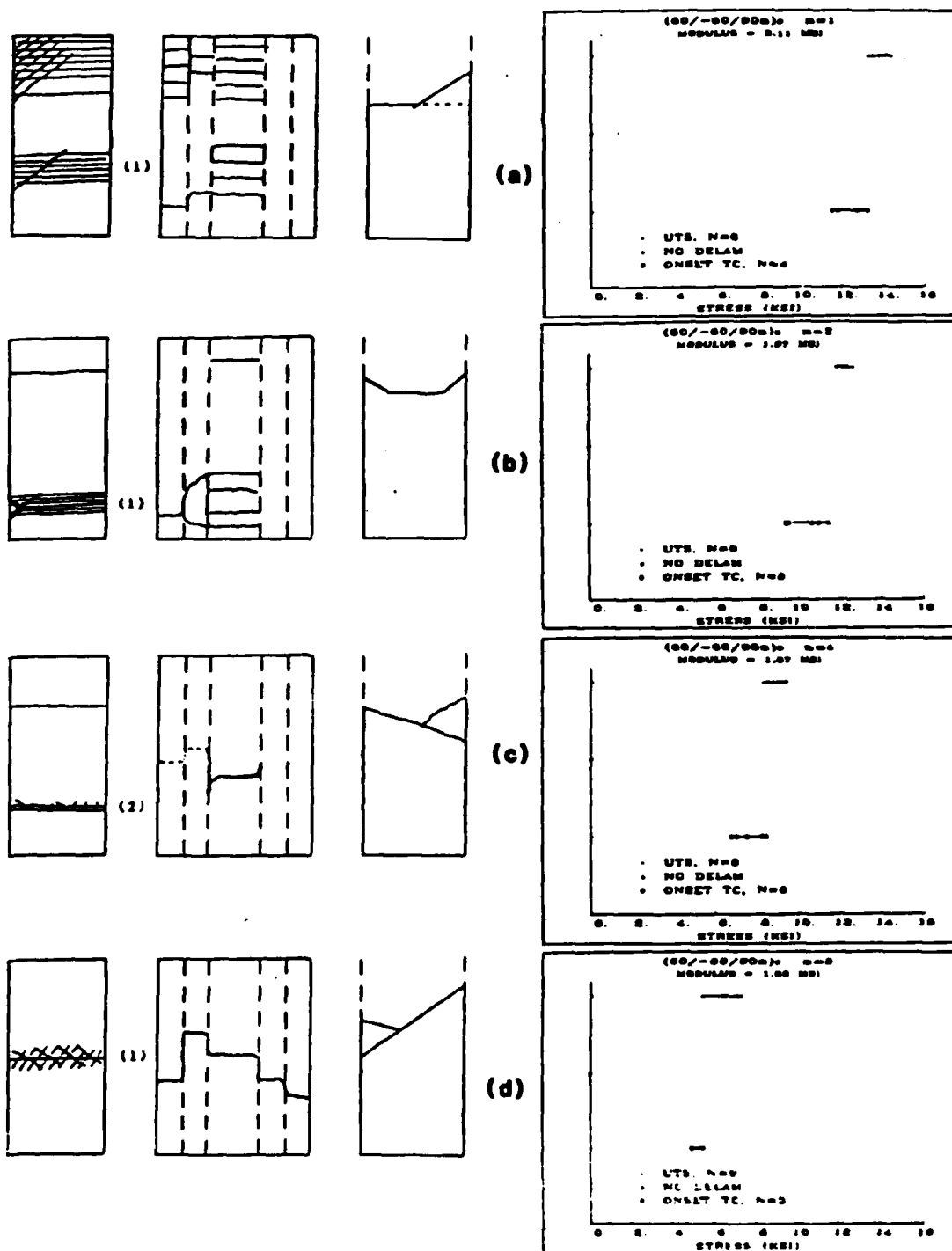


Figure 7. Sequence of Fracture in $(60/-60/90)_{n_s}$ Laminates. (a) $n = 1$; (b) $n = 2$; (c) $n = 4$; (d) $n = 8$.

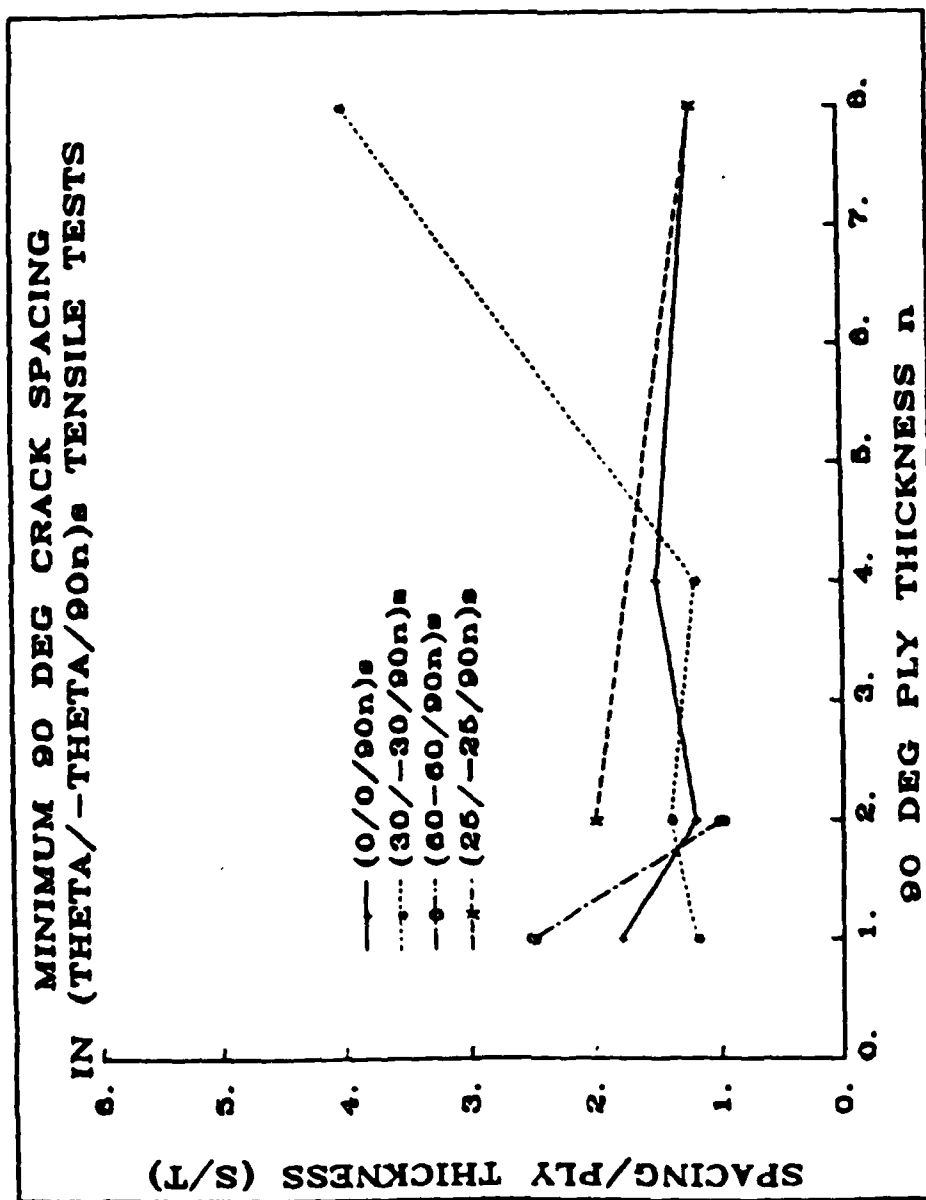


Figure 8. 90-Degree Ply Crack Spacing Before Failure In (theta/-theta/90)_n T300/934 Laminates.

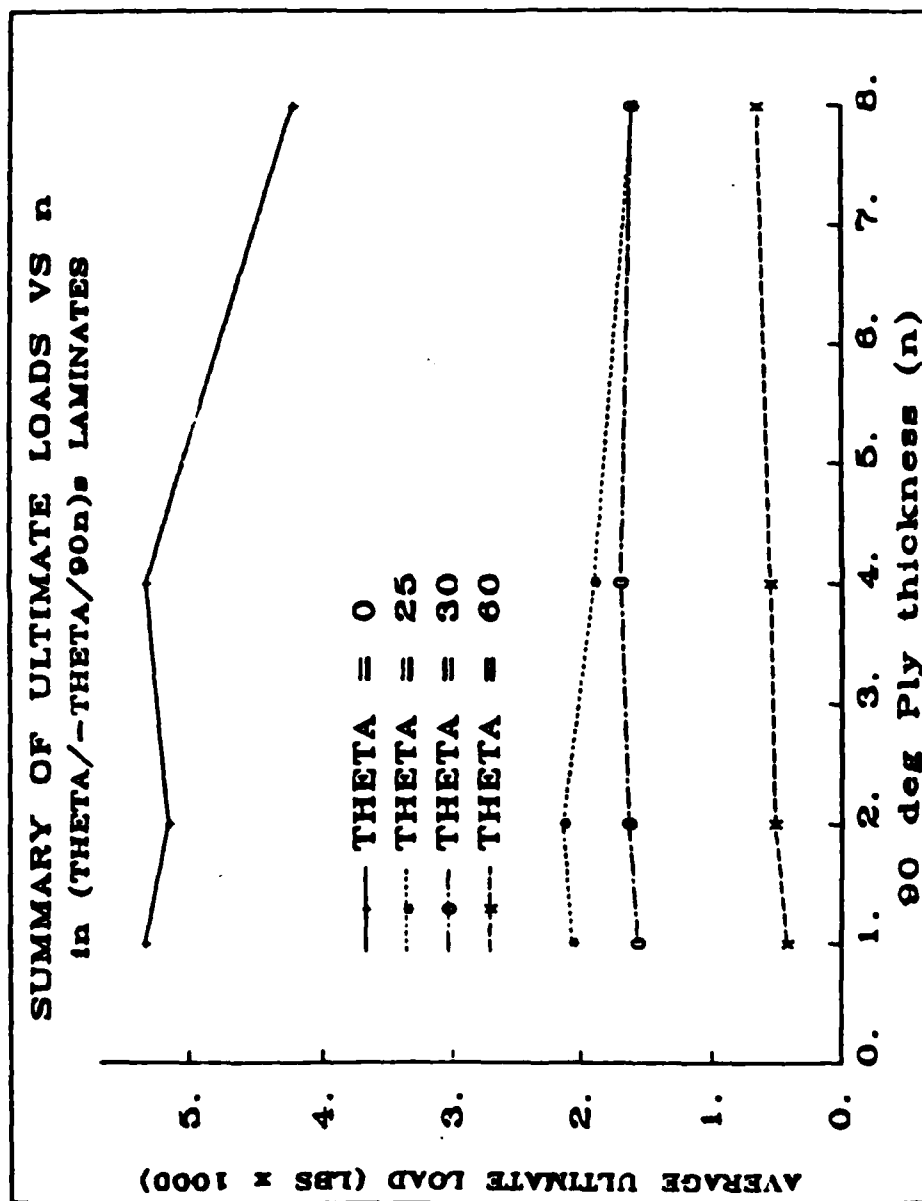


Figure 9. Average Ultimate Tensile Load As A Function of Angle and Ply Thickness In
(theta/-theta/90)_n T300/934 Laminates.

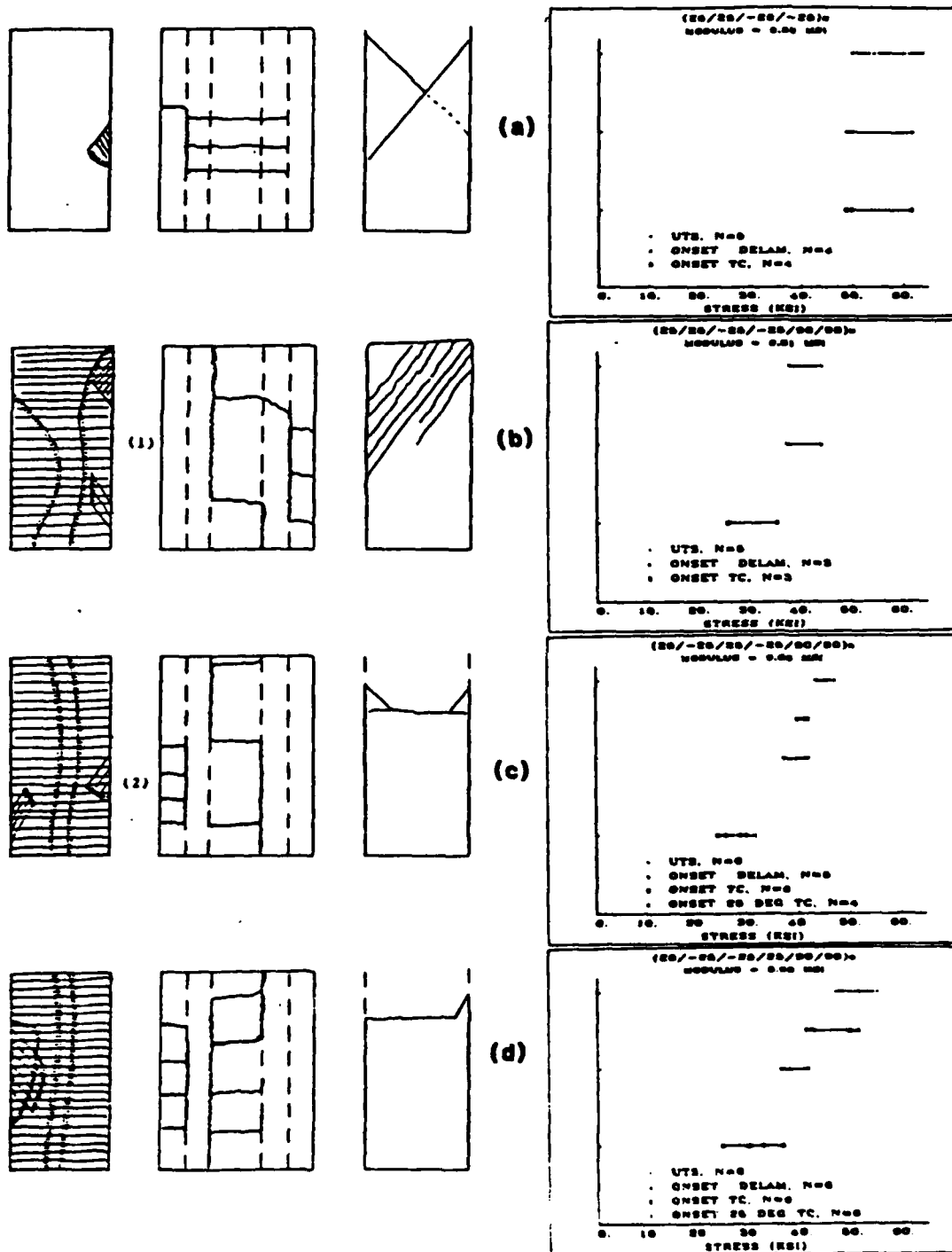


Figure 10. Summary of Fracture Morphology and Sequence in (25/-25/90)₈ T300/934 Tension Loaded Laminates.

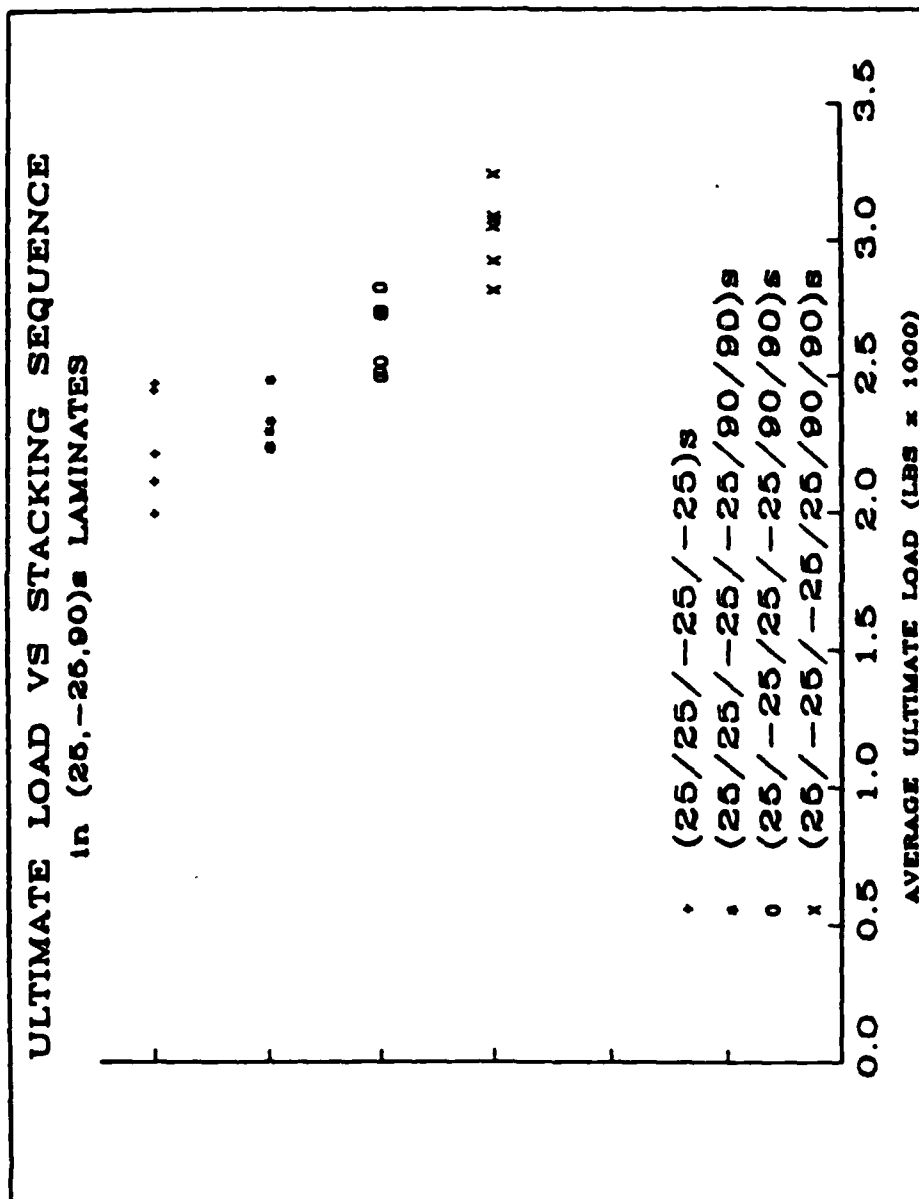


Figure 11. Range of Ultimate Tensile Load As A Function of Stacking Sequence In (25/-25/90)_s

T300/934 Laminate family.

APPENDIX D

ON CRACK DEVELOPMENT IN GRAPHITE-EPOXY
[0₂/90_n]_s LAMINATES UNDER UNIAXIAL TENSION*

A. S. D. Wang, N. N. Kishore and C. A. Li
Drexel University
Philadelphia, PA 19104

*Paper to be presented at the International Symposium
on Composites: Materials and Engineering, University
of Delaware, September, 1984.

ON CRACK DEVELOPMENT IN GRAPHITE EPOXY
[0₂/90_n]_s LAMINATES UNDER UNIAXIAL TENSION

A. S. D. Wang, N. N. Kishore and C. A. Li
Drexel University
Philadelphia, PA 19104

ABSTRACT. When a graphite epoxy laminate of cross ply (0/90) lamination are subjected to uniaxial tension, transverse cracks in the 90° ply can be induced at strains as low as 0.3%. As the applied tension increases, the cracks continue to form in increasing numbers.

At some late stage of loading and before the breaking of fibers in the 0° ply, several other matrix dominant cracking modes may emerge, all stemming from the sites of the transverse cracks. Among them are (1) splitting cracks in the 0° ply that cross over one or more 90° ply transverse cracks; (2) localized delamination in the 0°/90° interface emanating from the point where a 0° ply split crosses a 90° ply transverse crack; and (3) localized edge delamination in the 0°/90° interface emanating from the corner point where a transverse crack meets the free edge of the laminate coupon.

These late stage matrix cracking modes have been observed to form under either static or cyclic loads. Their individual growth and mutual coalescence often precipitate disintegration of the lamination structure and eventuate its total failure.

The physical mechanisms and the load-dependent crack development process of the 90° ply transverse cracks have previously been described by a stochastic model that combines the general concept of fracture mechanics and a random distribution of material flaws.

The objective of this paper is to apply the previously developed approach and describe the various cracking events in cross-ply laminates as they occur subsequent to the formation of 90° ply transverse cracks.

The particular laminates modelled are the $[0_2/90_n]_s$, $n = 1, 2$ and 4 family, subjected to static tensile loading. Emphasis is placed on determining why a certain mode of cracking occurs while other modes do not. Especially for the cracking state which exists during late stage loading, an analysis will be made to explain why that state is critical to the final strength of the laminate.

All predicted results will be compared with the experimentally obtained data. The details of the experiment have been reported in an earlier paper.

I. INTRODUCTION

Structural laminates made of unidirectional fiber reinforced plies frequently suffer interply and intraply matrix cracks well before the final rupture of the laminates [1]. Consider as an example the graphite-epoxy cross-ply $(0/90)_s$ type laminates subjected to uniaxial tension. Matrix cracks in the 90° ply known as transverse cracks have been observed to occur at laminate tensile strains as low as 0.2 to 0.3% [2,3]. Since the final rupture of the laminate is primarily controlled by the 0° plies, whose ultimate tensile strain exceeds 1%, matrix cracking of this kind has often been tolerated in design as some benign internal failure mode.

Actually, it has been known that the formation of intraply matrix cracks signifies the beginning of a complex sublaminar crack development process, which almost always leads to cracks in multiple plies and internal load redistribution. In the case of the cross-ply laminate cited above, onset of 90° ply transverse cracking is followed by multiple cracks in that ply if the applied tension is increased. Or, if it is cyclically applied, multiple cracks in that ply will form in time. In either case, the presence of a distribution of the cracks in the laminate can reduce the threshold condition for other matrix crack modes to emerge [4,5,6,7]. One such mode, for instance, is the intraply splitting of the 0° ply, the split being parallel to the applied tension. Under ascending load, or in time, 0° ply splitting also occurs in multiple numbers. At each crossing point where a 0° ply split intersects a 90° ply transverse crack, interaction between the two crossing cracks causes a localized but highly magnified three dimensional stress field. The tensile and the shearing components in this stress field may in turn cause 0/90 interface delamination around the crossing point [4,5]. Coalescence of the many localized delaminations eventuates a massive 0/90 interface separation at some critical loading level. This is often the last matrix cracking event before the catastrophic failure of the 0° ply by fiber breaking [5].

Laminates of more practical lay-up suffer similar matrix crack development, though the sequence of events may not necessarily follow the same order. Experiments have generally established that the entire process, including the cracking state which exists just prior to final laminate failure, is a generic phenomenon unique to the laminate type and the nature of the load; the phenomenon may be amenable to some form of analytical description [4].

While such a prospect remains largely unreached at the present time, several successful efforts have been made to describe crack development in laminates of simpler forms. The basic mechanisms of 90° ply transverse crack and free edge induced delamination have been explained and predicted by the energy release rate concept of the classical fracture mechanics [8,9,10]. Multiple cracks in the 90° ply are described by a stochastic procedure incorporating a new concept of effective flaw distribution as an inherent ply material property [11]. The utility of the same approach to predict the growth behavior of free edge delamination under fatigue loading has also been established [12].

However, matrix cracks in multiple plies and their mutual interactions have scarcely been analytically approached. In particular, an understanding is needed regarding the crack state which exists just prior to final failure of the laminate. Questions pertaining to why and how that state has come about, and why is it critical to the laminate's final failure are yet to be answered.

In an effort to understand the mechanisms of matrix crack interactions, a research has been conducted which included an experimental investigation and an analytical simulation.

The experiment detailed the chronological matrix cracking events in a family of laminate coupons in the form of $[\pm\theta/90_n]_s$. The coupons were made of the T300/934 graphite-epoxy composite system, and were tested under static

uniaxial tension. The outer angle-ply orientation θ varied from 0° , 25° , 30° and 60° ; the number of the 90° plies in the core varied from $n = 1, 2, 4$ and 8 . The ranges of these lamination variables were so chosen because they effect different matrix cracking events at distinctly different threshold stress conditions. All cracking patterns were detected and documented throughout the entire course of loading.

Results from this experimental investigation have been presented in an accompanying paper [13].

This paper presents the results from the analatical investigation. The energy release rate method developed earlier for modelling the 90° ply transverse cracks and free edge delaminations was employed again to model matrix crack interactions. The stress fields near several important crack-interaction regions were analyzed first by a three dimensional finite element routine, and the same routine was used to simulate any possible crack growth stemming from the interacting cracks. Special attention was placed on the various material and geometrical factors which play dominant role in the interaction effects.

For conciseness, however, only the results for $[0_2/90_n]_s$, $n = 1, 2$ and 4 will be reported here. As it may become clear later, the same method of analysis can be equally applied to laminates of any lay-up form.

II. CRACK DEVELOPMENT IN $[0_2/90_n]_s$

Let us consider the laminate family $[0_2/90_n]_s$, for $n = 1, 2$ and 4 . Coupons of 25 mm (1 in.) width and 225 mm (9 in.) length were made and tested under monotonic tension in room temperature condition. The material properties of the T300/934 unidirectional ply have been previously characterized and are listed here in Table I. As has been mentioned, the details of the test and test results are reported in Ref. [13]; and the energy method used for modeling is found in Refs. [8,9,10]. The three dimensional finite element routine, its development and user's instructions are contained in Ref. [14]. In this section, we simply apply these techniques and predict the sequential crack events as the laminates are loaded in monotonic tension.

Transverse Cracking Versus Free Edge Delamination.

When the $[0_2/90_n]_s$ laminates are loaded, two competing crack modes exist during the initial stage of loading. One mode is due to the in-plane stress in the 90° ply which causes multiple cracks in that ply as shown schematically in Fig. 1. The other possible cracking mode is free edge delamination caused by interlaminar tensile stress which is concentrated near the free edge [15, 16]. A schematical view of the latter is shown in Fig. 2.

It will be determined next that the free edge effect in the $[0_2/90_n]_s$ family under tension is negligible; and edge delamination alone cannot occur. Consequently, 90° ply transverse cracking is the first failure event.

To show this, we first calculate the energy release rate coefficient functions $C_e(a)$ and $C_T(a)$ associated with 90° ply transverse cracking. The significance of these coefficients is that the available energy release rate G for a flaw in the 90° ply to become a transverse crack can be expressed as

$$G(\bar{e}_x, \Delta T, a) = [\sqrt{C_e} \cdot \bar{e}_x + \sqrt{C_T} \cdot \Delta T]^2 t \quad (1)$$

where \bar{e}_x is the applied laminate tensile strain, ΔT is the temperature load experienced by the laminate after curing and t is a length parameter taken here as one ply thickness. The quantity a represents the size of the assumed effective flaws ($=2a$) which distribute in the 90° plies(for details see [10] or [11]).

Figures 3 and 4 show the calculated $C_e(a)$ and $C_T(a)$ functions for the laminates $[0_2/90_2]_s$ and $[0_2/90_4]_s$. Using these curves, the threshold stress condition for the first transverse crack and the subsequent cracks can be obtained. This will be shown later in this section.

If we assume that free edge delamination will occur before transverse cracking, we then calculate the energy release rate coefficient functions C_e and C_T associated with an edge flaw of size a (for details see [10] and [12]). Figures 5 and 6 show the calculated $C_e(a)$ and $C_T(a)$ curves for $[0_2/90_2]_s$ and $[0_2/90_4]_s$ assuming the edge flaw in the laminate mid-plane causes delamination. These curves can be used to predict the onset load condition for delamination.

The criterion for the flaw to become a crack is

$$G(\bar{e}_x, \Delta T, a) = G_c \quad (2)$$

where G_c is the appropriately determined critical energy release rate of the material(see discussions in [17]).

Onset of Transverse Cracking. To determine the onset load for 90° ply transverse cracking, the size of the most dominant effective flaw, $2a_0$, in the effective flaw distribution must be identified. Following the reasoning given in Ref. [11], a_0 is defined as the 99 percentile of the effective flaw distribution $f(a)$. As it will be shown later, a_0 for both $[0_2/90_2]_s$ and $[0_2/90_4]_s$ is in the order of $1.5t$. Thus, from Figs. 3 and 4 we obtain,

$$\begin{aligned} \text{for } n = 2, \quad C_e(a_o) &= 41.3 \times 10^9 \text{ J/m}^3 \\ &\quad (6 \times 10^6 \text{ in-lb/in}^3) \\ C_T(a_o) &= 26.1 \text{ J/m}^3/\text{C}^2 \\ &\quad (11.7 \times 10^{-4} \text{ in-lb/in}^3/\text{F}^2) \end{aligned}$$

$$\begin{aligned} \text{for } n = 4, \quad C_e(a_o) &= 48.3 \times 10^9 \text{ J/m}^3 \\ &\quad (7 \times 10^6 \text{ in-lb/in}^3) \\ C_T(a_o) &= 26.05 \text{ J/m}^3/\text{C}^2 \\ &\quad (11.7 \times 10^{-4} \text{ in-lb/in}^3/\text{F}^2) \end{aligned}$$

Substitution of these values into Eq.(1) and using $\Delta T = 125^\circ\text{C}$ (225°F), $t = 0.132 \text{ mm}$ (0.0052 in.) and $G_c = 228 \text{ J/m}^2$ (1.3 in-lb/in^2) from Table I, we obtain from Eq.(2) the respective onset strains for transverse cracking:

$$\begin{aligned} \text{for } n = 2, \quad (\bar{\epsilon}_x)_{tc} &= 3.3 \times 10^{-3} \\ \text{for } n = 4, \quad (\bar{\epsilon}_x)_{tc} &= 3.1 \times 10^{-3}. \end{aligned}$$

Onset of Free Edge Delamination. If we assume free edge delamination in the mid-plane to occur before transverse cracking, the associated threshold stress can be determined by using the maximum values of the C_e and C_T curves in Figs. 5 and 6. In essence, we assume the size of the effective edge flaw $a_o > 2t$; and the prediction yields the lower bound. Hence,

$$\begin{aligned} \text{for } n = 2, \quad C_{e,\max} &= 0.73 \times 10^9 \text{ J/m}^3 \\ &\quad (0.106 \times 10^6 \text{ in-lb/in}^3) \\ C_{T,\max} &= 7.03 \text{ J/m}^3/\text{C}^2 \\ &\quad (3.15 \times 10^{-4} \text{ in-lb/in}^3/\text{F}^2) \end{aligned}$$

$$\begin{aligned} \text{for } n = 4, \quad C_{e,\max} &= 0.41 \times 10^9 \text{ J/m}^3 \\ &\quad (0.06 \times 10^6 \text{ in-lb/in}^3) \\ C_{T,\max} &= 3.73 \text{ J/m}^3/\text{C}^2 \\ &\quad (1.67 \times 10^{-4} \text{ in-lb/in}^3/\text{F}^2) \end{aligned}$$

Using the same values for ΔT and t as before, but $G_c = 158 \text{ J/m}^2$ (0.9 in-lb/in^2) for mode-I mid-plane delamination as indicated in Table I, we obtain from Eqs. (1) and (2) the respective onset strains(lower bounds) for free edge delamination:

$$\text{for } n = 2, \quad (\bar{\epsilon}_x)_{de} = 36 \times 10^{-3}$$

$$\text{for } n = 4, \quad (\bar{\epsilon}_x)_{de} = 52 \times 10^{-3}.$$

Clearly, the assumed free edge delamination will never occur, because the laminate final failure by fiber breaking is likely to take place at about 10×10^{-3} to 12×10^{-3} strain.

Influence of θ in $[\pm\theta/90]_s$ Laminates. The previous examples showed that free edge effect is relatively unimportant. However, when the angle θ increases slightly from being 0° , the role of free edge effect increases dramatically. Fig. 7 shows a family of the $C_e(a)$ curves associated with delamination in the laminate mid-plane for $[\pm\theta/90]_s$ with $\theta = 0^\circ, 10^\circ, 20^\circ$ and 30° . It is seen that C_e rises sharply with θ . On the other hand, Fig. 8 shows the corresponding family of the C_T curves, which decrease with θ . Between these two sets of curves, the angle $\theta = 25^\circ$ yields approximately the optimum free edge effect. In fact, if we use the same calculation procedure as before, the onset strains for mid-plane delamination in $[0_2/90]_s$ and in $[\pm 25/90]_s$ are:

$$\text{for } [0_2/90]_s, \quad (\bar{\epsilon}_x)_{de} = 24 \times 10^{-3}$$

$$\text{for } [\pm 25/90]_s, \quad (\bar{\epsilon}_x)_{de} = 6. \times 10^{-3}.$$

From these results, it may be concluded that free edge delamination is not possible for the case of $\theta = 0^\circ$, but is definitely possible for the case of $\theta = 25^\circ$. It is not known however, whether transverse cracks in the 90° ply

occur before or after free edge delamination. So, let us investigate the influence of θ on transverse cracking. Fig. 9 shows the $C_e(a)$ family associated with a transverse crack; and the corresponding $C_T(a)$ family is displayed in Fig. 10. It is seen that θ , in the range indicated, has only a small effect on transverse cracking. In fact, the calculated onset strains for $[0_2/90]_s$ and $[\pm 25/90]_s$ are:

$$\text{for } [0_2/90]_s, \quad (\bar{\epsilon}_x)_{tc} = 5.9 \times 10^{-3}$$

$$\text{for } [\pm 25/90]_s, \quad (\bar{\epsilon}_x)_{tc} = 6.3 \times 10^{-3}.$$

From the above results, we can readily determine that transverse cracking in $[\pm 25/90]_s$ laminate should occur after free edge delamination.

Summary. In this section, we have demonstrated the profound influence of lamination variables on the formation mechanisms of two competing matrix crack modes; namely, transverse cracking and delamination. The energy release rate method takes into account these variables and provides a quantitative prediction. Table II summarizes the predicted results obtained in this section; and these are compared with the corresponding experimental results extracted from Ref. [13].

90° Ply Multiple Cracks in $[0_2/90_n]_s$.

In the previous section, it was shown that free edge delamination as a first matrix failure mode will never occur in the $[0_2/90_n]_s$ family when they are loaded in tension. Rather, the first matrix failure mode is the 90° ply transverse cracking which initiates at distinctively different laminate tensile strains, depending on the value of n or the number of the 90° plies. Following the onset of the first crack in the 90° plies, multiple cracks can occur as the applied tension increases, resulting in a characteristic crack density versus applied load relationship. The stochastic search procedure based on an assumed effective flaw distribution can be applied to simulate the crack de-

velopment process. The procedure was previously formulated in Ref. [10] and was discussed in more details in Ref. [11]. We shall therefore omit the computational details here and simply present the simulated results.

The simulation will be based on the assumed flaw distribution which is characterized by the flaw size distribution and the flaw spacing distribution. These two distributions are represented by the probability density functions,

$$f(a) = \frac{1}{a\sqrt{2\pi}} \exp [-(a - \mu_a)^2/2v_a^2] \quad (3)$$

$$f(s) = \frac{1}{s\sqrt{2\pi}} \exp [-(s - \mu_s)^2/2v_s^2] \quad (4)$$

where μ and v denote the mean and the standard deviation of the normal distribution function $f()$.

For the T300/934 material system used here, the parameters μ and v in the assumed flaw distribution functions were previously determined as (see Ref. [10]),

for $n = 1$,	$\mu_a = 0.053 \text{ mm}$ 0.0021 in.	$v_a = 0.019 \text{ mm}$ 0.00075 in.
	$\mu_s = 0.313 \text{ mm}$ 0.0125 in.	$v_s = 0.115 \text{ mm}$ 0.0046 in.
for $n = 2, 4$,	$\mu_a = 0.091 \text{ mm}$ 0.0036 in.	$v_a = 0.033 \text{ mm}$ 0.0013 in.
	$\mu_s = 0.313 \text{ mm}$ 0.0125 in.	$v_s = 0.115 \text{ mm}$ 0.0046 in.

Now, let the size of the most dominant flaw in each case be denoted by $2a_o$ and let a_o be the 99 percentile of $f(a)$. Then, for the normal distribution expressed in (3), a_o can be approximated by [18],

$$a_o = \mu_a + 3v_a \quad (5)$$

It follows that the largest flaw determines the onset of transverse

cracking, and their size is found using (5). Hence, for $n = 1$, $a_0 = 0.112$ mm (0.0044 in.); for $n = 2$ and 4 , $a_0 = 0.191$ mm (0.0075 in.). The former is about 0.8 times the ply thickness t , while the latter is about $1.5t$.

The stochastic procedure actually mimics the cracking process as it would occur naturally. The result is a simulated crack density versus applied load relationship. Figures 11, 12 and 13 display such a relationship for, respectively, the $n = 1, 2$ and 4 laminates. The simulated results were generated for four or five specimens in each case; they collectively form a scatter bend as shown in each of these figures. The corresponding experimental result is shown by the shaded bend.

Of course, the simulation assumes that the applied tension can be monotonically increasing; and the resulting transverse cracking process can go on forever. This, clearly, does not happen in reality since other modes of matrix cracking may emerge at higher load levels. As it will be shown next, any late-stage matrix cracking invariably involves interactions with the transverse cracks in the 90° plies. These distributed cracks act like local defects, each is capable of causing localized stress concentration.

Matrix Cracks At High Load Levels.

When a transverse crack is formed in the 90° ply, the load formerly carried by the 90° ply must now be taken by the 0° ply near the vicinity of the transverse crack. This extra load, however, is gradually transferred back to the unbroken part of the 90° ply through the bonding strength of the $0/90$ interface. Thus, near the transverse crack root, a stress concentration zone exists which may cause both in-plane and out-of-plane matrix cracking modes.

In addition, the presence of free edges now becomes important factor. As is shown schematically in Figure 14, a highly concentrated stress zone exists near the intersection of a transverse crack and the coupon free edge.

We shall label this point as the 'corner point'. The high stresses near this point are caused by the compound effects from the transverse crack and the free edge.

The effects of these localized stress concentrations on matrix cracking at high loads will be investigated in this section. Since these local stress fields are three dimensional, the finite element routine developed previously [14] will be employed.

Stress Field Near A Transverse Crack. The tensile coupon shown in Fig.14 already has multiple transverse cracks in the 90° ply. For purpose of analysis, consider only a section of the laminate which contains one crack. Due to lamination symmetry, it is sufficient to model one-eighth of this section by a net-work of finite elements. The actual sizing, meshing and other related computational details are found in Ref. [14]. Here, we shall discuss primarily the stresses which act on the $0/90$ interface near the crack root, and the stresses acting in the 0° ply above the crack root. It is noted that the interface stresses can cause delamination, while the in-plane stresses can cause several possible failure modes in the 0° ply.

Figures 15, 16 and 17 show, respectively, the interlaminar stresses σ_z , τ_{xz} and τ_{yz} which are acting on the $0/90$ interface. Figures 18, 19 and 20 show the in-plane stresses σ_x , σ_y and τ_{xy} , respectively, which are acting in the 0° ply but close to the $0/90$ interface. Both sets of figures are for the cases of $n = 2$ and 4 . And, the magnitude of the stresses is due to a unit tensile strain applied at the far-field, $\bar{\epsilon}_x = 10^{-6}$.

Similar display for the interlaminar and the in-plane stresses due to a unit of temperature change is shown in Figures 21 to 26, the unit temperature being $\Delta T = -0.56^\circ\text{C}$ (-1°F).

In all the stress displays, the xy -plane coincides with the $0/90$ interface,

with the x-axis lying along the free edge of the laminate, and the y-axis lying along the transverse crack root; the origin of the axes is the corner point shown in Fig. 14.

A cursory examination of these stress displays reveals the following general features:

1. The influence of laminate free edge on the interlaminar and the in-plane stresses is relatively insignificant compared to the influence of the 90° ply transverse crack. But the two effects compound each other near the corner point, resulting in a much amplified stress concentration zone. The amplification of stress near this point is not a simple addition of these two individual effects.
2. The influence of the 90° ply thickness (the value of n) on the stresses continues to dominate. An increase of n increases both the magnitudes of the stresses and the size of the stress concentration zone. Clearly, any material damage inside this zone will be likewise controlled by the same factor.
3. The stress fields caused, respectively, by $\bar{e}_x = 10^{-6}$ and by $\Delta T = -0.56^\circ\text{C}$. have their corresponding stress components in the same sign inside the concentration zone. For instance, σ_z due to tension is positive near the corner point and along the transverse crack root (Fig. 15); and σ_z due to the temperature load is also positive in the same region (Fig. 21). Thus, they combine to give a stress field of much higher magnitude in the actual laminate.

It will be shown in the sequel that the local stress concentration which surrounds a transverse crack in the 90° ply is capable of causing different modes of material damage at high loads. And the thickness factor (the value of n) plays an important role in this regard.

Effects of the Interlaminar Stresses - Localized Delamination. As has

been shown in Figures 15 and 21, the normal stress σ_z acting on the 0/90 interface is tensile near the corner point and along the transverse crack root. This stress alone can debond the interface at least locally. In addition, the shearing stresses τ_{xz} and τ_{yz} are also of considerable magnitude (see Figures 16, 17 and 22, 23). Hence, the actual debonding will be essentially mixed-mode in nature. When the applied load reaches a certain magnitude, a contour-shape delamination will occur emanating from the corner point. This is schematically illustrated in Figure 27.

In order to make a prediction for the onset and the growth behavior of the contour delamination, we begin with the assumption that a small interface flaw is located near the corner point. This assumption is, of course, an out-growth of the effective flaw concept which was discussed earlier in this paper. Under the applied load, the assumed flaw will become a local delamination crack having a contour shape. The growth of the contour is mimicked by a sequence of nodal point release in the finite element net-work. This is represented by an approximate sequential nodal release as displayed in Figure 27. As each of the finite element nodes is released, the corresponding delaminated area as well as the strain energy lost can be computed (for details, see Ref. [14]). In this manner, a relationship between the delaminated area and the strain energy release rate is obtained for the assumed contour-shaped growth.

Figure 28 shows the computed energy release rate coefficient C_e (for $\bar{e}_x = 1$) as a function of the assumed delamination contour for the $[0_2/90_2]_s$ laminate. Note that C_e consists of all three modal components, each of which is also shown in the figure. In this case, the mode-I component is slightly larger than the mode-II component, while the mode-III component is negligible. Also, the release of those nodes along the transverse crack root yields the largest

energy release rate.

Figure 29 shows the C_T coefficient for the laminate subjected to $\Delta T = -1^\circ\text{F}$. or -0.65°C . The general character of C_T and its three modal components are similar to those of C_e .

Although the calculated C_e and C_T coefficients are based on the assumed nodal release sequence (shown in Figure 27), which may not represent the best possible choice, the general trend of these coefficient functions indicates that the delamination growth is basically a stable process. This qualitative result agrees with the actual behavior observed in experiment.

Furthermore, if we assume that the actual delamination becomes macroscopically observable when its area grows to about t^2 (t is one ply thickness), we then define such a state as the onset of the contour delamination. Thus, we take the maximum values of C_e and C_T from Figures 28 and 29 at $A/t^2 = 1$ and compute the total energy release rate $G(\bar{\epsilon}_x, \Delta T, A)$ via Eq. (1). Let, as before, $\Delta T = -125^\circ\text{C}$ (-225°F) and $G_c = 289 \text{ J/m}^2$ (1.65 in-lb/in^2) for mixed-mode crack growth, see Table I. It follows from Eq. (2) that the threshold tensile strain for the onset of the contour delamination is predicted as

$$(\bar{\epsilon}_x)_{de} = 11.0 \times 10^{-3} \quad (\text{for } n = 2) \quad (6)$$

Similarly, the computed C_e and C_T coefficient functions for $[0_2/90_4]_s$ are shown in Figures 30 and 31, respectively. It is seen that the values of C_e and C_T are significantly increased as a result of doubling the number of the 90° plies. Consequently, the predicted threshold strain for onset of the contour delamination is much reduced;

$$(\bar{\epsilon}_x)_{de} = 7.8 \times 10^{-3} \quad (\text{for } n = 4) \quad (7)$$

Now, if we consider the fact that the breaking strain of the 0° ply is

10 to 12×10^{-3} , it becomes clear that the assumed contour delamination near the transverse crack will occur in the $[0_2/90_4]_s$ laminate well before any fiber break in the 0° ply, though it is not likely to occur at all in the $[0_2/90_2]_s$ laminate.

It is also clear from the results in (6) and (7) that such a type of delamination will never occur in the $[0_2/90]_s$ laminate before the final laminate failure.

Effects of the In-plane Stresses - Fiber Break and 0° Ply Split. Let us examine next possible failure modes effected by the in-plane stresses which exist in the 0° ply and are magnified by the presence of the transverse crack. These in-plane stresses are shown in Figures 18, 19 and 20 for tensile load of $\bar{e}_x = 10^{-6}$, and in Figures 24, 25 and 26 for thermal load $\Delta T = -0.65^\circ\text{C}$ (-1°F). Note that in both cases, the normal stresses, σ_x and σ_y , are tensile and are much magnified near the transverse crack; but the shear stress, τ_{xy} , is of small amplitude except near the corner point. It will be shown here that σ_x may cause local fiber break while σ_y causes 0° ply splitting cracks.

First, consider σ_x which is taken by the fibers. The part due to the applied tension is shown in Figure 18; its amplitude is seen to increase 30% to 50% near the transverse crack root, depending on the value of n . The part due to the thermal load is shown in Figure 24. This stress is compressive throughout the 0° ply except near the transverse crack root where it becomes tensile. Again, the magnitude of the localized tensile stress depends also on the value of n . Hence, in the vicinity of the transverse crack, the combined σ_x in the 0° ply could be as much as 50% to 100% higher than the far-field value. As illustrated in Figure 32, σ_x exhibits a singular behavior approaching the 0/90 interface, and reduces magnitude away from the interface. It is clear that the localized concentration of the tensile stress will have varying effect

on the breaking mechanisms of the 0° ply fibers, depending on the 90° ply thickness. But the exact nature of fiber breaking mechanisms in laminates is not the object of this paper, and we shall not attempt to make any prediction based on the calculated σ_x here. It is sufficient to note that experimental observations [6,13] have verified fiber breakage near the site of 90° ply transverse cracks.

Consider next σ_y which is normal to the fibers of the 0° ply, see Figures 19 and 25. In this case, both the mechanical part and the thermal part are tensile throughout the 0° ply, but are especially amplified near the transverse crack. Like σ_x discussed earlier, σ_y also becomes singular near the $0/90$ interface as is illustrated in Figure 33. And, depending on the value of n , the maximum amplification can be as much as more than 500%. Such a high stress is capable of causing matrix cracks in the interior of the 0° ply, known as longitudinal splitting.

The actual mechanisms of 0° ply splitting are similar to that in the 90° ply transverse cracking. Hence, the crack-closure procedure and the criterion used for defining the onset of transverse cracking can be applied to 0° ply splitting. But we shall omit the details of the calculation, and present here simply the simulated results. Namely, matrix splits in the interior of the 0° ply will occur over the transverse crack when the applied tensile strain \bar{e}_x reaches the following critical value:

$$\text{for } n = 2, \quad (\bar{e}_x)_{sp} = 10.5 \times 10^{-3} \quad (8)$$

$$\text{for } n = 4, \quad (\bar{e}_x)_{sp} = 7.8 \times 10^{-3} \quad (9)$$

According to the above prediction, 0° ply splitting may or may not occur in $[0_2/90_2]_s$ when under static tension; but will definitely occur in $[0_2/90_4]_s$

before fiber breaking. Note that in the case of $[0_2/90_4]_S$, the threshold condition for 0° ply splitting is about the same as the threshold condition for transverse crack induced $0/90$ interface delamination (see Eq.7). Thus, these two types of matrix cracks may actually occur at the same load level for this particular laminate.

Delamination at the Crossing Cracks. When a splitting crack is formed in the 0° ply, it makes a cross with the transverse crack in the 90° ply, see Figure 34. In the close vicinity of the crossing point, a severe stress concentration is developed. Especially the interlaminar stresses acting on the $0/90$ interface are capable of causing localized delamination as shown by the shaded area in Figure 34. Hence, we shall examine only the distributional nature of these interlaminar stresses.

Figure 35(a) shows the $0/90$ interface plane. Note that the x-axis is made parallel to the 0° ply split and the y-axis is parallel to the 90° ply transverse crack; the origin of the axes is the intersection point of the two cross cracks. The first-quadrant distribution of the computed stresses σ_z , τ_{xz} and τ_{yz} are displayed, respectively, in Figures 36, 37 and 38. Again, these are for the $[0_2/90_2]_S$ and the $[0_2/90_4]_S$ laminates only; and the mechanical part of the stresses is due to $\bar{e}_x = 10^{-6}$ while the thermal part is due to $\Delta T = -1^\circ\text{F}$, or -0.56°C . It is seen that all the stresses are highly amplified near the crossing point; and σ_z is tensile (both the mechanical and the thermal parts) around this point.

In order to determine the threshold condition for delamination near the crossing point, a crack growth simulation is performed using the finite element routine. The simulated delamination followed the nodal release sequence shown in Figure 35(b). The point-by-point energy release rate coefficients C_e and C_T are shown in Figures 39 and 40 for $[0_2/90_2]_S$ and in Figures 41 and 42

for $[0_2/90_4]_s$.

From the energy release rate coefficient curves, it is apparent that the behavior of the delamination is in mixed-mode, mode-I and mode-II being about equal and mode-III negligible. The total energy release rate is slightly decreasing with delaminated area A. This again indicates that the delamination growth is essentially stable.

If we compare the four energy release rate curves with those shown in Figures 28, 29, 30 and 31, we see the close similarity between this case and the one discussed earlier for delamination emanating from the transverse crack/free edge intersection. However, the calculated energy release rate for delamination at the cross cracks is slightly higher.

Indeed, if we follow the same procedure as before, we obtain a prediction for the threshold condition. Thus, onset of delamination occurs when the applied strain reaches the following values:

$$\text{for } n = 2, \quad (\bar{\epsilon}_x)_{de} = 10.9 \times 10^{-3} \quad (10)$$

$$\text{for } n = 4, \quad (\bar{\epsilon}_x)_{de} = 7.5 \times 10^{-3} \quad (11)$$

It appears that delamination at the cross cracks occurs at about the same time when the 0° ply splitting is formed. Physically, of course, the splitting must occur before delamination. It is also noted that for the $[0_2/90_2]_s$ laminate the splitting and the delamination are unlikely to occur before fiber break.

Summary of Results. All results predicted in this section are summarized in Table III. Whenever possible, the predicted results are compared with their experimental counterparts. The latter were actually extracted from Ref. [13]. A cursory examination of Table III indicates readily that the predicted events and the associated threshold strains agree well with the experimentally obtained

results. It should be emphasized that the predictions involved some degree of approximation, both in numerical accuracy and in setting the criterion for the threshold condition.

In spite of such reservations, it seems that the energy release rate concept continues to be applicable to matrix cracking simulation problems at high load levels where complicated crack interactions take place. This concept, however, could not at least at the present time predict the failure of the fibers, although the event of fiber failure (hence also the final failure of the laminate) is affected by matrix crack interactions at high loads. The adversity of the interactions intensifies if the matrix cracks can become large. For instance, among the three laminates of $[0_2/90_n]_s$, $n = 1, 2$ and 4 , matrix cracks in $n = 1$ are the smallest in size, while in $n = 4$ are the largest. Thus, at least qualitatively, we may conclude that the threshold strain for fiber break should be the highest in $n = 1$ and lowest in $n = 4$. This observation is reasonably supported by experiment (see results in the last column of Table III).

Finally, let us note that the predicted threshold strains for (a) 0° ply splitting, (b) delamination at the cross cracks and (c) delamination at the free edge/transverse crack corner point are practically all the same for the $[0_2/90_n]_s$ laminate family, although for laminates with $n \leq 2$ these crack modes are not likely to occur before fiber break. This observation has also been experimentally supported in at least one instance: Figure 43 shows a sequence of x-ray photographs taken during tension loading of a $[0_2/90_3]_s$ laminate. At about 90% of the ultimate load, cross cracks were seen to form in increasing numbers and delaminations around the cross cracks followed almost instantly. And, the coalescence of the numerous local delaminations finally triggered the failure of the laminate. An identical specimen loaded by the same procedure developed instead delaminations near the free edge/transverse crack corners,

also at about 90% the laminate ultimate load, see Figure 44. While the general appearances of the two crack events at high load are different, the actual threshold conditions separating them are close. The fact that such results can be predicted at all is in itself surprising.

In Table III, experimental results for $[0_2/90_8]_s$ were listed for comparison. An analytical prediction using the same method can be readily performed, but it was not attempted in this paper.

III. CONCLUSIONS

In this paper, we have demonstrated that the development process of matrix cracks and crack interactions at high loads can be analytically described by a three dimensional stress analysis based on the method of ply elasticity and by a crack growth simulation routine based on the method of fracture mechanics in conjunction with a new concept of material "effective" flaw distribution. The $[0_2/90_n]_s$ laminate family made of T300/934 graphite-epoxy system was used to illustrate and to obtain specific results which can be compared by a parallel experiment. To conclude this paper, we wish to make the following comments:

1. Matrix cracks in off-axis plies, the 90° ply transverse cracks being examples, are important precursors in the laminate damage accumulation process. In time, or at high loads, these cracks eventually cause secondary matrix cracks into the load-carrying plies. When this happens, it is often the beginning of the end of the laminate's failure process. In this paper, we have shown that the matrix crack development process is influenced largely by the lamination geometry, given the material and the loading environment. And, the geometrical factors can be explicitly included in the predictive models. Consequently, it appears that the final laminate failure event could also be much influenced by the same factors. The present and past experiments [1,13] have demonstrated convincingly this fact. To emphasize, let us examine briefly the experimental results [13] shown in Table IV, where the final failure (tensile) strains of the $[\pm\theta/90_n]_s$ laminate family ($n = 1, 2, 4$ and 8 ; $\theta = 0^\circ, 25^\circ$ and 30°) are displayed. It is seen that the failure strains are influenced by the value of n . And, as we have already shown, the value of n has been the prime factor in the matrix crack development processes observed in these laminates. Clearly, it is important to know when and how a certain matrix cracking pattern is reached at high loads, and

why it is critical to the final failure of the load-carrying plies.

2. In practice, however, the analysts have generally ignored the detailed matrix crack patterns in the off-axis plies, but simply assume that all loads will eventually be taken by the load-carrying plies. This approach is typified by the so-called progressive ply failure analysis. The approach is simple to use and may be adequate for preliminary static strength prediction. The reason may be that matrix cracks can branch into the load-carrying plies only at very high loads (except for some extreme but impractical laminates); the threshold condition for such event is almost synonymous to the breaking of the load-carrying plies alone. But, the situation will be quite different when the applied load is cyclic in nature. Then, matrix cracks in the load-carrying plies can be developed at low stress amplitudes [5,7]. When this happens, both the laminate residual strength and fatigue life may not be predicted based on the properties of the load-carrying plies alone. Then, the detailed matrix cracking patterns could become important; and an accurate account for their effects is essential. As has recently been remarked by Reifsnider, et. al. [5], we quote:

".... in order to make an absolute (meaning, quantitative) association between these (matrix cracks) patterns and laminate residual strength, an accurate stress analysis of such a pattern must be obtained. Such an analysis is indeed complex. However, the nearly ubiquitous nature of these types of pattern in many situations involving the long-term cyclic loading of composite laminates suggests that further study of such patterns by investigators concerned with long-term strength and life is merited."

This paper demonstrated that such an analysis is indeed complex, but

also seems possible.

Acknowledgments: The results reported in this paper were obtained in the course of research conducted under the contract F49620-79-C-0206 from the Air Force Office of Scientific Research to Drexel University. The preparation of this manuscript was completed during the period when the first author was an National Research Council Senior Research Associate visiting Naval Air Development Center during October 1983 to September 1984.

REFERENCES

- [1] Crossman, F.W. and Wang, A.S.D., "The Dependence of Transverse Cracking and Delamination on Ply Thickness in Graphite Epoxy Laminates," in Damage in Composite Materials, ASTM STP 775 (1982), pp. 118-139.
- [2] Harrison, R.P. and Bader, M.G., "Damage Development in CFRP Laminates Under Monotonic and Cyclic Stressing," Fibre Science and Technology, Vol. 18 (1983), pp. 163-180.
- [3] Flaggs, D.L. and Kural, M.H., "Experimental Determination of the In-situ Transverse Lamina Strength in Graphite Epoxy Laminates," Journal of Composite Materials, Vol. 16 (1982), pp. 103-116.
- [4] Bailey, J.E., Curtis, P.T. and Parvizi, A., "On the Transverse Cracking and Longitudinal Splitting Behavior of Glass and Carbon Fibre Reinforced Epoxy Cross-ply Laminates and the Effect of Poisson and Thermally Generated Strain," Proceedings, Royal Society of London, Vol. A-366 (1979), pp. 599-623.
- [5] Reifsnider, K.L., Stinchcomb, W.W., Henneke, E.G. and Duke, J.C., "Fatigue Damage-Strength Relationships in Composite Laminates," AFWAL-TR-83-3804, (1983), Air Force Wright Aeronautical Laboratories, Ohio.
- [6] Jamison, R.D. and Reifsnider, K.L., "Advanced Fatigue Damage Development in Graphite Epoxy Laminates," AFWAL-TR-82-3103, (1982), Air Force Wright Aeronautical Laboratories, Ohio.
- [7] Ryder, J.T. and Crossman, F.W., "A Study of Stiffness, Residual Strength and Fatigue Life Relationships for Composite Laminates," NASA-CR-172211, (1983), Langley Research Center, Hampton Va.
- [8] Wang, A.S.D. and Crossman, F.W., "Initiation and Growth of Transverse Cracks and Edge Delamination in Composite Laminates," Journal of Composite materials, Suppl. Vol. 14 (1980), pp. 71-106.
- [9] Wang, A.S.D., "Growth Mechanisms of Transverse Cracks and Ply Delamination in Composite Laminates," Proceedings, International Conference on Composite Materials, III, Vol. 1 (1980), p. 170.
- [10] Wang, A.S.D., "Fracture Mechanics of Sublaminar Cracks in Composite Laminates," in Characterization, analysis and Significance of Defects in Composite materials, Pub. No. 355, NATO Advanced Group on Aeronautical

Research and Development, London (1983), p. 15-1.

- [11] Wang, A.S.D., Chou, P.C. and Lei, S.C., "A Stochastic Model for the Growth of Matrix Cracks in Composite Laminates," in Advances in Aerospace Structures, Materials and Dynamics, ASME AD-06 (1983), New York. pp. 7-16.
- [12] Wang, A.S.D., Slomiana, M and Bucinell, R., "A Three Dimensional Finite Element Analysis of Delamination Growth in Composite Laminates: Part 1. The Energy Method and Case Studies," NADC-84017-60 (1983), Naval Air Development Center, Pa.
- [13] Crossman, F.W., Warren, W.J. and Wang, A.S.D., "Influence of Ply Thickness on Damage Accumulation and Final Fracture," in Advances in Aerospace Structures, Materials and Dynamics, ASME AD-06 (1983), New York. pp. 215-226.
- [14] Wang, A.S.D., Kishore, N.N. and Li, C.A., "A Three Dimensional Finite Element Analysis of Delamination Growth in Composite Laminates: Part 2. The Finite Element Code and User's Manual," NADC-84018-60 (1983), Naval Air Development Center, Pa.
- [15] Pipes, R.B. and Pagano, N.J., "Interlaminar stresses in Composite Laminates Under Uniform Axial Tension," Journal of Composite Materials, Vol. 4 (1970) pp. 538-
- [16] Wang, A.S.D. and Crossman, F.W., "Some New Results on Free Edge Effects in Symmetric Composite Laminates," Journal of Composite Materials, Vol. 11 (1977), pp. 92-
- [17] Wang, A.S.D., Kishore, N.N. and Feng, W.W., "On Mixed-mode Fracture in Off-axis Unidirectional Graphite Epoxy Composites," Proceedings, International Conference on Composite Materials, IV, Vol. 1 (1982), pp. 599.
- [18] Juvinall, R.C., "Stress, Strain and Strength," McGraw Hill, New York, (1967), p. 346.

TABLE I

Material Constants For T300/934 Unidirectional Ply

Property	SI Unit	English Unit
E_{LL}	144.8 Gpa	21×10^6 psi
E_{TT}, E_{zz}	11.7 Gpa	1.7×10^6 psi
ν_{LT}, ν_{Lz}	0.3	0.3
ν_{Tz}	0.54	0.54
G_{LT}, G_{Lz}	6.5 Gpa	0.94×10^6 psi
G_{Tz}	3.5 Gpa	0.5×10^6 psi
α_T, α_z	$28.8 \times 10^{-6} / ^\circ C$	$16 \times 10^{-6} / ^\circ F$
α_L	$0.36 \times 10^{-6} / ^\circ C$	$0.2 \times 10^{-6} / ^\circ F$
<hr/>		
t, nominal ply thickness	0.132 mm	0.0052"
ΔT , temperature drop	125 $^\circ C$	225 $^\circ F$
G_{Ic} (0/0 interface)*	158 J/m ²	0.9 in-lb/in ²
G_{Ic} (90/90 interface)*	228 J/m ²	1.3 in-lb/in ²
$G_{(I,II)c}, G_{II}/G_I = 0.5^*$	288.75 J/m ²	1.65 in-lb/in ²

* See discussions in Ref. [17].

TABLE II

Summary of Results in Section 2.1

Laminate Type	1st Cracking Event (threshold strain)	Experimental value (strain ranges)
$[\pm 25/90]_s$	Free edge Delam. (0.60%)	Free edge Delam. (0.58 to 0.61%)
$[0_2/90]_s$	Transv. Cracking (0.59%)	Transv. Cracking (.55 to 0.57%)
$[0_2/90_2]_s$	Transv. Cracking (0.33%)	Transv. Cracking (0.29 to 0.36%)
$[0_2/90_4]_s$	Transv. Cracking (0.31%)	Transv. Cracking (0.24 to 0.28%)

TABLE III

Summary of Predicted(Experimental) Cracking Events in the $[0_2/90_n]_s$ Laminate Family.

Laminate Type	Laminate Tensile Strain at Onset of Predicted(Experimental) Events, 10^{-3} .				
	90° Ply T. C.	0° Ply Split	Delam. @ X-Cracks	Delam. @ TC/FE	Final Failure
$[0_2/90]_s$	pr. 5.9 ex. (5.6)	> 12 (not observed)	> 12 (not observed)	> 12 (not observed)	---- (12.3)
$[0_2/90_2]_s$	3.3 (3.2)	10.5 (9.2)	10.9 (>9.2)	11.0 (>10)	---- (11.2)
$[0_2/90_4]_s$	3.1 (2.6)	7.8 (<8.0)	7.5 (<8.0)	7.8 (8.0)	---- (10.3)
$[0_2/90_8]_s$	--- (1.9)	--- (4.7)	--- (4.7)	--- (4.1)	---- (7.5)

TABLE IV

Influence of Matrix Cracking on Load-Bearing Plies.

Number of 90° Plies	Experimental Failure (Tensile) Stain $\bar{\epsilon}_x$, 10^{-3}		
	$[0_2/90_n]_s$	$[\pm 25/90_n]_s$	$[\pm 30/90_n]_s$
n = 0	12.2	6.70	---
n = 1	12.3	6.66	6.15
n = 2	11.2	6.51	6.06
n = 4	10.3	5.37	5.70
n = 8	7.50	3.90	4.33

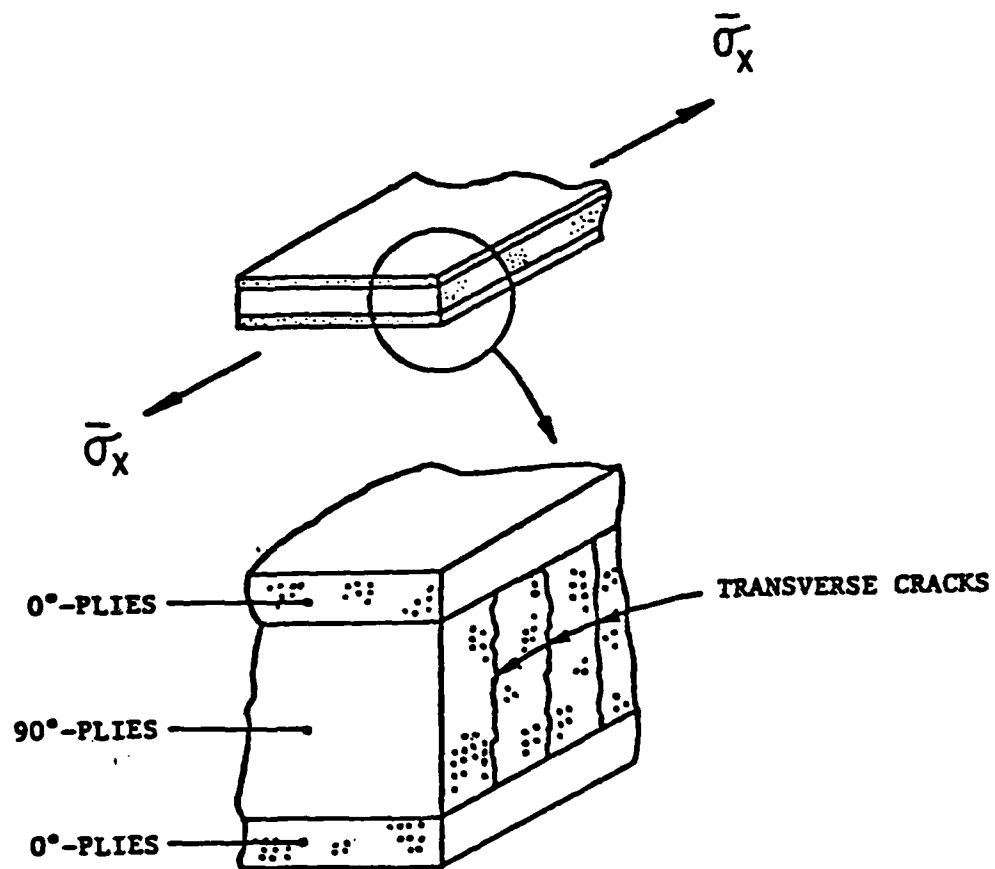


Figure 1 Schematic View of Multiple Transverse Cracks

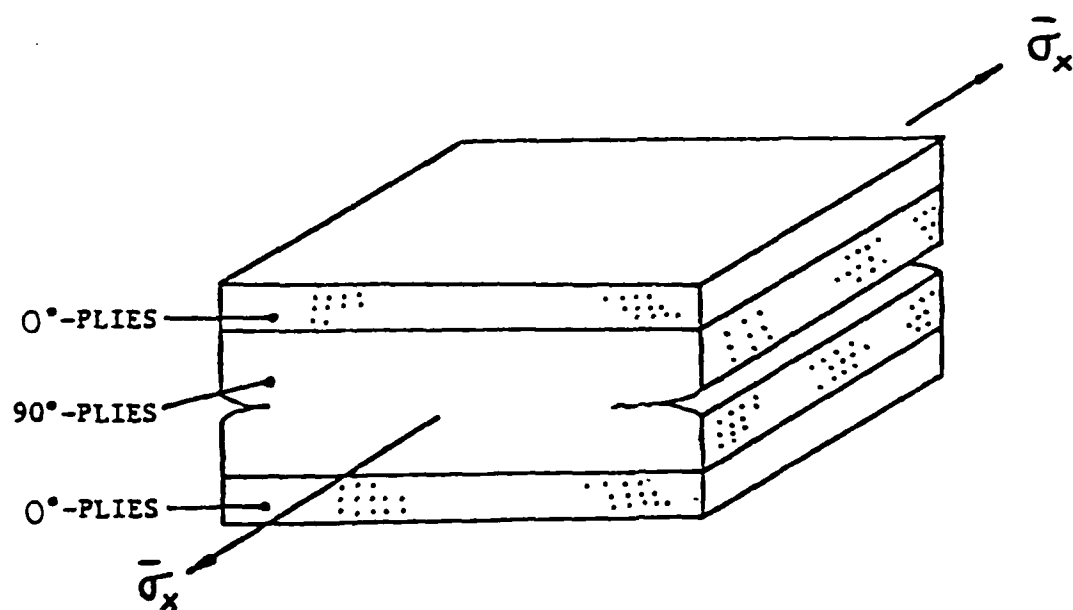


Figure 2 Schematic View of Free Edge Delamination.

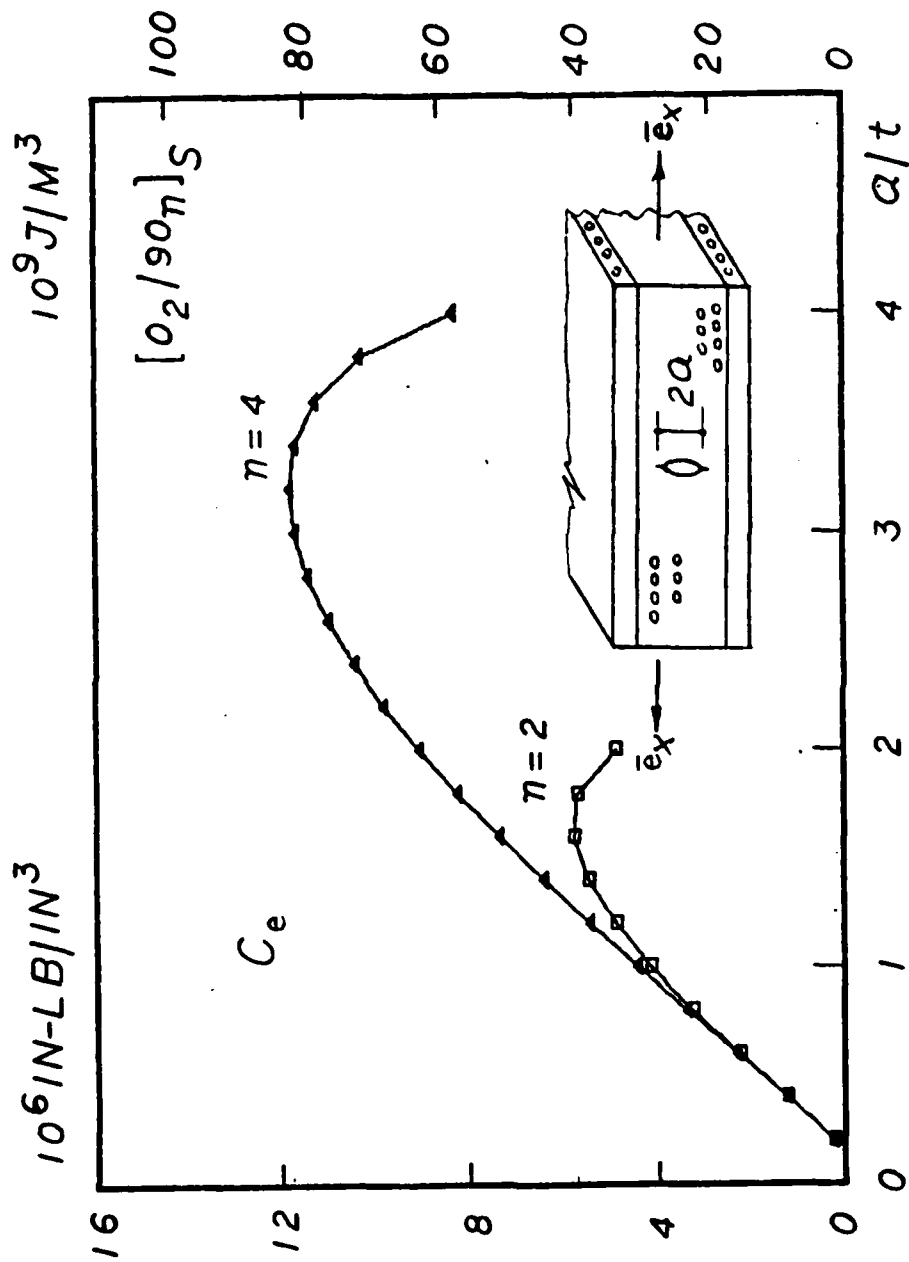


Figure 3 Strain Energy Release Rate Coefficient, C_e , for Transverse Cracking ($\bar{e}_x = 1$)

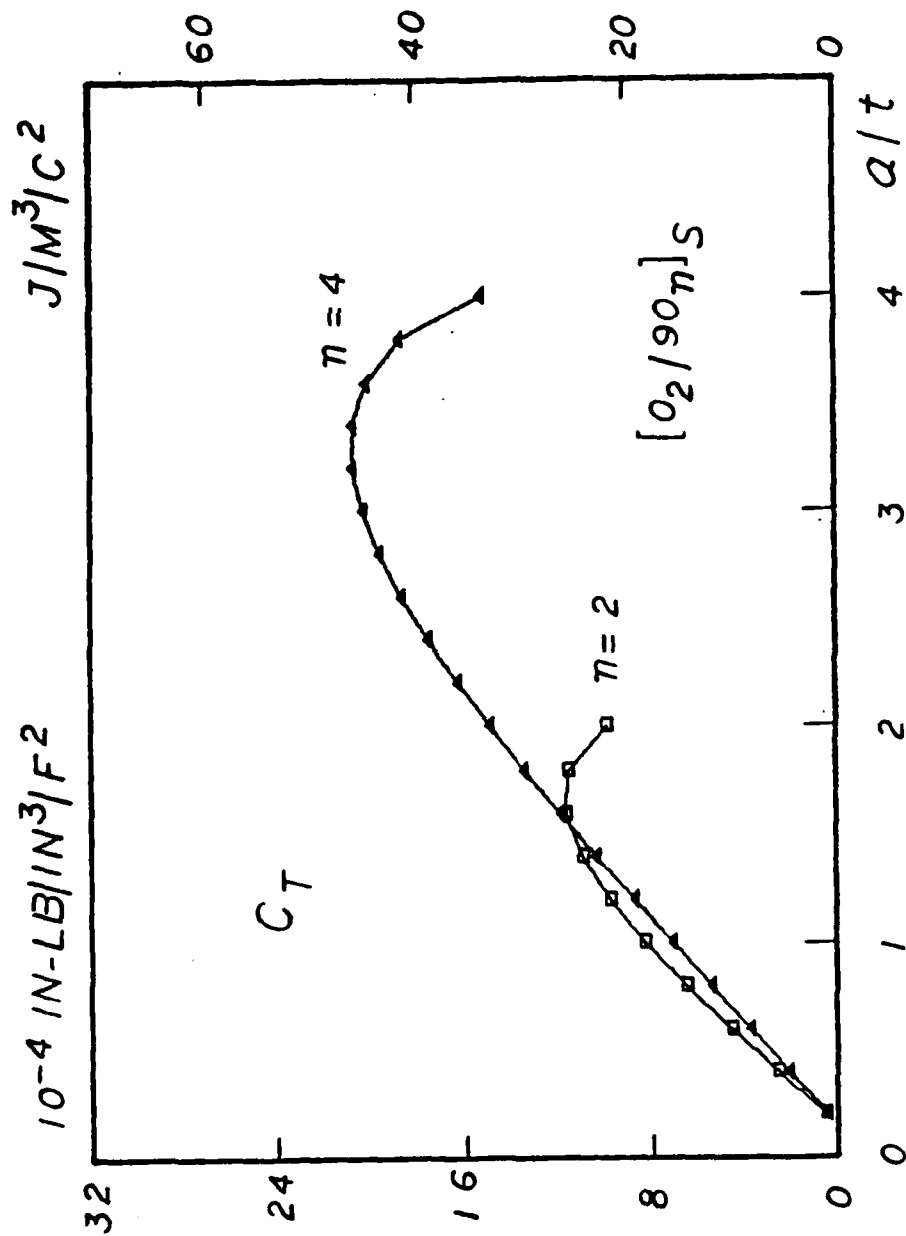


Figure 4 Strain Energy Release Rate Coefficient, C_T , for Transverse Cracking ($\Delta T = 1^\circ \text{F}$)

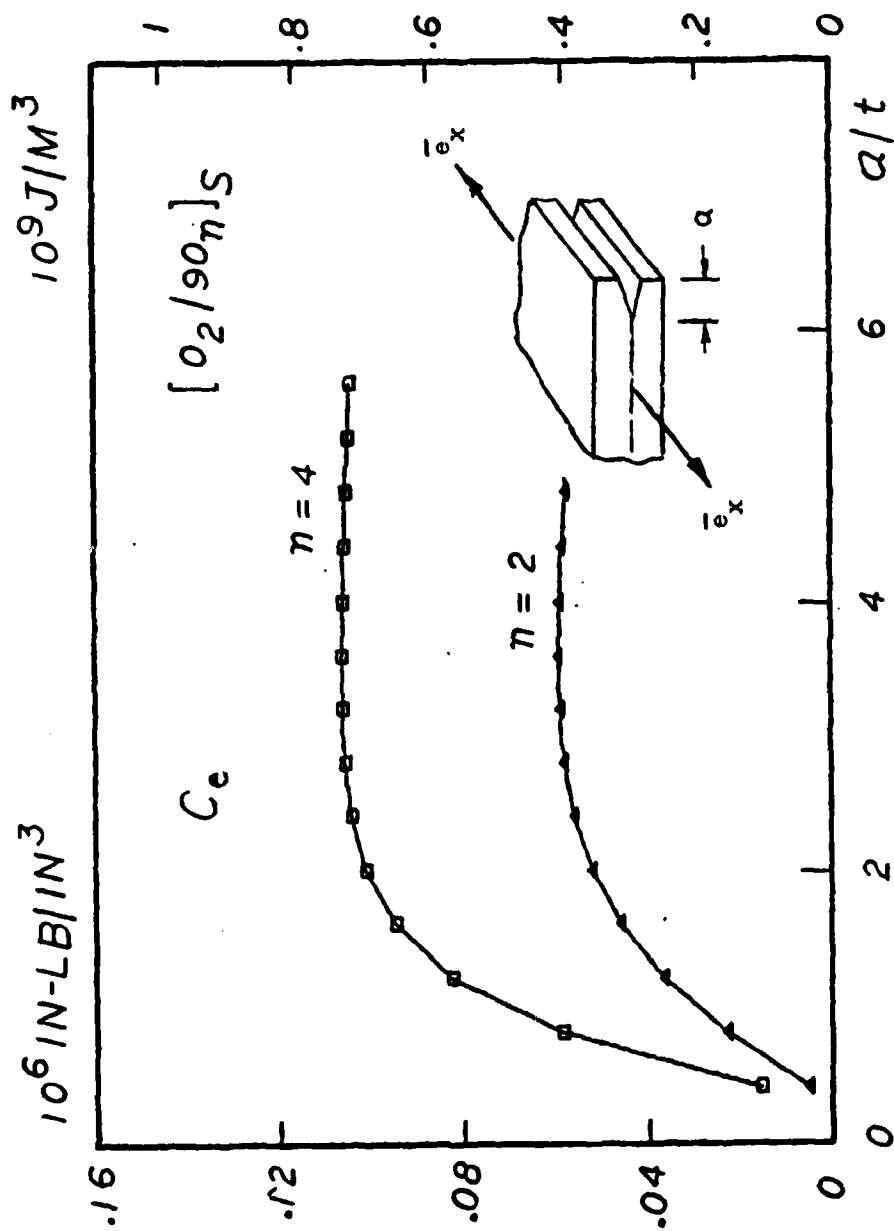


Figure 5 Strain Energy Release Rate Coefficient, C_e , for Free Edge Delamination ($\bar{e}_x = 1$)

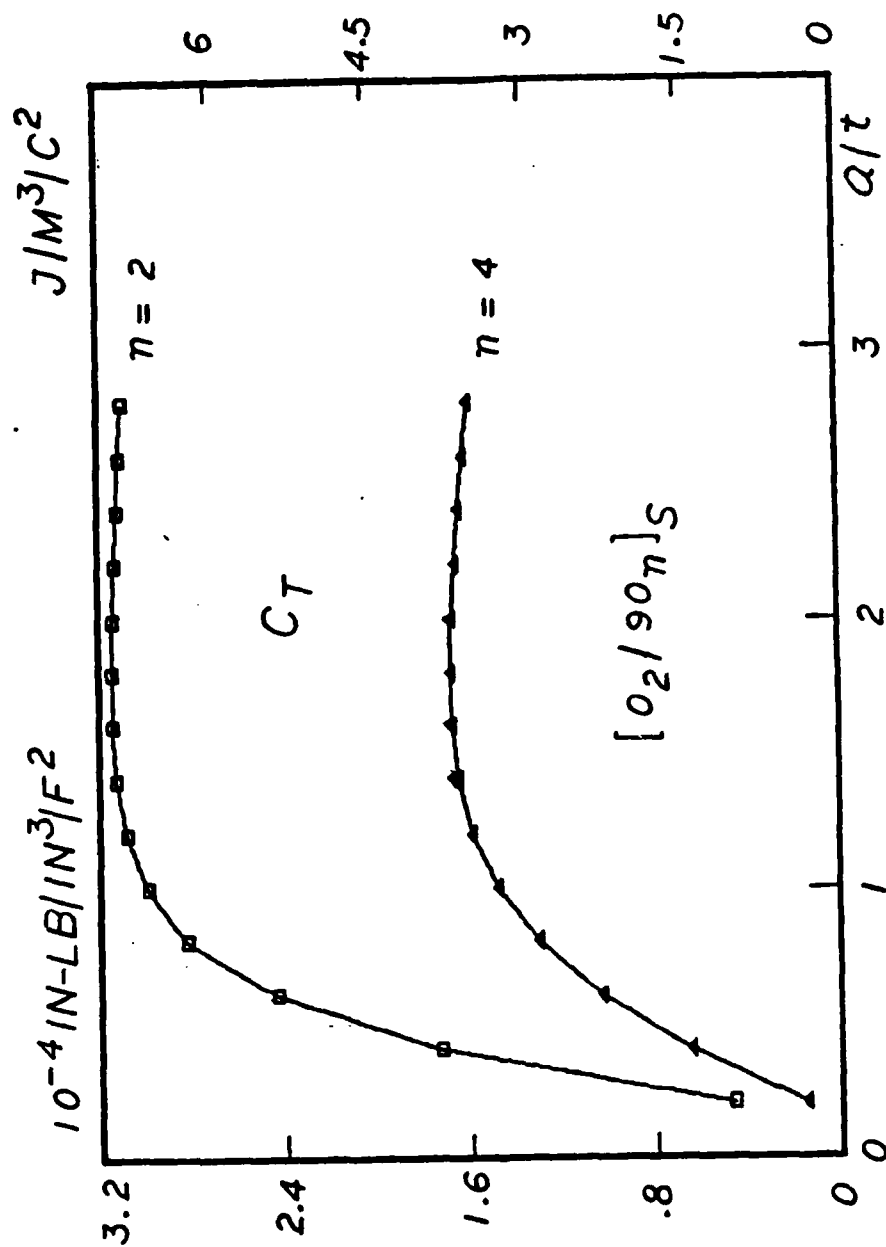


Figure 6 Strain Energy Release Rate Coefficient, C_T , for Free Edge Delamination ($\Delta T = 1^\circ \text{F}$)

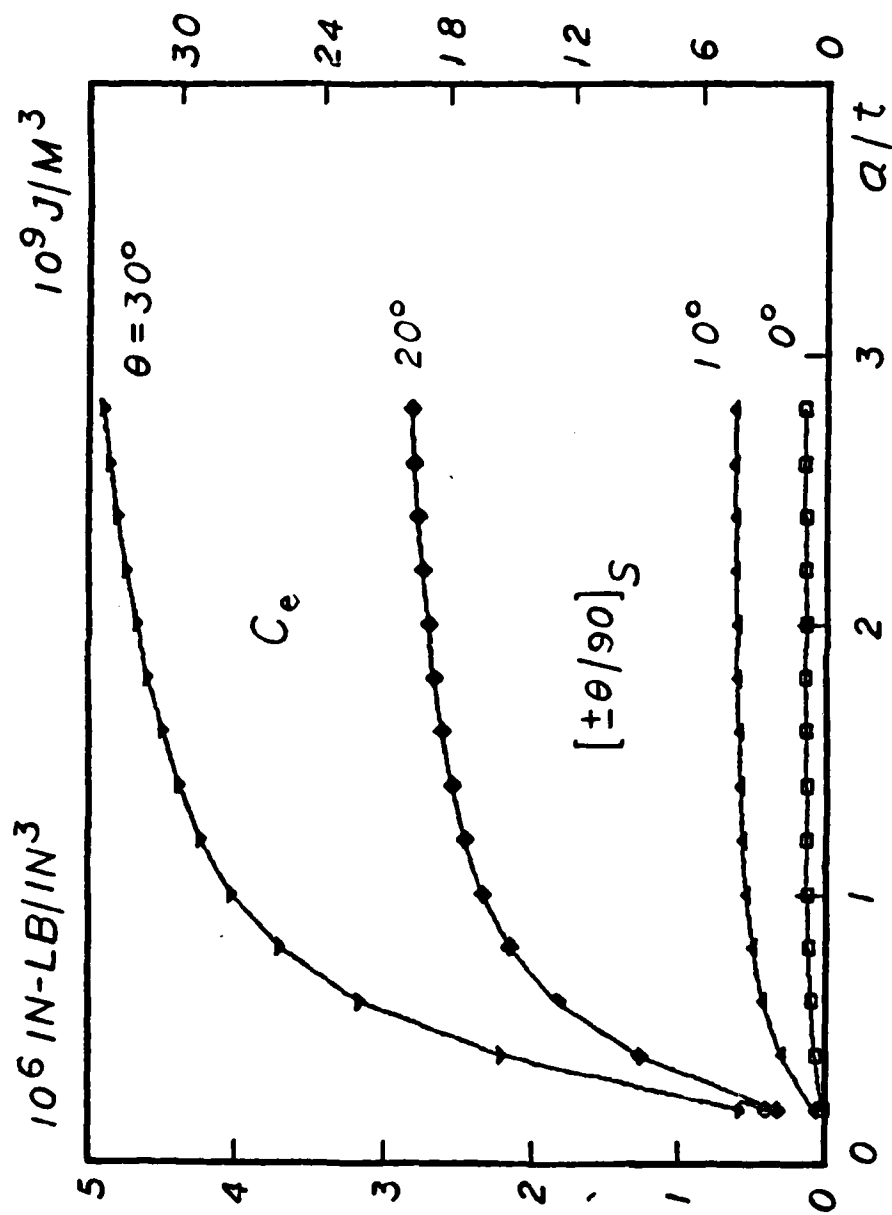


Figure 7 Strain Energy Release Rate Coefficient, C_e , for Free Edge Delamination ($\bar{e}_x = 1$)

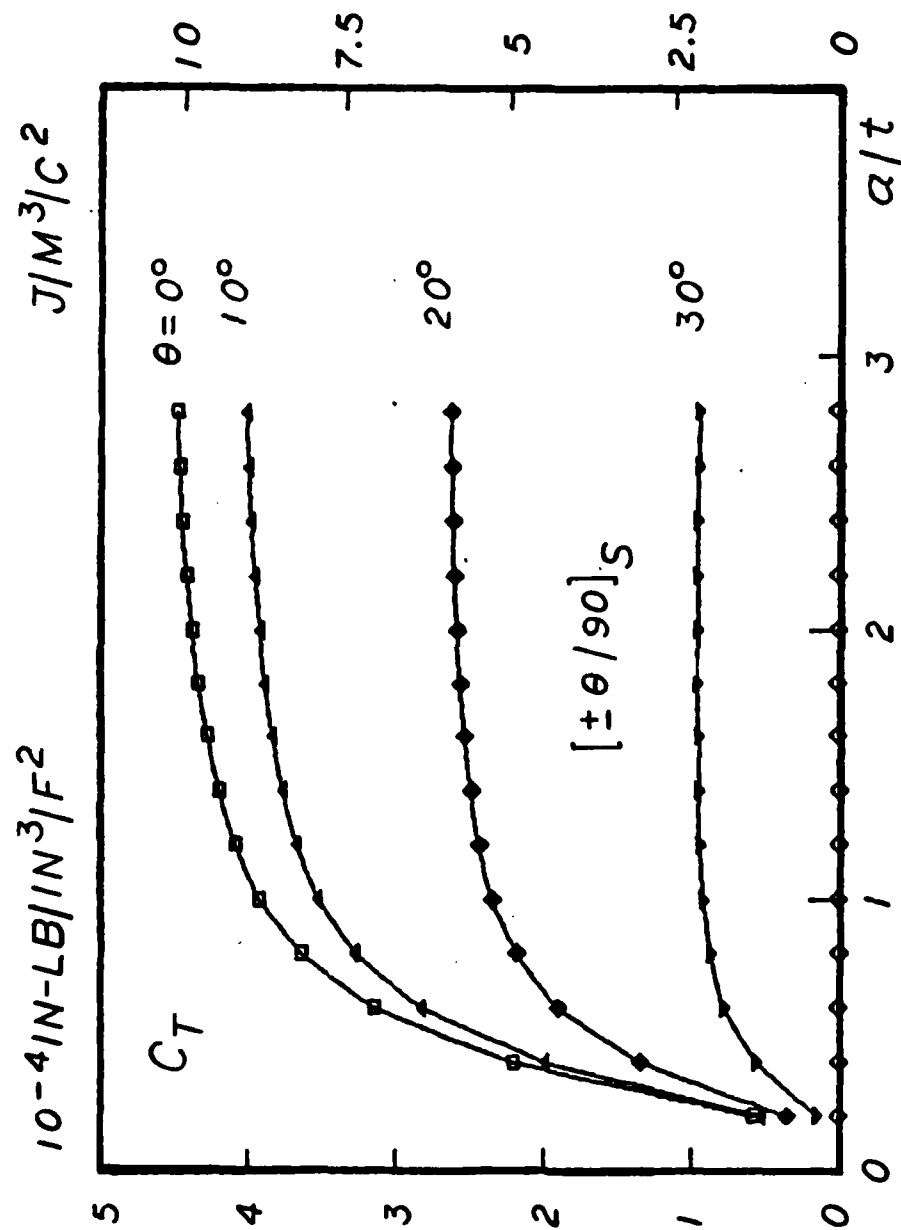


Figure 8 Strain Energy Release Rate Coefficient, C_T , for Free Edge Delamination ($\Delta T = 1^\circ\text{F}$)

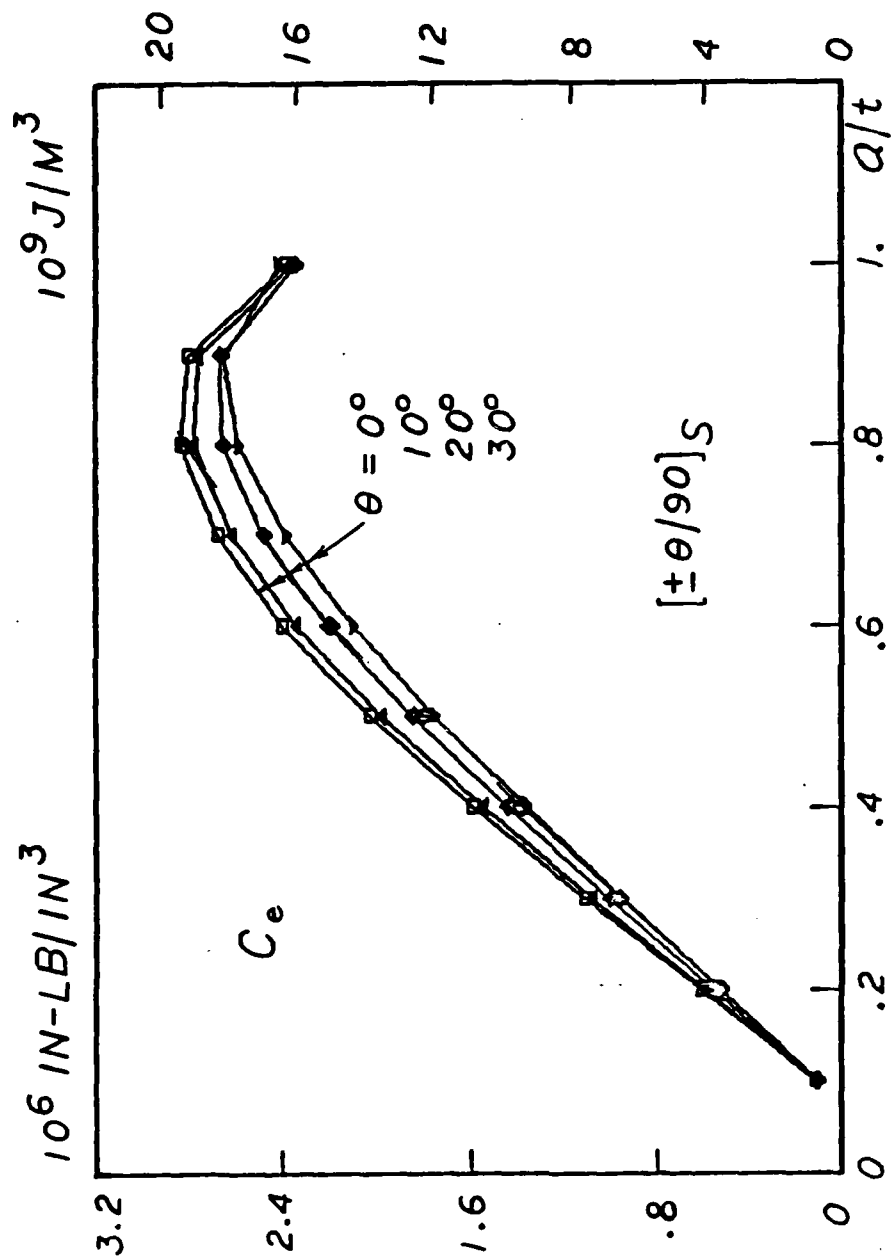


Figure 9 Strain Energy Release Rate Coefficient, C_e , for Transverse Cracking ($\bar{e}_x = 1$)

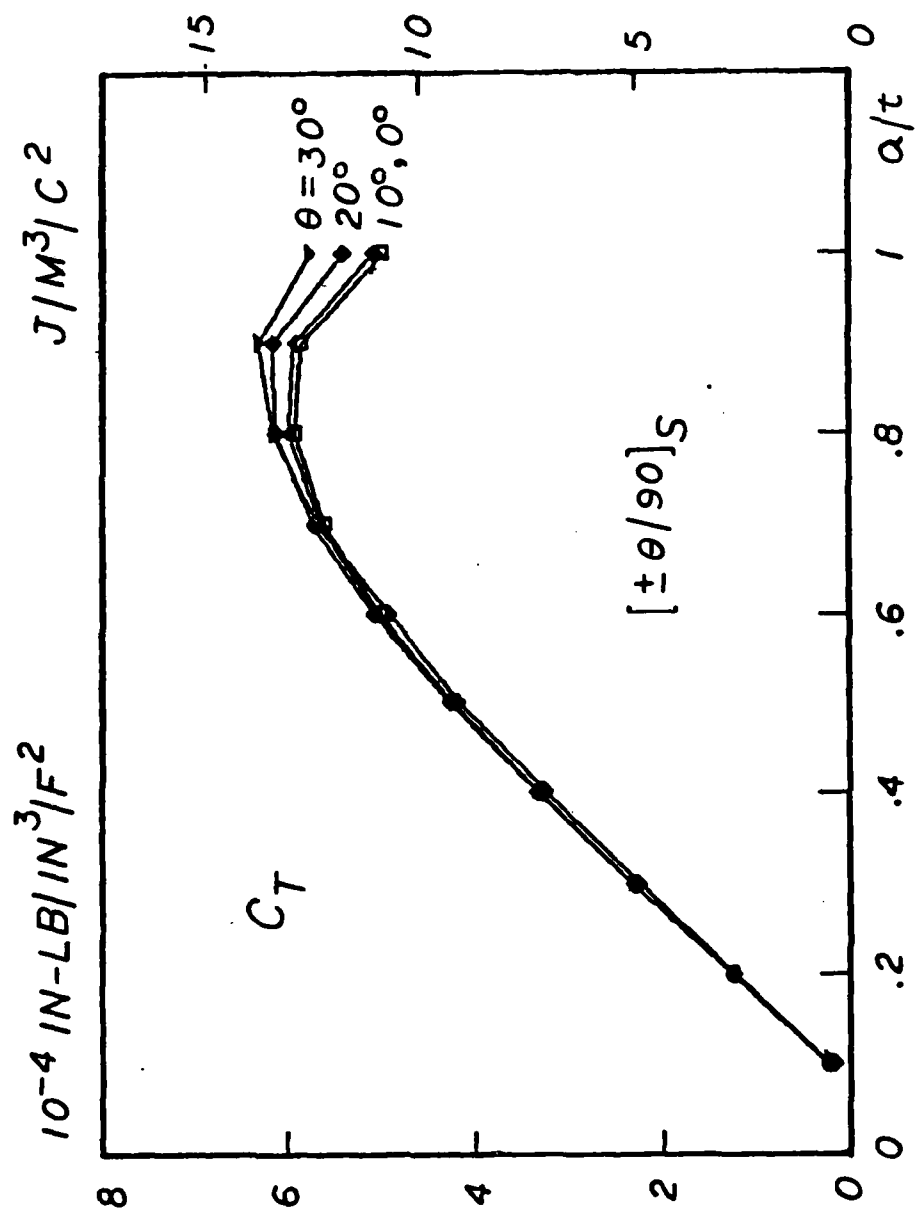


Figure 10 Strain Energy Release Rate Coefficient, C_T , for Transverse Cracking ($\Delta T = 1^\circ \text{F}$)

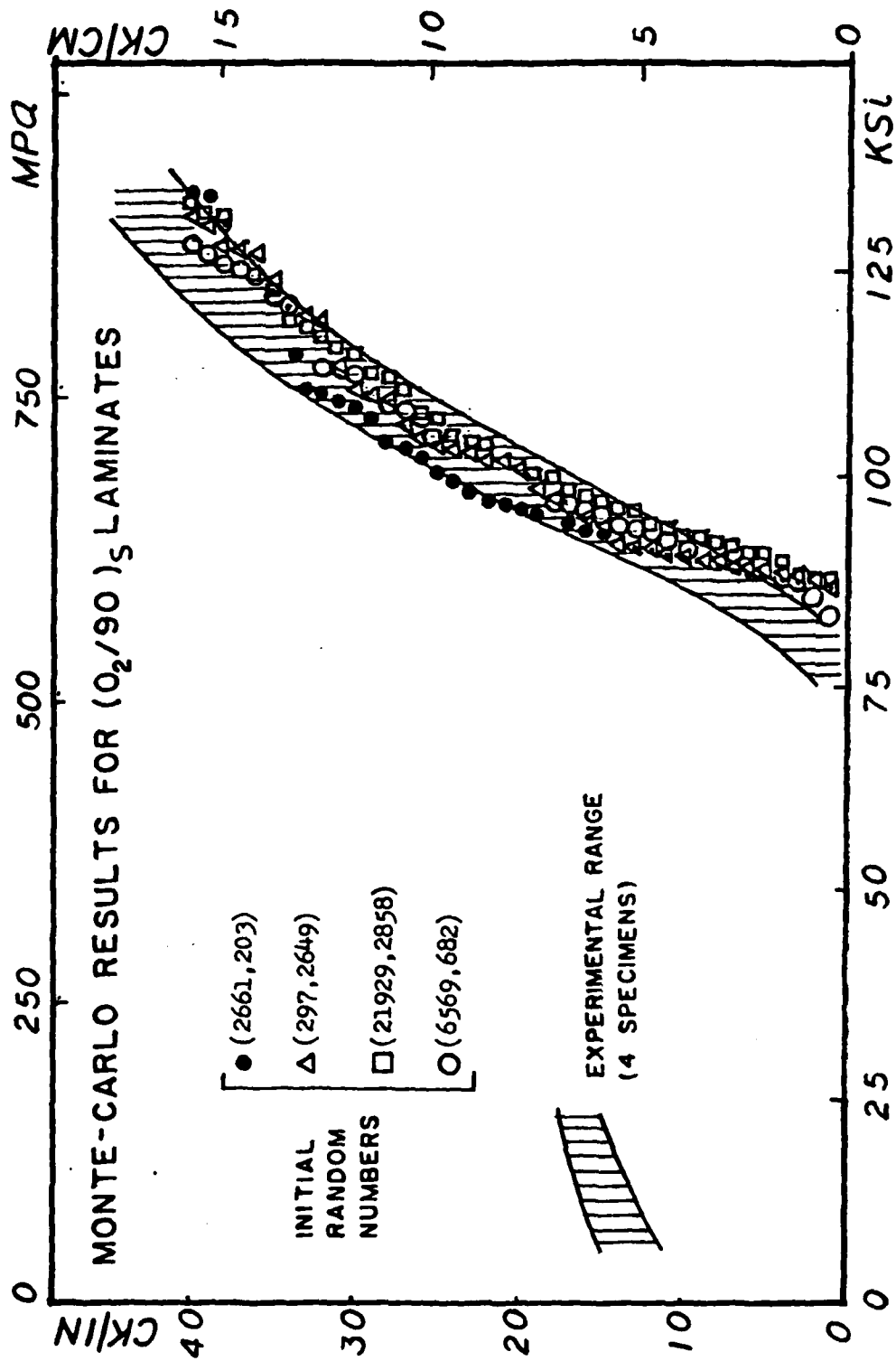


Figure 11 Simulated Transverse Crack Density vs. Applied Tension Relationship for $[O_2/90]_S$.

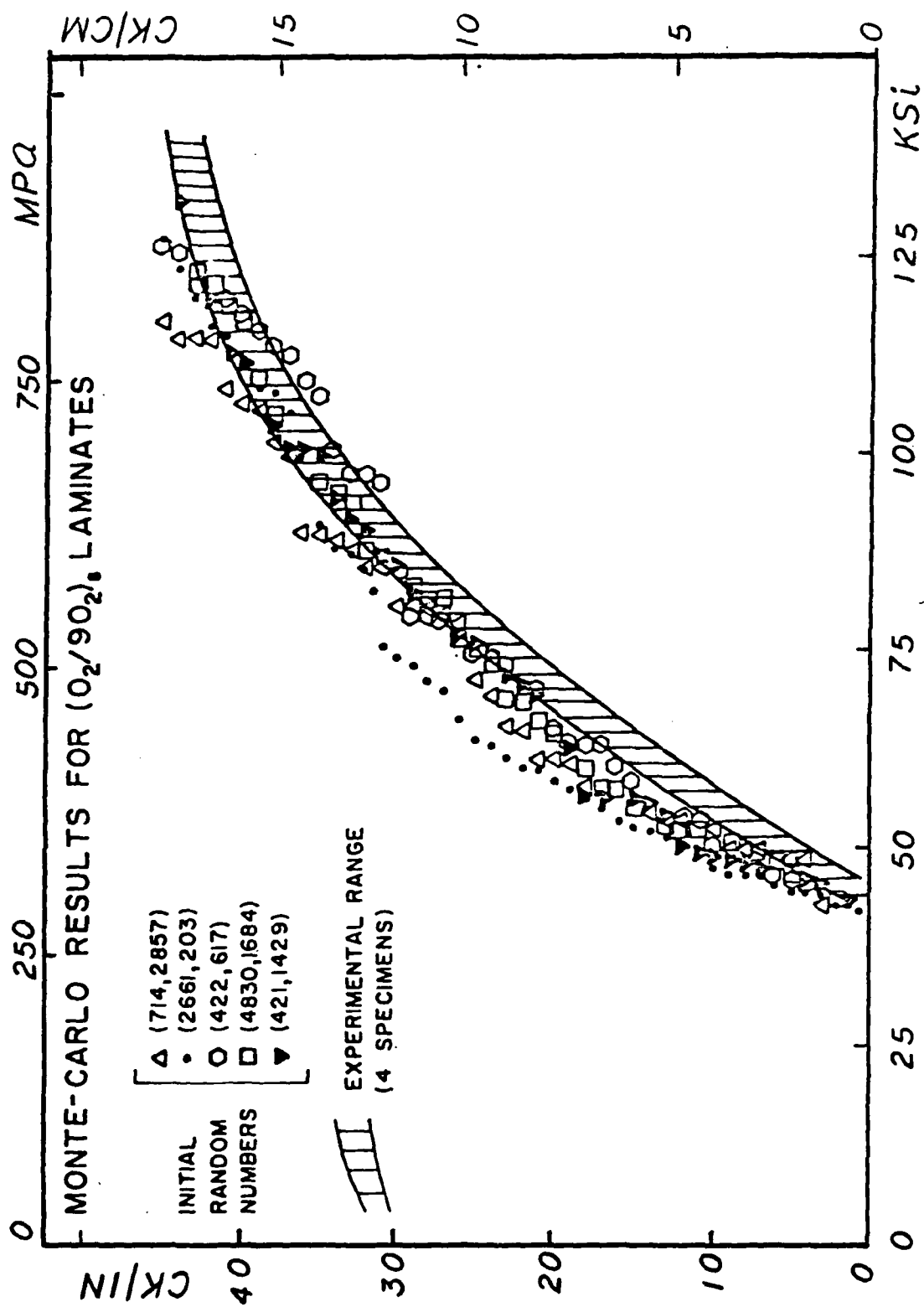


Figure 12 Simulated Transverse Crack Density vs. Applied Tension Relationship for $[O_2/90_2]_s$.

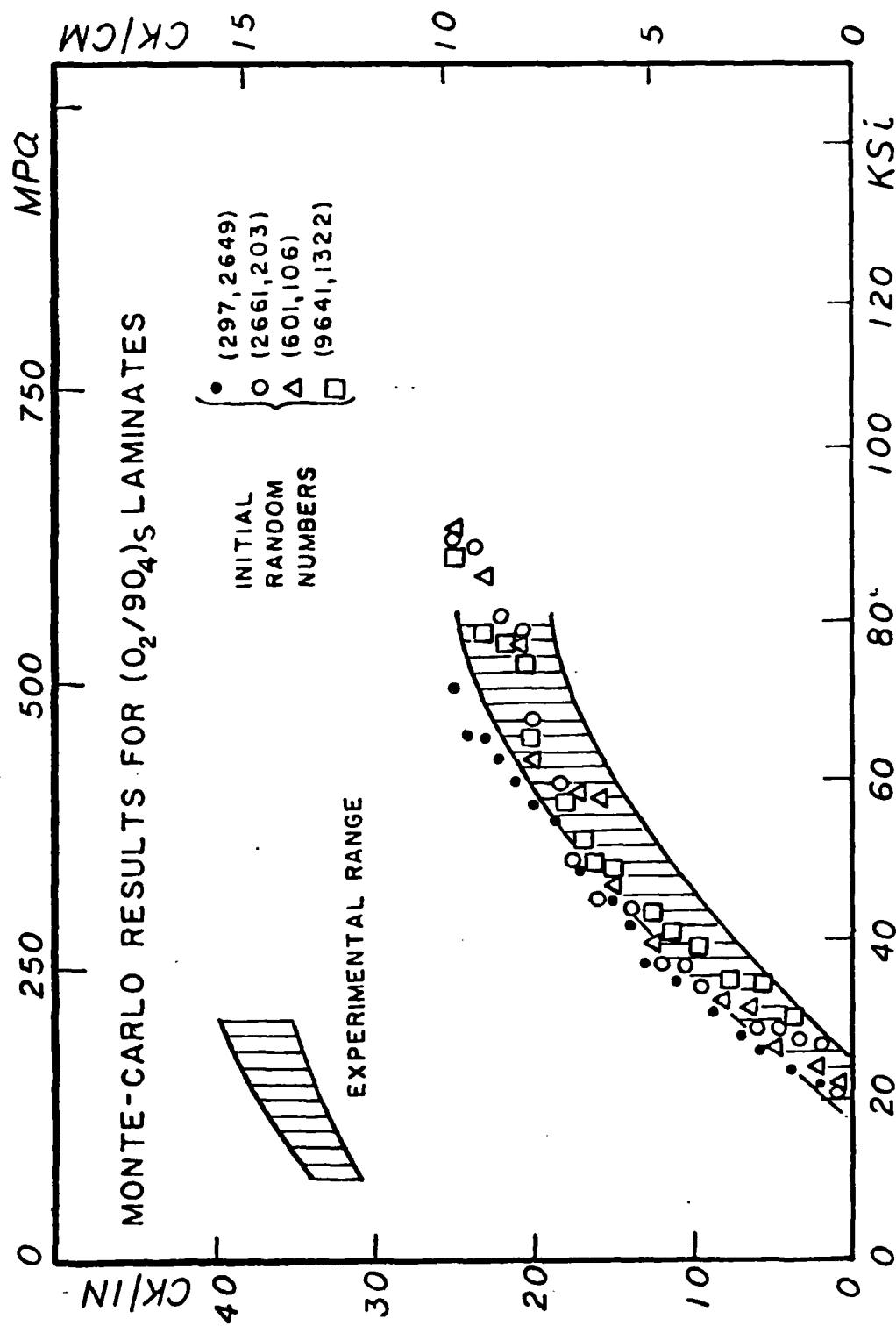


Figure 13 Simulated Transverse Crack Density vs. Applied Tension Relationship for $[O_2/90_4]_S$.

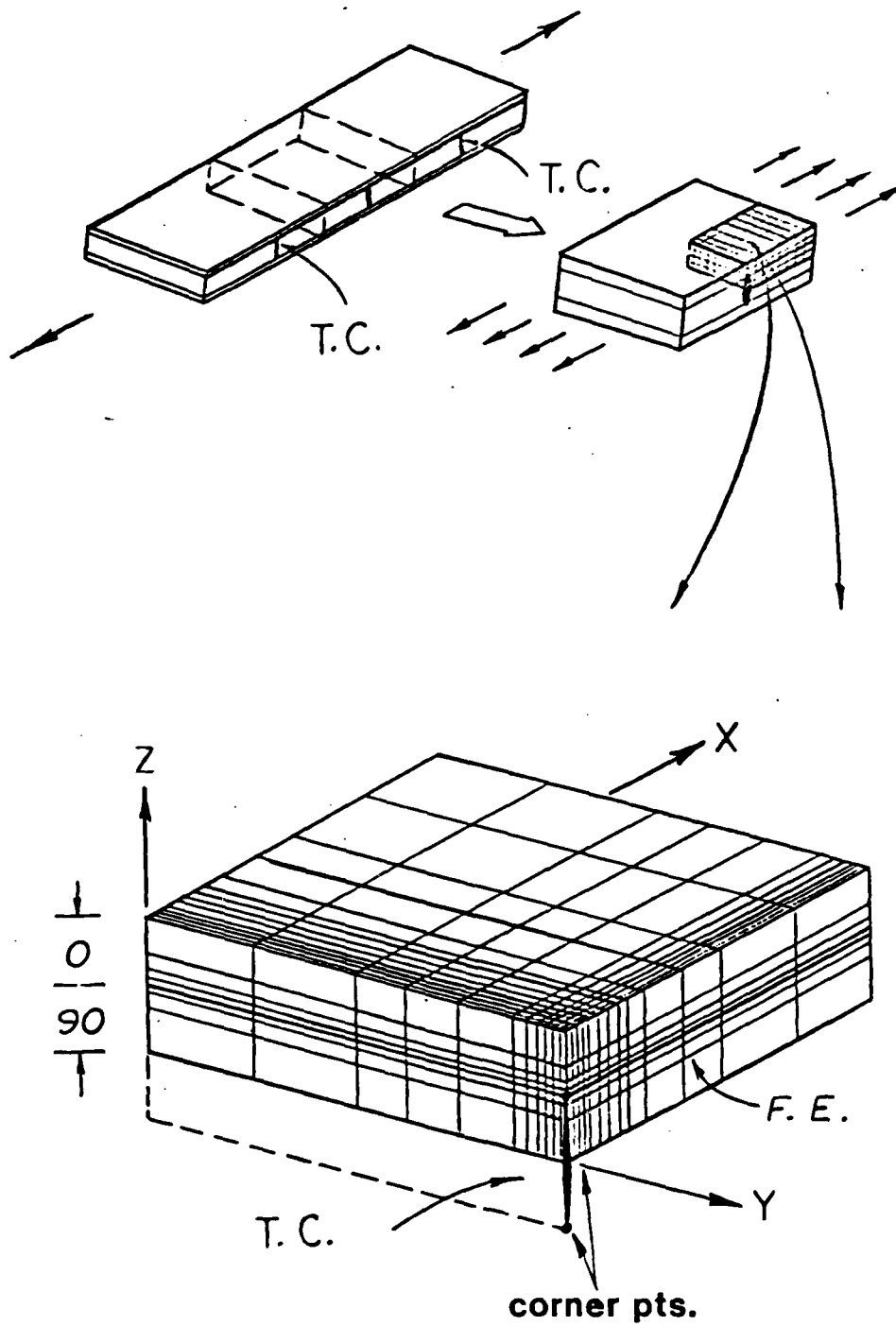


Figure 14 Finite Element Network for Stress Field Analysis.

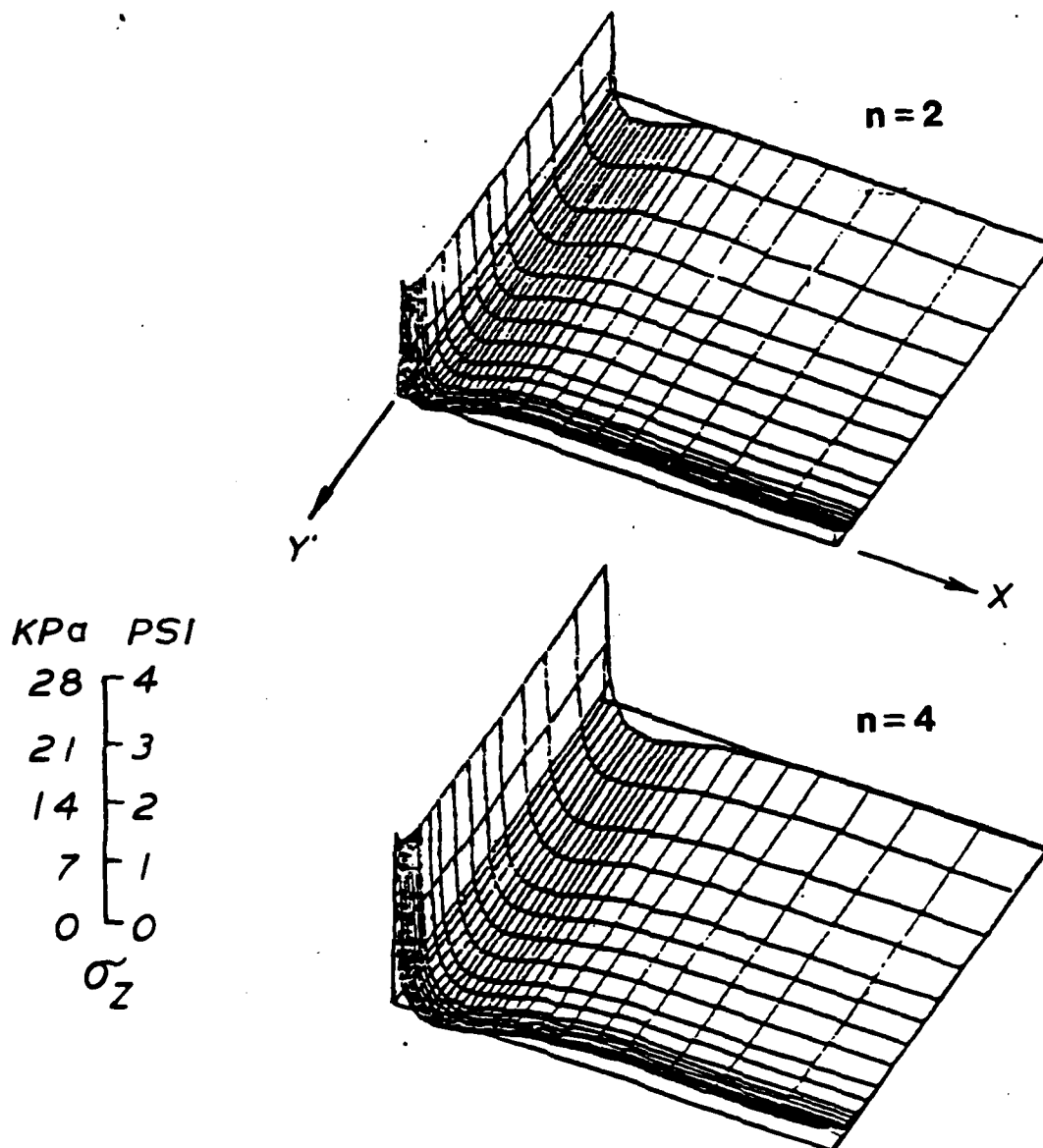


Figure 15 σ_z Distribution on 0/90 Interface Due to $\bar{e}_x = 10^{-6}$.

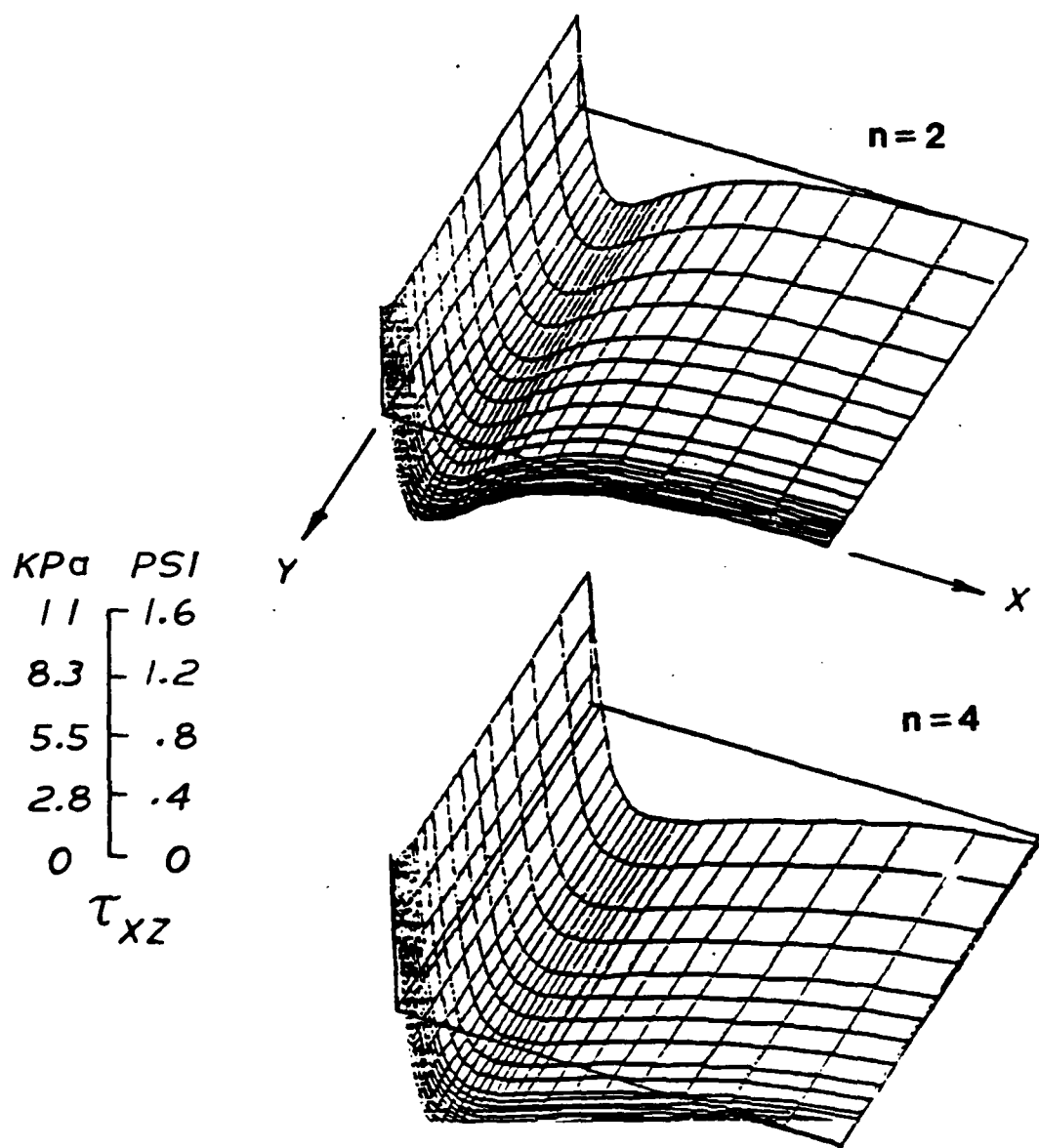
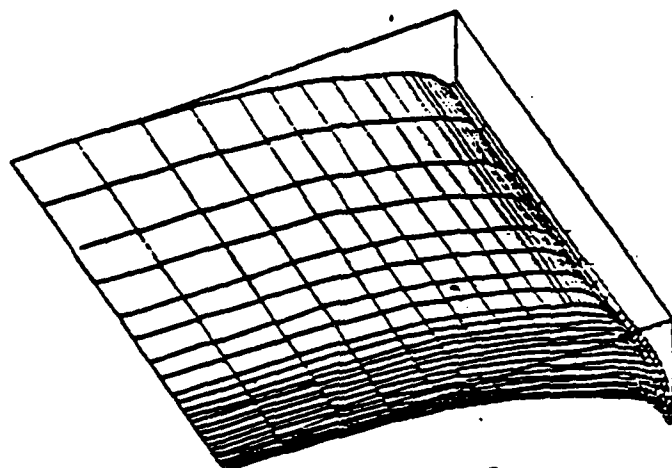


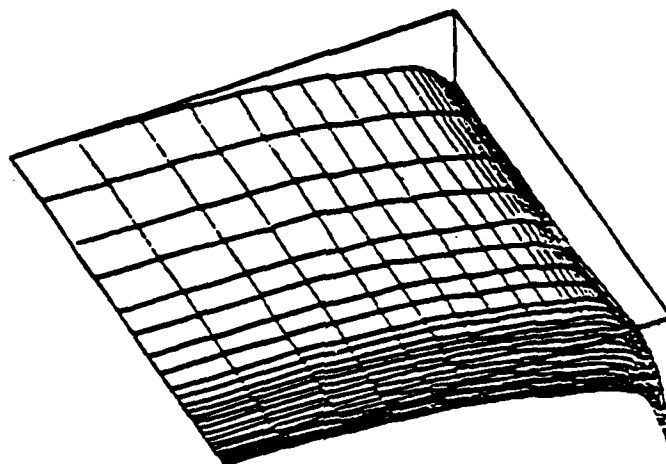
Figure 16 τ_{xz} Distribution on 0/90 Interface Due to $\bar{e}_x = 10^{-6}$.

KPa	PSI
5.5	.8
4.1	.6
2.8	.4
1.4	.2
0	0

τ_{yz}



$n=2$



$n=4$

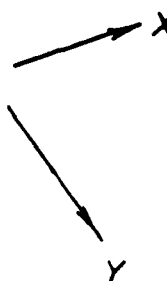


Figure 17 τ_{yz} Distribution on 0/90 Interface Due to $\bar{e}_x = 10^{-6}$.

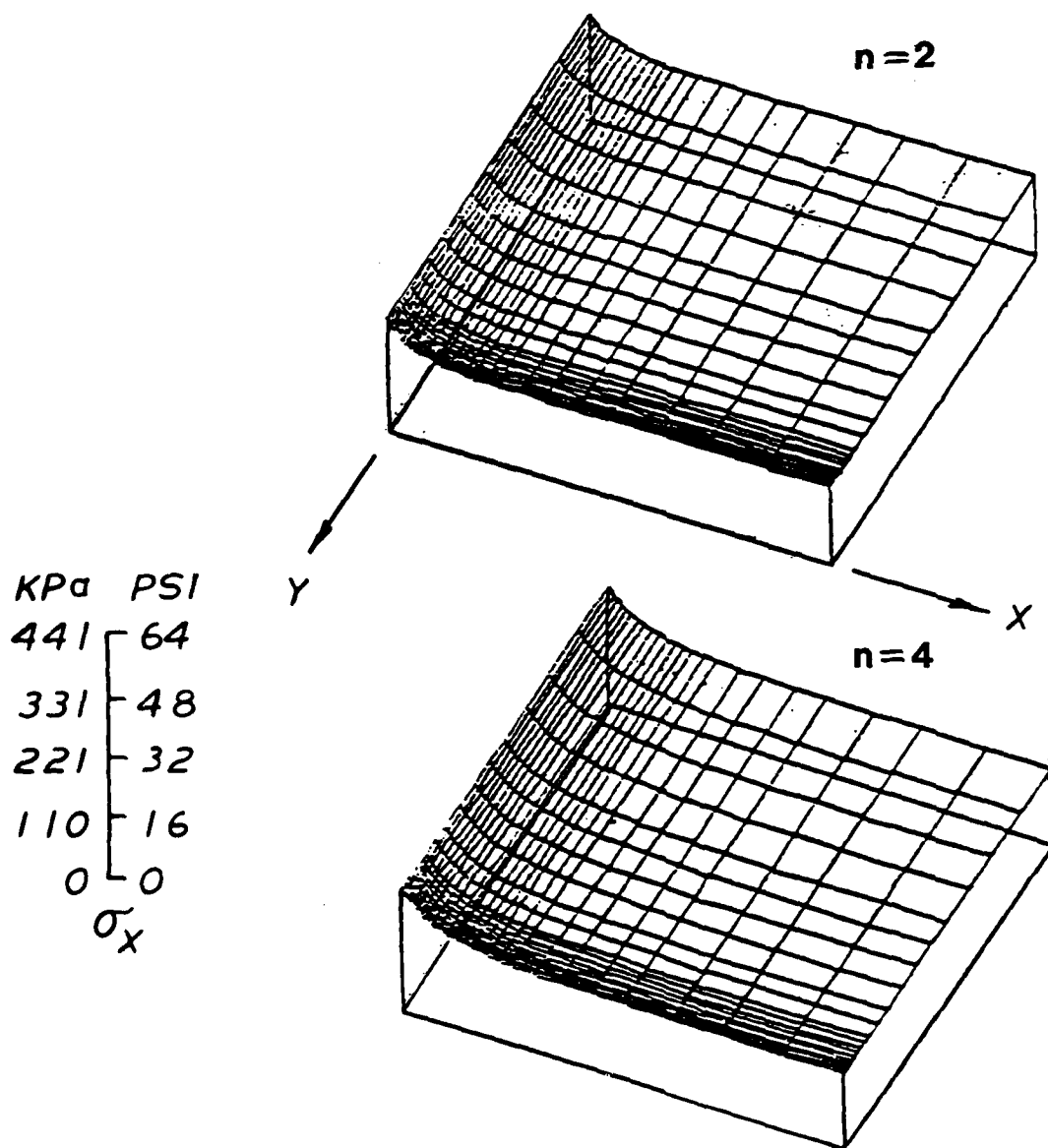


Figure 18 σ_x Distribution in the 0° Ply (near $0/90$ interface) Due to $\bar{e}_x = 10^{-6}$.

KPa	PSI
11	1.6
8.3	1.2
5.5	.8
2.8	.4
0	0

σ_y

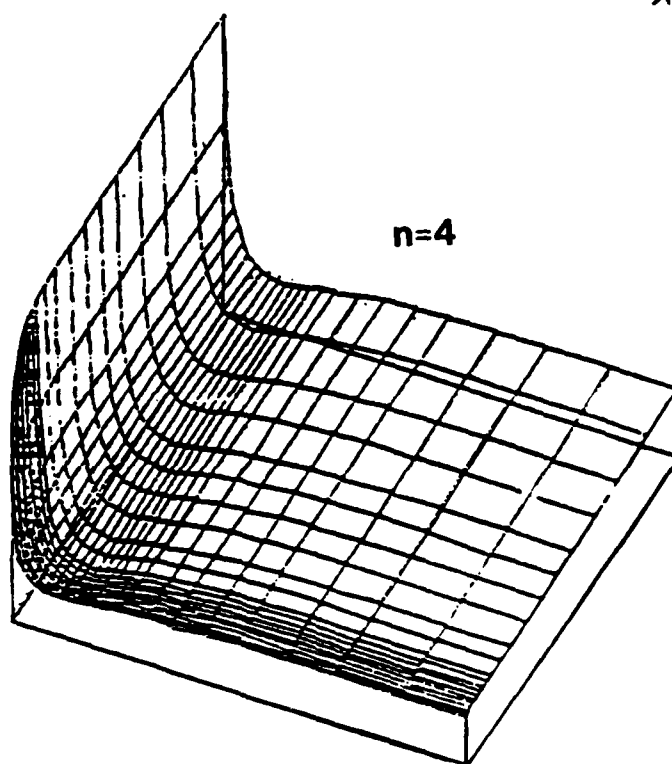
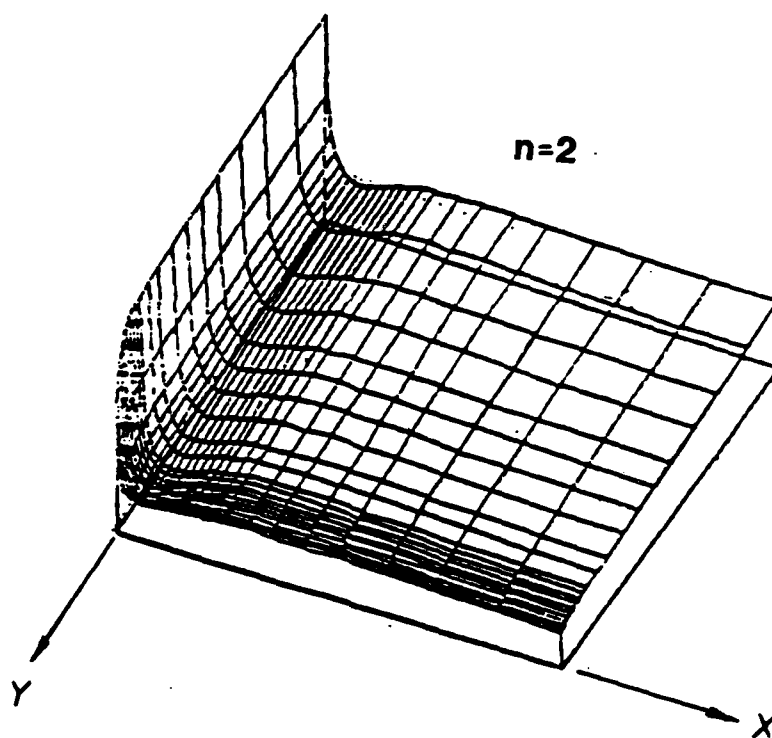


Figure 19 σ_y Distribution in the 0° Ply (near $0/90$ interface)
 Due to $\bar{\epsilon}_x = 10^{-6}$

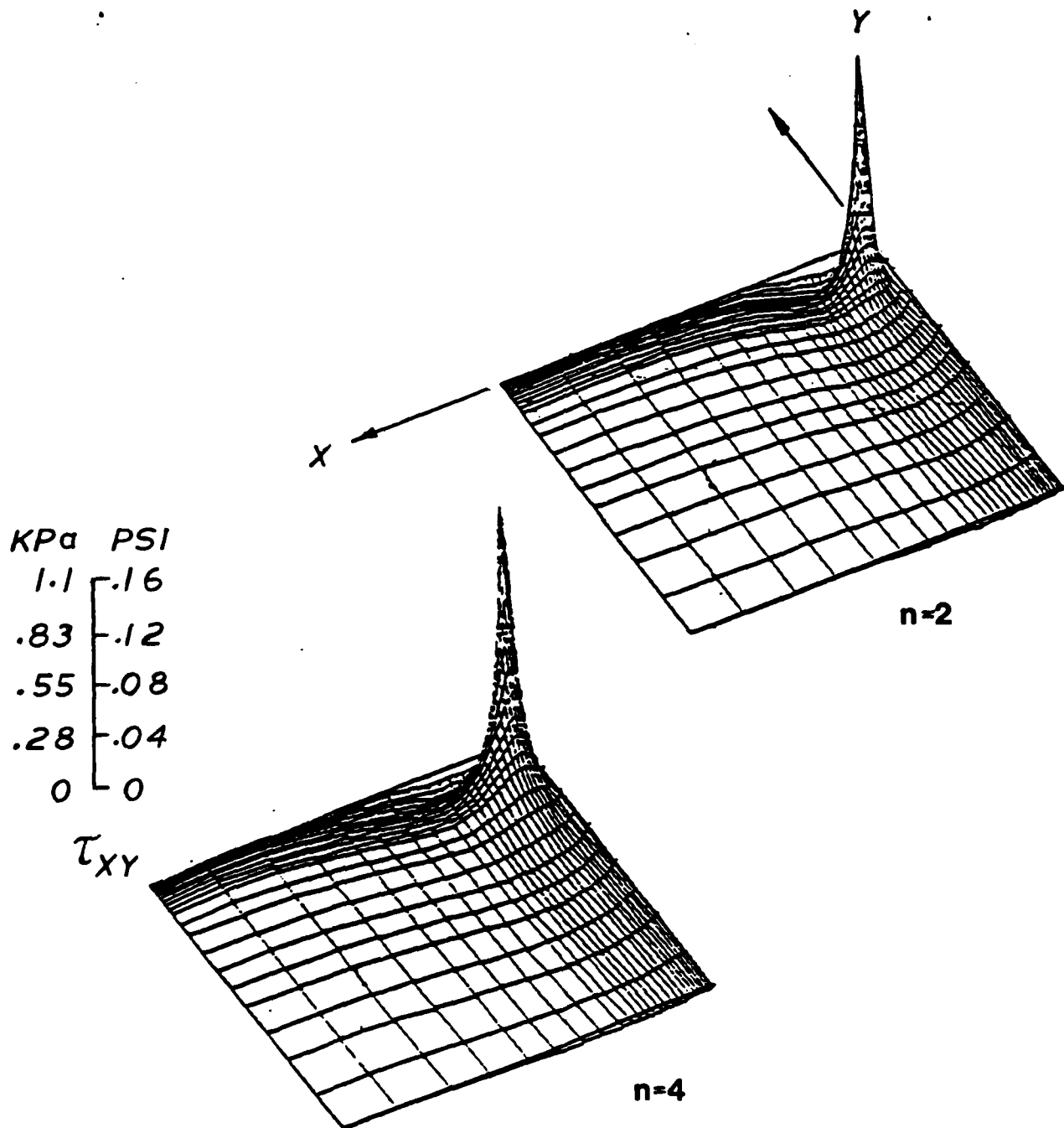


Figure 20 τ_{xy} Distribution in the 0° Ply (near $0/90$ interface)
 Due to $\bar{e}_x = 10^{-6}$.

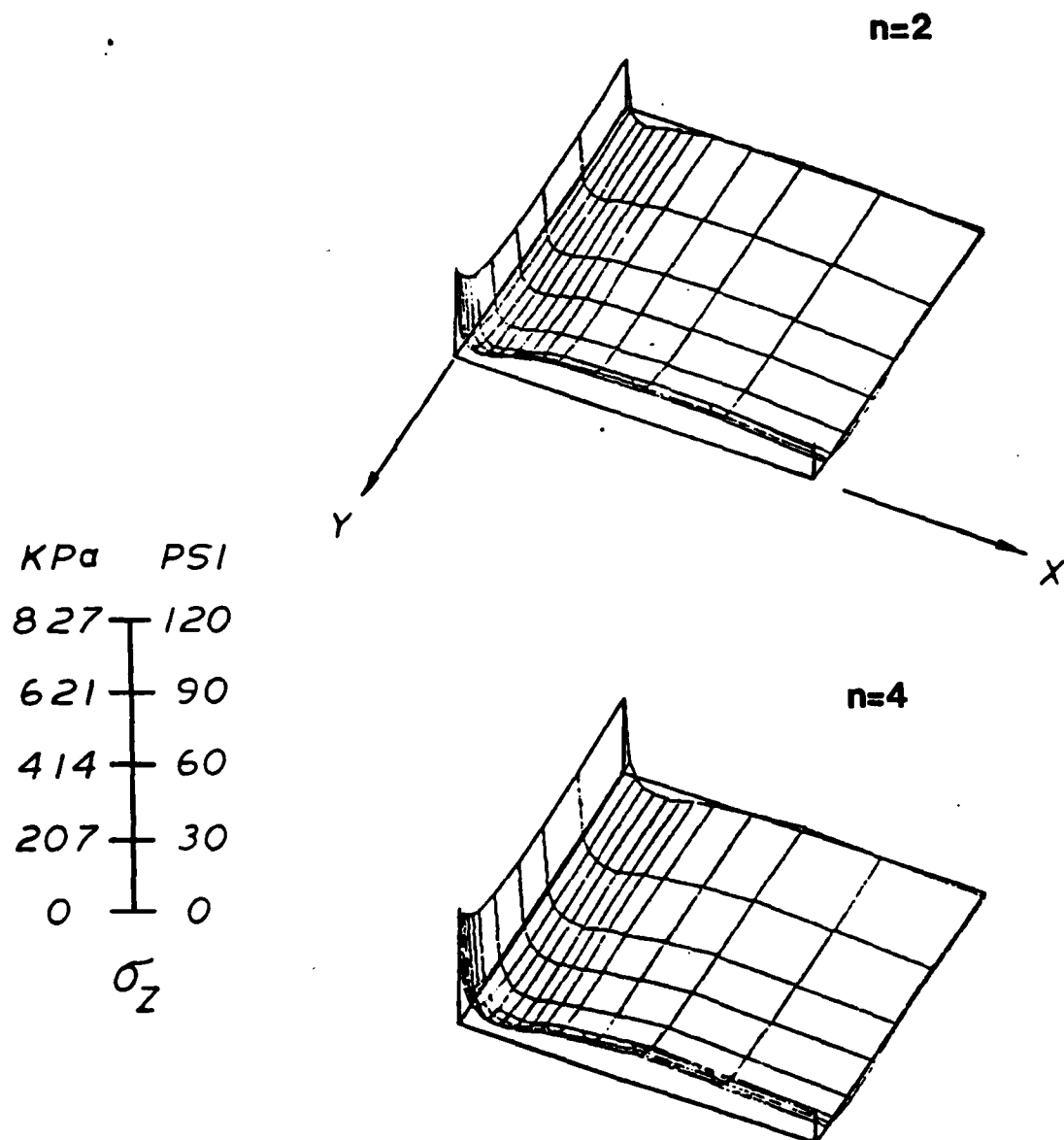


Figure 21 σ_z Distribution on 0/90 Interface Due to $\Delta T = -1^\circ\text{F}$.

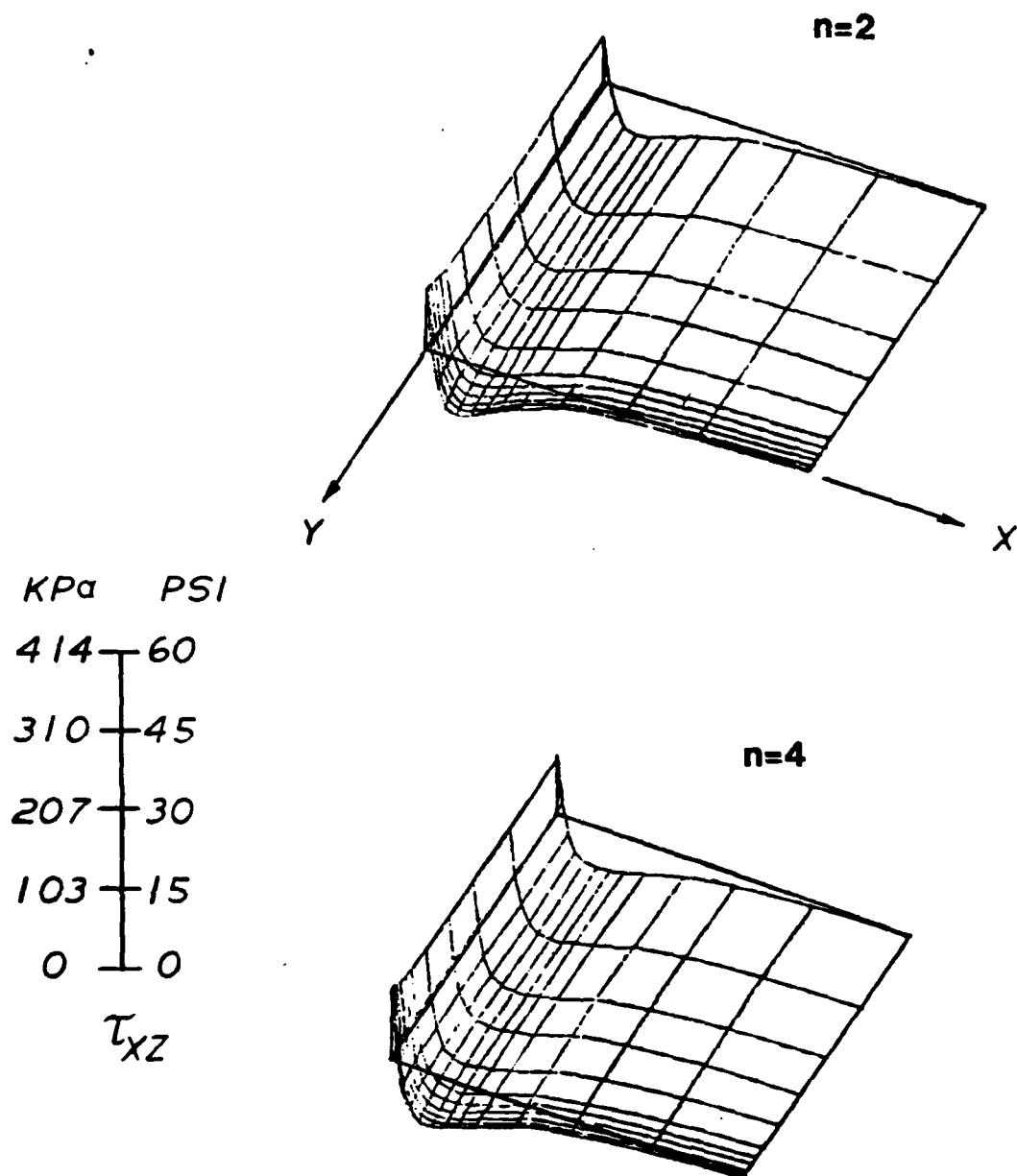


Figure 22 τ_{xz} Distribution on 0/90 Interface Due to $\Delta T = -1^{\circ}\text{F}$.

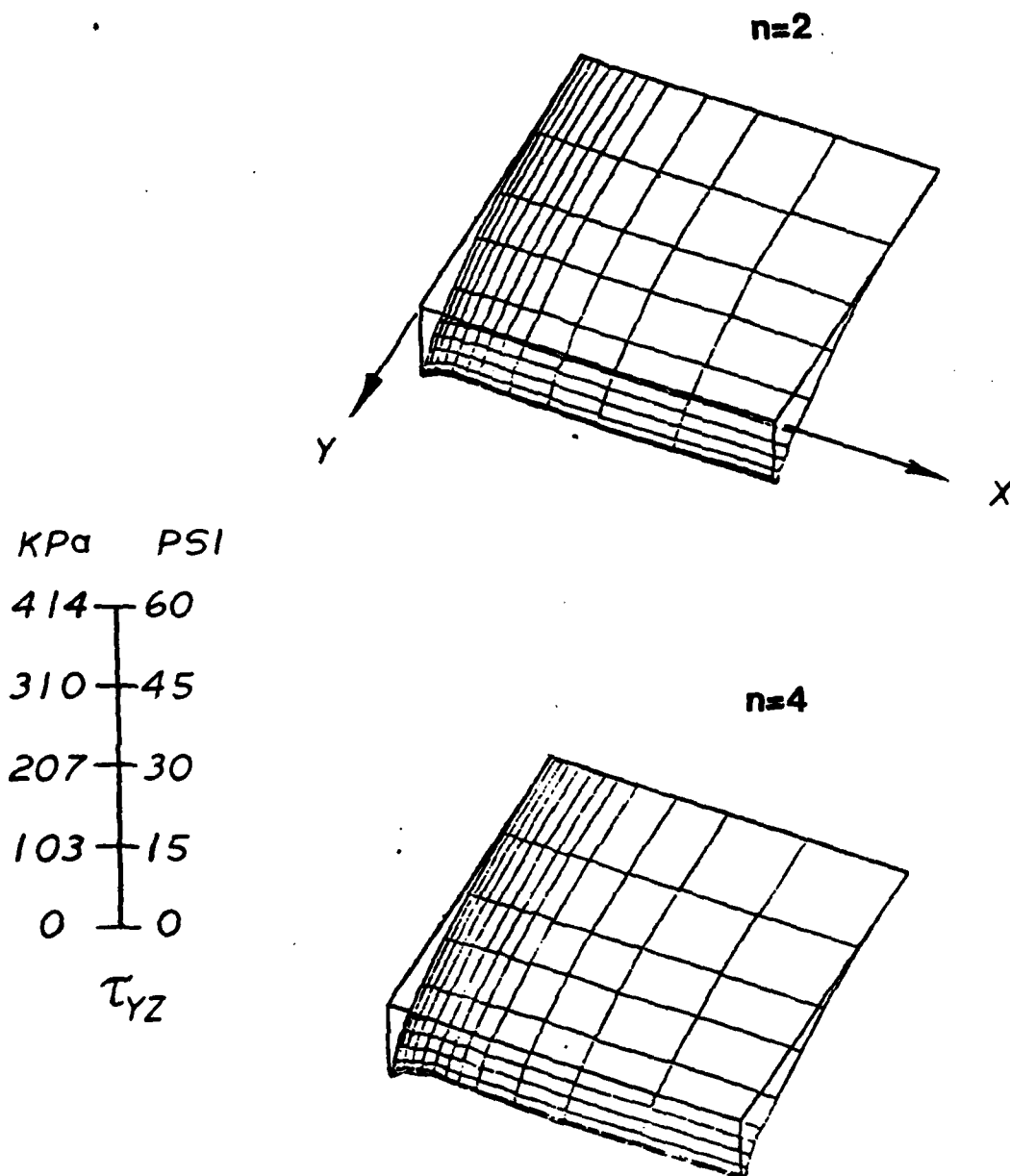


Figure 23 τ_{yz} Distribution on 0/90 Interface Due to $\Delta T = -1^{\circ}F$

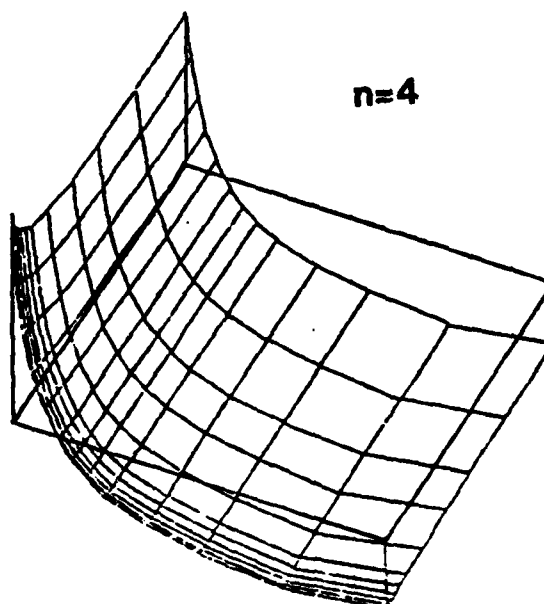
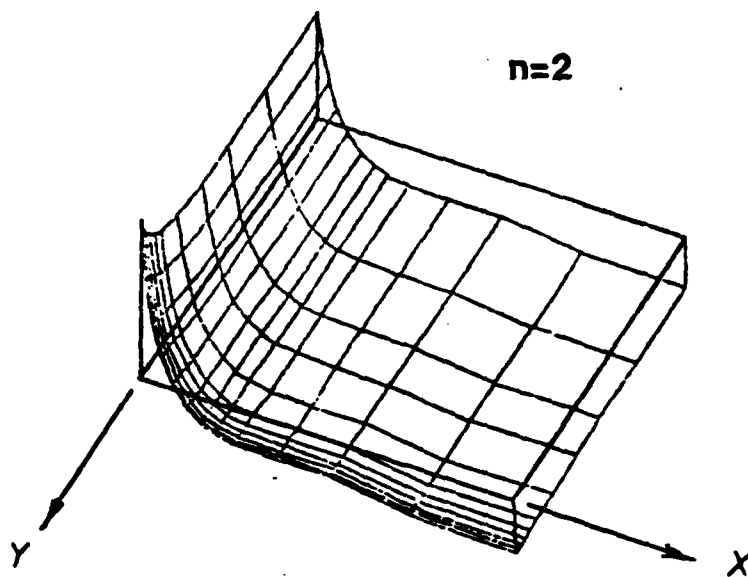
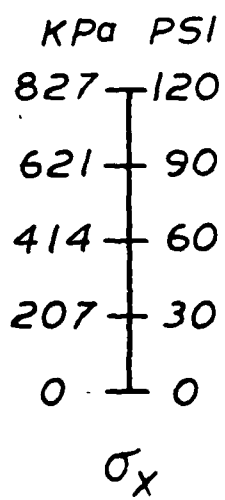


Figure 24 σ_x Distribution in the 0° Ply (near $0/90$ interface)
Due to $\Delta T = -1^\circ F$.

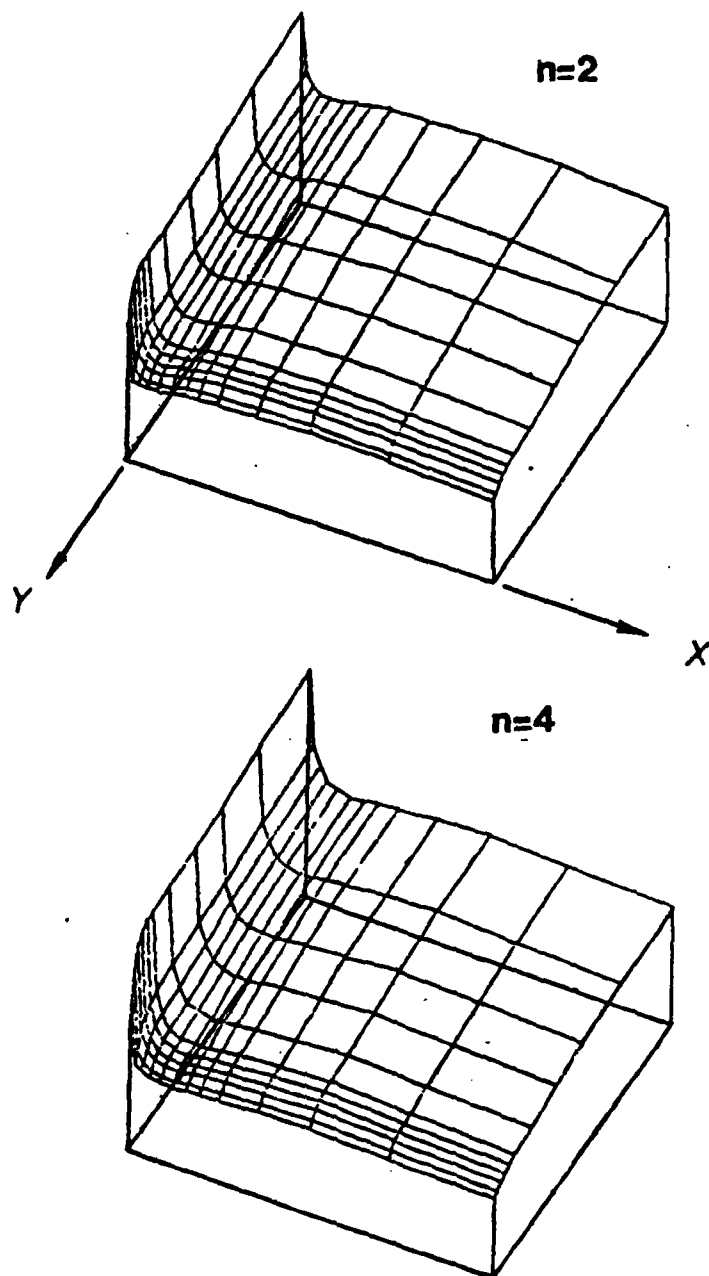
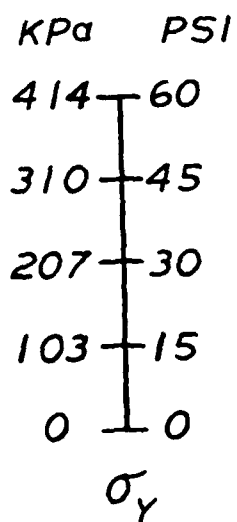


Figure 25 σ_y Distribution in the 0° Ply (near $0/90$ interface)
Due to $\Delta T = -1^\circ\text{F}$.

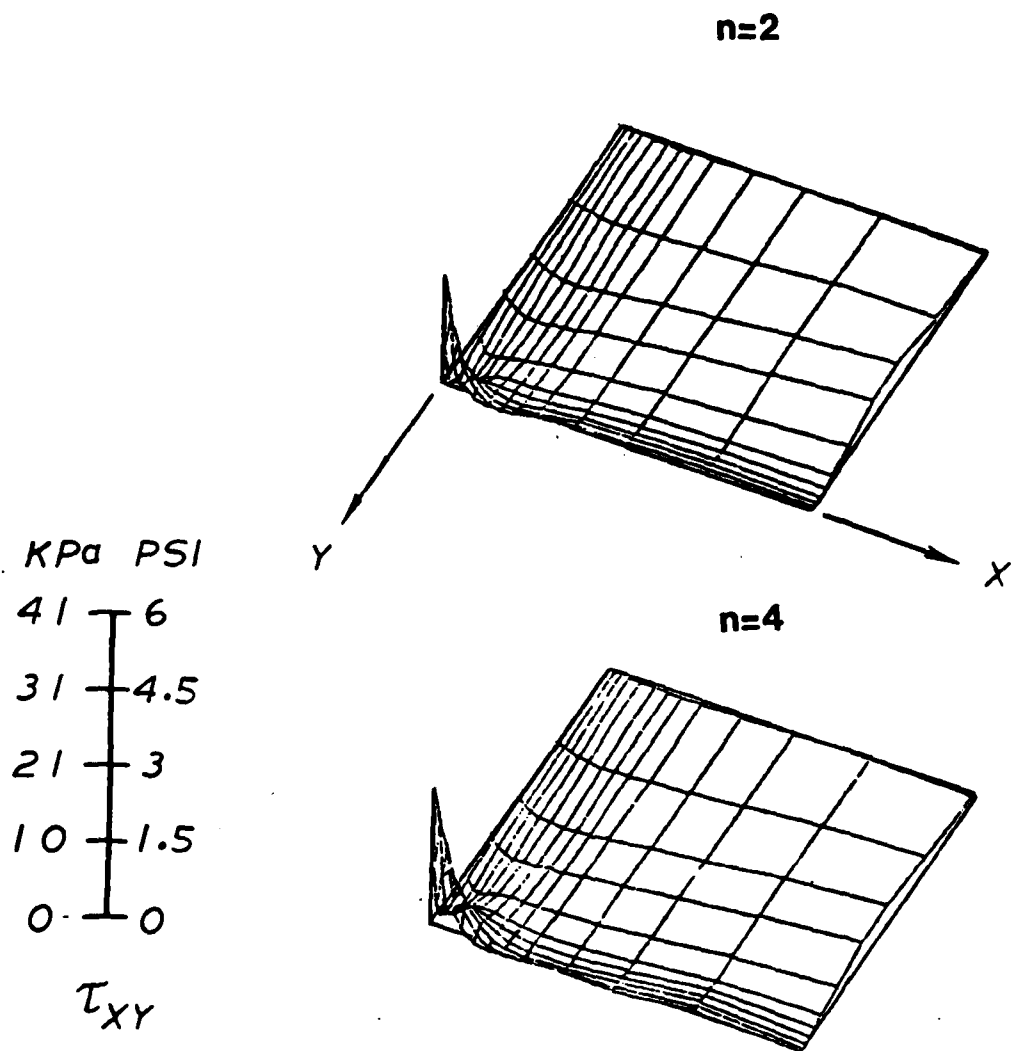


Figure 26 τ_{xy} Distribution in the 0° Ply (near $0/90$ interface)
Due to $\Delta T = -1^\circ\text{F}$.

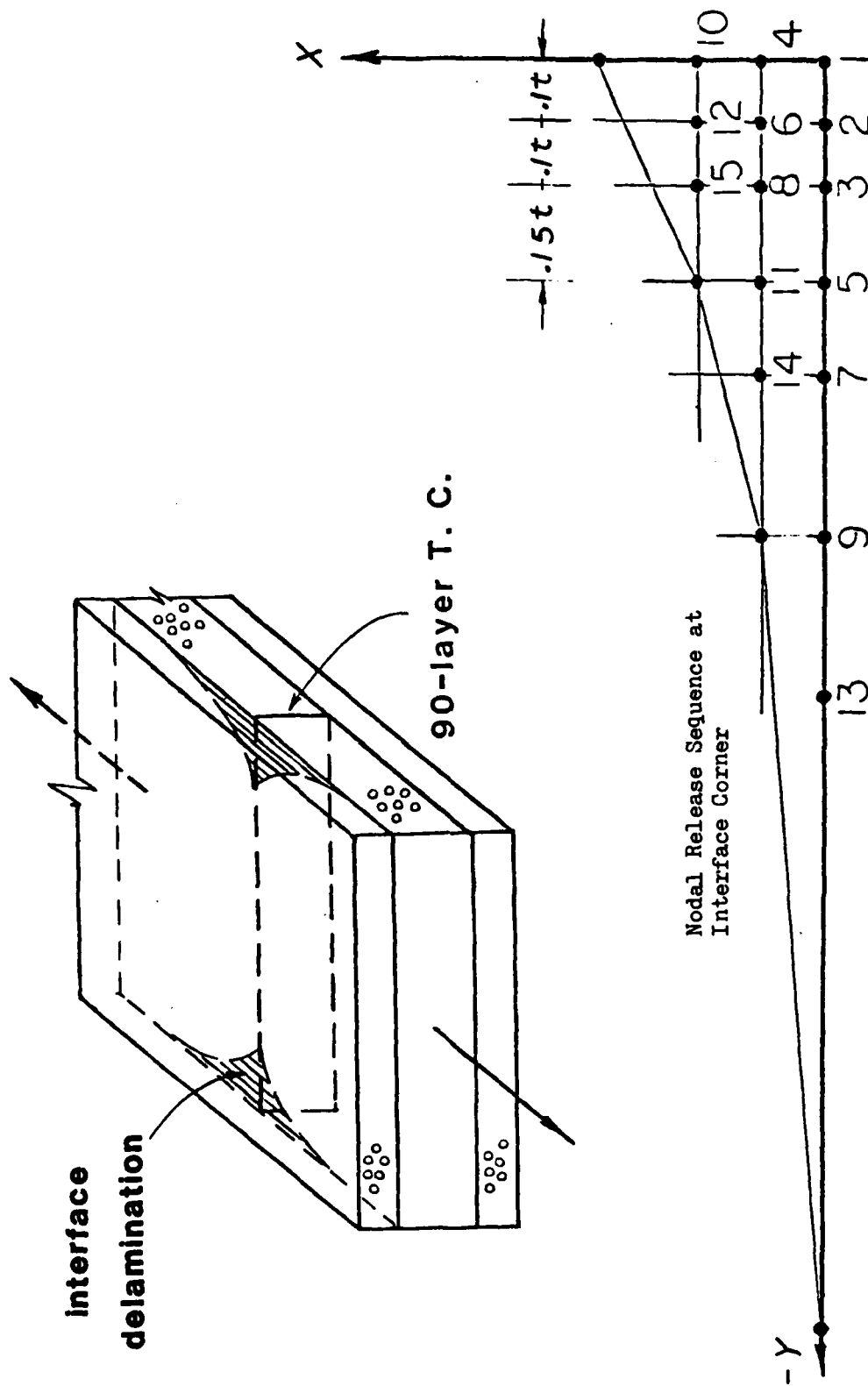


Figure 27 Schematic View (above) of Interface Delamination Near Free Edge/Transverse Crack Corner Point; and the Nodal Release Sequence (below) for Delamination Simulation.

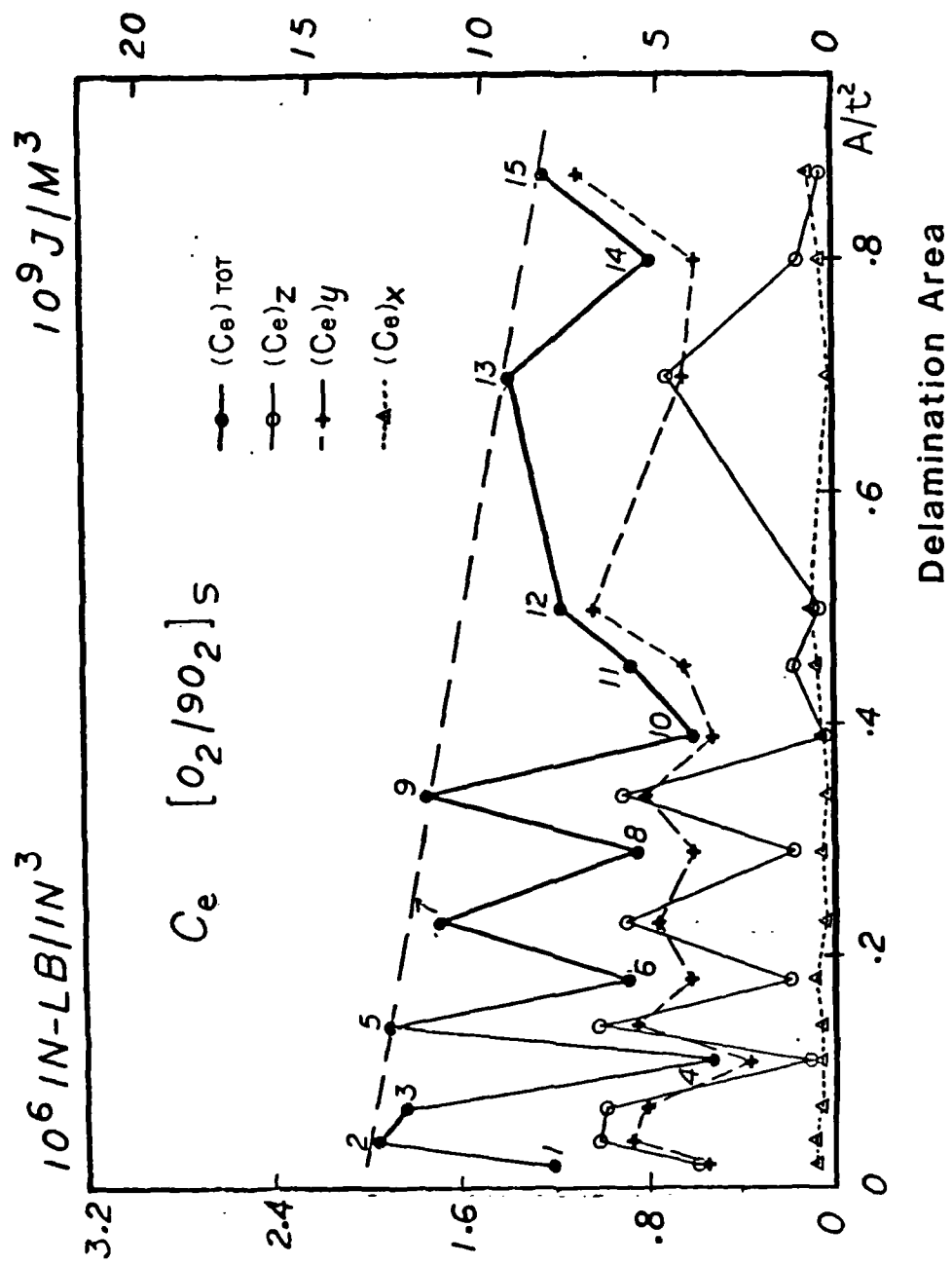


Figure 28 Strain Energy Release Rate Coefficient, C_e , for Delamination at Corner Point.

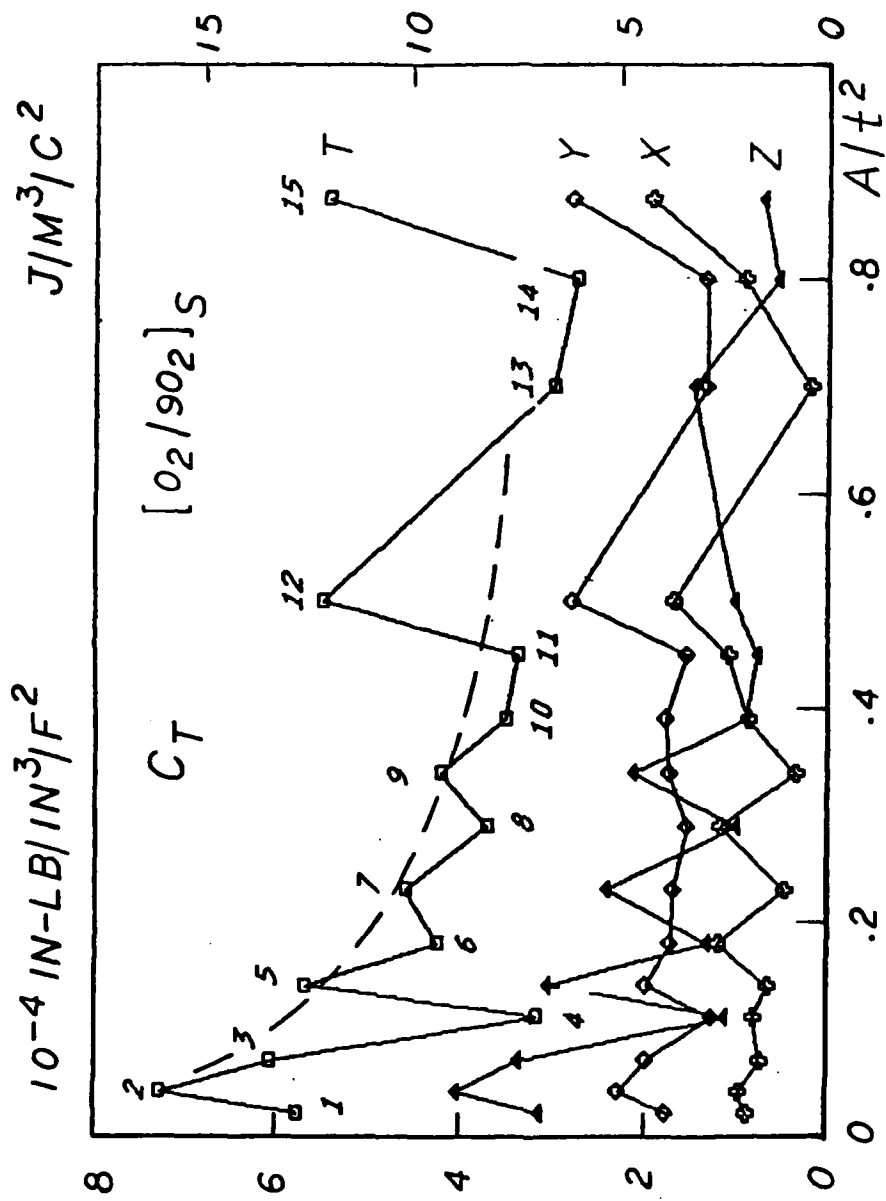


Figure 29 Strain Energy Release Rate Coefficient, C_T , for Delamination at Corner Point.

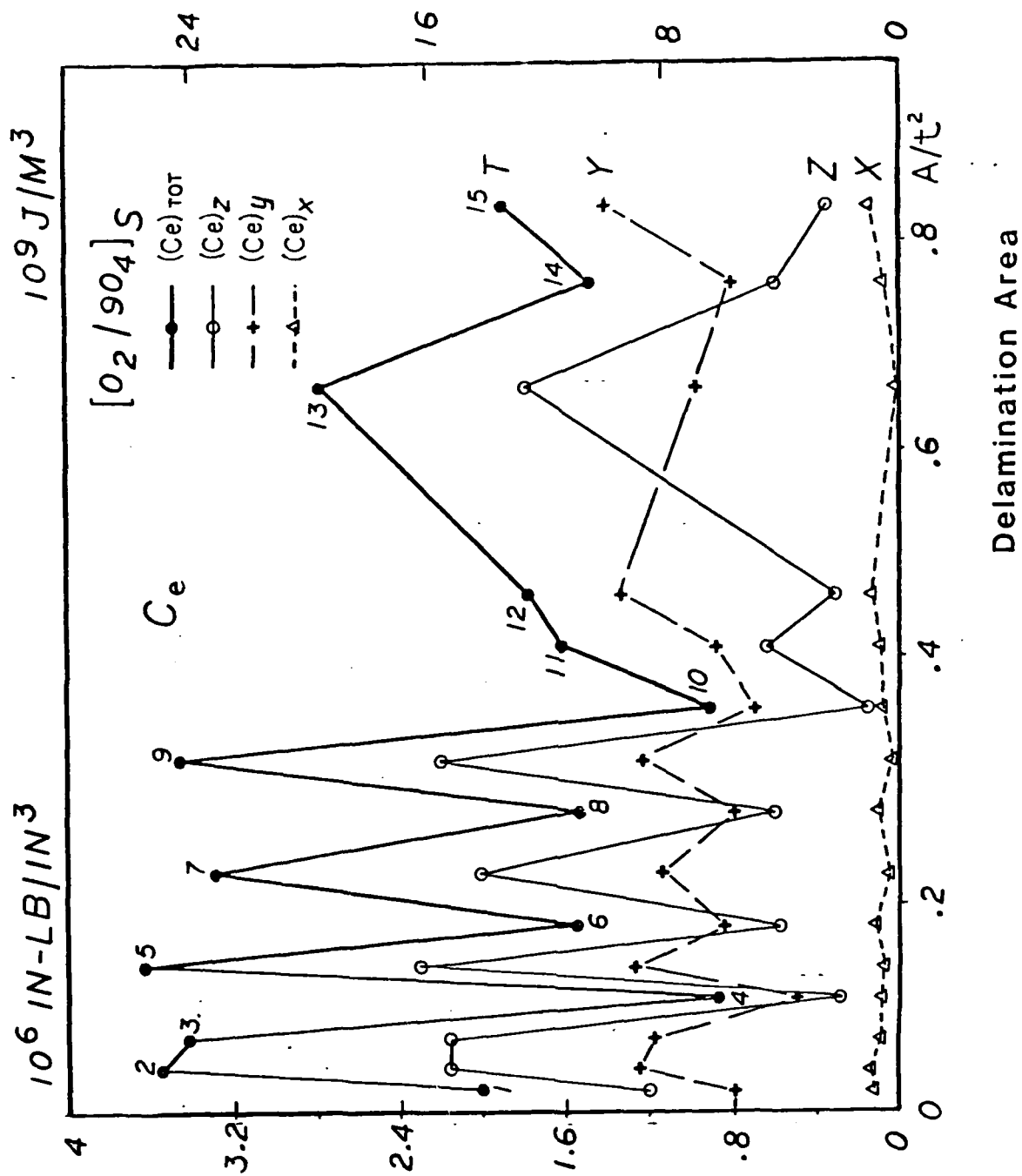


Figure 30 Strain Energy Release Rate Coefficient, C_e , for Delamination at Corner Point.

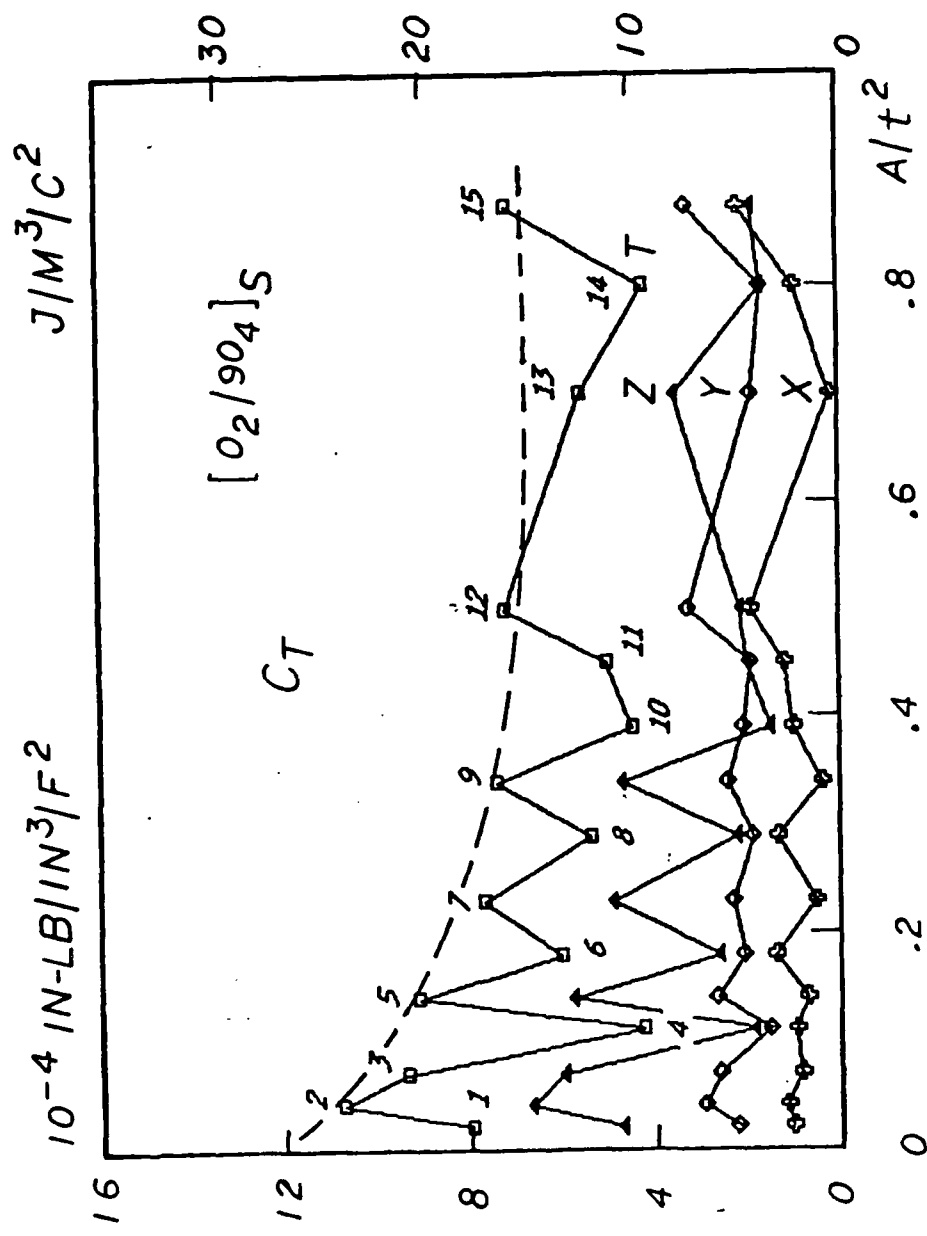


Figure 31 Strain Energy Release Rate Coefficient, C_T , for Delamination at Corner Point.

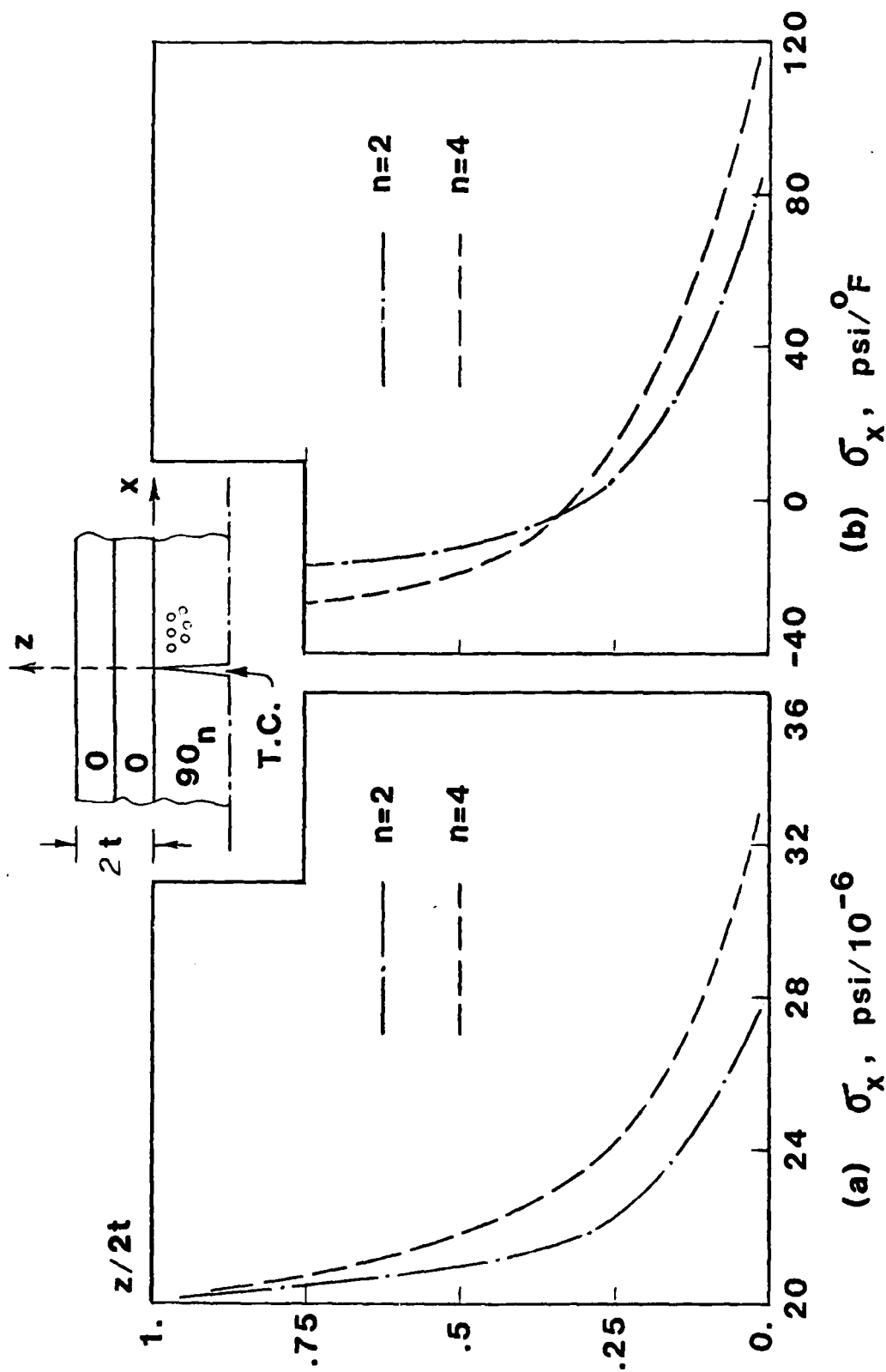


Figure 32 Through-thickness Distribution of σ_x in the 0° Ply and Near A 90° Ply Transverse Crack.

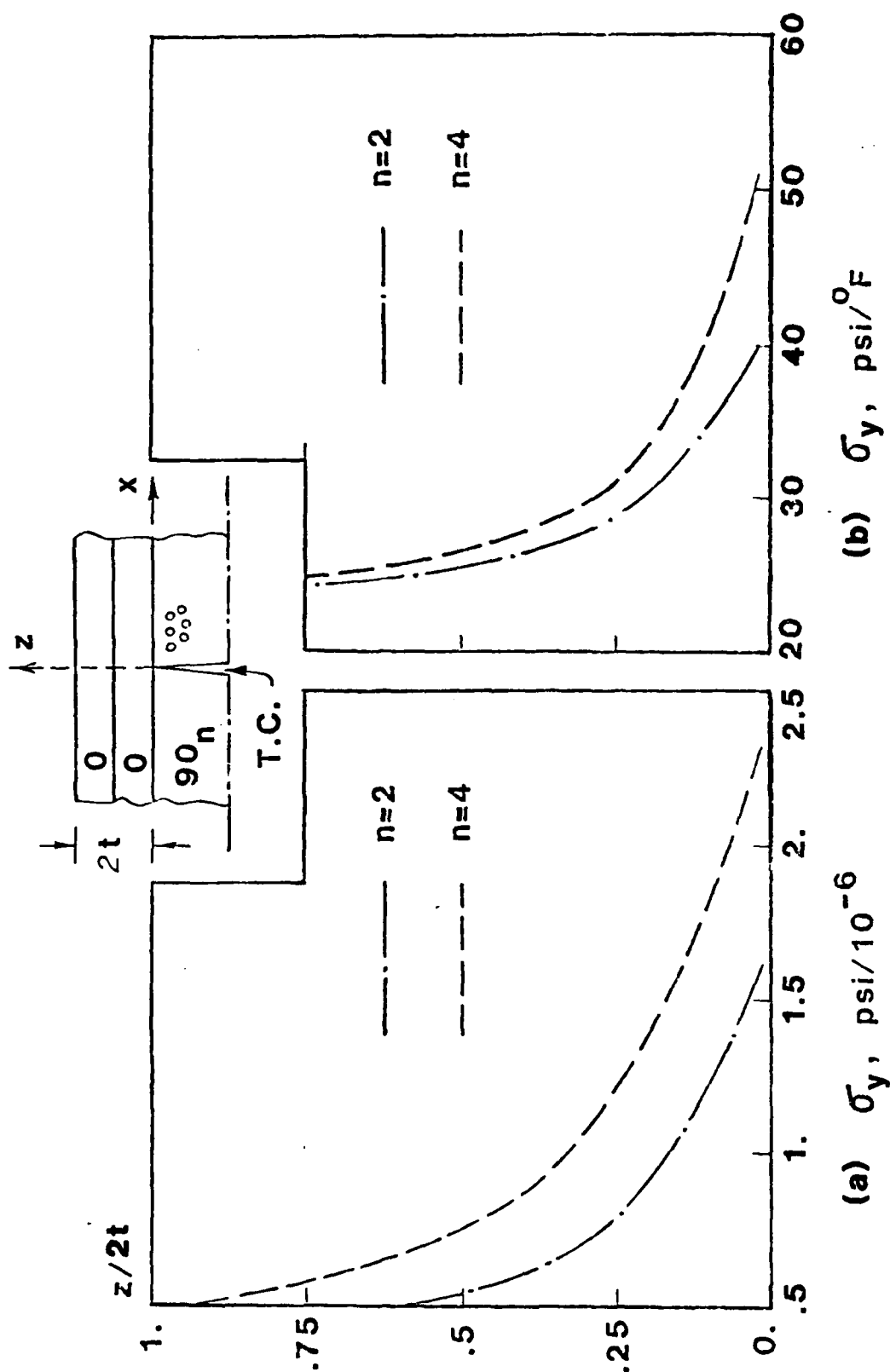


Figure 32 Through-thickness Distribution of σ_y in the 0° Ply and Near A 90° Ply Transverse Crack.

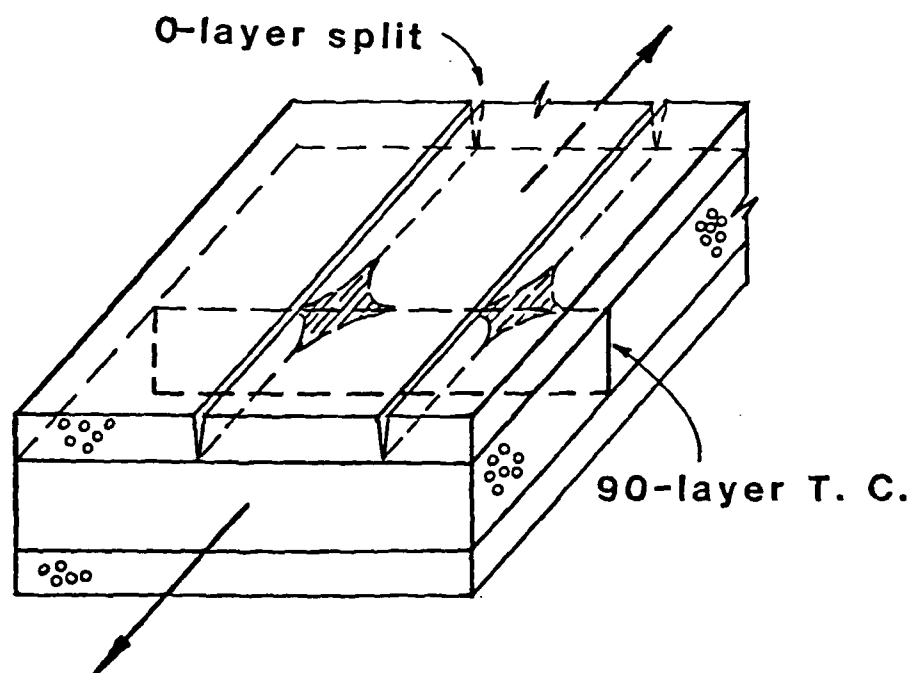


Figure 40 Schematic View of Cross Cracks and Delamination
at the Cross Cracks.

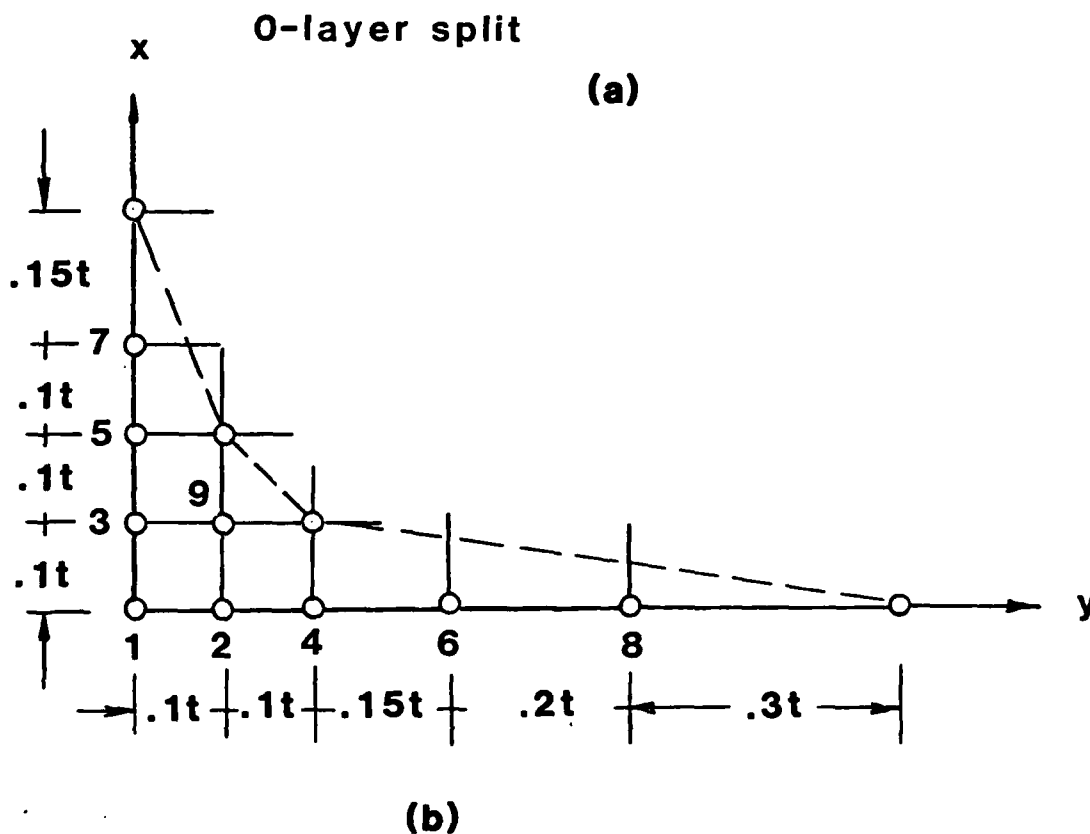
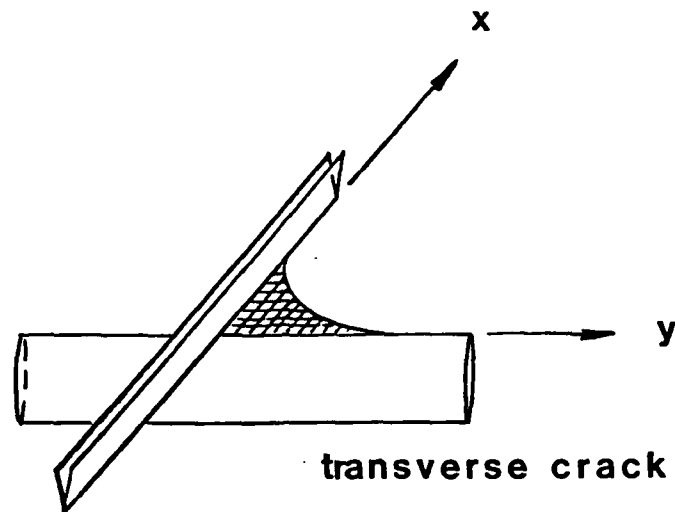


Figure 35 (a) Plane of Delamination at the Cross Cracks; and (b) The Simulated Nodal Release Sequence of Delamination Growth.

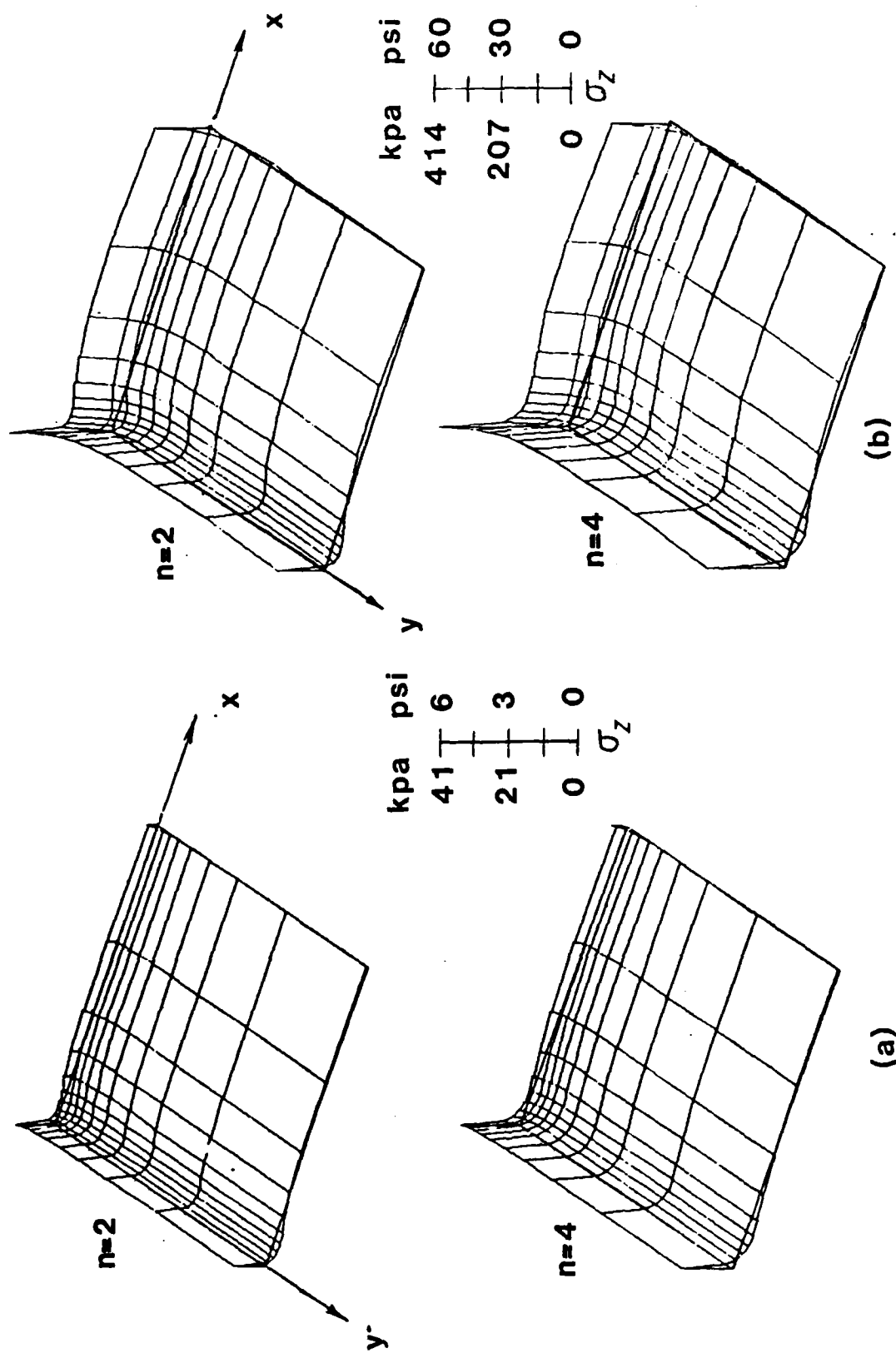


Figure 36 σ_z Distribution on the 0/90 Interface Near the Cross Cracks; (a) $\bar{\epsilon}_x = 10^{-6}$, (b) $\Delta T = -1^\circ\text{F}$

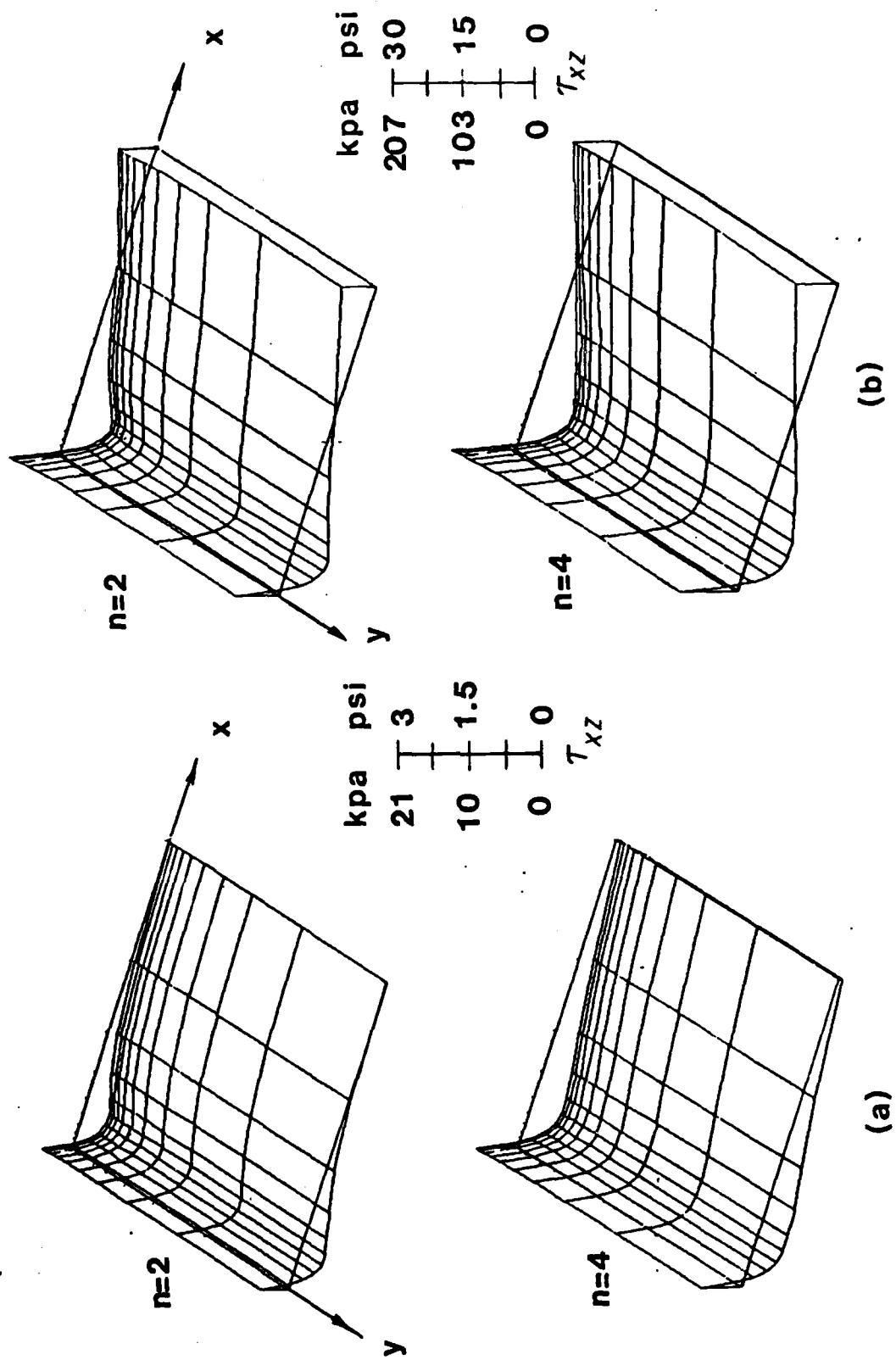


Figure 37 τ_{xz} Distribution on the 0/90 Interface Near the Cross Cracks; (a) $\bar{\epsilon}_x = 10^{-6}$, (b) $\Delta T = -1^\circ F$

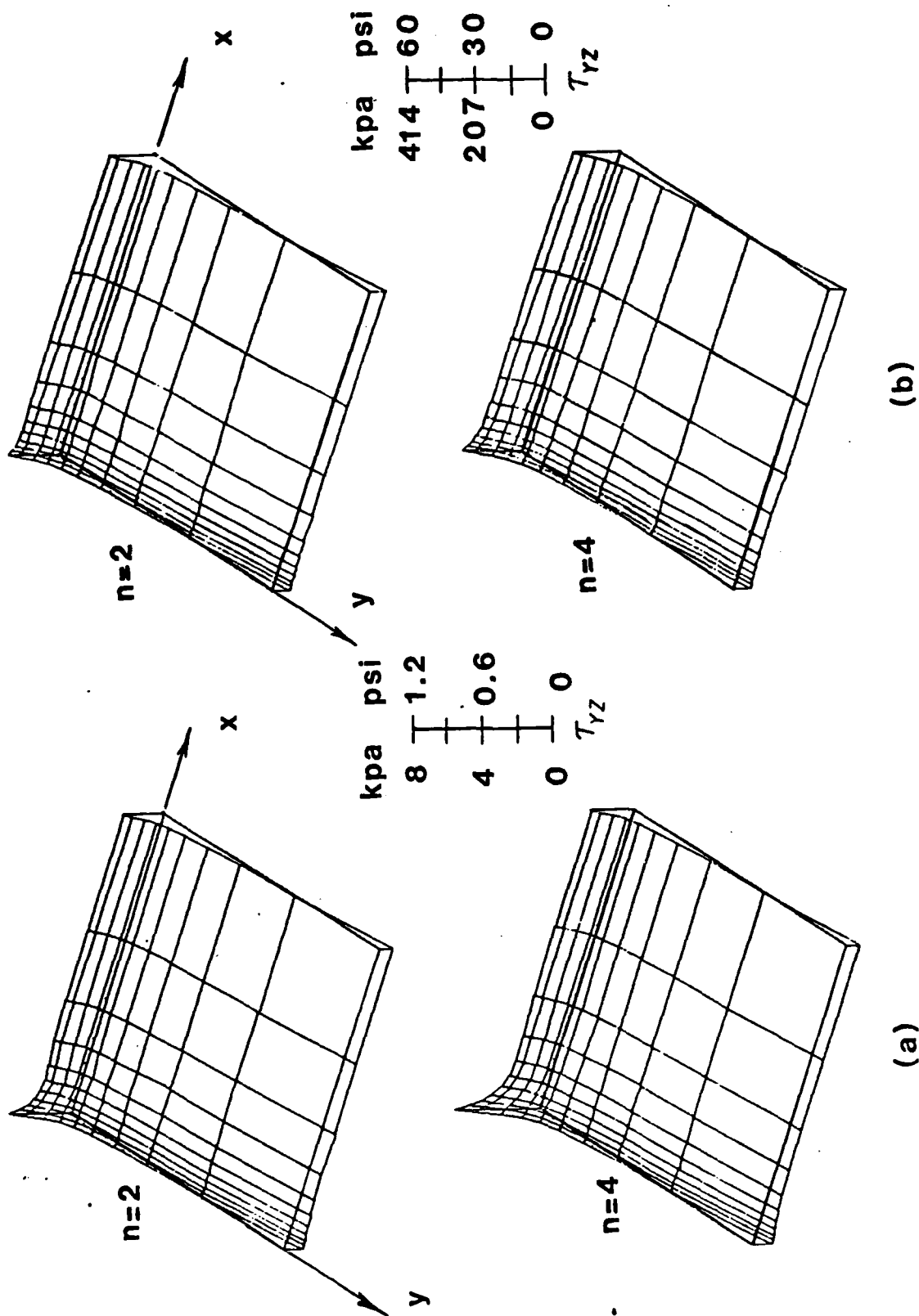


Figure 38 τ_{yz} Distribution on the 0/90 Interface Near the Cross Cracks; (a) $\bar{e}_x = 10^{-6}$, (b) $\Delta T = -1^\circ F$

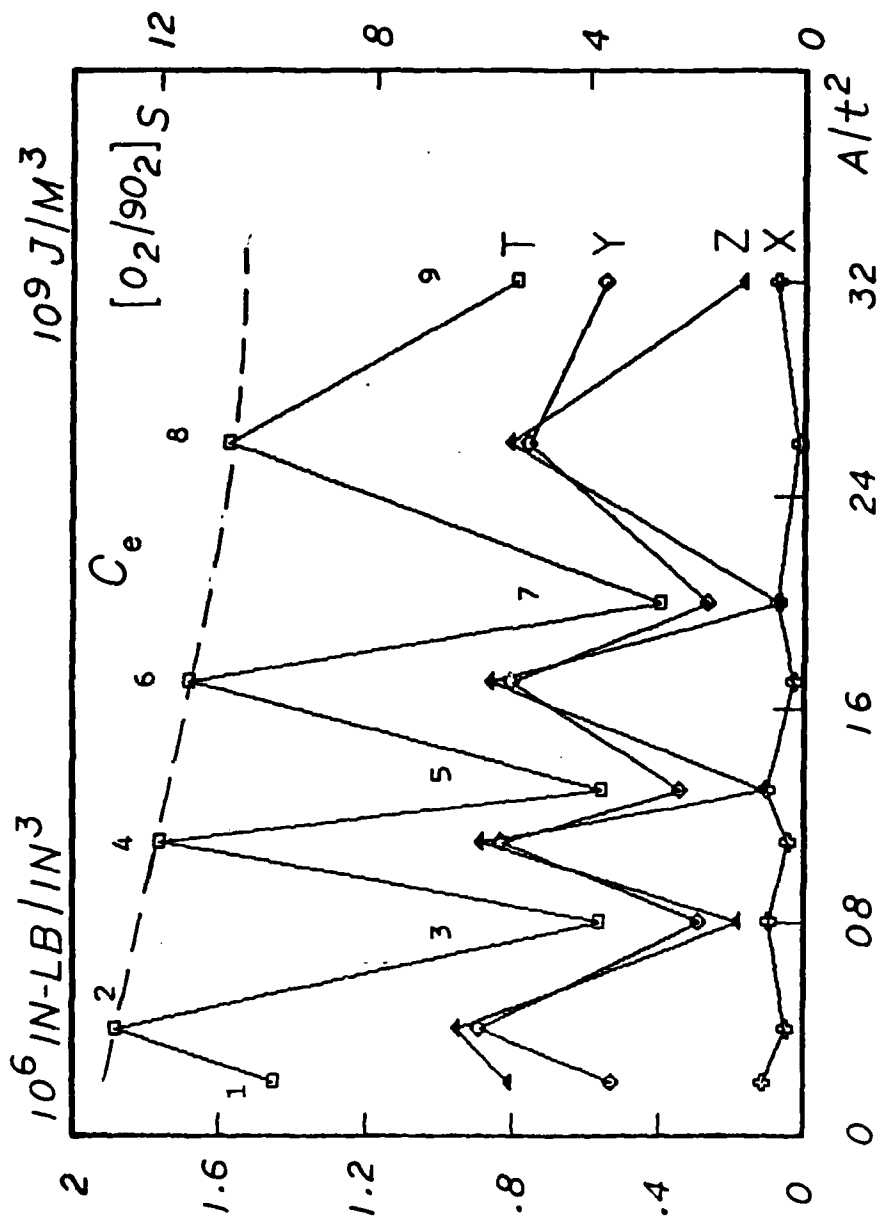


Figure 39 Strain Energy Release Rate Coefficient, C_e , for Delamination at Cross Cracks.

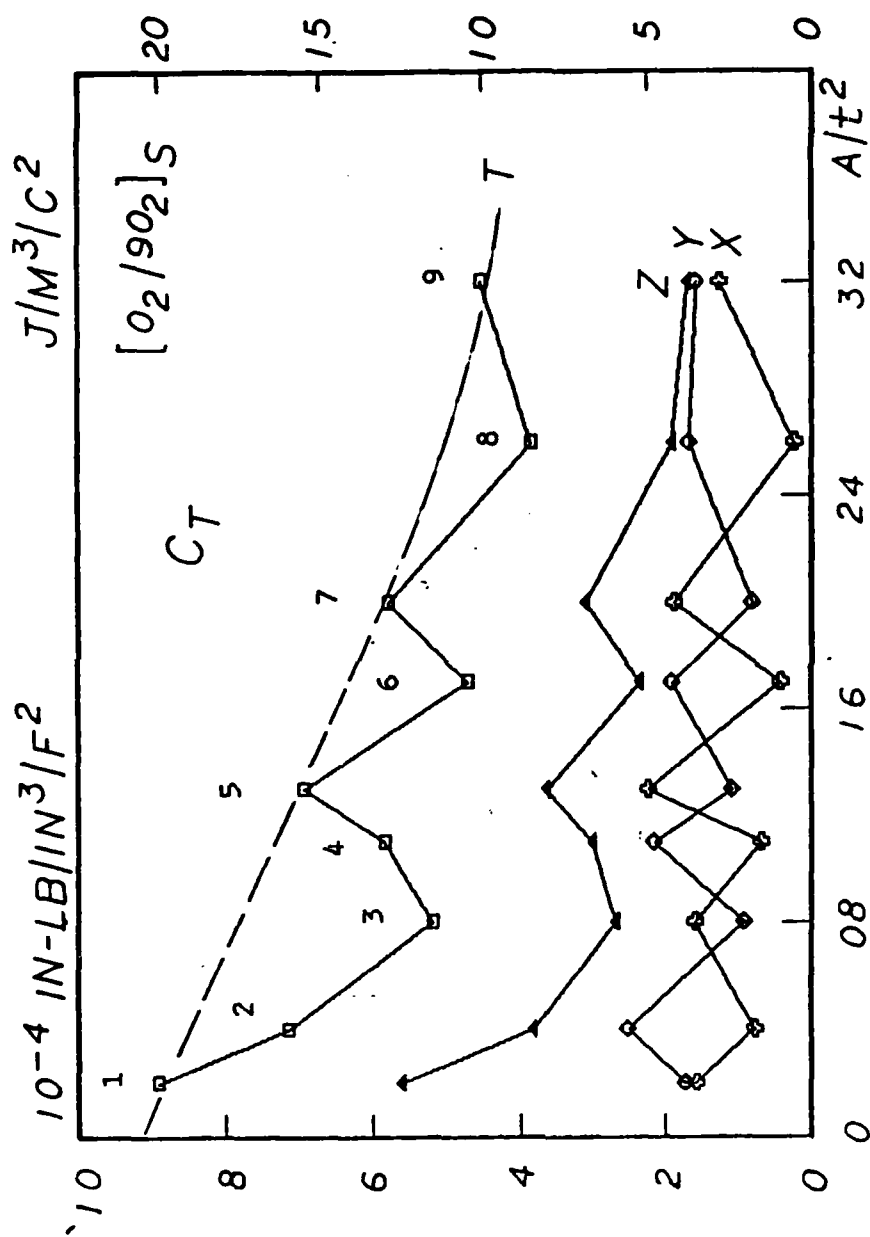


Figure 40 Strain Energy Release Rate Coefficient, C_T , for Delamination at Cross Cracks.

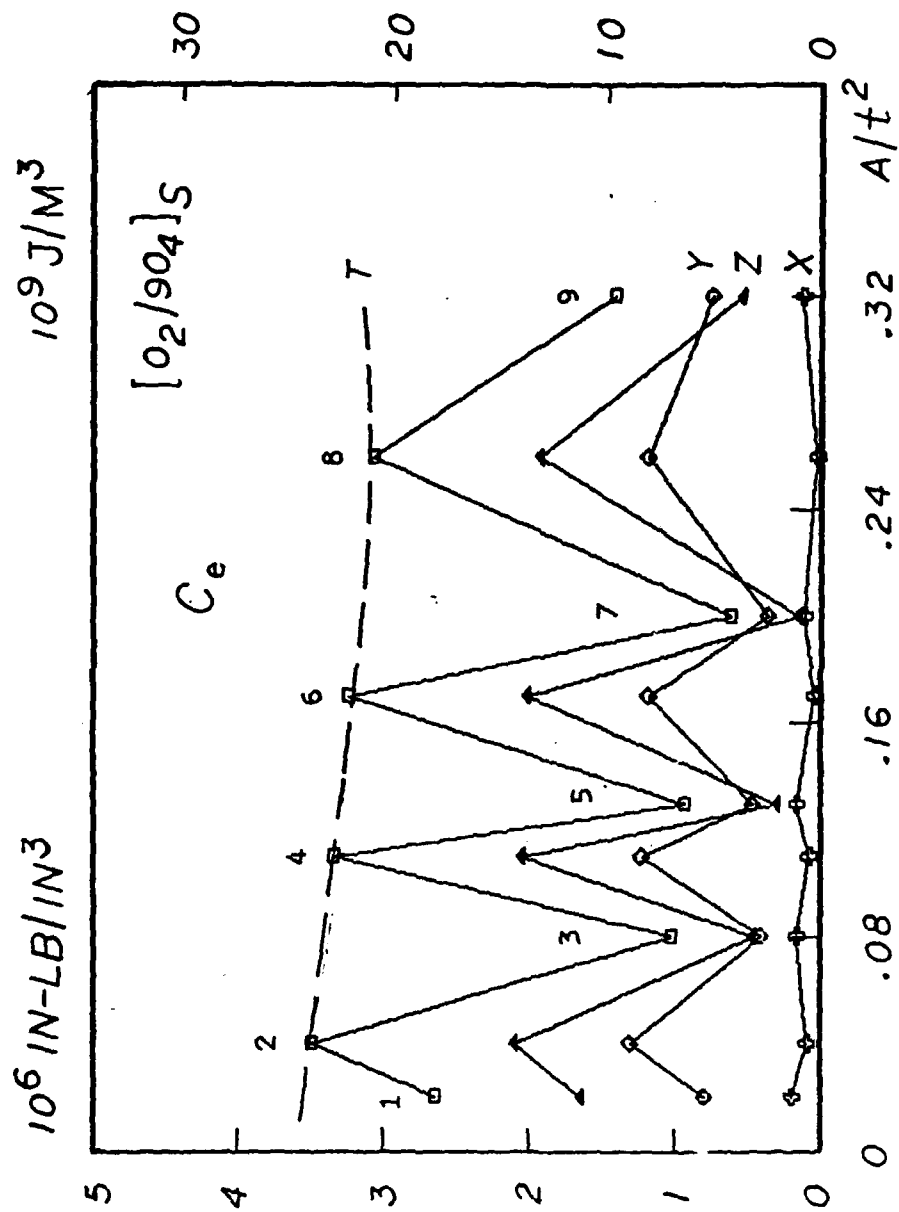


Figure 41 Strain Energy Release Rate Coefficient, C_e , for Delamination at Cross Cracks.

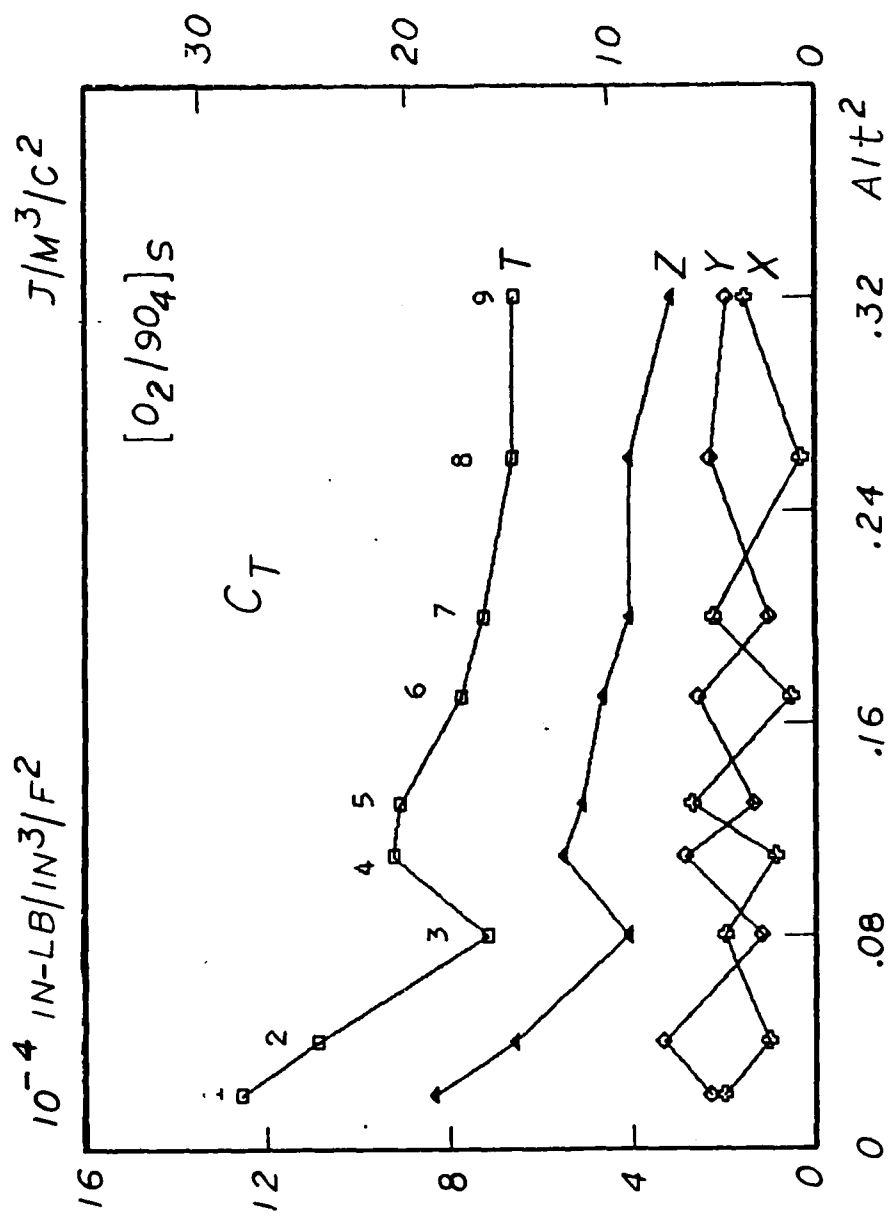


Figure 42 Strain Energy Release Rate Coefficient, C_T , for Delamination at Cross Cracks.

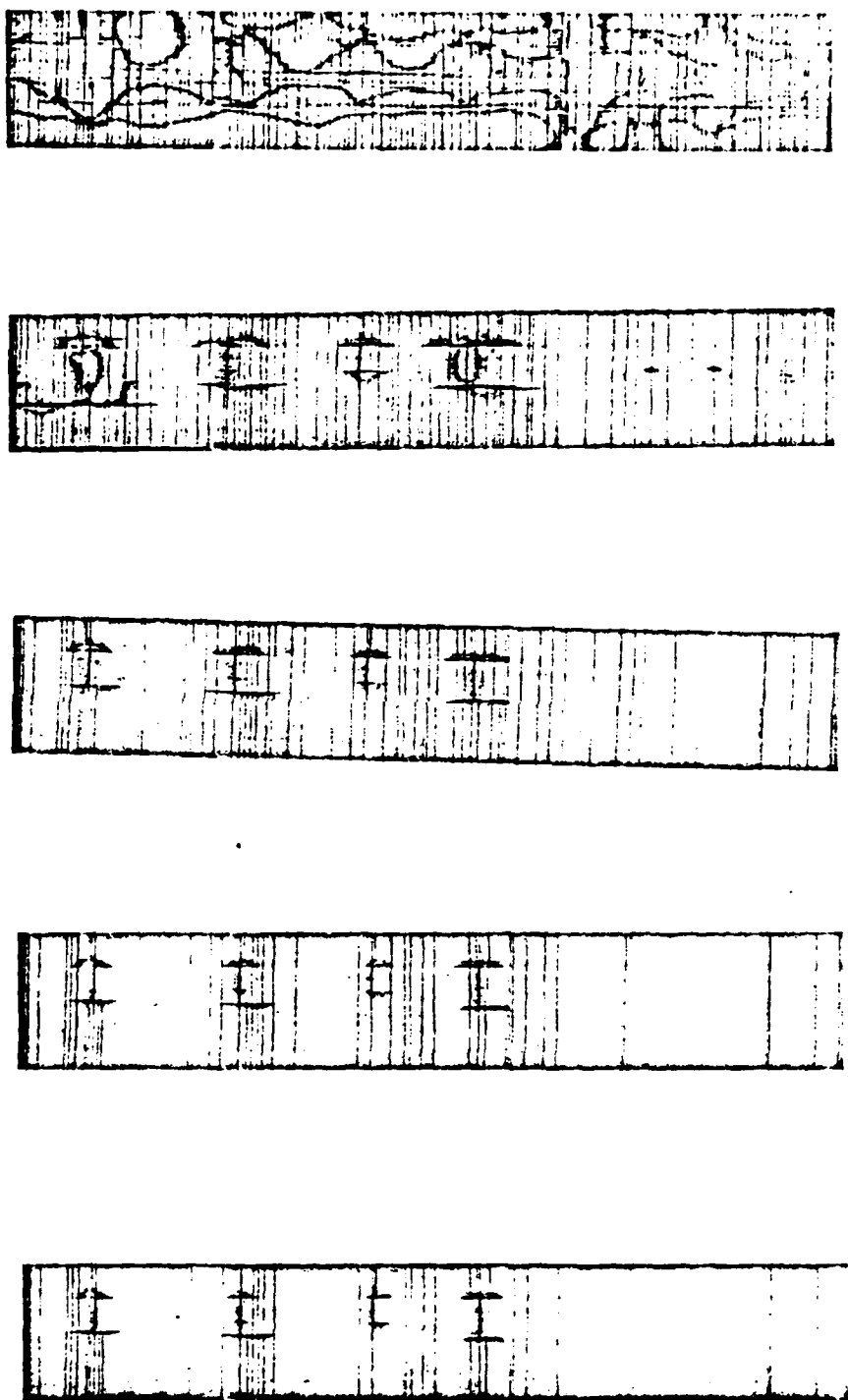


Figure 43 Load-Sequence of X - Radiographs Showing Delamination Growth at Several Cross Cracks.

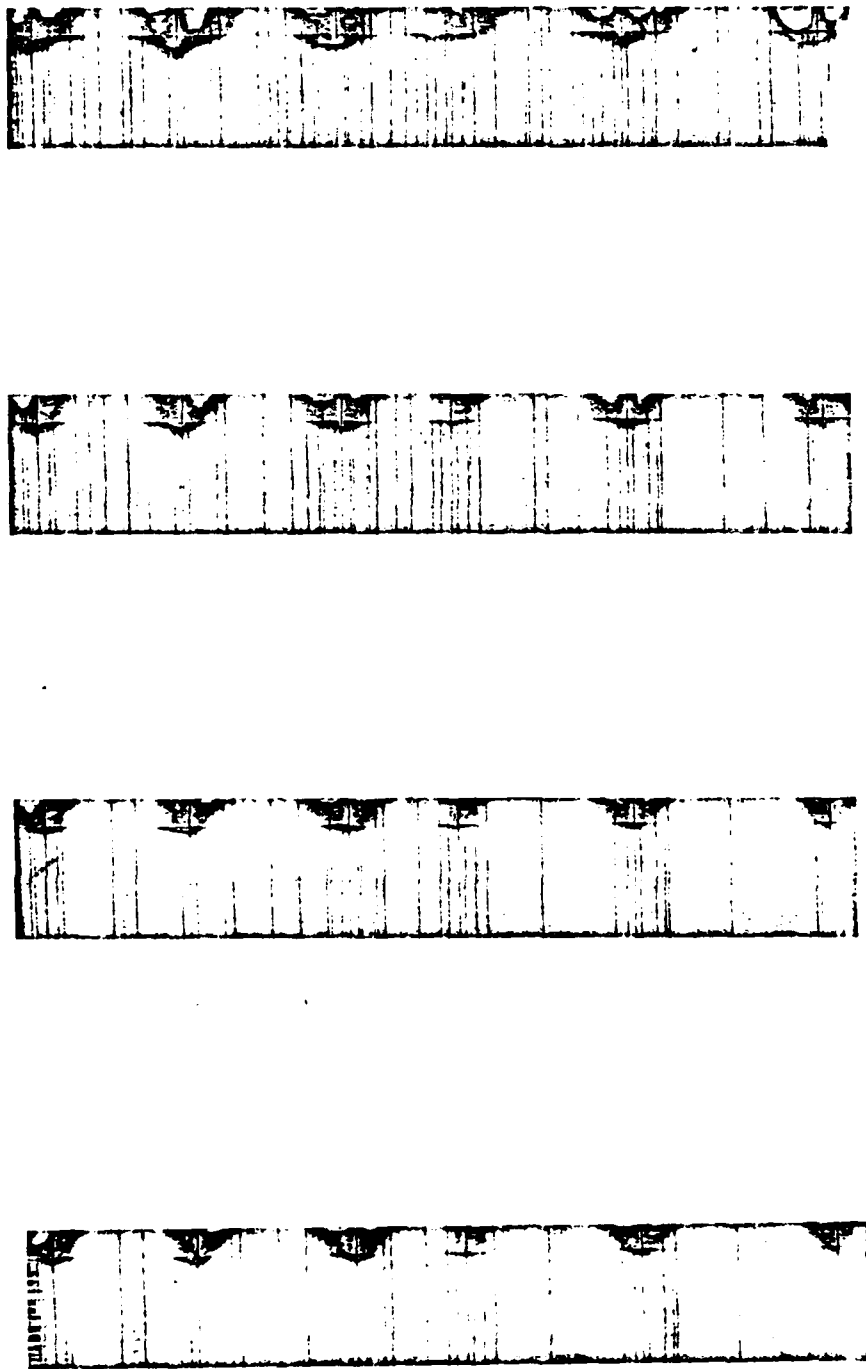


Figure 44 Load-Sequence X - Radiographs Showing Delamination Growth at Free Edge/T. C. Corner Points.

END

FILMED

2-85

DTIC